JANUARY
1977

MICROWAVES

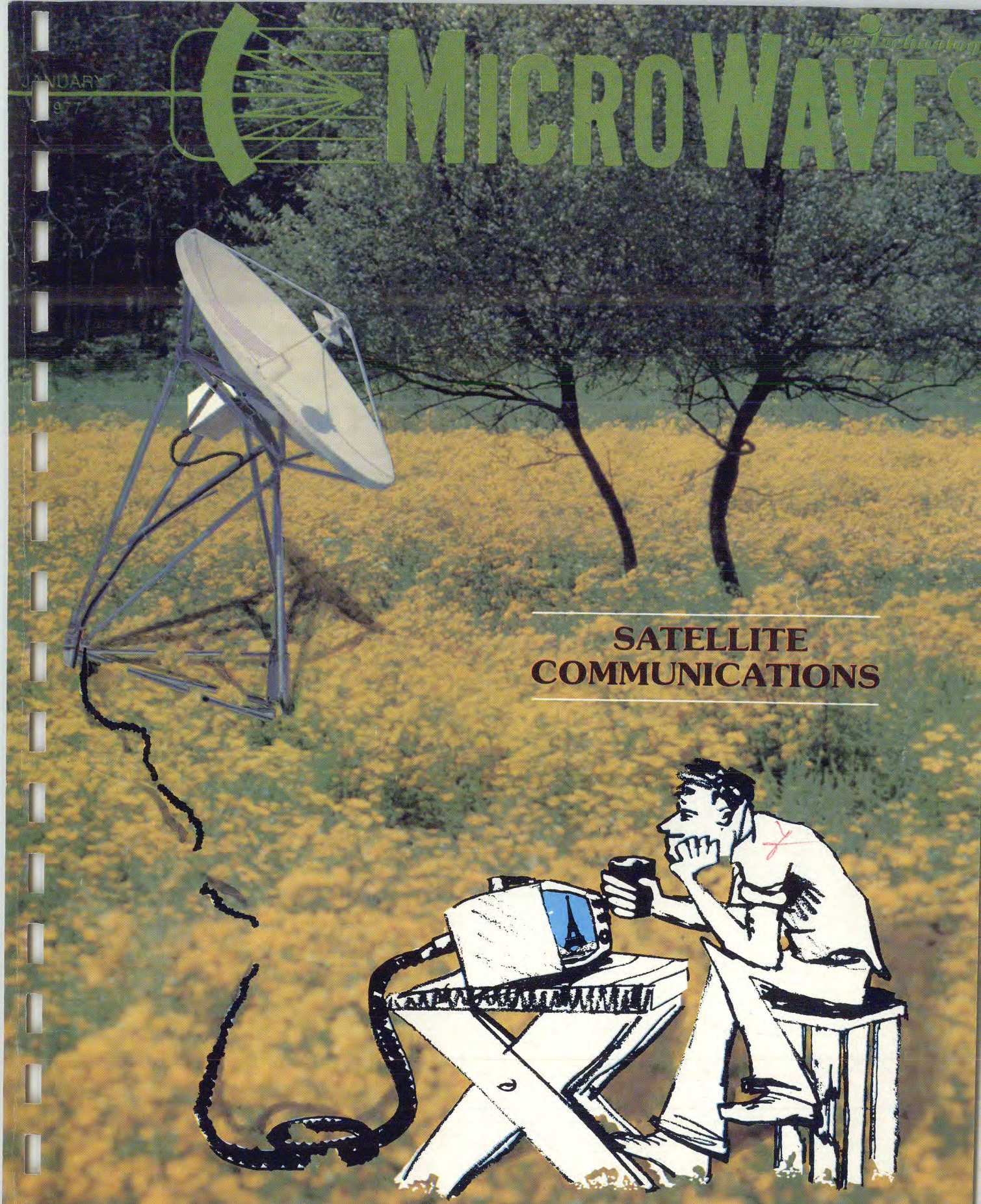

SATELLITE COMMUNICATIONS

Earth stations slim down to meet grass-root demands

Also: Upgrade coax switches for Satcom • Synthetic array radar to chart Venus • 1976 Annual index

MICROWAVES

January 1977
Vol. 16, No. 1

news

9 **Tube manufacturers stress power and efficiency gains**
12 **Synthetic array radar to map the surface of Venus**
14 **Illumination improves Trapatt performance**
17 **Industry**
18 **Washington**
22 **International**
28 **Meetings**
30 **For Your Personal Interest...**
32 **R & D**

editorial

34 **Will today's policy decisions choke tomorrow's technology?**

technical

Communications

36 **Earth Stations Slim Down To Meet Grass-Root Demands.** Higher-power satellites, improved low-noise amplifiers and cost-effective antennas are bringing the back yard earth station closer to reality.

48 **Upgrade Coax Switches For High Power Transfer.** R.G. Winch of Teledyne Microwave, proposes a simple scheme to modify a standard, SP2T switch for satellite applications. Tradeoff curves guide the way toward optimum switch design.

54 **Edge-Guide: One Path To Wideband Isolator Design (Part I).** Michael Dydyk of Motorola Government Electronics Division, examines propagation characteristics in the first half of a two part series.

60 **1976 Annual Index**

departments

64 **Product Features:** Sweeper and signal generator features combined in one package. Bandpass multiplexers now cover 9:1 bandwidths.
66 **New Products**
69 **Feedback**
74 **Application Notes**
76 **New Literature**
78 **Bookshelf**
79 **Advertisers' Index**
80 **Product Index**

About the cover: An earth station in your back yard ? Well not today, but if earth station trends continue it can't be too far off. Cover composition by Art Director Robert Meehan.

coming next month-Semiconductors

Is there a power FET in your future? System designers are just beginning to enjoy the impact that the GaAs FET has made on the low-noise amplifier scene, but component manufacturers are already bracing for the second wave of GaAs FET technology—the power FET. Next month, a staff-written status report reviews efforts behind the development of this potential TWT replacement.

An applications view of the Josephson junction. Applications in super-conducting microstrip—where component Qs of 300,000 can be approached—are suggested along with a futuristic view of the devices might slash the weight of relay satellites by a factor of 20.

Publisher/Editor
Howard Bierman

Managing Editor
Stacy V. Bearse

Associate Editor
George R. Davis

Washington Editor
Paul Harris
Snyder Associates
1050 Potomac St. NW
Washington, DC 20007
(202) 965-3700

Editorial Assistant
Gail Murphy

Production Editor
Sherry Lynne Karpen

Art Director
Robert Meehan

Production
Dollie S. Viebig, Mgr.
Sandra N. Bowen

Circulation
Barbara Freundlich, Dir.
Trish Edelmann
Sherry Karpen,
Reader Service

Directory Coordinator
Janice Tapp

Editorial Office
50 Essex St.,
Rochelle Park, NJ 07662
Phone (201) 843-0550
TWX 710-990-5071

A Hayden Publication
James S. Mulholland, Jr.,
President

MICROWAVES is sent free to individuals actively engaged in microwave work. Prices for non-qualified subscribers:

	1 Yr.	2 Yr.	3 Yr.	Single Copy
U.S.	$25	$40	$ 60	$3.00
Foreign	$40	$70	$100	$4.00

Additional Product Data Directory reference issue, $15.00 each (U.S), $27.00, (Foreign), POSTMASTER, please send Form 3579 to Fulfillment Manager, MicroWaves, P.O. Box 13801, Philadelphia, PA. 19101.

Back Issues of MicroWaves are available on microfilm, microfiche, 16mm or 35mm roll film. They can be ordered from Xerox University Microfilms, 300 North Zeeb Road, Ann Arbor, MI 48106. For immediate information, call (313) 761-4700.

Hayden Publishing Co., Inc., James S. Mulholland, President, printed at Brown Printing Co., Inc., Waseca, MN.

Copyright © 1977 Hayden Publishing Co., Inc., all rights reserved.

SATELLITE COMMUNICATIONS

Earth stations meet grass-



AN earth station in your backyard? Well not quite yet, but if earth station trends continue, it can't be too far off. Already dishes are popping up on the frozen plains of Alaska and tiny hamlets in Indonesia. Pick up a copy of the Wall Street Journal and you will be reading copy transmitted by satellite. Satcom technology is now within the grasps of the entrepreneur who brings you cable TV and similar technology is available today to enable voting, shopping and banking to be carried out from your living room.

In the next few years, earth terminals will continue to shrink, and when the public satellite responsible for the viewing entertainment of our friend on the cover is launched, earth-station engineers will be ready for it.

This unalterable course is a result of three major trends bringing about less complex, less expensive earth terminals:

- Higher frequency utilization.
- Increased satellite efficiencies and higher EIRP (effective isotropic radiated power).
- Demand for cheaper use oriented terminals.

The trend to higher frequencies is, in itself, perhaps the most significant and the most immediate movement. Already there are numerous satellite experiments being carried out at frequencies as high as 30 GHz. The irony in the shift to higher frequency is that it is being forced on the satellite common carrier, not by a transponder shortage but rather by spectrum overcrowding caused by terrestrial activity. But the move to approve small aperture terminals by the FCC may rapidly fill S-band transponders and force users to the higher bands.

Next step is to 11 and 14 GHz

This is one instance where the technology will be ready when the demand is imposed. Higher frequency satcom experiments have been carried out almost since the beginning of the satellite communications era. Intelsat V will use the 11 and 14-GHz bands and Satellite Business Systems (SBS) plans to deploy a number of five-meter earth terminals operating in the 12-and-14 GHz bands.

The Communications Technology Satellite (CTS) system, a joint NASA and Communications Research Center of Canada project, is currently using one- and three-meter transportable terminals to carry out experiments in the 11 and 14-GHz bands.

The three-meter terminals are housed in a trailer and contain essentially the same electronics as the system's nine-meter main terminal which provides TV transmission and reception, sound program and digital data. The system's smallest deployed stations, the transportable one-meter terminals, are used for two-way telephone traffic.

The 11 and 14-GHz European Communications Satellite (ECS), planned as a complement to European public terrestrial systems, is currently scheduled for a 1980 launch. Experimental use of the bands will begin this year with the launch of the European Space Agency's (ESA) Orbital Test Satellite (OTS), using three-meter earth stations for propagation tests. In Japan, an experimental communications satellite will be launched later this year to perform studies at both 20 and 30 GHz. In this country, Comsat is presently evaluating 20 and 30-GHz communication possibilities with beacons operating at 19.0 and 28.56 GHz.

Frequency feasability studies are only the tip of the experimental iceberg. Experiments on these same satellite systems include higher power traveling-wave tubes (TWTs) for increased EIRP, beam-shaping techniques for greater radiated efficiency and a number of frequency reuse schemes to increase transponder availability. The most important of these to future earth station designers are EIRP studies.

EIRP dictates terminal design

Because on-board power is limited by payload weight and most modern satellites are called on to blanket large areas, the average output power is relatively low. Most spacecraft transponders have power outputs of 4 to 5 watts and with the most commonly used antennas produce "footprints" in the 30 to 36 dBw region. The highest power concentration naturally aligns with the spacecraft beam center and falls off as indicated in Fig. 1. With the present limitation on power payloads, the EIRP actually becomes a function of the area covered. Intelsat satellites with their extremely large footprints —covering one third of the earth with three birds—provide an average 26 dBw EIRP. On the other hand, RCA's domestic Satcom I, with its much smaller coverage provides 36 dBw in the central US. The earth terminal constraints then for these two EIRPs are quite different.

In addition to available power, station end use further constrains the terminal designer. The most convenient common denominator of earth

slim down to root demands

George R. Davis,
Associate Editor



station applications is the figure-of-merit or G/T. System G/T is defined as the ratio of antenna gain to total system noise measured in degrees Kelvin. Again a wide varient exists; a heavy route Intelsat station requires a G/T of 40.7 dB/°K while 27.7 dB/°K is sufficient for TV reception in most US locations. The long-term challenge from a systems' point of view is in increasing EIRP. Shaping spacecraft beams to cover only those areas containing customers is the aim of numerous experiments. Here the advent of millimeter-wave communications is the key. A prime example is Japan's CS system. The spacecraft will spotlight all of the Japanese islands with large, circular radiation patterns at 4 and 6 GHz. But at 20 and 30 GHz, the craft will generate patterns tailored to cover only the larger islands as seen in Fig. 2. The shape of the graphite-epoxy reflectors create far field radiation patterns that match the shape of the islands. The advantages of this scheme include not only more efficient power distribution but also closer compliance with international guidelines governing energy spillover.

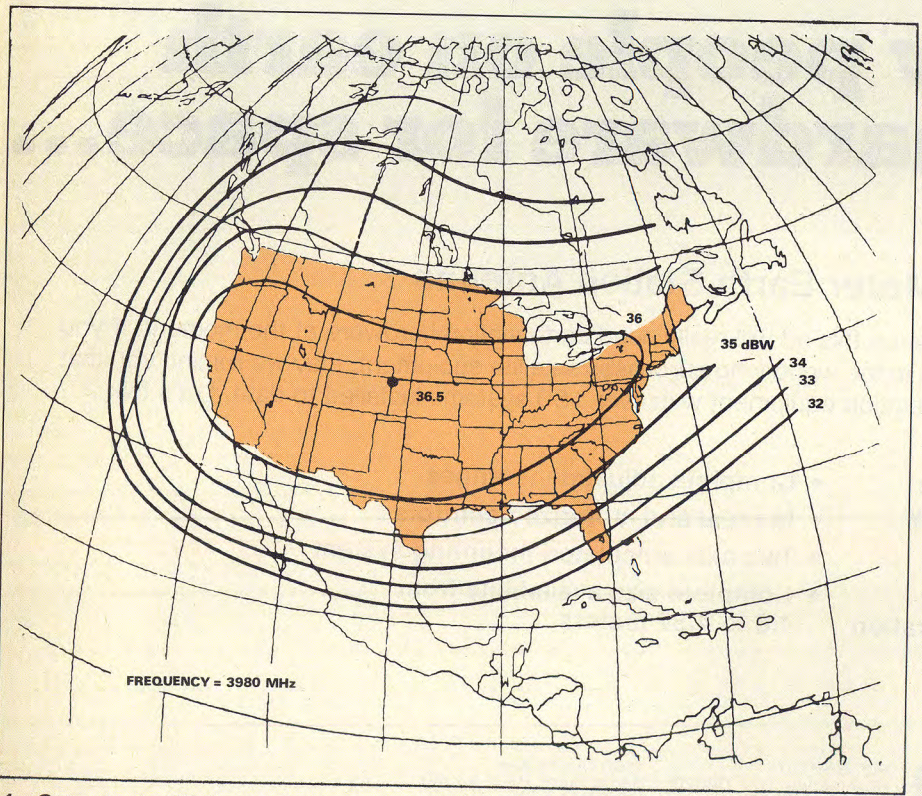

*1. **Comstar's US footprint** has maximum EIRP in the central US. Areas near Miami are 4 dB down from maximum power.*

Satcom TWT puts out 200 watts

The effects of incrreased EIRP are also under study by NASA and the Canadian Department of Communications with their CTS satellite. The CTS approach is simply to make more power available. NASA engineers developed the 12-GHz, 50 per cent efficient, 200-watt TWT now aboard the spacecraft. This power level represents the first major jump in available satellite power and the satellite is, in fact, only licensed to perform experimental tasks. Looking still further to the future, NASA has begun development on 100 and 200 watt space qualified TWTs for operation in the 41 to 43- and the 84 to 86-GHz bands. These millimeter bands were allocated by the World Administrative Radio Conference in 1971 for broadcast satellite service.

Taken together, the propounderance of new satellite technology will do much to promote lower cost, user orientated earth stations. The advantages of all these trends, however, will be amplified with the availability by 1980 of the space shuttle.

Shuttle launches to boost power

Satellite payload costs determine the amount of RF power aboard todays spacecraft. Although premature, NASA's projected savings for shuttle-launched Intelsat spacecraft are extremely encouraging. NASA estimates the cost of a shuttle launch to position a 2,000-pound payload in synchronous orbit at about $15-million in current dollars, compared with $25-million for

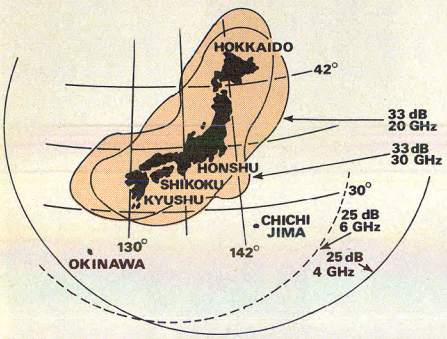

2. *Japanese engineers have created a kidney shaped contour* *by tailoring the spacecraft's graphite-epoxy reflectors.*

an Atlas-Centaur launch. The 94-nation Intelsat organization plans to launch the last three of its initial seven Intelsats with the shuttle to reap the significant cost savings.

Interestingly, the shuttle's emergence on the scene will coincide with the promised advances in lighter weight microwave power sources. The pounds per dB balance will therefore be effected from both a launch cost and a microwave technology aspect.

Demand for lower cost, less complex earth stations are coming from virtually every corner of the globe. Surveying numerous marketing experts involved in earth station enterprises, results in an almost undigestible series of numbers and predictions. The US manufacturers surveyed by *Microwaves* all have cut out their own piece of the pie and have reams of numbers to back up their predictions. Sorting through the data, however, does produce some common agreement in terms of the demand sectors. Key among these are:

- Intelsat—approximately 30 heavy-route stations still to be built.
- Domestic stations—this sector promises to use a mix of large and small aperture systems (see "Domsat and regional markets set to explode.").
- US domestic network—ranging from 10-to-11 meter earth stations, fully redundant for TV broadcast to 2-to-3 foot stations for news wire services.
- Cable TV receive only (TVRO) stations—perhaps the largest market for the simple non-redundant station. The near future promises 4-to-5 meter stations for CATV.
- Maritime and special use markets—very small (1-to-2 meter) stations for use in ship-to-ship voice traffic, earthquake detection and offshore oil recovery operations.

Although the Intelsat market may have passed its peak, there are still at least 30 new stations to be supplied, according to Bill Osborne, director of systems engineering of the Satellite Communications Operation at Harris Corp., Melbourne, FL. These super-engineered stations with G/T of 40.7 dB/°K and 45°K low-noise amplifiers sell for approximately $5-million each. The sophistication of the Intelsat stations is a result first of the low EIRP at the site because of the global footprint and secondly, Intelsat's operating guidelines.

Intelsat market still healthy

Earth stations used in the system (Fig. 3), although not owned by Intelsat are nevertheless, designed, built and operated to conform with Intelsat operating and performance specifications. With first and second generation commercial communications satellites, the limiting feature of the system was always the power transmitted by the satellite which resulted, inevitably, in the establishment of earth stations with very large antennas and reflectors —the so-called Intelsat A installation. A station of this type consists of three principal elements—the antenna system, the communications equipment and the buildings and services. A typical antenna will have a parabolic reflector 29 to 33 meters in diameter, mounted so as to be fully steerable through programmed or auto-tracking mechanisms, in both azimuth and elevation, so that the antenna beam can be pointed towards the satellite to within a one-fiftieth of a degree.

Frost and Sullivan, the New York based marketing forecaster, identifies these Intelsat customers in its September, 1976 report E-190, "Communication Satellite Systems Market In Developing Countries For The Period 1976 to 1990." Although most of the stations will be standard A, between 4 and 14 class B stations will be needed. Intelsat B calls for a G/T of 31.7 dB/°K offering a less complex, less expensive alternative to the $5-million class A installation. An additional market will soon appear in the Intelsat network. Established Intelsat stations require retrofits of dual-polarized feeds to reap the benefits of the frequency reuse schemes used in Intelsat V. Added to the feeds will be two additional LNAs to maintain full capacity redundancy. "This market will definitely be substantial," claims Osborne, "and lucrative considering feeds of this complexity will cost between $200,000 and $300,000."

Intelsat, in order to grab a larger share of the world communications market, may in the future, allow stations with lower G/T than the 31.7 dB/°K Class B limit. As Frost and Sullivan point out, "During the past ten years, Intelsat has discouraged the use of smaller earth stations through the application of higher tariffs. Nevertheless, it is the obvious intention of Intelsat to encourage the use of cheaper and smaller stations and thereby secure an additional share of the telecommunications traffic in the face of planned and proposed regional and domestic systems."

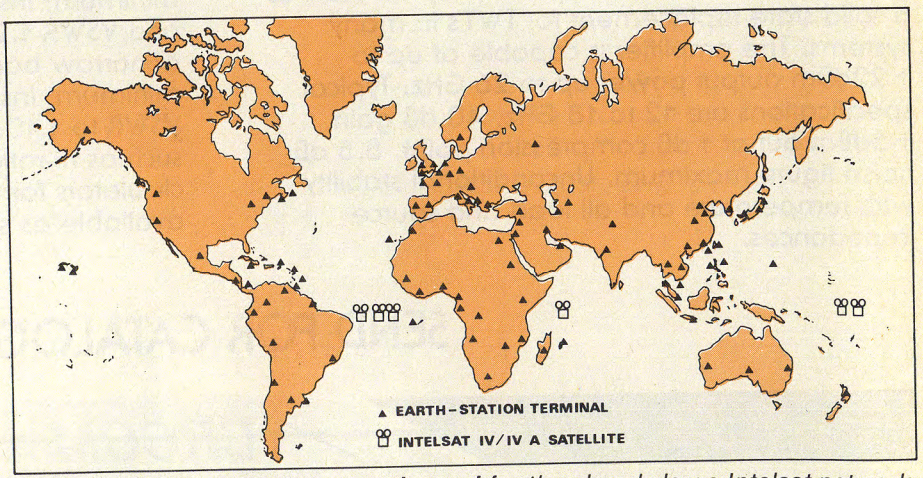

3. *At least 30 new stations are planned* *for the already large Intelsat network. Installations shown are as of late last year.*

Intelsat has good reason to fear competition from the proposed domestic and regional satcom systems. Present plans call for at least five regional systems in the world with three domestic systems already in operation using dedicated satellites.

Domsats will be a mixed bag

A review of the domestic station requirement includes a number of possibilities ranging from 10 to 12-meter stations using paramps to 3 to 4-meter terminals with GaAs FETs. As most domestic systems will comprise a mix of these, it is convenient to describe them by function. The main stations in these networks will have 10 to 12-meter antennas, figure of merit 28 to 32 dB/°K used for heavy trunk route multi-channel telephony, two-way television transmission and distribution.

A second class of domestic stations that will be used for TV network broadcasting will have slightly smaller antennas. The need here, at least in the US, is potentially large. A number of TV broadcasters plan to use this type of system to eliminate programming tariffs imposed by AT&T.

The trend toward smaller stations will affect all these networks but small station designers have not yet decided on the optimum designs.

The first choice to be made by a small earth station supplier centers on antenna type and size. In the majority of existing markets, choice of size and geometric shape is limited. Parabolic dishes abound, ranging in size from 33 feet for Intelsat A to 4 feet diameters in the Marisat system. (Fig. 4).

For foreign, domestic and CATV TVRO sockets, however, it's not as clear. Both Brazil and Indonesia, for example, plan to use a mix of 13-meter terminals and some number of small aperture stations, probably 4 to 5 meters in diameter. In countries contemplating a total system where none presently exists, it is even possible that the primary stations would be outfitted with 4-to-5 meter antennas. According to Jim Smith, sales manager at California Microwave, Sunnyvale, CA, "The 4.5-meter earth station could very well become the fundamental link in some foreign-domestic markets. Before that comes about, however, it would require an increase in satellite power." For the many domestic sockets, the choice goes beyond size. Recent filings at the FCC for TVRO station approval have included two small aperture parabolic dishes (Fig. 5), and a horn antenna approach.

According to some observers, the horn performs best when measured to the critical $32-25 \log \Theta$ requirement. Orest Hanas, a staff engineer at RCA's Astroelectronics Division, Hightstown, NJ, points out, "Mathematically, it can be proven that the 4.5-meter horn will meet the published $32-25 \log \Theta$ sidelobe requirements. For the 4.5-meter dish, however, it's not really clear."

The $32-25 \log \theta$ is the standard sidelobe interference criteria imposed by the FCC Rules and Regulations 25.209 Antenna Performance Standard which states, *"Any antenna to be employed in transmission at an earth station in communication-satellite service shall conform to the following standard:*

Outside the main beam, the gain of the antenna shall lie below the envelope defined by:

$32 - 25 \log_{10}(\Theta)$ dBi $1° \leq \Theta \leq 48°$

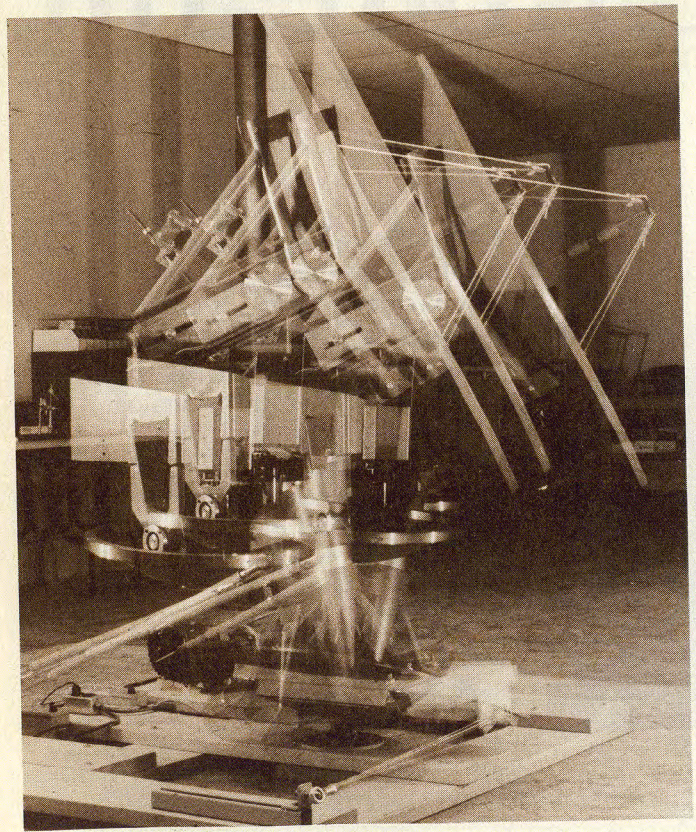

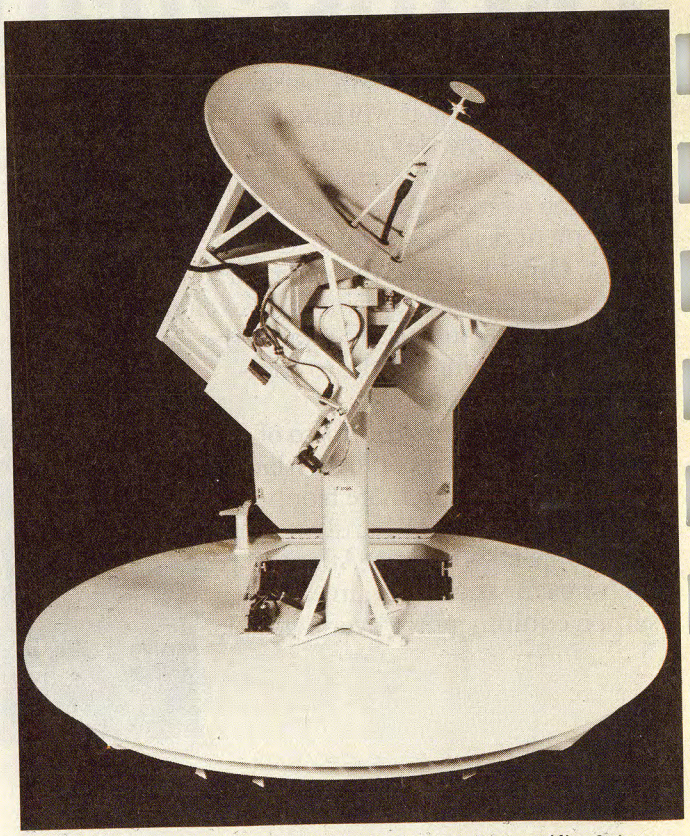

***4. Antenna systems dominate the engineering** and cost of the Marisat earth terminals. At BE Industries, an antenna system is simultaneously tested for pitch, roll and yaw (left). Complete system built by Scientific-Atlanta (right) includes aluminum antenna which is enclosed in a radome when installed aboard ship.*

Domsat and regional markets set to explode

Planned regional and domestic satellite communications markets around the world will create a $2-billion non-US earth station market by 1990, according to Frost and Sullivan forecasters. Most important among these are five regional systems in a planning stage and three foreign domestic systems already in operation. In addition to the foreign explosion, the US earth station market promises to grow at an excellerated pace due primarily to the TVRO infusion.

The first regional system to be operational will be Arabsat with a 1977 launch projection. The space segment of this 19-member Arab League program will consist of two 450-kilogram spacecraft, each capable of at least 2,000 voice circuits, three or four broadcast TV channels plus two high-power channels for community television.

Three terminal types for Arabsat

Investment in the ground segment will be made by the separate national administrations, and the distribution of ground facilities will vary according to the needs of the various member states. There is, however, a common element in that there will be at least one large earth station in each country for public telecommunications and television program exchange. These stations will operate in the 4 and 6-GHz band and use 10 to 12-meter diameter antennas to transmit and receive television and multi-channel and single channel per carrier (SCPC) telephony between the capital cities of each country.

Two kinds of earth stations are envisaged for the reception and distribution of national television programs. The first, using 8-meter diameter antennas will receive television signals from the satellite, via a low-power transponder and rebroadcast or distribute them through conventional local terrestrial networks. Many of these stations on thin telephony routes will also have SCPC terminal and telephony transmission equipment for use on pre-assigned circuits. The second type of station is much smaller and designed for community reception of television or radio signals directly from a high-power transponder in the satellite. These stations will receive signals in the 2.5-GHz band using 3-to-4 meter diameter antennas.

Frost and Sullivan estimate an initial need for 30, 8-meter and 100 CATV terminals to establish program and operation techniques. After this, the market for CATV terminals alone is predicted to reach 30,000 to 40,000 by 1990.

A European system, the European Communications Satellite (ECS) is also in the planning stage although political hassles prevent any thorough analysis of the earth station picture. What is known, however, is that ECS will be charged with providing an operational network to member nations with about 5,000 voice channels by 1980 and 15,000 to 20,000 by 1990. ECS will operate at 11 and 14 GHz using cross polarization.

Other regional markets include Serla, the Regional System of Telecommunications in Latin America. Plans here include the use of 2 to 3-meter earth stations for TV reception. Not likely to be implemented before 1985, Serla will eventually need about 100,000 community TVRO stations by 1990 according to Frost and Sullivan. In addition, the Association of South East Asian Nations (Asean) is projecting a need for 10,000 small terminals for TV programming by the mid-1980s.

Africa promises major market

The final identified regional system is in Africa. The present telecommunications network in Africa is, at best, sparse. Numerous satellite broadcasting systems for countries south of the Sahara have been proposed in recent years. While no specified plan has been adopted, experts are predicting that Africa may represent the largest earth station market of the 1990s.

Domsats are only beginning

Domestic systems with dedicated satellites already exist in Brazil, Indonesia and India, but all are considered in the infant phase. Demand from this sector is immediate, especially for less complex secondary systems. Among other nations planning to launch a dedicated satellite system are the Philippines and possibly Mexico.

The market picture in the US contains two important sectors. A substantial market exists for 10- to 11-meter stations for network TV broadcasts. The Public Broadcast System (PBS) plans at least a 155 earth station network to interconnect PBS stations. These stations, at least initially, will be 10 to 13-meters outfitted with GaAs FET LNAs. Satellite Business Systems (SBS) has projected a need by 1986 for 8,000 earth stations operating in the 11 and 14 GHz bands. SBS approval has for some time been before the FCC, and the final outcome is still in question. This sector of the US Domestic market, which includes 10 to 13-meter stations is expected to grow to about $50-million in just the next three years according to Arthur D. Little marketing estimates.

The other sector of the US market is the small aperture TVRO sector. With FCC agreement to licence stations based on performance rather then size, predictions for this market have been numerous. Manufacturers have told MicroWaves that the US market could reach 10,000 stations within 10 years. This prediction, if only partially correct, will herald a beginning for very inexpensive, non-redundant 4-to-5 meter terminals.

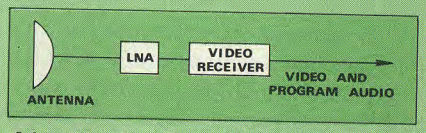

A1. Block diagram shows the simplest, least expensive video earth station. *Stations used in today's CATV market usually have some redundancy added.*

As Prodelin's Renner points out, "The 4.5-meter antenna isn't going to be all things to all people, but I can say most assuredly that it's going to cover 90 per cent of the US for RTVO applications. There are a few places in Maine, a spot in Florida and possibly a place in Texas where it won't fit but these are the exceptions."

The other fact affecting earth station engineers in the RTVO market is price. Most purchasers from this sector will be concerned almost exclusively with price. Redundancy and noise interference protection may simply cost too much for the typical buyer. The non-redundant system shown in Fig. A1 will probably cost about $25,000 today and predictions of stations with $1,000 price tags in the near future are not hard to find.••

- 10 dBi $48° < \Theta \leq 180°$

where Θ is the angle in degrees from the axis of the mainlobe, and dBi refer to dB relative to an isotropic radiator. For the purposes of this section, the peak gain of an individual sidelobe may be reduced by averaging peak level with the peaks of the nearest sidelobes on either side, or with the peaks of two nearest sidelobes on either side, provided that the level of no individual sidelobe exceeds the gain envelope given above by more than 6 dB."

Feeds and sidelobes

Perhaps the best indication of the wide range of differing design philosophies for small aperture systems is the question regarding antenna feeds. There are really only two contenders, prime focus and Cassegrain, with good arguments for each. Some system manufacturers, in fact, are offering either one. Scientific Atlanta's Mason believes it is in the customer's interest to offer both types. The Cassegrain, he remarks, has a higher efficiency, is slightly more costly but is more susceptible to terrestial interference because of reflections from the sub-reflector structure. The prime focus on the other hand, has no sub-reflector and with a direct feed waveguide reduces sidelobes.

It's actually a matter of choosing where to spend design time. The Cassegrain has inherently higher gain, so the design challenge is in sidelobe reduction. The prime focus designer must expend his energy on increasing the gain and surface accuracy of the antenna. In the end, the application will dictate the individual feed selection. In high fade regions with the current LNA state-of-the-art, a Cassegrain may be necessary to get that extra dB of gain. In a good footprint sector with a high EIRP, the question of gain may not be as important as sidelobes and hence, a prime focus might better fill the bill.

GaAs FETs challenge paramps

This question of EIRP also governs the paramp/GaAs FET choice for the earth station LNA. The parametric amplifier, long the mainstay of earth station LNAs, are currently being severely challenged by GaAs FET amplifiers. Manufacturers are producing GaAs FET LNAs for the 3.7-to-4.2 GHz region with noise figures as low as 1.55 dB and the battle-lines are only just forming. Paramp manufacturers are gearing up for a cost/performance war especially in the lucrative TVRO area. "For an TVRO application with a 4.5-meter antenna, you can get a good enough signal-to-noise ratio with a 150 to 180°K (1.8 to 2.1 dB) GaAs FET amplifier," according to Jack Golin, a staff engineer at IT&T Space Communications, Inc., Ramsey, NJ.

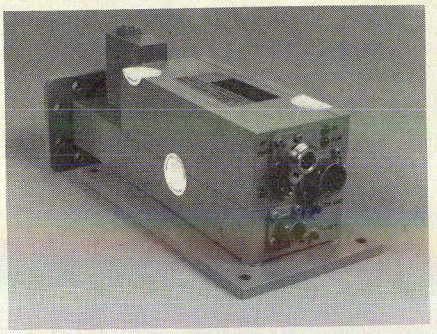

6. GaAs FET for the 3.7 to 4.2 GHz satcom band *includes fault indicators (upper right) for power supply and transistor failures.*

It must be pointed out that the GaAs FET amplifiers will only fill those sockets where high satellite powers are available, at least today. The cable TV market presents a good view of the cost performance options available to satellite subscribers. There are essentially four combinations being considered to receive signals via satellite. An operator could call for either a large aperture or small aperture system with either a parametric or a GaAs FET low-noise amplifier. The combination chosen depends a great deal on the received satellite signal strength and cost to the operator. The small stations, using a state-of-the-art GaAs FET amplifier, similar to the one in Fig. 6, are the least expensive, but it should be kept in mind that at best, the GaAs FET amplifier is operating "full out" to meet the performance. A better combination may be a larger antenna with a GaAs FET amplifier. This would produce some gain margin but it would be more costly. Another factor to consider is that small antennas offer an advantage to the less well financed CATV operator because of its mobility and ease of installation. Also as Conrad Fioretti, manager of systems engineering at IT&T Space Communications suggests, the 4.5-meter dish is more easily shielded against terrestrial interference.

It seems clear then that the cable operator would prefer a smaller station if he can get acceptable performance. But what then does he use for the LNA? The best noise performance for a commercial 3.7-to-4.2 GHz GaAs FET amp to date is the NEC LA-0412 which boasts a 1.55-dB noise figure (125°K) at 60-dB gain for $4,000. With these performance figures and a $4,000 price tag, the paramp may seem doomed. Not so, says Dick Domchick, business development manager of AIL's applied electronics division, Melville, NY. "The 4.5 meter earth station for a cable TV application would require something about 100°K (1.285 dB) for a comparative performance with a 10-meter station using a 2.6-dB noise figure GaAs FET." Domchick further explains that the 100°K noise figure would be necessary if a cable operator were to redistribute the received signal. This requirement is imposed because of losses incurred during the receive-to-transmit mode.

Most industry experts agree, at least, in principle with Domchick. Andrew's Carl van Hecke notes, "If a CATV operator wants to resell service from a 4.5-meter terminal, he has got to go with very expensive LNAs in order to start out with broadcast quality." Broadcast quality, according to IT&T's Fioretti, is a signal with a signal-to-noise ratio between 55 and 50 to 1. Starting with an 11-meter dish, on the other hand, the same quality could be realized with a GaAs FET amplifier. The decision to implement either approach would be one of cost. Don Busher, marketing manager at IT&T Space Communications, explains, "The redundant paramp with a 4.5-meter dish would be as expensive, if not more expensive than an 11-meter dish with two GaAs FET amplifiers."

It's important to point out that these requirements hold only for CATV operators reselling entertainment. For a receive-only station, it seems reasonable to expect small aperture terminals with GaAs FET amplifiers at least in higher EIRP areas.

FET amps must be rugged

Although NEC America is presently leading in what many are calling the GaAs FET noise figure race, competition is stiff. A number of manufacturers have delivered 3.7 to 4.2-GHz

amplifiers at noise figures in the 1.8 to 2.1 dB range. Most are using an FET input to establish noise figure, coupled to a bipolar for the required gain. All suppliers participating in the broadcast market are quick to point out the new problems posed by non-microwave users. "They just don't have experience with microwave devices," explains Marvin Wallace, marketing sales manager of Garland, TX's Scientific Communications. Keith Kennedy, manager of Watkins-Johnson's Solid State Division, Santa Clara, CA, reports, "Basically, you must make a very rugged unit. Our first return was run over by a truck. Then we got four in a row from a very angry customer. It turns out the units were deployed in a high thunderstorm area and our amplifier with its power cord to ground was the best path for lightning. What you must supply is a unit that can sit out in the rain and survive."

The next thrust for the GaAs FET amplifier will be the higher frequencies, but here the parametric amplifier will be a stiffer competitor. Dick Domchick addressing the question of the FET price advantage told Micro-Waves, "In quantities purchased, we plan to sell 3.7 to 4.2-GHz paramps at 125°K under $4,000." The significance of this is that if indeed the paramp is competitive at lower frequency, it will also enjoy a price/noise figure edge for the newer satcom bands, because higher frequency ultra low-noise GaAs FETs must be considered still in the development phase. Watkins-Johnson, for instance, has developed a 12 to 15-GHz GaAs FET amplifier with a 6.8 dB NF, but it was a single unit development contract.

For the more sophisticated applications like the new Intelsat systems, paramps have a wide lead in the market. A recently announced 40°K paramp from LNR Communications may set the tone for competition. Priced at $25,000, the non-cooled unit represents a major price decline for paramp technology, according to LNR's Len Lazarus.

The new Intelsat V frequencies, 11 and 14 GHz, offer still another choice to the earth station owner: The image recovery mixer. George Spacek, president of Spacekom, Inc., Santa Barbara, CA, points out, "We have delivered 5 to 5.5-dB noise figure image recovery mixer-preamplifiers to Intelsat V systems for as low as $1,800." The approach here is to downconvert a low-noise amplifier output to a K-band IF.

Satcom and social benefits

Perhaps the best view of things to come is the wide range of social experiments being carried out in the CTS program. The US portion of this program is concentrating on education, health care and community special services.

In health care, for instance, emphasis will be on two-way video transmission linking hospital to hospital, studio to hospital and hospital to medical teaching center. Five experiments, each taking advantage of the satellite's unique capabilities, are being carried out by the Veterans Administration through weekly broadcasts using CTS to interconnect 30 VA hospitals in the Western United States. The list includes individual discrete telecommunications and a weekly national medical journal for physicians, dentists and nurses.

The ground systems will include CTS downlink receivers at each of the 30 participating hospitals and a portable uplink transmitter. Mobile production capabilities will enable program origination from any of the hospitals over an 11-state area.

CTS decentralized education experiments are planned for the first half of this year. Tests are planned to investigate the practical use of satellites for medical science education in four state universities. An experimental library information network is already in existence in the CTS system. The satellite is linking a consortium of libraries with the University of Denver Graduate School of Librarianship, offering training programs and catalog information.

The most significant experiment, at least to earth station engineers, being carried out via CTS is a study of transportable earth stations. The experiment is intended to show that a transportable, small, earth terminal can quickly establish reliable communications between the site of a disaster and relief agencies. For this experiment, Comsat has fabricated a lightweight earth terminal that can be transported by a small van, a helicopter or even a small boat. The terminals can be set up by two persons and be operational in less than one hour.

The small terminal includes a rugged metalized fiberglass antenna 4 ft in diameter mounted on a lightweight tripod. The other end of the communications link consists of an earth terminal using a 15-ft diameter antenna mounted on a modified boat trailer.

The era of the personal terminal?

In the near future, the personal, portable earth terminal could indeed be as commonplace as the portable television. Reducing the size and complexity of earth stations to this point, however, will require a quantum step in available satellite power. The combined effect of the space shuttle and improved microwave power sources will go a long way toward this realization by 1990. Lee Farnam, general manager of General Electric Space Center, has predicted a "Five-thousand watt plateau of usable satellite power for a single bird by 1990." This is 50 times the limit of today's commercial systems and 25 times as powerful as the experimental CTS. "Future systems will have over 100 spot beams and reuse frequency several times. In the not too distant future, direct broadcast TV satellites, similar to Japan's experimental bird with large EIRPs will permit earth stations a few feet in diameter costing less than $500," Farnam continues.

The idea of a direct TV broadcast satellite is not new but its actual realization is another question. Sid Topol, president of Scientific Atlanta, states the case for the realist. "It seems silly to keep talking about this romantic idea of earth stations on every rooftop. The question is, who's going to put up the broadcast satellite? It will cost $100-million to design, develop and launch. How will it be paid for? Will the government put it up in the national interest? Intelsat and Marisat are there because they make money."

One thing is clear, however, when a public broadcast satellite is launched, earth station engineers will have the technology to respond to the demand it will create. ••

For satcom hot-switching. . .

Upgrade Coax Switches For High Power Transfer

Many satellite transmission schemes demand continuous transmissions while changing antennas. A simple coax switch can be easily modified to handle these hot switching requirements.

IS the coaxial switch suffering the fate of the vacuum tube? Definitely not! While PIN diode switches are rapidly becoming the standard switching element in numerous microwave applications, the blossoming satellite communications market is heralding a rebirth of the coax work horse. As satcom systems demand greater power levels and uninterrupted transmission, the coax switch is being called upon to fulfill the requirements.

In circumstances where the spacecraft has several antennas, it becomes necessary to actuate the switches while the power is being applied to provide non-interrupted transmission during rotational motion. This "hot-switching" must be carried out at power levels in the order of several hundred watts. PIN diodes become less attractive at these levels because shunt designs incorporating PINs exhibit insertion losses of about 0.7 dB for an SP2T circuit at 2 GHz compared to 0.1 dB for their coaxial counterparts. A series PIN scheme is likewise ruled out because of thermal dissipation limitations.

Although the standard coax switch isn't capable of performing hot-switching without modification, the inclusion of a simple dielectric medium between the poles is essentially all that's required to insure an arc-free transition. Tradeoffs of course, must be accepted. A computer-aided analysis has been performed detailing the modified switch's peak power performance and frequency/VSWR relationship.

Hot switching is a killer

"Hot-switching" has historically been confined to relatively low power levels (approximately 10 watts). Even at this low power, severe degradation of the contacts can be observed after several thousand actuations. Contacts fabricated from various combinations of noble metals like silver cadmium oxide improve, but do not eradicate the problem.

Coaxial switches are hermetically sealed with an internal pressure of 1 atmosphere[1] to eliminate multipacting or ionization phenomena. Figure 1 illustrates a simplified construction of an SP2T coaxial switch. When power is transmitted from J2 and J1, the reed is intimately contacted with the connector pins at its extremities. In this condition, the other reed rests against the side wall forming the ground plane and this combination produces a single ridge waveguide below cutoff. Consequently, high isolation is maintained between J2 and J3. Actuating the switch with the power applied creates an arc as the reed breaks away from the connector pin.

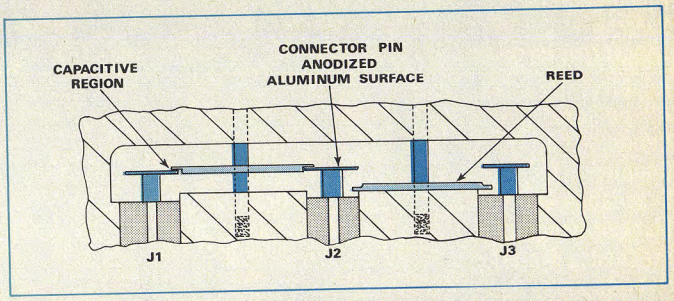

1. The reed in the non-contact position (J2 to J3) forms a single-ridge waveguide below cutoff. The capacitive region formed by the contacting reed (J1 to J2) becomes more dominant when dielectric is added to the pin.

Actually, ionization should not occur between the pin and reed because the frequency (1-18 GHz) and pressure (1 atmos) conditions dictate a below threshold state for the voltage breakdown phenomena.[2] Ionization does occur, however. The reasons for this are not at all mysterious. Considering the contact area on a microscopic level, it is known that there are very small area bridges between peaks of the two metal surfaces caused by imperfect surface finishes. Just before the contacts are absolutely separated, the current is concentrated in the minute surface area of a few interconnecting peaks. Rapid heating in these bridge regions locally elevates the peaks in the surface of the metals. Temperatures become high enough to create thermionic emission. The electrons have enough energy to produce air ionization resulting in sustained arcs. At current levels associated with a few hundred watts CW power at microwave frequencies, significant contact erosion and subsequent RF performance degradation takes places after just a few hundred cycles of hot switching.

Dielectric eliminates arcs, erosion

Complete arc-suppression is the only solution to the problem. As noted earlier, dielectric media are the most attractive means of achieving this goal. But dielectrics often create more problems than they solve.

During a program undertaken to design and construct an S-band switch matrix for spacecraft applications, several materials were tested for their ability to suppress arcs. This investigation considered numerous dielectric and connector

(continued from p. 50)

R. G. Winch, M. S. Ph. D., Microwave Subsystem Designer, Teledyne Microwave, 1290 Terra Bella Avenue, Mountain View, CA 94043.

pin material combinations measuring their effect on the overall switch performance as well as breakdown voltage.

The final design uses an aluminum connector pin with a thin-anodized layer. The use of this scheme is desirable because the dielectric breakdown voltage is directly proportional to the layer thickness. These hard anodized contacts are almost resistant to wear and offer long life times in hot switching environments. In fact, a life of 500,000 actuations is typical. A problem does arise, however, due to the capacitance created by the aluminum oxide. This capacitance increases inversely proportional to layer thickness. The capacitance introduced at each reed edge gives rise to a high pass characteristic and consequently, switch operation around 1 GHz is only possible for very high values of capacitance.

Unfortunately, realizing such capacitances is only possible with a very thin anodized layer, placing a limit on the peak power capabilities.

For instance, an S-band switch with a 250-watt CW rating in a 50-ohm system would require an oxide layer approximately 0.0003 inch (for a two-fold safety factor) to withstand the associated 141 volts (peak).

Predict other dielectric effects

A computer-aided analysis was performed to fully examine the tradeoffs between the maximum peak power capability, bandwidth and mismatch. The equivalent circuit of the discontinuities is simply two capacitors separated by a 50-ohm transmission line as shown in Fig. 2.

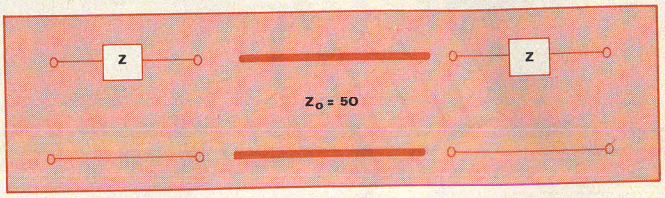

2. The equivalent of a coaxial SP2T is simply two capacitors separated by a 50-ohm transmission line.

The analysis, based on general circuit parameters (see "Parameter tradeoff program based on a matrix approach") results in a unique set of data helpful in determining proper material thickness.

As indicated in Fig. 1, the area of overlap between the reed and connector pin is limited. There are two reasons for this. Firstly, the conductors must be spaced far enough apart to allow mating connectors to be located. This defines the minimum distance between connector center pins. Isolation, of course, degrades as this distance decreases. The second limitation is the width of the flat on the end of the connector pin. Device VSWR is directly affected by this diameter. A maximum useful diameter is reached after which an increase creates a capacitative discontinuity that rapidly reduces the bandwidth.

Having placed a maximum value on the diameter for a given dielectric, the capacitance simply becomes a function of the thickness, which in turn, defines the maximum peak

(continued on p. 52)

Millimeter Sources from TRG

12.4 to 300 GHz

- fundamental oscillators to 65 GHz
- high power sources up to ½ watt
- varactor tuned GUNN oscillators
- high efficiency multipliers to 300 GHz

Need flatness? TRG GUNN oscillators are varactor tuned and offer ±0.25 dB (max power variation over ±100 MHz). For more bandwidth our ±200 MHz unit has a flatness level of ±0.4 dB.

Want high power? Our high power oscillators can deliver up to ½ watt over ±100 MHz mechanical tuning range with ±0.25 dB flatness.

Up there in frequency and bandwidth? The TRG series 9400 55 GHz GUNN oscillator has 4 GHz mechanical tuning with 50 mW power output and ±2dB flatness. For operating above 65 GHz, the TRG series 936 doublers and triplers develop 35% efficiency at up to 300 GHz. Call or write the Millimeter Team at TRG for more information.

TRG ai Alpha DIVISION **Our limits are your imagination.**

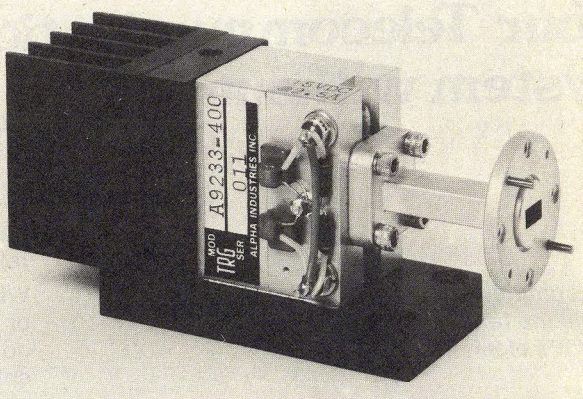

35 GHz, 400 mW GUNN Oscillator

ALPHA INDUSTRIES, INC. • 20 Sylvan Road, Woburn, Massachusetts 01801 • (617) 935-5150 • TWX: 710-393-1236 • TELEX 949436

READER SERVICE NUMBER 37

Parameter tradeoff program based on a matrix approach

Using the general circuit parameter, A, B, C, D, a simple matrix analysis can be performed to determine the input impedance of the SP2T network shown in Fig. 2 as follows:

$$E_i = A E_o + B I_o \qquad (1)$$
$$I_i = C E_o + D I_o$$

Where E_i and I_i are the input voltage and current, respectively, and E_o and I_o are the output voltage and current, respectively. Rewriting Eq. (1) in matrix form:

$$\begin{bmatrix} E_i \\ I_i \end{bmatrix} = \begin{bmatrix} A & B \\ C & D \end{bmatrix} \begin{bmatrix} E_o \\ I_o \end{bmatrix} \qquad (2)$$

Consider the two series impedances cascaded with an intervening transmission line as in Fig. 2.

$$\begin{bmatrix} E_i \\ I_i \end{bmatrix} = \begin{bmatrix} 1 & z \\ 0 & 1 \end{bmatrix} \begin{bmatrix} \cosh \theta_o & Z_o \sinh \theta_o \\ \frac{\sinh \theta_o}{Z_o} & \cosh \theta_o \end{bmatrix}$$

$$\begin{bmatrix} 1 & Z \\ 0 & 1 \end{bmatrix} \begin{bmatrix} E_o \\ I_o \end{bmatrix} \qquad (3)$$

Where $\theta_o = \gamma L$

$$\gamma = \alpha + j \frac{2\pi f_o}{V_g}$$

and
- α is the attenuation constant
- f_o is the frequency
- V_g is the guide wavelength
- L is the transmission line length
- Z is the discontinuity impedance.

From which

$$\begin{bmatrix} E_i \\ I_i \end{bmatrix} \begin{bmatrix} \cosh \theta_o + \frac{Z}{Z_o} & \sinh \theta_o \; Z_o \sinh \theta_o \\ \frac{\sinh \theta_o}{Z_o} & \end{bmatrix}$$

$$+ 2Z \cosh \theta_o + \frac{Z^2}{Z_o} \sinh \theta_o \Bigg] \begin{bmatrix} E_o \\ I_o \end{bmatrix} \qquad (4)$$

$$\cosh \theta_o + \frac{Z}{Z_o} \sinh \theta_o$$

The input impedance of the network with a matched load is:

$$Z_i = \frac{E_i}{I_i} = \frac{AZ_o + B}{CZ_o + D} \qquad (5)$$

Therefore

$$Z_i = \frac{(Z_o + 2Z) \cosh \theta_o + (Z_o + Z + \frac{Z^2}{Z_o}) \sinh \theta_o}{(1 + \frac{Z}{Z_o}) \sinh \theta_o + \cosh \theta_o} \qquad (6)$$

From the input impedance, the VSWR can be obtained for various values of f_o and Z. The discontinuity impedance, Z, is equal to $\frac{1}{2\pi f_o C}$ where C is the capacitance due to the aluminum oxide.

This capacitance is simply $C = \frac{0.225 \; \epsilon_r \; A \text{ pf.}}{t}$

where
- ϵ_r is the relative permittivity
- t is the thickness of the dielectric layer
- A is the area of overlap between the reed and connector pin

The results then are in terms of those factors controlling bandwidth and VSWR for the coaxial switch.••

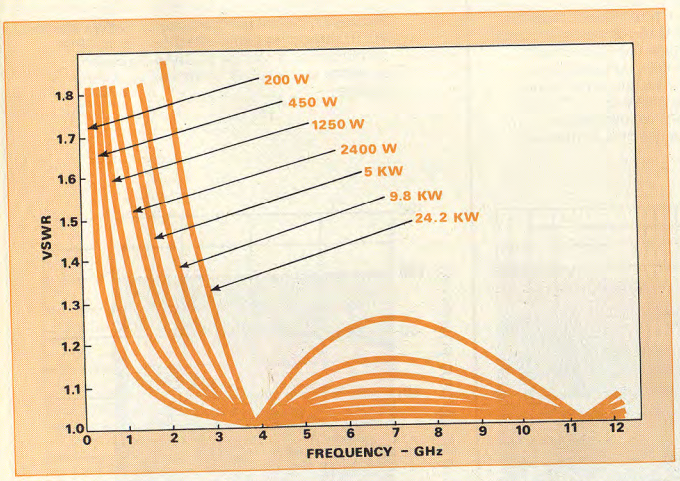

3. Increasing dielectric thickness increases the maximum power capability but results in a frequency shift. Use this chart to predict frequency when a peak power capability is known.

power handling capability. The voltage breakdown of aluminum oxide formed by anodizing aluminum is 100 volts per 0.0001 inch.[3]

The results of the computations shown in Fig. 3 illustrate the high pass nature of the switch with the discontinuities varying in magnitude. At low capacitance values (high P max), the VSWR becomes prohibitively large and therefore, presents a cutoff situation at relatively high frequencies. At 750 MHz, for example, a 1.2 VSWR results in a maximum power capability of 200 watts. The same parameters in a modified form are shown in Fig. 4 to allow peak power assessment given frequency and VSWR.

For the case where high peak power is needed at low frequency and low VSWR, it becomes necessary to vary the dimensions of the transmission line between the two capacitances to alter the characteristic impedance (Z_o). This will produce a ripple response with a steeper cutoff skirt that is advantageous for narrow bandwidths at lower frequencies. Figure 5 illustrates the VSWR and frequency relationship for a switch having varying values of Z_o between the two capacitances.

Consider departures from ideal

It must be pointed out that these curves are all computed for a switch operating into a perfect load. Maximum power capability must be derated for loads departing from the perfect 1.0 VSWR. The VSWR values presented only include capacitive discontinuities. Other mismatches in the switches contribute to increasing or decreasing these values depending upon their phase. Worst case compounding should also be taken into account during actual design considerations because switch data sheets normally show a typical reading.

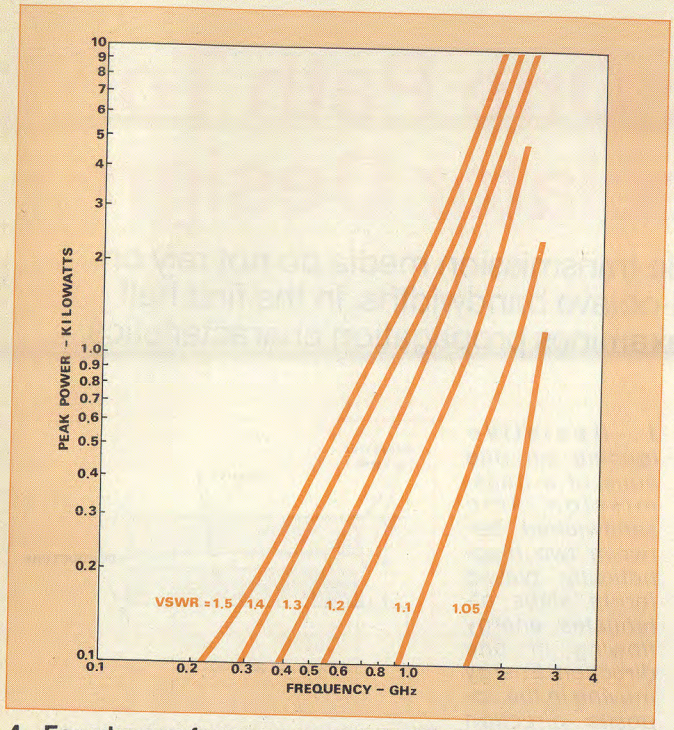

4. For a known frequency and VSWR, this graph predicts the maximum power capability.

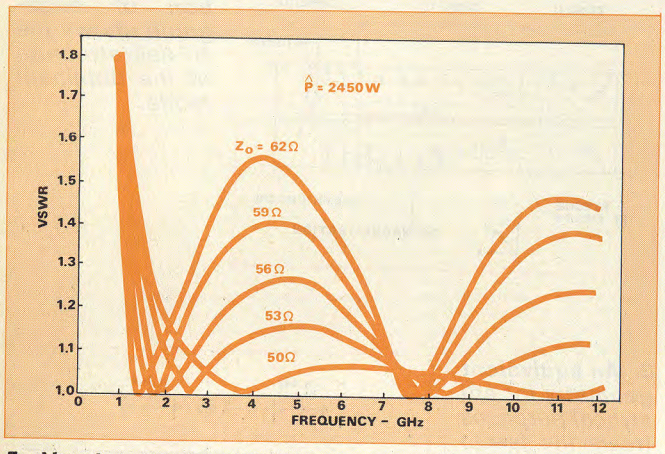

5. Varying the line impedance modifies the peak power capability at a fixed frequency. Data detailed here relates VSWR to frequency as the characteristics impedance is adjusted.

Tight tolerances are necessary for the high precision contact parts and extreme care must be exercised in assembling the switches to insure parallel reed and connector pin placement. The contact regions of the machined ports should be well polished and finally, precisely controlling the thickness of the hard anodized layer on the connector pin is essential.••

References

1. R. G. Winch, "High Power Coaxial RF Switches For Space Applications," *Microwave Journal*, pp. 56-58, (November, 1975).
2. R. Woo, "Final Report On RF Voltage Breakdown In Coaxial Transmission Lines," JPL Tech Rep 32-1500 (NASA), (October, 1970).
3. R. M. Burns and W. W. Bradley, "Protective Coating For Metals," Third Edition, Reinhold Publishing Corporation, P609.



- **1800 FDM Channels CCIR and/or Video Modulation**
- **Direct Baseband to RF** — eliminates 70 MHz FMT and upconverters in remodulating radios
- **Insert Baseband Modulation** — 300 Hz to 12 MHz at Heterodyne Repeaters
- **Crystal Stability** — to ±0.0005%
- **Output Power** — 25 mW to 1.0 W

An ideal update for older klystron equipped radios.

For complete technical information or applications assistance, call the Communications Specialists at: (408) 249-2850, TWX 910 338-0163, or write 3140 Alfred Street, Santa Clara, CA 95050.

FREQUENCY-WEST, INC.
Better Products for Communications

READER SERVICE NUMBER 39

Part I

Edge Guide: One Path To Wideband Isolator Design

Ferrite isolators using edge-guide transmission media do not rely on resonance, thus work over multi-octave bandwidths. In the first half of a two-part series, the author examines propagation characteristics.

IN the 18 years since Chair and Curry first announced a ferrite circulator/isolator[1], designers have feverishly tried to improve—or at least understand—the performance of the device over wide bandwidths. Yet today, even the best ferrite isolators and circulators based on the resonant junction principle offer acceptable performance over little more than one octave.

There is a relatively new transmission media on the horizon, however, that has the potential of broadening the performance of a ferrite isolator or circulator to more than two octaves. Edge-guide media, introduced several years ago by Hines[2], overcomes the limitations of junction devices by separating forward and reverse waves on opposite edges of a relatively wide, flat transmission line sandwiched between two magnetically based ferrite slabs. By applying a resistive film or bulk loading along one edge of the transmission line, it's possible to design a highly directional component (see Fig. 1). Significantly, the degree of isolation depends only on the amount of attenuation the lossy edge loading can provide, *independent of match quality*. In addition, theory predicts that there is no lower or upper limit on the frequency band of the mode of propagation. Combine these two characteristics, and it's apparent that multi-octave components providing high isolation are possible.

In contrast, the standard isolator or circulator is essentially limited to a 74 per cent bandwidth due to the frequency sensitivity of the ferrite junction and necessary equalizing networks, low-field losses and moding at high frequencies. It's important to note that the frequency constraints center on the heart of a traditional ferrite component: the resonant junction. The ferrite junction is cavity resonant, thus equalizing networks can only be the proper electrical length at one frequency. In addition, the physical dimensions of the ferrite junction are large enough to excite higher order modes and thus disturb the operation of the device.

A look at propagation constants in edge-guide

This article, the first of a two-part series, will examine the propagation characteristics of edge-guide transmission line, to illustrate how the frequency limitations of junction devices are overcome. Experimental data on edge-guide components reveal that more than 32-dB isolation can be provided over a 4-to-8 GHz bandwidth with a single, compact device. Although stripline and microstrip versions of edge-guide have been proposed, this analysis will deal strictly with the stripline case.

Michael Dydyk, Principal Staff Engineer, Motorola, Inc., Government Electronics Div., 8201 E. McDowell Road, Scottsdale, AZ 85252.

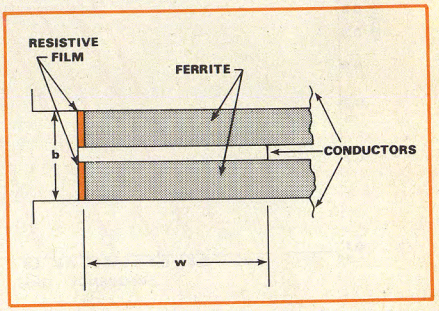

***1. Resistive loading** on one edge of a transmission line sandwiched between two magnetically biased ferrite slabs attenuates energy flowing in one direction. Energy moving in the opposite direction propagates freely along the non-loaded edge.*

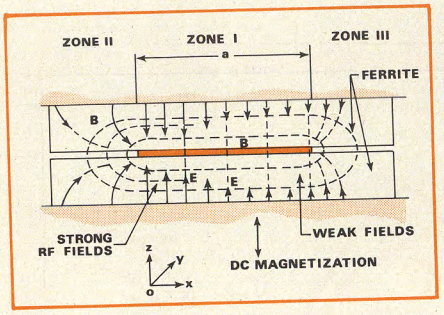

***2. A cross-section of edge-guide** shows the RF field structure of the dominant mode.*

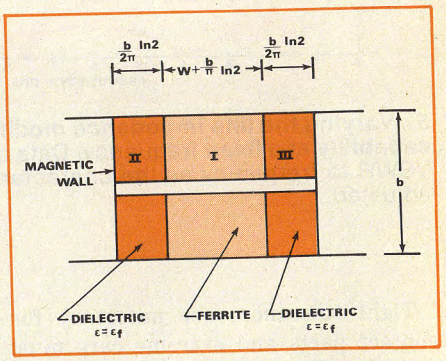

***3. An equivalent geometry** for analytical purposes treats the ferrite as fully magnetized (zone I) and as a non-magnetized (zones II and III) dielectric.*

To successfully design an edge-guide isolator and predict its performance characteristics, it is necessary to first determine propagation properties such as characteristic impedance, attenuation constant and higher-order mode propagation of the edge-guide transmission media. A knowledge of the characteristic impedance dictates the transducer design. The attenuation constant partially establishes the insertion loss and isolation of the component. The high-order mode propagation property sets the upper frequency of operation of the edge-guide isolator.

(continued on p. 56)

List of symbols

k and μ	elements of the Polder tensor
γ_x and γ_y	propagation constants in the x and y direction respectively
μ_{eg}	equivalent permeability of the ferrite
μ_o	permeability of free space
α_x	decay rate in the x-direction
β_y	phase constant in the y-direction
ϵ_o	permittivity of free space
ϵ_f	relative dielectric constant of ferrite
W	the width of the inner conductor of the edge-guide transmission line
β_x	phase constant in the x-direction
n	higher-order mode order
ω	frequency in radians
ω_m	$2\pi f_m$
f_m	$\gamma \times 4\pi M_s$
γ	2.8 MHz/Oe
$4\pi M_s$	saturation magnetization of ferrites
H_i	internal magnetic field in Oe.
P_y	magnitude of the Poynting vector in the direction of propagation
s	cross-sectional surface enclosed by the electric/magnetic walls
I_y	average value of the longitudinal current
b	ground plane spacing
Z_o	characteristic impedance of the edge-guide transmission line
η	free space impedance
c	speed of light
K(k)	complete elliptic integral of the first kind of modulus k,
d	$\frac{b}{2\pi} \ln 2$
a	$W + \frac{b}{\pi} \ln 2$
Z	characteristic impedance of unknown transmission line
$\tan\delta_\epsilon$	electric loss tangent of ferrite
$\tan\delta_m$	magnetic loss tangent of ferrite
ΔH	linewidth of ferrite
R_s	resistivity of ground planes
E	width of the inner conductor with lossy material
μ_{eg} and ϵ_{eg}	are the equivalent permeability and permittivity of the lossy bulk material
f_{min}	minimum frequency of interest
Y	the width of the inner conductor in the coupled area

Figure 2 illustrates the field patterns near one edge of a wide inner conductor sandwiched between two magnetically biased ferrites and shows the stripline geometry to be considered. Note that the RF magnetic fields do not end abruptly, but curve around the edges of the inner conductors and basically form closed loops. There, the H fields are vertical (in the z direction), and parallel to the DC magnetization, in which case, the ferrite behaves as a simple non-magnetic dielectric. Perhaps the best analytical approach is that introduced by Oliner[3], where the effect of the fringing field is taken into account by means of an equivalent width. This width, D, is related to the actual inner conductor width, W, by:

$$D = b \frac{K(k)}{K(k')} \tag{1}$$

where

$$k = \tanh\left(\frac{\pi W}{2b}\right) \; ; \; k'^2 = 1 - k^2 \tag{2}$$

In Eq. (1), D is the "equivalent strip width", i. e., the width of a strip with an associated uniform field (without fringing) but with the same capacitance as the actual strip. When

$$\frac{W}{b} > \frac{1}{2} \; , \tag{3}$$

Equation (1) can be approximated by:

$$D = W + \frac{2b}{\pi} \ln 2 \tag{4}$$

In the case of edge-guide transmission media, the excess width is split into two: one half behaves as a fully magnetized ferrite and the other, as a non-magnetic dielectric of the same dielectric constant. The modified geometry is shown in Fig. 3.

Using Maxwell's equations, appropriate fields can be derived for all three regions of the geometry described by Fig. 3. For example, applying boundary conditions to the intersection of zones I and III yields:

$$Y_o \omega\mu_o = \frac{\left[\gamma_y^2 + \left(\frac{\omega}{c}\right)^2 \epsilon_f\right] \tanh(\gamma_x W) - \left[j\gamma_x - \frac{K}{\mu}\gamma_y\right] Y_o \omega\mu_o}{j\gamma_x + \left[Y_o \omega\mu_o \; \mu_{eq} - \frac{K}{\mu}\gamma_y\right] \tanh(\gamma_x W)} \tag{5}$$

where

$$Y_o = -j \frac{\gamma_{xx}}{\omega\mu_o} \tanh(\gamma_{xx} d) \tag{6}$$

and the separation parameters are given by

$$\gamma_x^2 = -\gamma_y^2 - \left(\frac{\omega}{C}\right)^2 \epsilon_f \mu_{eq} \tag{7}$$

$$\gamma_{xx}^2 = -\gamma_y^2 - \left(\frac{\omega}{C}\right)^2 \epsilon_f \tag{8}$$

Equation (5) is a transcendental equation for determining γ_y, the propagation constant. Once the propagation constant is known, it is possible to find the characteristic impedance of the edge-guide transmission media and account for the effects of the fringing fields.

The characteristic impedance of this or any transmission media can be determined using the power—current relation:

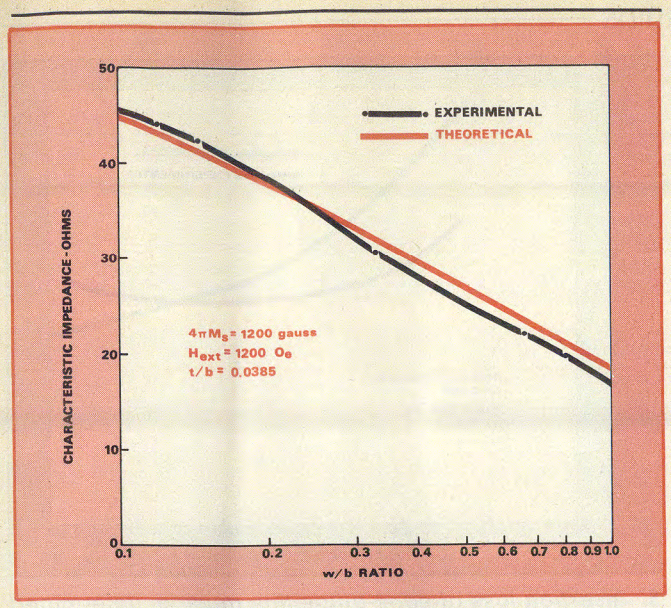

***4. Calculated characteristic impedance** agrees closely with experimental data.*

$$Z_o = \int_S \frac{P_y \, d_x \, dz}{|I_y|^2} \tag{9}$$

where

$$P_y = (\bar{E} \times \bar{H}^*) \cdot \bar{a}_y \tag{10}$$

$$I_y = \oint_c H_x \, dx \tag{11}$$

Performing the operations suggested in Eqs. (10) and (11) yields:

$$Z_o = \frac{\frac{\eta}{8} b \left(1 - \frac{t}{b}\right) \left\{ \sqrt{\epsilon_f} \, d \left[1 + \tanh^2\left(\frac{\alpha_x a}{2}\right)\right] + \frac{c}{\omega_m} \tanh\left(\frac{\alpha_x a}{2}\right) \right\}}{\left[\sqrt{\epsilon_f} \, d + \frac{C}{\omega_m} \tanh\left(\frac{\alpha_x a}{2}\right)\right]} \tag{12}$$

Figure 4 compares a plot of Eq. (12) with experimental results. Good agreement exists between theory and experiment.

Consider both dielectric and conductor losses

Practical transmission lines always have some loss caused by the finite conductivity of the conductors, in addition to the loss that is present in the dielectric material surrounding the conductors. For an edge-guide isolator, the dielectric material is ferrite, which suffers from both electric and magnetic dielectric losses.

Consider first the attenuation constant due to the dielectric losses. The method of solution considers the conductors to be perfect and the permittivity and permeability of the ferrite are modified accordingly.

$$\epsilon_{eg} = \epsilon_f \, (1 - j\tan\delta_\epsilon) \tag{13}$$

$$\mu_{eff} = \mu \, (1 - j\tan\delta_m) \tag{14}$$

(continued on p. 58)

From all angles, Anritsu's Power Meter ML81A meets your critical millimeter wave measurement requirements.

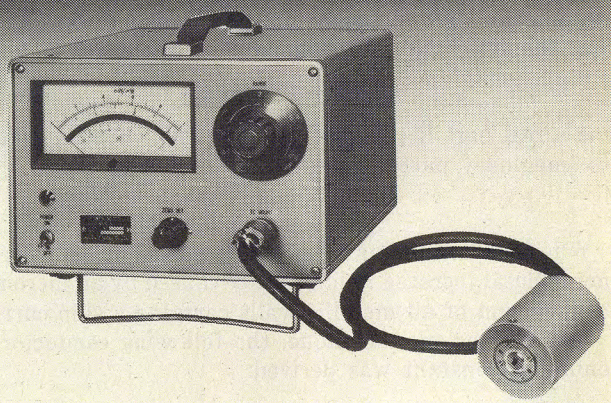

Advantage

❶ Typical VSWR less than 1.3 : 1

❷ Robust thin-film thermoelectric couple adopted to withstand up to 100mW C.W

❸ Low drift of less than 3% of full scale even in the most sensitive range

❹ 40-140 GHz wideband coverage with 5 fully interchangeable TC mounts, each TC mount covers the entire frequency band of a waveguide suited to it.

Take advantage of the ML81A now!

Anritsu
ANRITSU ELECTRIC CO., LTD.
MEASURING INSTRUMENTS DIVISION
SALES DEPARTMENT:
12-20, Minamiazabu 4-chome, Minato-ku, Tokyo 106, JAPAN
Phone: (03) 446-1111/Telex: 0-242-2353
Cable: ANRITDENKI TOKYO

U.S.A. Tau-Tron Inc. Tel: (617) 667-3874 • **West Germany** Knott Elektronik GmbH Tel: (0 8178) 4085 • **England** Dymar Electronics Limited Tel: Watford 37321 • **France** Tekelec Airtronic Tel: (1) 946-96-48 • **Italy** Vianello S.p.A. Tel: 544041 • **Holland** Uni-Office B.V. Tel: (010) 22 94 44 • **Sweden** Teleinstrument AB Tel: 08-38 03 70 • **Singapore** O'Connor's (Pte.) Ltd. Tel: 637944 • **Australia** NEC Australia Pty. Ltd. Tel: Melbourne 560-5233

READER SERVICE NUMBER 41

where the imaginary components reflect the loss mechanism.

This method of solution is based on the assumption that the introduction of a small loss does not substantially perturb the field from its loss-free value. The known field distribution for the loss-free case is then used to evaluate the loss in the system, and from this the contribution to the attenuation constant is calculated.

The complete analysis will be published elsewhere. The final results are:

$$\alpha_\epsilon = (4.34)\left(\frac{\omega}{c}\right)\sqrt{\epsilon_f}\tan\delta_\epsilon \quad \text{dB/in} \qquad (15)$$

$$\alpha_m = (4.34\,\pi)\left(\frac{f_m}{c^* f}\right)(\gamma)(\Delta H)\sqrt{\epsilon_f} \quad \text{dB/in} \qquad (16)$$

To obtain total attenuation constant for the edge-guide transmission line, the loss due to non-perfect conductors has to be determined. The technique used is based on Wheeler's "incremental inductance rule." This rule—really a formula—expresses the series skin resistance (R) per unit length which is attributable to the skin effect, that is, to the inductance produced by magnetic field within the metallic conductors. The formula is based on the known fact that the series skin impedance per unit length

$$Z = R + jx \qquad (17)$$

has a real part R (the desired quantity) which is equal to its imaginary part x, where

$$x = \omega L_i. \qquad (18)$$

Wheeler shows that L_i can be inferred from L as the incremental increase in inductance caused by an incremental recession of all metallic walls carrying a skin current.

Using Wheeler's technique, the following conductor attenuation constant was derived:

$$\alpha_c = \frac{8.68 * R_s * \sqrt{\epsilon_f}}{\eta}\left[\frac{1}{b} + \frac{(\omega_m/c)\sqrt{\epsilon_f}}{\sinh\left(\frac{\omega_m}{c} * a * \epsilon_f\right)}\left(1 - \frac{\ln 2}{\pi}\right)\right] \qquad (19)$$

The total attenuation constant is then given by the sum of Eqs. (13), (16) and (19). Typical theoretical and experimental results are shown in Fig. 5. From the experimental results, it can be seen that the line exhibits decreasing insertion loss as frequency increases. Lack of agreement between theory and experiment is due primarily to frequency dependent linewidth of ferrite material.[5] Probably, better correlation would have been obtained by characterizing the magnetic loss with an effective line width (Δ Heff) as was done by Patton.[6] However, the information on the material used was not available.

Pinpoint the threshold of higher-order modes

The final property of the edge-guide transmission media is higher-order mode propagation. The cutoff frequencies of these higher-order modes can be determined by the following substitutions into Eq. (7);

$$\gamma_x = j\beta_x \qquad (20)$$

$$\gamma_{xx} = j\beta_{xx} \qquad (21)$$

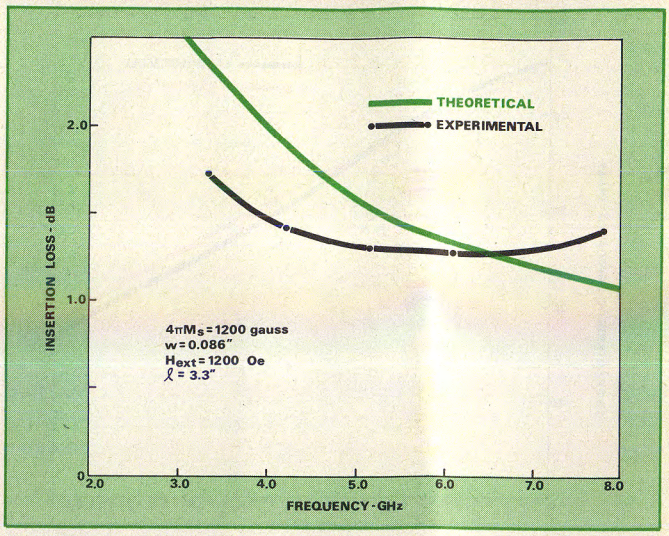

5. Insertion loss *of edge-guide line must be determined by considering conductor and dielectric losses.*

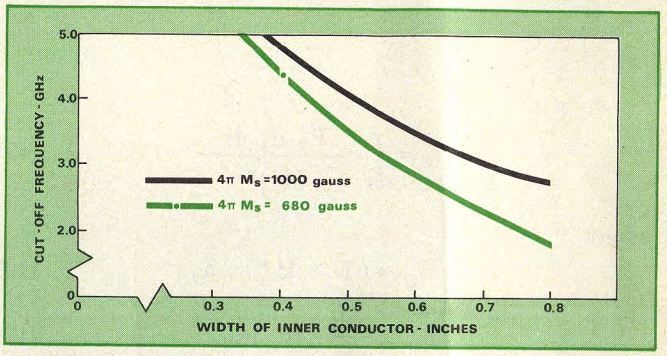

6. Cutoff frequency *of the first higher-order mode varies inversely with conductor width.*

$$\gamma_y = 0 \qquad (22)$$

Introducing these factors, the characteristic equation becomes:

$$\beta_x + 1 = -\beta_{xx}\tan\beta_x a\,\left[\mu_{eg} + \cot\beta_{xx} d\right] \qquad (23)$$

The above equation is also transcendental and must be solved by numerical techniques. Cutoff frequency plot of the first higher order mode as a function of W is shown in Fig. 6.

Next month, in Part II of this article, the theoretical propagation constants of edge-guide will be used to describe the design of two types of isolators. Each is capable of nominally providing 20-dB isolation over a 2-to-8 GHz bandwidth. A simple method of mode suppression will be introduced that results in an edge-guide component that provides greater than 32 dB isolation from 4 to 8 GHz. ••

References

1. H. N. Chair and T. R. Curry, "Y-Circulator," *Journal of Applied Physics*, Vol. 30, pp. 152-153S, (April, 1959).
2. M. E. Hines, "Reciprocal and Nonreciprocal Modes of Propagation in Ferrite Stripline and Microstrip Devices," *IEEE Transactions on Microwave Theory Tech.*, Vol. MTT-19, pp. 442-451, (May, 1971).
3. A. A. Oliner, "Equivalent Circuits for Discontinuities in Balanced Strip Transmission Line," *IEEE Transactions on Microwave Theory Tech.*, Vol. MTT-3, p. 135, (March, 1955).
4. H. A. Wheeler, "Formulas for the Skin Effect," *Proc. IRE*, Vol. 30, pp. 412-424, (September, 1942).
5. C. R. Buffler, "Effects on Surface Irregularities on Single Crystal Resonance Parameters," *Journal Applied Physics*, Vol. 31, p. 222S, (1960).
6. C. E. Patton, "Effective Linewidth Due to Porosity and Anisotropy in Poly-crystalline Yttrium Iron Garnet and Ca-V-Substituted Yttrium Iron Garnet at 10 GHz," *Physics Review*, Vol. 179, p. 352, (1969).

FEBRUARY
1977

MICROWAVES

NOW
CARD INSIDE COVER



SEMICONDUCTORS

ow The New Schottkys Detect Without DC Bias
InP Gunn-Effect Devices Begin To Surface In U.S.
pplications Emphasized At This Month's ISSCC

POWER GAAS FETS STAR IN NEW ROLE

MICROWAVES

February 1977
Vol. 16, No. 2

news

9 Semiconductor and circuit designers team up to score new performance highs
12 InP Gunn-effect devices begin to surface in the US
12 GaAs FETs step up to K-band
16 Industry
19 Washington
22 International
26 For Your Personal Interest...
29 R & D
32 Meetings

editorial

30 Gigabit logic: The next wave of excitement in semiconductors

technical

Semiconductors

36 **Power! GaAs FETs star in a new role.** System designers are just beginning to enjoy the impact that the GaAs FET has made on the low-noise amplifier scene, but component manufacturers are already bracing for this second wave of GaAs FET technology.

44 **How The New Schottkys Detect Without DC Bias.** Jack Lepoff of Hewlett-Packard Company, explains why the newest generation of Schottky-barrier diodes do not require bias to detect low-level signals.

50 **Edge-Guide: One Path To Wideband Isolator Design (Part II).** Michael Dydyk of Motorola, Inc., concludes his two-part series by relating theory to practice in the design of isolators with thick-film and bulk resistive loading.

58 **Is Video Leakage Your System Problem?** Lee Duter of Crown Microwave, suggests a lumped-element, high-pass filter design for reducing the video leakage of PIN diode switches.

departments

60 Bookshelf
60 Feedback
62 New Products
72 New Literature
74 Application Notes
75 Advertisers' Index
76 Product Index

About the cover: King Kong, an old performer in a new role, monkeys around with the latest addition to the growing cast of microwave power devices: the GaAs FET. To learn more about how this low-noise performer is making waves on the power scene, turn to page 36. Device photo courtesy of RCA Microwave Technology Center; King Kong photo copyright© 1976 by Dino De Laurentiis Corp., used by permission. Composition by Art Director Robert Meehan.

coming next month: Front Ends

The Sideband Channelizer: A Mixer Design for Future Wideband Front-Ends When the latest thin-film techniques are applied to image-terminated mixer design, the result is a component with improved image rejection, lower noise and wideband operation. A design example described in this article provides image rejection of greater than 20 dB over an 8 to 16 GHz bandwidth.

Is There a Josephson Junction in Your Future? This review of device physics and experimental results reveals potential applications in detector, mixer, parametric amplifier and switching circuits.

Publisher
Howard Bierman

Editor-in-Chief
Stacy V. Bearse

Contributing Editor
George R. Davis

Washington Editor
Paul Harris
Snyder Associates
1050 Potomac St. NW
Washington, DC 20007
(202) 965-3700

Editorial Assistant
Gail Murphy

Production Editor
Sherry Lynne Karpen

Art Director
Robert Meehan

Production
Dollie S. Viebig, Mgr.
Anne Molfetas

Circulation
Barbara Freundlich, Dir.
Trish Edelmann
Sherry Karpen,
Reader Service

Directory Coordinator
Janice Tapp

Editorial Office
50 Essex St.,
Rochelle Park, NJ 07662
Phone (201) 843-0550
TWX 710-990-5071

A Hayden Publication
James S. Mulholland, Jr.,
President

MICROWAVES is sent free to individuals actively engaged in microwave work. Prices for non-qualified subscribers:

	1 Yr.	2 Yr.	3 Yr.	Single Copy
U.S.	$25	$40	$ 60	$3.00
Foreign	$40	$70	$100	$4.00

Additional Product Data Directory reference issue, $15.00 each (U.S), $27.00, (Foreign), POSTMASTER, please send Form 3579 to Fulfillment Manager, MicroWaves, P.O. Box 13801, Philadelphia, PA. 19101.

Back Issues of MicroWaves are available on microfilm, microfiche, 16mm or 35mm roll film. They can be ordered from Xerox University Microfilms, 300 North Zeeb Road, Ann Arbor, MI 48106. For immediate information, call (313) 761-4700.

Hayden Publishing Co., Inc., James S. Mulholland, President, printed at Brown Printing Co., Inc., Waseca, MN.

Copyright © 1977 Hayden Publishing Co., Inc., all rights reserved.

POWER!

GaAs FETs Star In A New Role

Stacy V. Bearse, Editor-in-Chief

If, like the film world, the microwave industry gave Academy Awards for outstanding performances, there's little question that the gallium arsenide field-effect transistor would sweep all small-signal categories for 1976. But like other versatile performers, the FET has changed costume for 1977 to star in a new role—the power amplifier.

Power GaAs FETs have only been on the scene for a brief period, yet they are already receiving rave reviews. Low distortion, ultra-wideband operation, the highest efficiency yet demonstrated for any microwave semiconductor, predictable gain characteristics and respectable power levels are the major attributes of these newcomers.

Perhaps the most important role earmarked for the power FET is as a replacement for medium power TWT amplifiers. Programs are underway to wring 4 W at 10 GHz from a single device, and the next several years will see government contracts aimed at getting several watts at frequencies as high as 21 GHz.

There's also a good chance that the power FET will displace some semiconductors now in use. High-frequency bipolar transistors, high-power Gunn devices and low-power Impatts are all fair game.

Circuit designers accustomed to working with small-signal GaAs FETs will discover a number of differences in the requirements of the new power FETs. In addition to the obvious differences in thermal circuit design (see Fig. 1), the new devices require higher drain voltage (V_{DS}) and saturation current (I_{dss}). For comparison, a typical low-noise FET, the NEC 244, is rated at V_{DS}= 5 V and I_{dss} = 100 mA. A 500 mW power FET, the NEC V464, is specified at V_{DS}= 10 V and I_{dss} = 500 mA.

"A high breakdown voltage design is generally contrary to the high-frequency, high-gain design," observes Yoshiyuki Mizuta of Nippon Electric Company, Kawasaki, Japan, "but in the present design situation, the breakdown voltage is governed by such factors as current or electric field concentration. Therefore, a high-voltage design can be achieved through improved structural design."[1]

Larger drain and source lengths and smaller active-layer impurity density are two major structural differences that set the higher-voltage power devices apart from their low-noise counterparts. Although these conditions tend to degrade gain, power FETs exhibit fairly healthy gain levels with a predictable, intrinsic rolloff of about 6 dB per octave. Thus, to design a wideband circuit, either reflective or absorptive gain tapering must be added to the input or output matching networks.

"People just don't realize how much gain they can get with a power FET chain," claims Yozo Satoda, president of Dexcel, Santa Clara, CA. Satoda's firm plans soon to introduce a 500 mW device with 8 to 12 dB gain at 12 GHz. "With a simple driver stage, it would be no problem to get 20 dB gain at 500 mW," he predicts.

Cells determine impedance

From the circuit designer's point of view, the steps taken by device manufacturers to control the power FET's large saturation drain current are by far the most important. Power FETs are fabricated with a very large gate width (not to be confused with gate length, usually in order of a micron) to handle high I_{dss}. This is usually accomplished by paralleling a number of interdigitated gate fingers. Thus, ten parallel gate strips, each typically 1-μm long and 150-μm wide, would add to form a 1500 μm gate width.

On the surface, it would appear that gate fingers could be paralleled ad infinitum to reach any power level. But the linear dependence of output power with total gate width eventually flattens out. Work reported by Masumi Fukuta and colleagues from Fujitsu Laboratories, Kawasaki, Japan, indicates that the practical limit on total gate width is in the order of 6000 μm.[2] Most device designers are fabricating power cells, each containing 600 to 1500μm of gate width, and bonding these cells together within a package to construct a high power device.

Just as there is a limit to the total gate width per cell that the device designer can provide, the circuit designer faces bandwidth constraints when specifying high-power (multicell) devices. "If the bandwidth requirement is zero, you can parallel a large number of cells, pretty much without limit," explains Robert Neidert, research electronic engineer at Naval Research Laboratories, Washington, DC. "But for wider and wider bandwidths, you cannot put that many together, partly because of the larger and larger departure from 50 ohms."

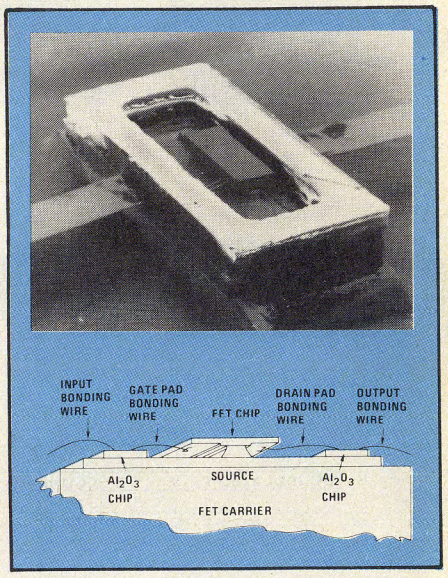

***1. The "flip-chip" mounting technique** designed by RCA is perhaps the most drastic departure from familiar low-noise packaging. Raised source pads are bonded to a pedestal formed as part of the carrier, providing heat sinking and RF ground. The mounting technique decreases both thermal resistance and common-source inductance, and results in a 1.5 to 2 dB increase in small signal gain.*

Input and output impedance levels drop by roughly a factor equal to the number of cells, reports a Texas Instruments research team.[3] An increase in the magnitude and decrease in the phase of S_{11} and S_{22} can be expected. The calculated gain of multi-cell devices should be slightly less than that of a single cell device, typically 1 or 2

dB, primarily due to the multi-cell interconnect scheme and corresponding increase in parasitics.

A single power FET cell in chip form with about 600 μm gate width can be approximated by an input series RC network, with R roughly equal to 6.1 ohms and C about 1.5 pF. The equivalent output network looks like a rather high resistance, about 350 ohms, in parallel with a small capacitance, about 0.13 pF. The reverse transmission parameter, S_{12}, is high enough to neglect feedback elements.[4]

A figure of merit proposed by a research team from RCA Laboratories, Princeton, NJ, illustrates the effect of total gate width.[5] This expression:

$M_F = P_A f^2/W$

where P_A is the RF added power ($P_{out} - P_{in}$) in mW, f is the frequency in GHz and W is the total gate width in microns, gives a measure of the intrinsic device capability and is useful for comparing different devices. "If you compare two 1-W C-band devices, for example, then the one with the higher M_F will permit easier matching," comments Ira Drukier, GaAs FET manager at Microwave Semiconductor Corporation, Somerset, NJ. "Also, for the same input, a higher power can be matched."

Although internally matched packages could ease many design problems, few FETs are so equipped. But an experimental device described at this month's International Solid-State Circuits Conference by researchers from NEC might represent a future production transistor. The FET produces a 1-W output at the 1-dB gain compression point, with 6.5-dB linear gain over a 4.6-to-7.6 GHz bandwidth. This performance was achieved without *any* type of external matching network.[6]

Linearity looks excellent

The power FET has all the characteristics necessary to design excellent linear amplifiers with very low intermodulation distortion. " It has very good third order intermodulation characteristics," reports Chern Huang, project engineer at the Air Force Avionics Laboratory, Wright-Patterson Air Force Base, OH. "Researchers at Texas Instruments, for example, were able to build at 8.5 GHz amplifiers with 1.5-W output and third-order IMD of about 28 dB below the carrier."

At this month's International Solid State Circuits Conference, two researchers from RCA Laboratories, Franco N. Sechi and Ho C. Huang, reported 500-mW of output power at 40-dB intermodulation for a 3.7-to-4.2 GHz amplifer design.[7] The amplifier, designed for Intelsat, relies on two hybrid coupled power FETs, each featuring five cells connected in parallel for a total gate width of 3000 μm, for the power stage. A four-cell FET is used in a driver stage.

The RCA team reports that at a C/I ratio of 40 dB, the output power of one-half of the output circuit stage is 320 mW with an efficiency of 14 percent and gain of 12 dB. "Such value of efficiency, obtained at a point only 5 dB below saturation, is very high," they contend. "Moreover, the output power, efficiency and gain vary only 0.2 dB, 1 per cent and 0.7 dB, respectively, over the 3.7 to 4.2 GHz range. This is a result of our design techniques that, by using IMD contours of the active device, allows the optimization of power and gain over bandwidth independently."

Another outstanding example of the exceptional distortion characteristics of the power GaAs FET is provided by a 6-GHz amplifier developed by Fujitsu Laboratories for application in an FM radio relay system. The third-order intermodulation product is reported to be 31.5 dB below the carrier at an output of 1 W. The four-stage amplifier builds 26-dB gain and operates with an efficiency of 22 per cent.[8]

Measurements of four-cell (2400 μm) power devices at Texas Instruments show that third-order distortion is not sensitive to the frequency separation of the two test signals used. Furthermore, the TI report points out that the third-order distortion of a power FET amplifier is essentially independent of frequency within the amplifier passband.[3]

All things considered, the power FET looks very attractive for applications in communications systems. It should also be noted that the power GaAs FET is inherently a very efficient device—a plus for spacecraft applications. In fact, class-B devices operating at 4 GHz have been reported by RCA with power-added efficiencies as high as 68 per cent. This is an exceptional result, and represents the highest efficiency reported for any microwave semiconductor at this frequency.

High efficiency makes the devices very attractive as replacements for medium-power TWTs. "The FET efficiency of 68 per cent at 4 GHz compares to about 44 per cent for the best practical TWT," comments Fred Sterzer, director of RCA's Microwave Techno-

(continued on p. 40)

Electro-optics, Optomechanics, Infrared, Laser, Computer Hardware Development, Radar

The professionals: EEs, physicists
The tasks: advanced and conceptual design; electro-optical sensor analysis; performance analysis; advanced image and signal processing; stabilization/tracking analysis; systems design, including space-based programs; circuit design that uses MOS or bipolar; design of CCDs and microprocessor/microcomputer techniques.

The professionals: EEs, physicists, MEs
The tasks: device development; high-energy-laser alignment-control systems; servos; precision gimbals and mechanisms.

The professionals: EEs
The tasks: computer-controlled test equipment and system integration and checkout, including systems design and application.

The professionals: radar circuit designers
The tasks: analog or digital circuit design and development; radar transmitters; RF subsystems—all using RF power-amplifier components/subsystems, modulators, high-voltage power processing, and control/protection circuits and techniques.

The professionals: radar systems engineers
The tasks: systems design using Fourier analysis, pattern recognition, and radar signal processing using digital techniques.

Degree from an accredited institution required. Please send resume to: Professional Employment, Hughes Aircraft Company, 11940 West Jefferson Blvd., Culver City, CA 90230.

HUGHES
HUGHES AIRCRAFT COMPANY
AEROSPACE GROUP

US citizenship required
Equal opportunity M/F/HC employer

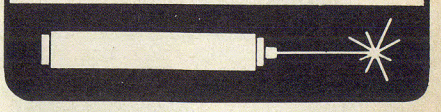

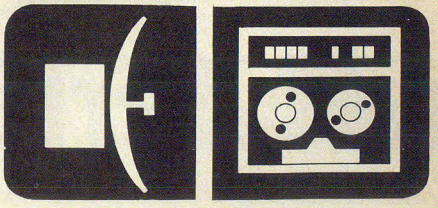

READER SERVICE NUMBER 31

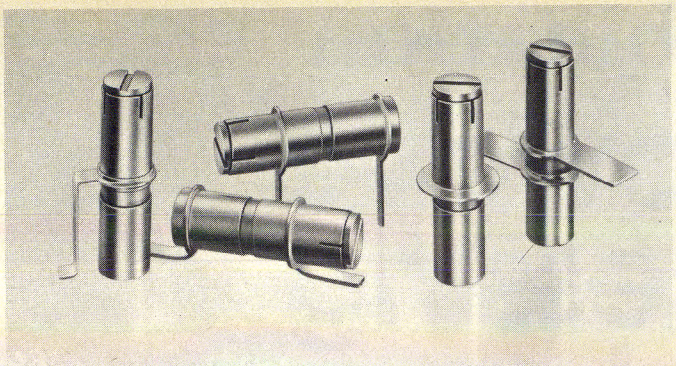

GIGA-TRIM CAPACITORS
FOR MICROWAVE DESIGNERS

GIGA-TRIM (gigahertz-trimmers) are tiny variable capacitors which provide a beautifully straightforward technique to fine tune RF hybrid circuits and MIC's into proper behavior.

APPLICATIONS

- Impedance matching of GHz transistor circuits
- Series or shunt "gap trimming" of microstrips
- External tweaking of cavities

Available in 5 sizes and 5 mounting styles with capacitance ranges from .3 - 1.2 pf to 7 - 30 pf.

Johanson®

MANUFACTURING CORPORATION
Rockaway Valley Road
Boonton, N.J. 07005
(201) 334-2676 TWX 710-987-8367

READER SERVICE NUMBER 37

Power GaAs FETs

gy Center in Princeton, NJ. NASA is sponsoring a program at RCA aimed at developing a 1 W device at 15 GHz.

Sources and amps for USAF

Most of the progress in power FET technology in the US has been underwritten by the Army, Navy and Air Force. Although the Army has postponed all power FET funding until fiscal year 1978, Navy and Air Force contracts continue to develop devices aimed specifically at airborne phased array applications in X-band.

"We believe that GaAs FETs will, for the first time, make solid-state airborne phased arrays possible," forecasts RCA's Sterzer. RCA is partway through the first year of a two-year Air Force program with the goal of developing a 4 W (CW) device operating at 10 GHz with 8-dB gain and better than 25 per cent efficiency. "Right now," Sterzer continues, "state-of-the-art at that frequency is in the order of 1 W, depending on what you consider to be reproducible."

William Wisseman, manager of a parallel Air Force program at Texas Instruments, Dallas, TX, reports that the 4 W level has been demonstrated in a narrow-band (chip-tuned) amplifier circuit at 8 GHz. "Although we haven't tried to build a broadband version yet, we've achieved 4.1 W at 8 GHz with 4 dB gain and 31 per cent efficiency," Wisseman told *Microwaves*. "The device used here had four, 1200-μm cells (4800-μm total gate width). Gates were delineated with e-beam technology."

"Reproducible" is a key word in the program funded by the Air Force. "In a laboratory demonstration, people can probably demonstrate 4 to 6 W at one time or another," explains AFAL'S Chern Huang, who is monitoring the work at RCA and TI, "but in terms of applications, this demonstration is probably not very useful. It shows capability not usefulness." Thus, a performance demonstration is only one of the four goals of the Air Force program. The others deal with developing a well-defined manufacturing technology and obtaining reproducible results.

"Another objective is a demonstration of applications to be used in a 9 to 10 GHz, 26-dB gain amplifier with 2 W output power," Huang continues. "We are interested in the power GaAs FET as a pulse source for radar applications, and for that we plan a 9 to 10 GHz, 26-dB gain amplifier with a 3-W peak output at 60°C."

In addition, the Air Force is evaluating the power FET as an oscillator element. "The oscillators we have developed should be pretty competitive with the Gunn-effect circuits at frequencies up to 25 GHz," points out TI's Wisseman. He reports fixed-frequency sources that produce 50 mW at 10 GHz with 45 per cent efficiency, 500 mW at 9 GHz with 26.8 per cent efficiency and 150 mW at 15.2 GHz with 9 per cent efficiency. A 25.2-GHz oscillator reported by TI with in-house funds produces 6.5 mW with 4.7 per cent conversion efficiency.

Varactor-tuned FET oscillators have also been designed at TI. Performance includes a frequency range of 8.2 to 12.4 GHz with 50-to-100 mW output and 10-to-15 percent conversion efficiency. A higher frequency circuit produced 20 mW over a 12.8-to-16.8 GHz bandwidth with 5-to-10 per cent efficiency.

Most of the oscillator work at TI relies on a common-gate circuit.

Although close-in noise performance has not been fully explored, it is generally believed that the power FET will find many applications at power levels that lie between Gunn and Impatt capabilities. "The GaAs FET is an intermediate device between the Impatt diode and the Gunn diode, when considering its output noise level," observes NEC's Yoshiyuki Mizuta.

The 1/f noise of an oscillator using a GaAs FET is 10 dB greater than that obtained from a silicon bipolar transistor," adds Youichi Arai and Hidemisu Komizo of Fujitsu Laboratories. "Further device improvement in the noise property is much awaited.[10]"

Navy compares FETs and Trapatts

Phased array applications for power FETs also interest the Navy. In what Elliot Cohen, head of the high-frequency device section at NRL, terms "a successor to the Westinghouse MARE program," RCA and TI will submit amplifier modules to the Navy for evaluation by March, 1978. The performance of the amplifiers developed in this program will be compared with the results of an X-band Trapatt program now underway at Hughes. But industry experts see no real contest.

Where can you buy a power GaAs FET?

Eighteen months ago, if you wanted to purchase a low-noise GaAs FET, you simply called NEC, Plessey or Fairchild. Today, Fairchild is out of the business, but there are at least two dozen manufacturers to take its place. And, if you thought 1976 was a hectic year for the FET business, wait until 1977. With NEC entering the component business and many amplifier houses developing in-house production facilities, the topsy-turvy world of GaAs FET marketing will spin even faster.

Will a similar avalanche of manufacturers invade the power GaAs FET marketplace? Probably, unless the current suppliers can perform processing miracles to increase yields substantially and slash today's dollar per milliwatt prices.

Fujitsu, Texas Instruments and RCA are out to an early lead with the really "high" power devices. NEC and Plessey are in production with what could be called "medium" power designs, while Microwave Semiconductor Corporation, Dexcel and Alpha Industries have plans to enter the competition shortly.

MSC president Ronald Rosenzweig, confidently predicts that the power GaAs FET market will grow to the size of the present microwave silicon bipolar market in less than ten years. His firm will introduce sample quantities of devices for the 4-to-10 GHz range early this year. "Only packaged devices will be sold initially," Rosenzweig confirms. "Our package, made in-house, is 100 mils² and called Micropac. Devices in the Micropac will be usable through C-band." In two to three years, MSC expects to be shipping 5 W C-band devices, although specifications for its initial device was not available at presstime.

Intent on maintaining its lead in the overall GaAs FET market, NEC has introduced two power devices for oscillator and amplifier applications to X-band. The NE464A has a power output in excess of 250 mW at the 1-dB compression point with an associated gain of 7.5 dB at 6 GHz. An output of 400 mW with 6 dB gain is featured. According to Jerry Arden, marketing manager at California Eastern Laboratories, Burlingame, CA, the packaged devices sell for $385 and $495, respectively. Either device may be ordered in chip form, and the 550 mW FET is available in a new package with an internal matching network.

Plessey now offers two medium power devices, PGAT 100 and 200, producing 100 and 200 mW, respectively, at 5 GHz. Marketing manager Rand Burke says that a single-chip device producing 250 mW at 5 GHz is close to introduction, while FETs delivering 500 mW at 12 GHz and 1 W at 8 GHz are currently under development.

Texas Instruments recently introduced three devices, the MSX 801, 802 and 803, producing 250 mW, 500 mW and 1 W, respectively, at 8 GHz with 30 per cent efficiency. Gain for all devices is 4 dB. TI will bond the devices common-source or common-drain for amplifier or oscillator applications. Prices are $250, $500 and $1,000.

RCA's Microwave Technology Center in Princeton offers three developmental models producing 500, 250 and 100 mW at 4.5, 8 and 12 GHz. Models MTC-T450, MTC-T825 and MTC-T1210 feature power-added efficiencies of 25, 20 and 15 per cent.

Fujitsu's FLC series is intended for common-source Class-A linear power amplifier and oscillator applications. Model FLC30 offers 3.0, 2.4 and 1.0 W at 4, 6 and 8 GHz, respectively. Model FLC15 is rated at 1.5, 1.2 and 1.0 W, model FLC08 is specified at 800, 700 and 600 W.••

"Efficiency will surely be a major obstacle to the Trapatt approach," one source told *MicroWaves*. "They might achieve 16 or 18 per cent efficiency with the Trapatt, while the FET approach should yield closer to 25 per cent."

RCA's approach to the 5 W module design is strictly FET, with perhaps two, 2.5-W devices paralleled for the necessary output power. The Navy requires that the module provide a gain of 25-dB—no easy chore over a bandwidth of 1 GHz. Although the 9.5 GHz amplifiers will be used in a pulsed radar, duty cycle is said to be in the neighborhood of 40 to 50 per cent, calling for near-CW thermal considerations.

Texas Instruments proposes two alternatives to meet the Navy requirement. Like RCA, they plan to submit a design based strictly on power GaAs FETs. However, a hybrid design involving an FET driving a Read-profile Impatt amplifier will be developed as a back up.

More pulsed work needed

Designing devices and circuits with the power and frequency capabilities for the Navy and Air Force phased array programs is only part of the developmental efforts that lie ahead. Much work remains to be done in characterizing the FET under pulsed conditions and in designing appropriate gate circuits.

There are two basic schools of thought concerning how the power FET of the future will function in a pulsed radar module. Both plans call for the device to be turned off between RF pulses by increasing the gate voltage to pinchoff. Many designers believe that the level of RF power required to turn the device back on is low enough for the incident signal to do the job. If this is not the case, then some type of

(continued on p. 43)

a winning combination

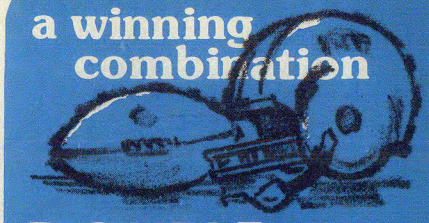

DOUBLE BALANCED MIXERS

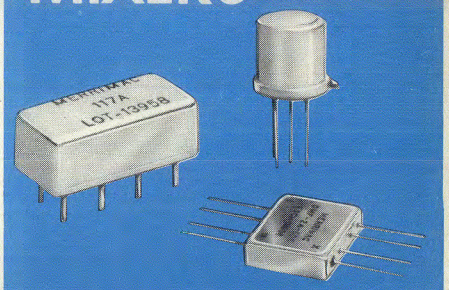

DC to 1 GHz — in TO-5, Flat Pack or Relay Header

Check our minimum performance characteristics and see for yourself why Merrimac has the winning combination for you...

DC-500 MHz MODELS				
PACKAGE	MODEL NO'S	PRICE	CONVERSION LOSS	ISOLATION (DB-MIN)
RELAY HEADER	117A	$ 9.45	5.5 dB Typ. 8.0 dB Max.	L-R 40-30 L-X 35-20
FLAT PACK	DMF-2A-250	$29.00	7.0 dB Typ. 8.0 dB Max.	L-R 40-35 L-X 30-20
TO-5 (0.3" HIGH)	M-109	$25.00	6.0 dB Typ. 8.5 dB Max.	L-R 40-25 L-X 30-18
DC-1000 MHz MODELS				
RELAY HEADER	M-119	$15.00	7.0 dB Typ. 8.0 dB Max.	L-R 30-20 L-X 25-15
FLAT PACK	DMF-2A-505	$26.00	7.5 dB Typ. 8.0 dB Max.	L-R 35-25 L-X 30-20
TO-5 (0.3" HIGH)	M-122	$39.00	6.5 dB Typ. 9.5 dB Max.	L-R 40-25 L-X 30-20

LO POWER (ALL MODELS) +7 DBM NOMINAL.

Send for complete data on the above Mixers and we will also include free MTBF data and information on our complete line of DC-3GHz "Connectorized" Single and Double Balanced Mixers.

send for our NEW '77 CATALOG OF IF SIGNAL PROCESSING COMPONENTS

Merrimac
INDUSTRIES, INCORPORATED
41 FAIRFIELD PL., W. CALDWELL, N.J. 07006
201 575-1300 • TWX 710-734-4314

now there is one...in signal processing

READER SERVICE NUMBER 32

sensing circuit would have to be designed to turn the device back on just prior to the arrival of an RF pulse. Risetime of the device is not expected to be a problem in either case—logic applications demonstrate that FETs can respond in the order of 100ps.

Army eyes K-band

The Army, having pulled all of its funding from X-band power FET development in deference to the large-dollar Air Force and Navy programs, plans to develop a series of Ku-band devices in early 1978. "Our next requirements are in the Ku-band area, around 14 through 16 GHz, for applications like the Army miniature RPV, Aquilla," states Vladimir Gelnovatch, an engineer at ECOM. "Right now, the RPV is being tested by Harris at C-band, but due to frequency allocations in Europe, it will go to Ku-band. There are also classified requirements at around 21 GHz, for secure communications."

According to Gelnovatch, a request for proposals will probably go out sometime in January or February of 1978 for K-band devices in the 1 to 3 W range. "Right now, the art seems to be about 0.5 W at these frequencies," he observes. "I don't think that we'll have to go to anything exotic like vertical structures to reach our goal. I suspect that it will be a multi-cell device, perhaps with 4800 to 5000 μm of gate width. I suspect that whomever does the work will go with a 0.5-μm gate length, but the present work (at RCA) is interesting. For instance, with nominal 1 μm of gate length, they have been getting 250 mW at 22 GHz."

"In fiscal year 1979, we hope to develop a 10 to 20 W Ku-band FET amplifier, using the devices developed in this program. This may require four combined devices in the output, and there is some interest in push-pull instead of a hybrid-coupled circuit.

"Obviously, what we're really going after are the TWTs."

Some practical points

If you have decided to pick up a power FET or two and try them in your own circuit design, there are a few things to consider (see, Where can you buy a power GaAs FET?). First, be prepared to spend about a dollar per milliwatt for the devices. It's a high price to pay, but power FET technology is relatively immature and manufacturers still have no yields to speak of.

Secondly, don't expect to succeed with a "seat of the pants" design approach—s-parameter analysis and computer-aided optimization are virtual requirements. If the input impedance-matching circuit is changed, for example, the output impedance of the device varies accordingly.

It must also be recognized that the input and output impedances of the FET change as input power is raised. Thus, although small-signal s-parameters may be used to roughly guide a design, matching circuits must be modified for large-signal conditions.

Finally, realize that although the devices are indeed powerful, sound and rugged, they are *not* made of silicon. Static discharge *can* destroy the fragile Schottky-barrier gate. And, remember to turn up the gate-source bias prior to applying the drain-source voltage. If the drain-source voltage is applied first, the device could go out to an I_{dss} condition and break into self-destructive oscillation.

Designers will often fire up a silicon bipolar transistor without proper heat-sinking to get a quick look at its DC characteristics. Try this with a power GaAs FET and in the words of TI marketing engineer, Bernie Landress, "you will smoke-test the device." Designers must pay immediate attention to heat-sink considerations, due to the poor thermal conductivity of GaAs.

Also watch for oscillations when performing DC tests. "The power FETs have such a high frequency response, that it could well break into oscillation and self-destruct before you have a chance to look at the DC characteristics," TI's Landress cautions. Small ferrite beads, placed around the test leads as close as possible to the FET package, are usually effective for safeguarding the device.••

References

1. Y. Mizuta, "GaAs FETs Have A Bright Future Insured By Technical Progress," *Journal of Electronic Engineering*, No. 120 p. 47, (December, 1976).
2. M. Fukuta, et al, "Power GaAs MESFET With A High Drain-Source Breakdown Voltage," *IEEE Transactions On MTT*, Vol. MTT-24, No. 6, p. 312, (June, 1976).
3. H. Tserng, et al, "Microwave Power GaAs FET Amplifiers," *IEEE Transactions On MTT*, Vol. MTT-24, No. 12, p. 936, (December, 1976).
4. R. Neidert, et al, "Wideband GaAs Power MESFET Amplifiers," *IEEE Transactions On MTT*, Vol. MTT-24, No. 6, p. 344, (June, 1976).
5. I. Drukier, et al, "Medium Power J-Band MESFETS," presented at the Conference on Active Semiconductor Devices for Microwaves and Integrated Optics, Cornell University, Ithaca, NY, (August, 1975).
6. Y. Takayama, et al, "Internally Matched Microwave Broadband Linear Power FET," to be published in Proceedings of 1977 International Solid-State Circuits Conference.
7. F. Sechi, et al, "High-Efficiency MESFET Linear Amplifier Operating at 4 GHz," to be published in Proceedings of 1977 International Solid-State Circuits Conference.
8. Y. Arai, et al, "A 6-GHz, Four-Stage GaAs MESFET Power Amplifier," *IEEE Transactions On MTT*, Vol. MTT-24, No. 6, p. 381, (June, 1976).
9. H. Huang, et al, "GaAs MESFET Performance," *1975 IEDM Technical Digest*, p. 236, (December, 1975).
10. Y. Arai, et al, "GaAs FET Applications Expand," *Journal of Electronic Engineering*, No. 120, p. 57, (December, 1976).

a winning combination



SINGLE AND DOUBLE BALANCED MICROWAVE STRIPLINE MIXERS

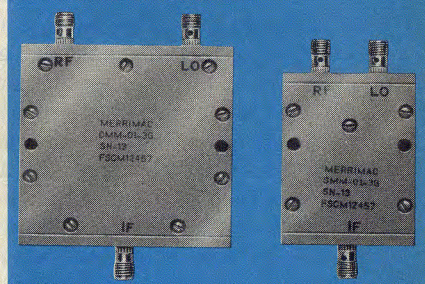

1.7-18 GHz

Check our minimum performance characteristics and see for yourself why Merrimac has the winning combination for you...

SINGLE BALANCED MICROWAVE STRIPLINE MIXERS

MODEL SMM-01-	RF & LO FREQ. (GHz)	IF BW (MHz)	ISOLAT'N dB (MIN)	NOISE FIG. dB (MAX)	CONV. LOSS dB (MAX)
2.95 G	1.7-4.2	DC-400	6	8.0	6.5
3 G	2.0-4.0	DC-400	8	7.5	6.5
3.90 G	2.6-5.2	DC-400	7	7.5	6.5
6 G	4.0-8.0	DC-400	6	8.0	7.0
10 G	8.0-12.4	DC-1000	6	8.5	7.5
15 G	12.4-18	DC-1500	6	9.0	8.0

DOUBLE BALANCED MICROWAVE STRIPLINE MIXERS

MODEL SMM-01-	RF & LO FREQ. (GHz)	IF BW (MHz)	ISOLAT'N dB (MIN)	NOISE FIG. dB (MAX)	CONV. LOSS dB (MAX)
2.95 G	1.7-4.2	DC-400	20	8.5	7.5
3 G	2.0-4.0	DC-400	20	8.0	7.0
3.90 G	2.6-5.2	DC-400	20	8.5	7.5
6 G	4.0-8.0	DC-400	20	9.0	8.0
8 G	6.0-12.4	DC-400	16	9.5	8.5
10 G	8.0-12.4	DC-700	18	9.0	8.0
15 G	12.4-18	DC-1000	15	10.0	9.0

send for our NEW '77 MICROWAVE CATALOG.

Merrimac
INDUSTRIES, INCORPORATED
41 FAIRFIELD PL., W. CALDWELL, N.J. 07006
201 575-1300 • TWX 710-734-4314

now there is one...in signal processing

READER SERVICE NUMBER 34

How The New Schottkys Detect Without DC Bias

The latest generation of Schottky-barrier diodes do not require bias to detect low-level signals. The key to this useful feature lies in higher saturation current and better impedance matching.

WHAT differentiates the newer, zero-bias Schottky-barrier detector diodes from conventional Schottky-barrier detectors? The main difference in the unbiased behavior of the different types of diodes is embodied in their saturation current, I_S.

Zero-bias diodes typically exhibit saturation currents that are two to four orders of magnitude greater than conventional detectors. This may seem contradictory since in theory detector diodes are most sensitive at zero bias when I_S is small, corresponding to large video resistance. However, it will be shown that there is a limit to sensitivity when the resistance is so large that it cannot be matched. Thus, the higher saturation current of zero-bias detectors involves a compromise between sensitivity due to large resistance and loss due to matching.

To review, a conventional Schottky-barrier diode detector requires no bias for high level input power—above 1 milliwatt. However, at low input levels, a small amount of DC bias is required for detection to take place. Even though this bias current is at the microampere level, the requirement is often difficult to supply.

The new generation of zero-bias diodes eliminates the need for a DC supply at low input levels. The new diodes are also two to three times more efficient as a detector compared to conventional biased detectors.

Compare forward voltage characteristics

Since both types of detectors are Schottky diodes, the forward current obeys the equation:

$$I = I_S \left(e^{\frac{q}{nkT}(V - IR_S)} - 1 \right) \qquad (1)$$

The ideality factor, n, is close to unity for these diodes, so the equation may be simplified:

$$I = I_S \left(e^{\frac{V - IR_S}{0.026}} - 1 \right) \qquad (2)$$

when values for the constants q (electron charge), T (room temperature) and k (Boltzmann's constant) are added.

The influence of saturation current on the forward voltage characteristic of a detector diode is clearly shown by the plots in Fig. 1. Curve A illustrates the performance of a conventional Schottky-barrier detector (Hewlett-Packard 5082-2750) with I_S of 7×10^{-10} amperes and series resistance (R_S) of 32 ohms. Curves B and C trace the characteristics of two zero-bias detectors (HP HSCH-3171 and HSCH-3486) with I_S of 7×10^{-8} and 6×10^{-6}, respectively. Series resistance is 15 ohms for both these devices.

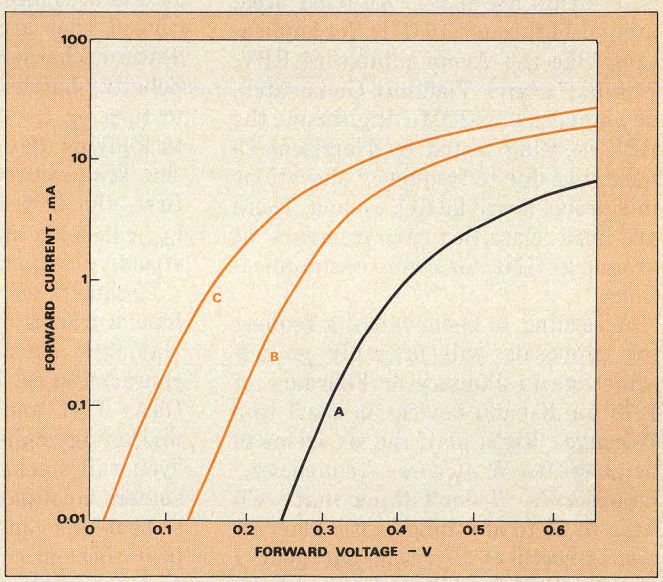

***1. The forward I-V characteristics** show that zero-bias detectors have lower forward voltages than conventional detectors.*

Predicting voltage sensitivity

A detector diode is classically treated as some current generator across the diode video resistance.[1] One encounters major problems, however, when attempting to apply this simple analysis to the case of a detector without bias.

Proceeding with the basic analysis, voltage sensitivity (β) is the product of current sensitivity (γ) and video resistance (R_V), the inverse of the derivative of current with respect to voltage. Neglecting parasitic and reflection losses:

$$\gamma = \beta \,/\, \frac{\delta I}{\delta V} \qquad (3)$$

For small values of current Eq. (2) becomes:

$$I = I_S \left(e^{\frac{V}{0.026}} - 1 \right) \qquad (4)$$

and,

$$\frac{\delta I}{\delta V} = \frac{I + I_S}{0.026} \qquad (5)$$

(continued on p. 46)

Jack Lepoff, Applications Engineer, Hewlett-Packard Co., Microwave Semiconductor Div., 3172 Porter Drive, Palo Alto, CA 94304.

The theoretical current sensitivity is 20 amperes per watt[2], so:

$$\gamma = \frac{0.52}{I + I_S} \quad (6)$$

or, for zero bias current:

$$\gamma = \frac{0.52}{I_S} \quad (7)$$

This simplified analysis indicates no improvement in using the new zero-bias diodes, because sensitivity varies inversely as saturation current and the conventional diodes have the lowest saturation current. In fact, Eq. (7) predicts that without bias, the conventional diode used as an example in Fig. 1 would exhibit a sensitivity of:

$$\gamma = \frac{0.52}{7 \times 10^{-10}} = 750 \times 10^6 \text{ volts per watt}$$

or 750,000 millivolts per microwatt.

This, of course, is considerably higher than the sensitivity the diode actually offers. In fact, the actual sensitivity of the HP 5082-2750 detector with zero bias is close to zero. The effects of junction capacitance, load resistance and reflection loss must be considered to bring this analysis closer to reality.

Enter capacitance and load resistance

The influence of junction capacitance on current sensitivity is derived in section 11.2 of Reference 1. Adding this effect to the voltage sensitivity analysis gives:

$$\gamma_1 = \frac{0.52}{I_S (1 + \omega^2 C_j^2 R_S R_V)} \quad (8)$$

For a typical case,

$C_j = 0.07$ pF, $R_S = 15$ ohms, and $R_V = \frac{0.026}{I_S}$

so that:

$$\gamma = \frac{6900}{f^2 + 1.33 \times 10^7 I_S} \frac{mV}{\mu W}$$

with frequency in gigahertz and saturation current in amperes. Figure 2 shows how capacitance modifies voltage sensitivity. Since the change is due to the RF current split between C_j and R_V, the reduction is more severe at higher frequencies, where the capacitive susceptance is higher. The inverse relationship with saturation current is still present at low frequencies or high saturation current values. However, predicted values of voltage sensitivity are still unreasonably high.

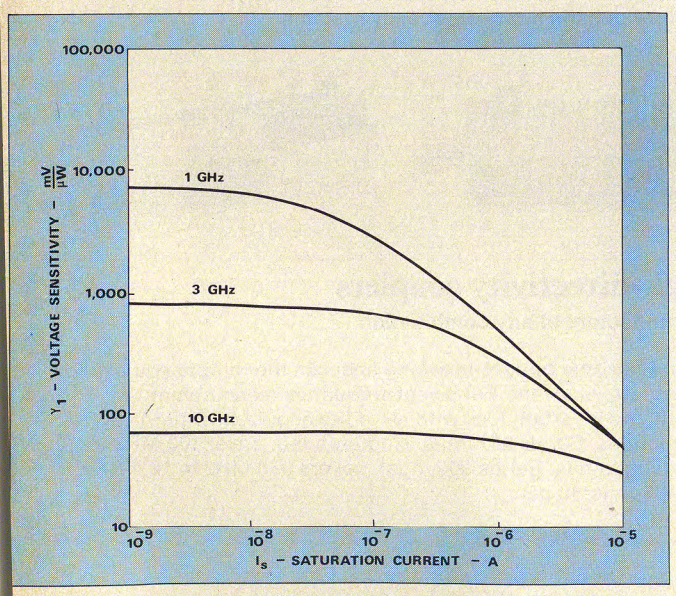

2. Junction capacitance modifies voltage sensitivity *by robbing a portion of the current assumed to flow through the equivalent video resistance.*

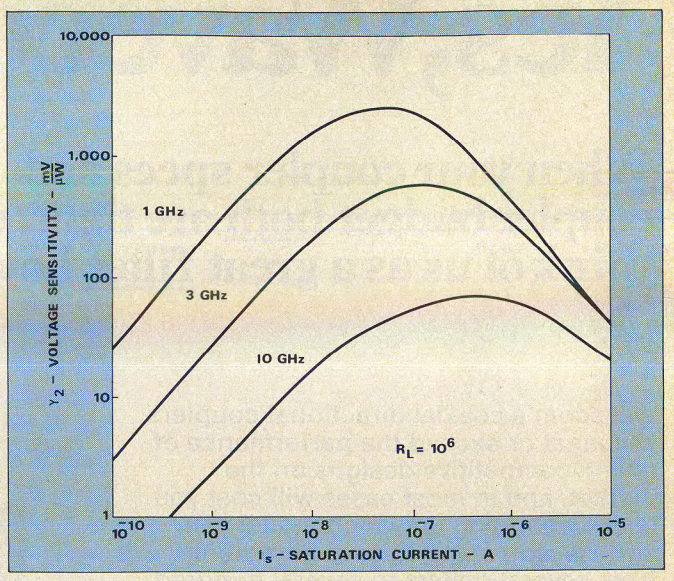

3. Load resistance becomes significant at zero bias. *Diode resistance is not small compared with load resistance, hence video voltage is reduced.*

A detector diode may be considered as a video voltage source of impedance R_V feeding a load resistance R_L. The voltage across the load, γ_2, is reduced by the ratio of R_L to $R_V + R_L$:

$$\gamma_2 = \gamma_1 \frac{R_L}{R_V + R_L} = \frac{\gamma_1}{1 + \frac{R_V}{R_L}} \quad (9)$$

When the ratio of video resistance to load resistance is small, $\gamma_2 = \gamma_1$. This is a common condition for biased detectors. However, at zero bias, the diode resistance is usually not small compared to load resistance. For a typical load resistance value of 1 megohm, the sensitivity is:

$$\gamma_2 = \frac{\gamma_1}{1 + \frac{26 \times 10^{-9}}{I_S}} \quad (10)$$

The effect of load resistance at zero bias is shown in Fig. 3. Note how load resistance tends to move the point of maximum sensitivity to the right, favoring diodes with higher saturation current, in spite of what Eq. (7) predicts. The inverse relationship between sensitivity and saturation current in γ_1 combined with the direct relationship due to load resistance results in a maximum voltage sensitivity when $I_s = 4.43 \times 10^{-8}$ f, where f is frequency in GHz. However, these theoretical results are still unreasonably high, particularly at lower frequencies.

Now, consider reflection loss

The analysis so far has assumed that all incident power is absorbed by the diode. Normally, this is a good assumption because low-loss matching circuits can be designed to eliminate reflection losses. At zero bias, however, the mismatch may be so severe that it is not possible to

(continued on p. 48)

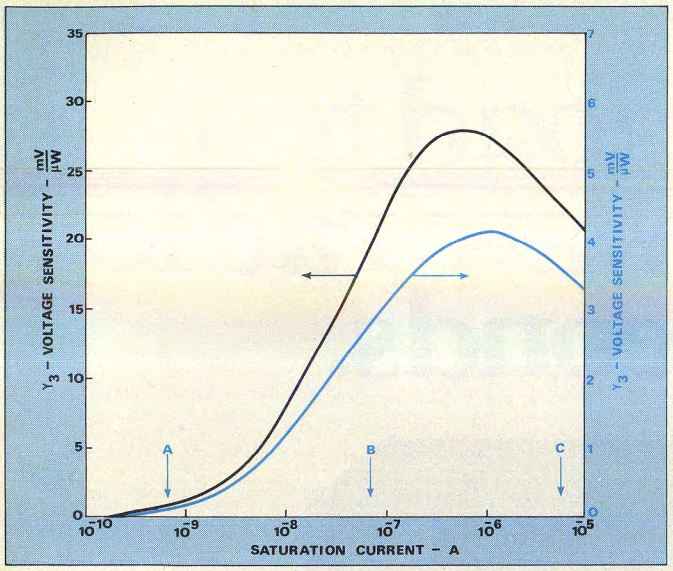

***4. Mismatch is by far the largest detriment** to voltage sensitivity at zero bias. The lower curve represents theoretical data on a variety of packaged devices; the upper curve is for an axial lead device at 10 GHz. Saturation currents corresponding to the three diodes used in Fig. 1 are indicated.*

eliminate these reflection losses. In fact, most of the incident power may be absorbed by losses in the matching network.

If we go to the other extreme and assume no matching, the sensitivity becomes:

$$\gamma_3 = \gamma_2 (1-\rho^2) \qquad (11)$$

where ρ is the reflection coefficient of the diode. Assuming the diode impedance, Z_D, terminates a 50-ohm system:

$$\rho = \frac{Z_D - 50}{Z_D + 50} \qquad (12)$$

Since diode impedance is a function of package parasitics as well as frequency, calculations were performed for three types of packages—axial lead, cartridge and pill—at 1, 3 and 10 GHz. Most of the results were quite close to the lower curve in Fig. 4. At 10 GHz, however, the axial lead component was considerably less sensitive (upper curve, left scale), because the package inductance resonates the junction capacitance. If this is compared with Figs. 2 and 3, it can be seen that mismatch is the largest factor to degraded sensitivity. Note that the effect of mismatch is to again skew the curve to the right to favor diodes with higher saturation current.

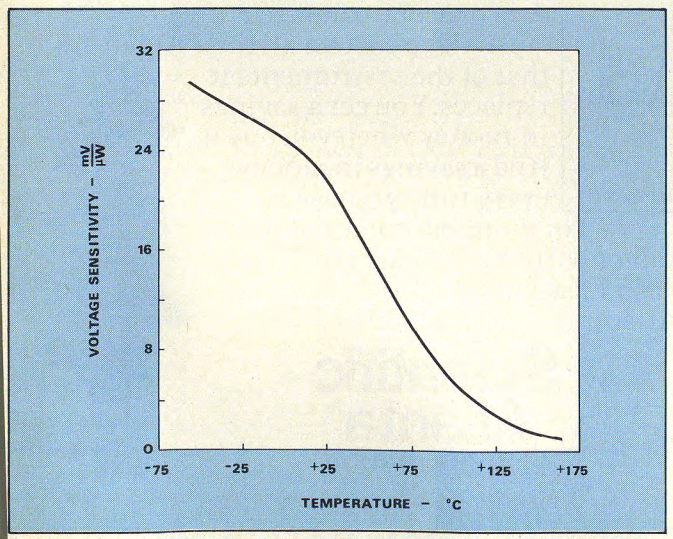

***5. Voltage sensitivity of zero-bias devices** with higher saturation current improves at lower temperatures.*

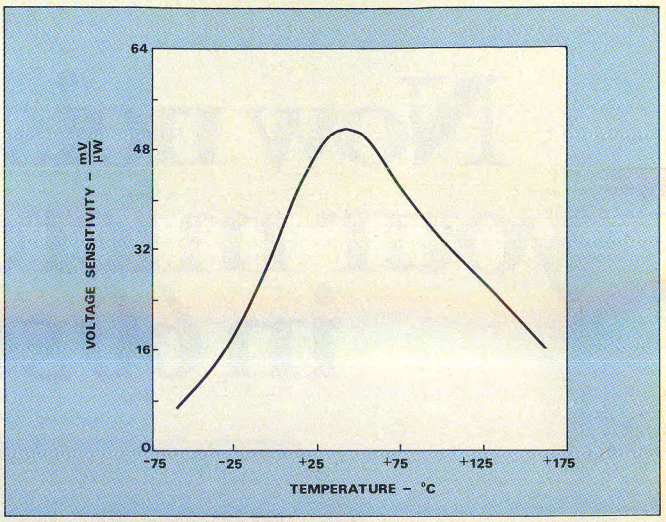

***6. Zero-bias detectors** with lower saturation current offer optimum sensitivity at some intermediate temperature.*

With the addition of tuning to overcome some of the reflection losses, the measured sensitivity of most zero-bias diodes is usually better than that shown in Fig. 4. However, the reflection losses for a conventional diode under zero-bias conditions are so great that tuners do not help much. Thus, these diodes are not useful without bias.

The effects of temperature vary

The sensitivity of conventional Schottky detectors improves at colder temperatures. This behavior is similar to that of the higher saturation current zero-bias devices, which have a temperature characteristic as shown in Fig. 5. When matching losses are small, sensitivity varies inversely with temperature because saturation current varies directly with temperature. This behavior is consistent with the high saturation current portion of Fig. 4, where sensitivity varies inversely with saturation current.

Figure 6 illustrates the temperature characteristic of a zero-bias detector diode with lower saturation current—closer to that of a conventional diode. This diode has maximum sensitivity just above room temperature, degrading at cold as well as at hot temperatures. The high temperature behavior is expected from the higher value of saturation current. The low temperature behavior indicates that the room temperature value of saturation current is nearly optimum for this diode. At lower temperatures, the reduced value of saturation current is not able to improve sensitivity because the corresponding large diode resistance causes a large mismatch loss which cannot be tuned out. This behavior is analogous to the left-hand portion of Fig. 4 with temperature corresponding to saturation current.••

References

1. H. C. Torrey and C. A. Whitmer, "Crystal Rectifiers," *MIT Radiation Laboratory Series*, McGraw-Hill, New York, Vol. 15, (1948).

2. H. A. Watson, *Microwave Semiconductor Devices and Their Circuit Applications*, McGraw-Hill, p. 379, (1969).

Part II

Edge-Guide: One Path To Wideband Isolator Design

Part I examined the propagation characteristics of symmetrical edge-guide media. This concluding installment relates theory to practice by tracing the design of isolators with thick-film and bulk loading.

PROPAGATION constants for symmetrical edge-guide transmission line were derived last month in Part I of this article, using Maxwell's equations to solve a set of partial differential equations subject to boundary conditions. Although a similar analysis can be used to characterize propagation along the asymmetrical edge-guide used in an isolator (see Fig. 1), it might be more efficient to try a transverse resonance procedure.

As one carries out the details of the boundary value problem it becomes apparent that the steps required by the analysis, even in the transverse dimensions, are similar to those found in straightforward transmission line problems. The solutions in the transverse dimensions consist of standing waves, and the condition of the solution is that the transverse transmission line be resonant.[7] That condition can be represented mathematically as:

$$Z_i(x) = \vec{Z} + \overleftarrow{Z} = 0 \qquad (24)$$

where $\vec{Z}$ and $\overleftarrow{Z}$ are the impedances looking to the left and right at some arbitrary reference plane.

When this procedure is applied to the resistive-film loading scheme shown in Fig. 7, the following transcendental equations results:

$$\frac{\omega}{c} \times \frac{\eta}{R_s} = \frac{\gamma_y^2 + (\omega/c)^2 \epsilon_f}{j \gamma_x \coth(\gamma_x W) + \gamma_y \frac{k}{\mu}} \qquad (25)$$

Equation (25) can now be used to determine the propagation constant γ_y. The real part of this propagation constant, α_y, will give either the isolation or insertion loss, whereas the imaginary part, β_y, yields the phase constant. To obtain both results from the equation, all that has to be done is to change the polarity of K.

Due to the complexity of Eq. (25), it is not possible to obtain a closed form solution without the use of the computer. This was done and the results will be presented shortly. However, to gain a prior understanding of the behavior of this loaded transmission line with regard to the isolation, first assume that the width of the inner conductor is large and the ferrite is lossless. For this case, Eq. (25) does have a closed-form solution, and the propagation constant is given by

$$\alpha_y = \frac{\omega_m}{c} \times \frac{\eta}{R_s} \qquad (26)$$

Michael Dydyk, Principal Staff Engineer, Motorola, Inc., Government Electronics Div., 8201 E. McDowell Road, Scottsdale, AZ 85252.

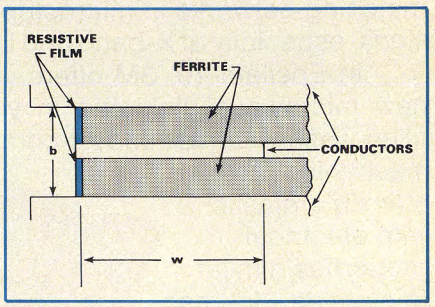

***7. Resistive loading** on one edge of a transmission line sandwiched between two magnetically biased ferrite slabs attenuates energy flowing in one direction. Energy moving in the opposite direction propagates freely along the non-loaded edge.*

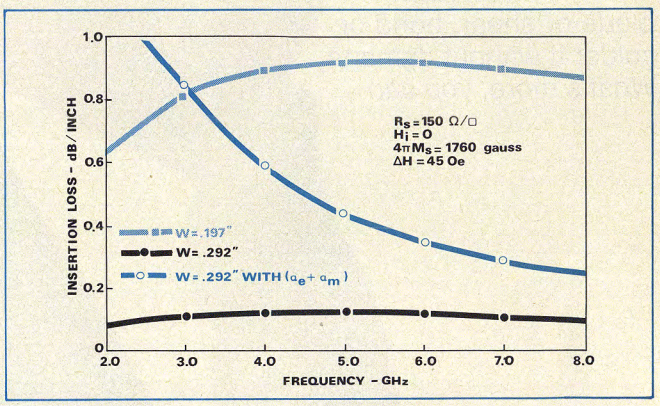

***8. Insertion loss** is lower for wider conductors.*

and

$$\beta_y = \frac{\omega}{c} \sqrt{\epsilon_f - \left(\frac{\eta}{R_s}\right)^2} \qquad (27)$$

Equation (26) gives the isolation in nepers/inch, and while it is a function of the characteristics of ferrite material and the resistivity of the resistive film loading, it is independent of frequency. The smaller the resistivity and the larger the saturation magnetization, the larger the isolation.

Equation (27) indicates something else of great interest: An optimum value of film resistivity for which no energy propagates in the desired direction. This optimum resistivity is given by:

$$R_{so} = \frac{\eta}{\sqrt{\epsilon_f}} \qquad (28)$$

Taking a closer look, we find that this describes a wave that is propagating in the x-direction with a decay rate in the y-direction (see Fig. 7). Since normal propagation is in the

(continued on p. 52)



9. Thick-film resistive loading *is used in this 2 to 8 GHz experimental isolator.*

y-direction, this optimum resistivity would enchance reverse isolation.

Two types of resistive loading tested

To determine the effect of the resistive film on the insertion loss for a finite width of the inner conductor, it was necessary to resort to computer analysis. A program was generated and used to study the behavior of this coupled transmission line. Typical results are presented in Fig. 8. Note that insertion loss increases as the width, W, decreases. A plot that considers the electric and magnetic losses of the ferrite material is also included in Fig. 8.

The isolation corresponding to a finite width inner conductor was also evaluated. The results closely comply with Eq. (26) and show little change with frequency.

An edge-guide isolator, using resistive-film loading and designed according to the computer-derived solutions of Eqs. (25), (26) and (27), was built to test the theory (see Fig. 9). Isolation and insertion loss characteristics, shown in Fig. 10, agree well with the calculations. Note that isolation is greater than 15 dB over two octaves, while maximum insertion loss is 1.7 dB. The thick-film compound used in the isolator measured 268 ohms-per-square.

A second type of edge-guide loading that can be considered is a bulk-lossy material such as the Eccosorb MF family from Emerson and Cuming, Canton, MA. The dielectric properties of this material properties are a function of frequency[8]. However, they increase or decrease monotonically with frequency, and therefore, can be represented by linear equations. For example, the permeability for type MF-124 can be described by

$$\mu_{eg} = \left[-4.0\times10^{-10}f+6.0\right]\left[1-j(8.7\times10^{-11}f+0.238)\right] \quad (29)$$

where f is in Hz.

The analytical approach to this problem is the same as for the case of resistive film loading. The result is

$$-j\gamma_{xx}\tanh\gamma_{xx}E = \frac{\gamma_y^2 + \left(\frac{\omega}{c}\right)^2 \epsilon_f}{j\,\gamma_x\coth(\gamma_x W) + \gamma_{yx}\,\frac{k}{\mu}} \quad (30)$$

where

$$\gamma_{xx}^2 = -\gamma_y^2 - \left(\frac{\omega}{c}\right)^2 \mu_{eq}\,\epsilon_{eq} \quad (31)$$

Equation (30) has no closed-form solution even for large conductor widths. Thus, this equation was programmed and used to study the behavior of bulk-lossy material loading an edge-guide transmission line.

The results, plotted in Fig. 11, show that as the width of the inner conductor is made finite, the insertion loss at the low end of the frequency band becomes larger for ferrite material with lower values of saturation magnetization.

The performance of actual components built according to Eqs. (30) and (31) (see Fig. 12) shows less agreement with theory, probably due to the change in dielectric constant of the material when an external magnetic field is applied. But as illustrated in Fig. 13, the isolation of this prototype is better than 23 dB over two octaves, and better than 15 dB over a bandwidth of 2 to 12 GHz. Insertion loss is less than 2.4 dB in the 2-to-12 GHz range. The bulk lossy material used in this design was based on Eccosorb CR-S-124.

Slot the conductor to suppress moding

In the edge-guide transmission line, the electric and magnetic fields are in the direction of propagation of the wave and are mutually perpendicular. For the components described here, this mode exists only about an octave and a half. The frequency where other modes begin to appear depends, in general, on the saturation magnetization and permittivity of the ferrite, the external magnetic field, the width of the inner conductor and the distance between the ground planes of the edge-guide transmission line.

(continued on p. 54)

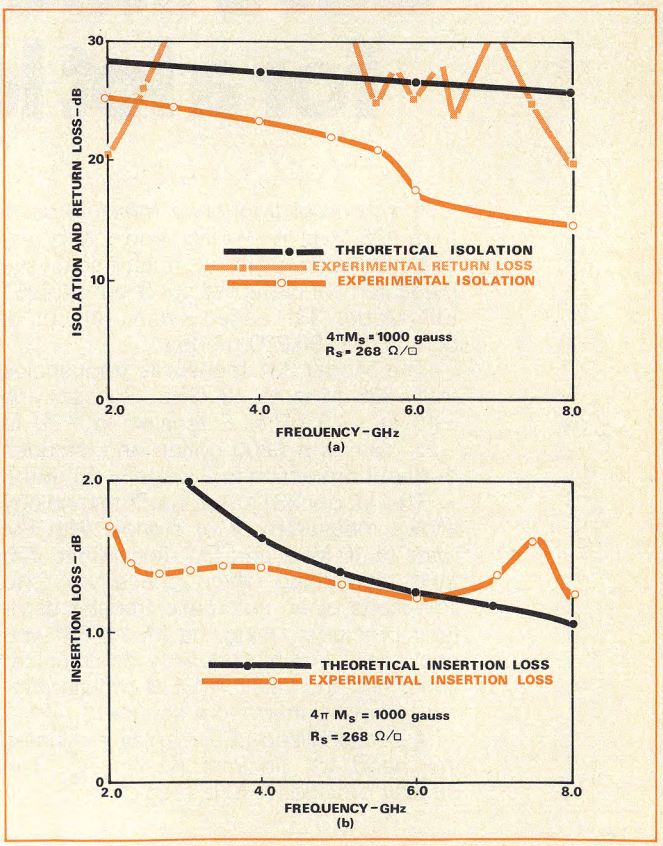

10. Performance of the film-loaded component *agrees quite well with theoretical predictions. Note that data was taken over a two-octave bandwidth.*

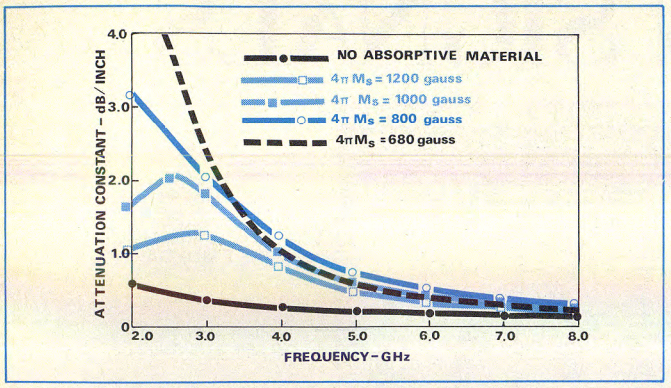

***11. Insertion loss** at the low end of the band increases as ferrites with lower saturated magnetization are used. Data are for bulk-loaded edgeguide.*

Although it must be emphasized that the performance of the edge-guide isolator deteriorates in the region of higher-order mode propagation, these modes can be prevented from forming, and those which do form, can be absorbed. For the normal edge-guide transmission mode, current is in the direction of propagation, but for higher-order modes, current lines also exist perpendicular to the direction of propagation. Therefore, if the outer conductors of this edge-guide transmission line are slotted parallel to the direction of propagation, current flow for the higher order modes will be interrupted, but the current flow for the edge-guide mode will be only slightly affected. In addition, high-loss material can be placed behind the slots to absorb any energy which is set up across the slots to further enhance the frequency of operation.

The outer conductor, in this case, has to be relatively thin so that the slots can be formed by conventional etching techniques. While any suitable number of slots can be used, it has been found that the arrangement shown in Fig. 14 works exceptionally well (see Fig. 15). The slots should be separated from each other by a quarter-wavelength at the highest anticipated operating frequency. The width of the slots for this type of mode suppressor should be made as small as possible. Contemporary etching processes are limited to about 3 mils.

The choice of the proper ferrite, and a corresponding external magnetic bias, are also key parts of both resistive

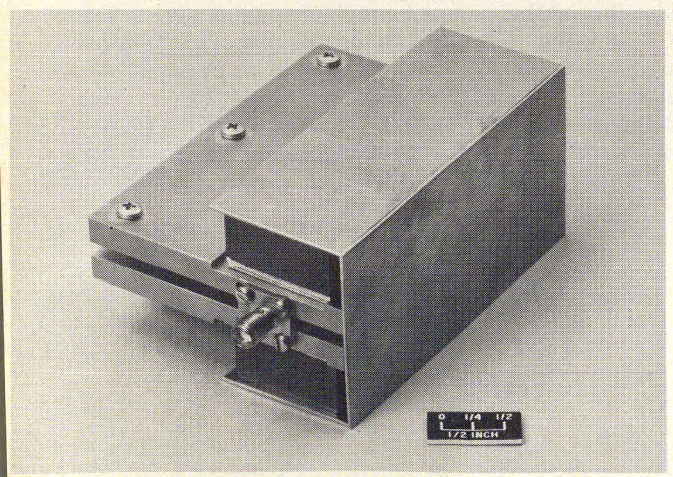

***12. Bulk loading** makes this isolator somewhat larger than its thick-film counterpart.*

film and bulk-loading edge-guide isolator designs. When selecting a ferrite material for an edge-guide isolator, it is necessary to pay attention to both electrical and magnetic characteristics, and particularly to loss behavior as a function of frequency. Magnetic losses in the ferrite may be traced to domain structure and magnetic resonance. To avoid these losses, it is necessary that the saturation magnetization ($4\pi M_s$) be determined so that the following is established:

$$f_{min} = \frac{2}{3}\gamma\,(4\pi M_s + H_a)$$

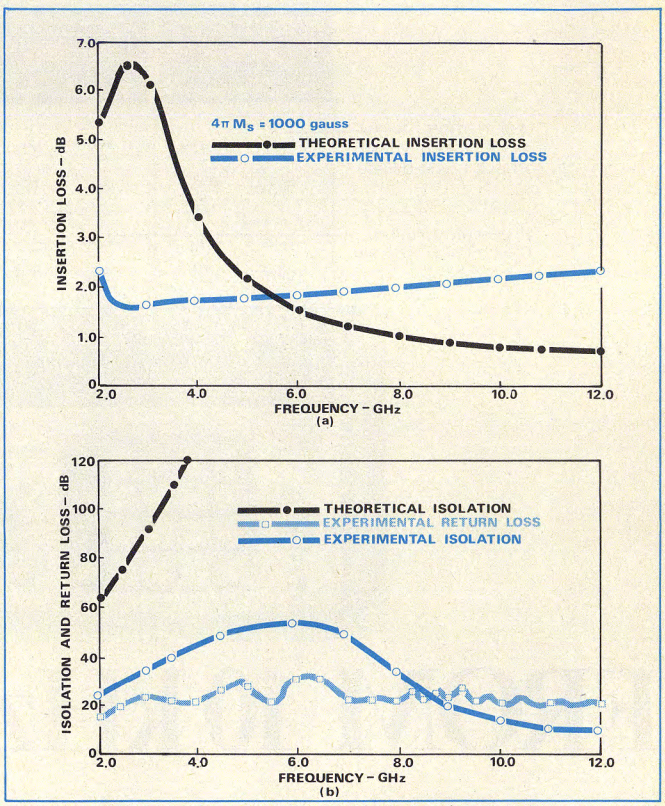

***13. Although larger, the bulk-loaded prototype outperforms** the thick-film design. Data were taken over a two and one-half octave bandwidth.*

where f_{min} = minimum frequency of operation in MHz
γ = gyromagnetic ratio of the ferrite and
H_a = anisotropy field in Oe (32)

Namely, to obtain a low-loss isolator, there is an upper limit of saturation magnetization that can be utilized. For example, for good performance at a minimum frequency of 2 GHz, saturation magnetization should be 970 gauss. The G-1010 material utilized in the both design examples has a saturation magnetization of 1000 (±5 per cent) gauss.

The electromagnetic properties of a ferrite, as described by the Polder permeability tensor[9] and used in the derivation of the edge-guide phenomena, are a function of the bias field and operating frequency. The actual dependence is described in terms of internal magnetic field, H_i. This internal field, in turn, is dependent upon external magnetic field, crystalline imperfections and sample shape.

The effect of crystalline imperfections is designated by the anisotropy field (H_a). Typical value of this field in

polycrystalline ferrites is approximately 100 O_e.

It is difficult to determine the effect of an arbitrary sample shape on the internal magnetic field. The problem is tractable, however, for a small ellipsoidal sample in a uniform magnetic field. Kittel[10] has shown that the microwave problem can be treated in a manner very similar to the static problem of a magnetic particle in a DC magnetic field.

For this case, Osborn[11] has carried out detailed computations for the general ellipsoid and has tabulated the results in terms of demagnetizing factors. The demagnetizing factor arises in the following way: When a homogeneous specimen is placed in a uniform magnetic field, the medium will become polarized. The magnetic dipoles induced on the surface by the applied field will create a component of magnetic field opposing the applied field.

Combining all factors, the internal field is given by

$$H_i = H_{ext} - H_a - N_z{*}4\pi M_s \qquad (33)$$

where $N_z{*}4\pi M_s$ is an opposing internal field due to the presence of the dipoles induced on the surface.

For the plane ferrite configuration where the applied DC magnetic field is perpendicular to the plane, the demagnetizing factor, N_z, is equal to unity.

To establish the non-reciprocal behavior (free of dispersion) and minimize insertion loss, it is merely necessary to provide $H_i = 0$, which results in

$$H_{ext} = 4\pi M_s + H_a \qquad (34)$$

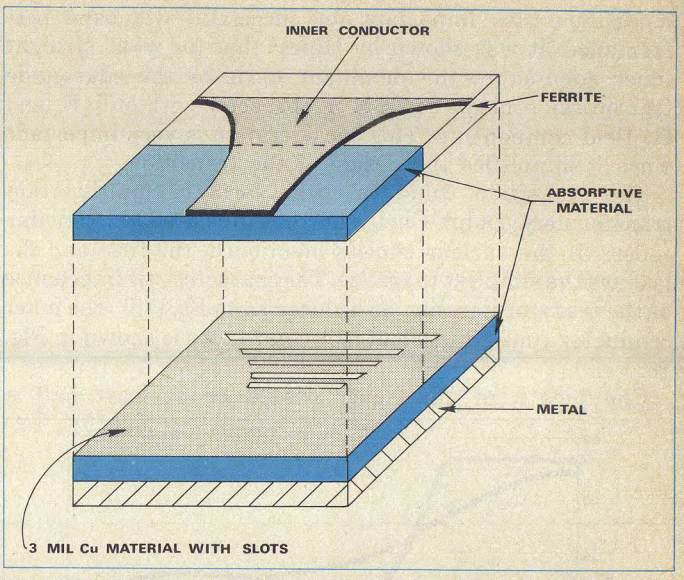

***14. Slots absorb energy** from higher-order modes in this bulk-loaded design.*

The magnetic circuits for the examples presented here were fabricated from Stackpole's A-50 ceramic permanent magnet and Carpenter's high permeability "49" material.

Changing from coax to stripline

Carefully designed transitions from coaxial input and output circuits to the composite edge-guide transmission

(continued on p. 56)

Low Post Tuning Drift from Alpha

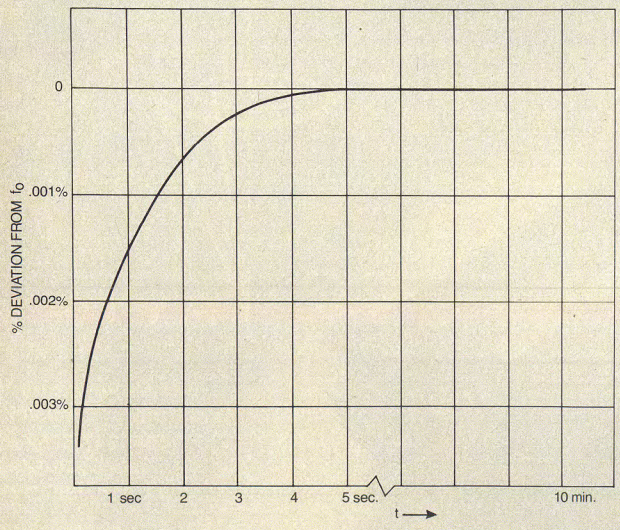

For those critical ECM applications, Alpha has the tuning diode for you! Available as standard or flip chip packaging for low thermal resistance, these diodes feature:

- Low Post Tuning Drift
- Highest Q Available
- Widest range of Capacitance, Voltage, and Package Styles.
- High Stability, Low Leakage
- Meet all Military Standard 750 Requirements

Alpha supplies diodes for many space and hi-rel programs. For more information, write for our data sheets and applications notes or call Frank Leith: x 314.

Alpha

Our limits are your imagination.

ALPHA INDUSTRIES, INC. • 20 Sylvan Road, Woburn, Massachusetts 01801 • (617) 935-5150 • TWX: 710-393-1236 • TELEX 949436

READER SERVICE NUMBER 41

media are also important for successful wideband performance. It was shown by Hines[2] that for wide, straight inner conductors the dominant mode of the edge-guide transmission media is TEM in character with only E_z and H_x field components. This consideration is very important since it simplifies the design of the transition.

The transition could take the form of multi-section transformers, Dolph-Chebyshev, Klopfenstein or a circular taper. Of the various choices mentioned, the first and the last are the simplest to realize. The characteristic impedance of the transformers can be deduced from Eq. (12). The inner conductor configuration of a circular taper is shown in Fig. 16.

The length of this taper should be at least half a

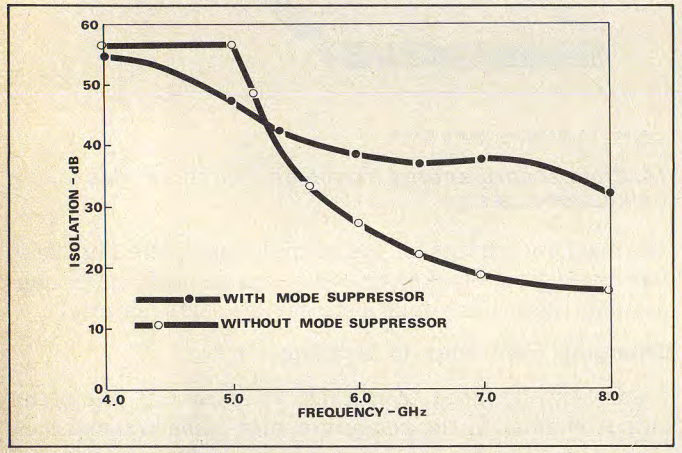

15. Simple mode suppression *levels out the performance of a one-octave design.*

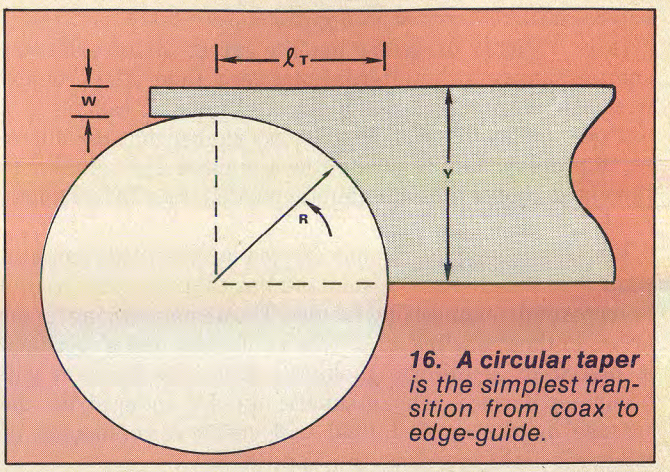

16. A circular taper *is the simplest transition from coax to edge-guide.*

wavelength at the lowest frequency of interest. The radius of this circular taper is given by:

$$R = \frac{Y-W}{2} + \frac{(c/f_{min})^2}{8\epsilon_f\ (Y-W)}$$

where Y - width of the composite media (depends on material, insertion loss and isolation);
W - width of 50-ohm ferrite loaded stripline.••

References

7. A. A. Oliner and L. Goldstone, "Leaky-Wave Antenna," *IRE Trans.*, Vol. AP-7, p. 307 (October, 1959).
8. Emerson and Cuming, Inc., Technical Bulletin 8-2-6.
9. D. Polder, "On the Theory of Ferromagnetic Resonance," *Philosophical Magazine*, Vol. 40, pp. 99-115, (January, 1949).
10. C. Kittel, "Interpretation of Anomalous Larmor Frequencies in Ferromagnetic Resonance Experiment," *Physics Review*, Vol. 71, p. 270, (1947).
11. J. A. Osborn, "Demagnetizing Factors of the General Ellipsoid," *Physics Review*, Vol. 67, p. 351. (1945).

The Multiplexer Problem:

Obtain a Diplexer-Filter to separate or combine the two broadband channels of DC-75 MHz and 2–18 GHz in a package size of 2.5 x 0.63 x 1.0 inches.

The Solution:

Call Filtronics Labs. We've already developed Model F3379, specified as follows—

Passbands:
Input to low band output: DC-75 MHz
Input to high band output: 2–18 GHz

Insertion Loss:
1.5 dB max in passbands

VSWR:
2.0:1 max

Interchannel Isolation:
10 dB min at 200 MHz
30 dB min at 865 MHz
40 dB min from 2–18 GHz

Whatever your filter needs may be—discrete or integrated, bandpass, highpass, lowpass, single or multi-channel, custom or standard—call or write Filtronics for reliable and low cost solutions to your requirements.

Filtronics Laboratories
A Division of
RYT INDUSTRIES
336 Mathew Street
Santa Clara, CA 95050
(408) 247-5750 or
(408) 246-8880
TWX 910-338-0189

Information Retrieval No. 52

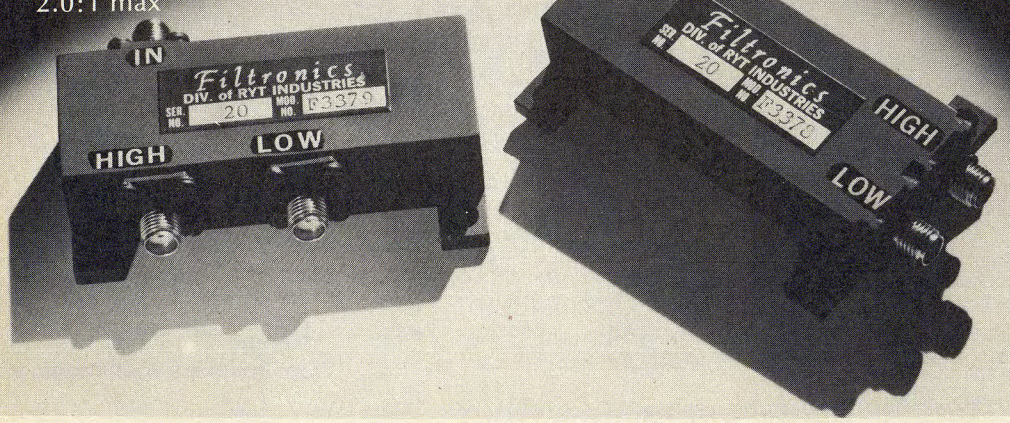

READER SERVICE NUMBER 42

Is Video Leakage Your System Problem?

High-pass filtering is the solution, and don't discount the classic lumped element approach. Distributed designs may look attractive, but a lumped-element circuit performs better over wide bandwidths.

A simple high-pass filter in lumped element form (Fig. 1) is an effective way to improve the video leakage characteristics of many PIN diode switches and attenuators. Uncontrolled, video leakage can raise the spurious signal level in any RF system.

PIN diode control components are normally driven by high-speed pulsed video circuitry that develops large current spikes at the leading and trailing edges of the video pulse. These current spikes are necessary to remove the stored charge associated with the diodes when they are switched from the forward conducting state to reverse bias. As specifications dictate faster switching time, the pulse video circuitry rise and fall times must be decreased, and the amplitude of the current pulses must be increased. The frequency components of the video pulse thus become higher in amplitude and frequency and can extend into the microwave region. Video components can thus show up in the system in many instances as spurious signals with power levels exceeding those of the desired signal.

In the past, system designers have gotten around this problem by allowing sufficient settling time for the video pulse, after switching has occurred. Video leakage levels of 500 mV were frequently tolerated without problem. Today, however, system requirements have tightened up considerably—video leakage of 50, 20 or even 10 mV is typical of present switch requirements. The problem of video leakage can no longer be skirted, but must be faced squarely.

Lee Duter, Engineering Manager, Crown Microwave, 6 Executive Park Drive, North Billerica, MA 01862.

Lumped element designs are best

There are several solutions to the video leakage problem. Component engineers have tried high-pass filtering using distributed or semi-lumped element designs, usually constructed of combinations of quarterwave stubs. These designs generally work well over narrow bandwidths, but tend to be periodic and have holes at higher frequencies where

Diode material influences video leakage

Video leakage can also be controlled by carefully selecting the PIN diode switching element. Minimum video leakage voltage is generated when the video driver pulse is as slow as possible and contains the smallest amount of current spiking necessary to meet the switching speed specification. Taken alone, this would call for the fastest switching material available.

But in most cases, PIN diode material must be selected on the basis of a tradeoff between power handling capability and switching speed. Unfortunately, these two diode characteristics are diametrically opposed.

Three constraints must be satisfied to ensure that the power handling properties of the material are not forsaken for switching speed. First, the reverse breakdown voltage (V_B) must be greater than the sum of peak RF voltage and reverse bias voltage. In practice, however, V_B may be exceeded somewhat if the time response of the PIN material is longer than the duration of the RF period.

The second criteria is the limiting property of the material. Limiting will occur when the peak RF voltage is greater than the reverse bias allowing the RF signal to go into the conduction region of the diode. This value, like reverse breakdown voltage, is a function of the response of the material in relation to the period of the RF. To assure reverse breakdown voltage and limiting values are not exceeded, the diode should be biased at one-half the breakdown voltage and the peak-to-peak voltage value of the RF signal should not exceed the value of the reverse breakdown voltage.

The third criteria is the effective temperature rise of the diode due to RF dissipation in the diode. This must not exceed the manufacturer's specifications.

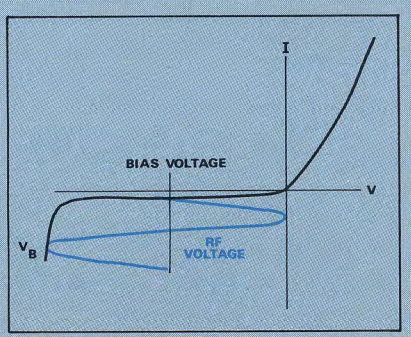

***Peak RF voltage and reverse bias** must both be considered when specifying breakdown voltage.*

Meeting all three power requirements with a minimum amount of tolerance results in a material with the minimum width intrinsic (I) region, and the fastest diode that will handle the desired RF power.

Once the diode material has been selected, three more switching speed optimizations are possible. The diode should be forward biased with a minimum of current, causing a minimum of stored charge, which will need a minimum amplitude current spike for removal. Second, the amplitude of the video driver current spike should be set at the minimum value that will give the desired switching speed. Third, the rise time of the video driver pulse should be as slow as possible and still meet the switching speed requirement. This will reduce the high frequency components of the video signal.••

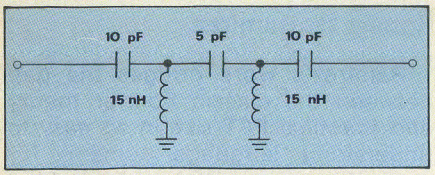

1. A five-element high-pass filter *in lumped-element form can significantly reduce video leakage.*

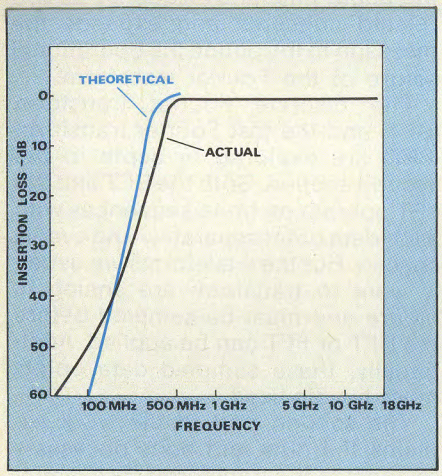

2. Performance *of the five-element Chebyshev filter is close to theory.*

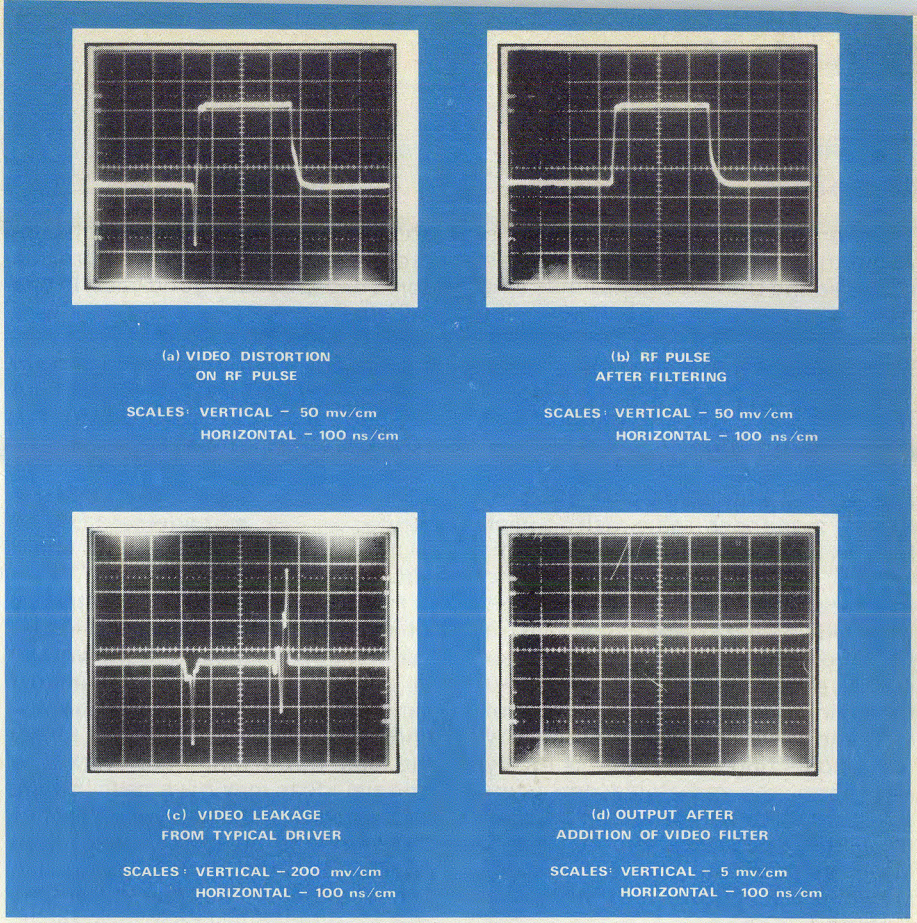

3. Oscilloscope photographs demonstrate the improvement *in performance of a 20 ns switch operating at 2 GHz after the addition of a high-pass filter.*

the stub lengths approach half wavelengths or multiples of half wavelengths.

A better solution is the use of lumped element high pass video filters. Many engineers have abandoned the use of lumped element designs at frequencies above 100 MHz, where the physical size of these elements approach a significant fraction of a wavelength. But in certain applications, these elements can be used successfully to 18 GHz. Microwave switch manufacturers, for example, have long been aware that lumped elements can be successfully used as biasing circuits for microwave switches with bandwidths that extend beyond 18 GHz.

The design of lumped-element filters is well documented, and it would serve no purpose to reproduce the classic equations and tables here. To outline the basic procedure, the amplitude and frequency of the video leakage present in the RF system is first determined by simple measurements with an oscilloscope or spectrum analyzer. The amplitude and frequency of the required filter rejection can then be determined from system requirements. Cutoff frequency and the number of filter elements required to attain the proper rejection are found using Chebyshev filter characteristics. Perhaps the best reference on this subject is "Microwave Filters, Impedance-Matching Networks and Coupling Structures," by Matthaei, Young and Jones.

The following results are for a lumped five-element, high-pass Chebyschev filter designed following the procedure outlined above. Using the cutoff frequency of 420 MHz, 50-ohm impedance and 0.01 dB ripple, the following elements were determined: C_1 = 9.93 pF, C_2 = 14.52 nH, C_3 = 4.8 pF, L_4 = 14.52 nH and C_5 = 9.93 pF. With the components available, a high pass filter (Fig. 1) was constructed using lumped elements on microstrip transmission line. The unit was packaged in a small microwave housing with SMA connectors. The resulting response, shown in Fig. 2, agrees very well with the theoretical response. The insertion loss measured in the above filter ranges from approximately 0.5 dB at 500 MHz to 0.8 dB at 12 GHz and 1.1 dB at 18 GHz. This insertion loss would, however, be reduced significantly if the filter is integrated into a microwave switch as the transmission line losses and connector loss would be removed. The only additional loss would then be the loss of the five filter elements themselves.

Improving a 2 GHz switch

The photographs in Fig. 3 show the results obtained when the above filter is used in series with a 20 ns switch operating at 2 GHz. Figure 3(a) shows the distortion present on the leading and trailing edges of the pulse caused by the video driving circuitry. Figure 3(b) shows the same detected RF pulse after passing through the high-pass video filter with the distortion removed.

A more graphic example of the results of the filtering are shown in the second set of photographs. Figure 3(c) shows the video leakage displayed on an oscilloscope, with the video leakage present on the leading and trailing edges of the pulse. From a typical fast switch driver, the spikes are approximately 600mV in amplitude. The second photo, Fig. 3(d) is with the filter in series with the switch output. As seen in the photographs, the video signal has been reduced by about 600 to 1 and the final video signal is less than 1 mV across 50 ohms. This response can be improved by the addition of more elements in the filter if necessary, at the expense of some increase in insertion loss. It is also possible to integrate the high-pass video filter into any switch with only a slight increase in insertion loss.••

bookshelf

Big Ear

John Kraus

Cover blurbs claim, "Big Ear is about the Ohio Telescope, how it has explored the Universe to its limits and now searches for intelligent life beyond Mars." But like the heavens it promises to explore, the book's treatment of radio astronomy is largely a dark void sprinkled with bright bits of information.

Contrary to cover descriptions, Big Ear is the autobiography of John Kraus, a pioneer radio astronomer long associated with Ohio State University. Actually only about half the book deals with Kraus' involvement with OSUs giant radiotelescope—a behemoth receiving system that occupies a good part of 20 acres and relies on a parabolic section 360 feet long and 70 feet high to reflect energy to its collecting horn. What is finally said about the radiotelescope is interesting and entertaining. Kraus traces the successes and failures of the project in an informal, almost conversational style. It's rather like reading a long letter that the author has written to a close friend.

Be prepared to wade through a long, rambling account of the author's experiences in the early days of radio before encountering the Big Ear, as the OSU observatory is called. But as the saying goes, getting there can be half the fun. Anecdotes liven up the early stages of the book, and again the conversational style is very effective. The years spent at Naval Ordnance Laboratory in Washington and at Harvard's Radio Research Laboratory during World War II provide some exceptionally good tales. In one unusual account, a wood and wire jammer antenna atop the RRL building caught fire due to the high level of RF power pumped to it. Cambridge firemen quickly responded to the scene, but ran into a barrier of red tape as they attempted to enter the high security area. The antenna burned as RRL management fiddled around trying to get security clearance for the firefighters.

History is replete with instances where two individuals in different locations have independently invented or discovered the same thing almost simultaneously. But consider the psychological letdown that must follow the bad news that hard work and original ideas may have been in vain. In a moving account, Kraus relates the emotions he experienced upon learning that the circularly polarized helical antenna he had developed had simultaneously been invented by Harold A. Wheeler.

Read the book if you would like to learn more about the life and times of John Kraus, and the developments in RF applications that paralleled his distinguished career.

However, if you are looking for a concentrated discussion of radio astronomy, look elsewhere. (222 pp; $2.95). **Cygnus-Quasar Books, P. O. Box 85, Powell, OH 43065.**

The FFT: Fundamentals and Concepts

Robert W. Ramirez

Ramirez's work bridges the gap between the classic Fourier theory and practical FFT use in an easy to understand language suitable for many disciplines. He has divided the work into two sections. The first, tackling basic time and frequency relationships, gets the reader thinking about time and frequency as two related concepts and expands the message to introduce the operational nature of the Fourier transform.

The discrete Fourier transform (DFT) and the fast Fourier transform (FFT) are explored in depth in the second section. Both the DFT and the FFT operate on finite sequences with each data point separately and evenly spaced. But the waveforms we usually want to transform are analog in nature and must be sampled before the DFT or FFT can be applied. Additionally, these sampled data points must be digitized.

The second part of the work explains the nuts and bolts necessary to apply to the transforms by examining the two basic concepts of analog-to-digital conversion, windowing and sampling. Once these operations are understood, the power of FFT becomes obvious.

The concluding chapters are dedicated to applications. More than 90 major illustrations make the book easily readable. (141 pp; $25; part number 070-1754-00). **Tektronix, Inc., P. O. Box 500, Beaverton, OR 97077.**

feedback

Missing copy department

To the editor:

The article by Anthony Paolantonio, "A Hybrid Ring You Can Build Yourself," appearing on p. 50 of the December issue, appears to have encountered a bit of sloppy cutting and pasting. Can you provide a copy which includes the referenced Eqs. (7) and (8), and any other material which appears to be missing? The problem appears to start right after Eq. (3).

Albert E. Hayes, Jr., Ph. D.
Fullerton, CA

Mr. Hayes was one of many alert readers who brought this error to our attention. Our apologies go out to all readers for the confusion caused by this misprint, and especially to Mr. Paolantonio. The following block of text was inadvertently omitted after Eq. (3) on page 54:

"The equation for the characteristic impedance of a twin-lead transmission line, as shown in cross-section C-C in Fig. 4, is:

$$Z_{OT} \approx \frac{276}{\sqrt{\epsilon}} \log_{10} \left\{ \left(\frac{2h}{d} \right) \left[\frac{1 - \left(\frac{h}{D} \right)^2}{1 + \left(\frac{h}{D} \right)^2} \right] \right\} \quad (4)$$

In order to produce a symmetrical, four-port hybrid ring, the characteristic impedance of all four arms must be a constant. Hence, it follows that:

$$Z_{OC} = Z_{OT} = Z_O \sqrt{\epsilon} \quad (5)$$

Let Eq. (1) be equal to Eq. (4) and solve for the optimum impedance of the transmission lines, Z_O, and the ratios D/d and h/d; hence:

$$Z_O = \frac{75.2}{\sqrt{\epsilon}} \text{ ohms} \quad (6)$$

$$\frac{D}{d} = 3.51 \quad (7)$$

$$\frac{h}{d} = 1.125 \quad (8)$$

Where ϵ is the dielectric constant of the insulating material inside the transmission lines."

MARCH
1977

MICROWAVES

laser technology

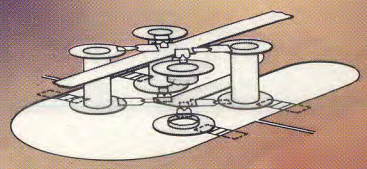

Trends in Front-End Design

- Thin-film Mixers Team Up To Block Out Image Noise
- BASIC Computer Algorithm Spots Spurious Responses
- Low-cost Detector Design Is Ideal For RF Monitors
- Is There A Josephson Junction In Your Future?

Also: PNP Transistor Works To 2 GHz

Defense Spending On The Rise

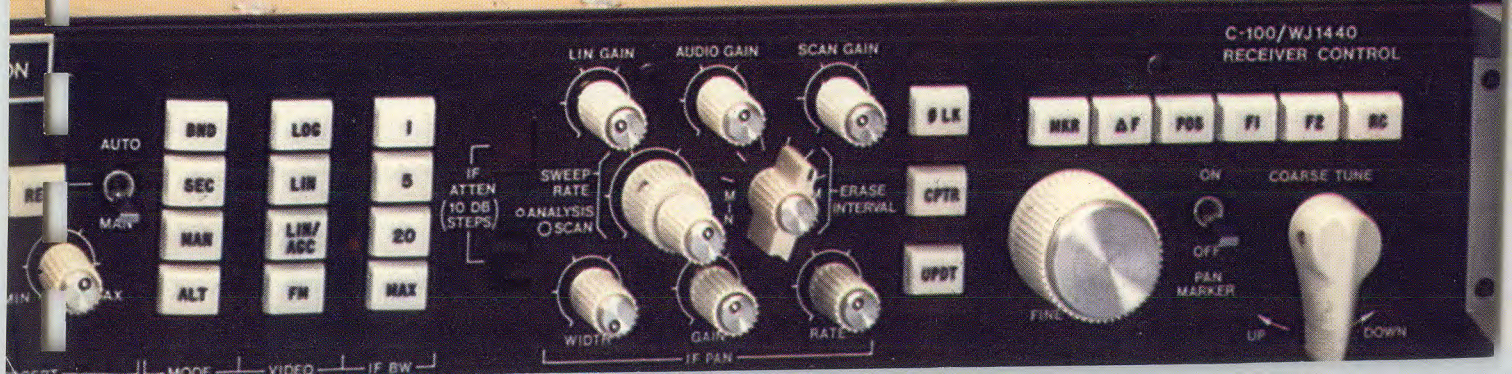

MICROWAVES

March 1977
Vol. 16, No. 3

news

9 **PNP bipolar transistor developed for high-speed complementary amplifier**

10 **Defense funding dominates FY 78 budget**

12 **FCC urged to allocate "communicasting" service frequencies**

14 **Western Union tapped for $796M satcom program**

Satellite links two radio observatories

16 **Industry**
19 **Washington**
24 **International**
26 **R & D**
28 **Meetings**
32 **For Your Personal Interest...**

editorial

30 **RF activities threatened by realignments at NBS**

technical

Trends in Front-Ends

34 **Thin-Film Mixers Team Up To Block Out Image Noise.** James B. Cochrane and Ferenc A. Marki of Watkins-Johnson Co., illustrate how a thin-film approach permits mixer pairs to be closely matched to build channelizer assemblies. Image can be easily separated from signal while intermod products are remixed for lower loss.

42 **BASIC Computer Algorithm Spots Spurious Responses.** Raymond P. Meixner of the Naval Research Laboratory, presents a computer program written in BASIC to predict the spurious response of a mixer/filter combination. Design examples compare single-ended, single-balanced and double-balanced mixer performance in a superheterodyne receiver.

50 **Is There A Josephson Junction In Your Future?** Roger Davidheiser of TRW Systems, provides an application-oriented introduction to the Josephson junction—a superconducting device with a wide range of microwave possibilities.

58 **Low-Cost Detector Design Is Ideal For RF Monitors.** Arthur Karp of Stanford Research Institute, shows how to combine two inexpensive axial-lead diodes to construct a detector with 200 mV/mW sensitivity.

62 **Active Circuits Keep Systems On The Level.** Jerry Hausner of The Narda Microwave Corp., compares open and closed-loop leveler designs, focusing on the active, closed-loop circuit for detailed analysis.

departments

72 **New Products**
86 **New Literature**
88 **Application Notes**
91 **Feedback**
92 **Catalog Update**
98 **Bookshelf**
99 **Advertisers' Index**
100 **Product Index**

About the cover: Thin-film circuit design allows mixers to be closely matched in terms of phase and amplitude. The result: channelizer assemblies to separate image and signal frequencies. Story begins on p. 34. (Cover artwork courtesy Watkins-Johnson Co.;composition by Art Director Robert Meehan).

coming next month: Test and Measurement

Speed Amplifier Testing With Swept Gain-Compression Measurements. Gain-compression measurement, traditionally a point-by-point process, becomes particularly tedious and time-consuming with today's ultra-broadband amplifiers. Here's how to update these tests using swept-frequency measurements.

Swept Measurement Accuracy Hinges On Coupler Design. Researchers from the Swiss Post Office show how to build waveguide couplers with 50-dB directivity, allowing simple measurement setups to handle complex chores.

Measure Complex Dielectric Constants Quickly. Developed in the Soviet Union, this method of measuring the complex dielectric constant of low-permittivity materials is presented to a Western audience for the first time.

PLUS: ON THE SCENE COVERAGE OF THE INTERNATIONAL SOLID-STATE CIRCUITS CONFERENCE.

Publisher
Howard Bierman

Editor-in-Chief
Stacy V. Bearse

Associate Editor
Frank G. Lynn

Contributing Editor
George R. Davis

Washington Editor
Paul Harris
Snyder Associates
1050 Potomac St. NW
Washington, DC 20007
(202) 965-3700

Editorial Assistant
Gail Murphy

Production Editor
Sherry Lynne Karpen

Art Director
Robert Meehan

Production
Dollie S. Viebig, Mgr.
Anne Molfetas

Circulation
Barbara Freundlich, Dir.
Sherry Karpen,
Reader Service

Directory Coordinator
Janice Tapp

Editorial Office
50 Essex St.,
Rochelle Park, NJ 07662
Phone (201) 843-0550
TWX 710-990-5071

A Hayden Publication
James S. Mulholland, Jr.,
President

MICROWAVES is sent free to individuals actively engaged in microwave work. Prices for non-qualified subscribers:

	1 Yr.	2 Yr.	3 Yr.	Single Copy
U.S.	$25	$40	$ 60	$3.00
Foreign	$40	$70	$100	$4.00

Additional Product Data Directory reference issue, $15.00 each (U.S), $27.00, (Foreign). POSTMASTER, please send Form 3579 to Fulfillment Manager, MicroWaves, P.O. Box 13801, Philadelphia, PA. 19101.

Back Issues of MicroWaves are available on microfilm, microfiche, 16mm or 35mm roll film. They can be ordered from Xerox University Microfilms, 300 North Zeeb Road, Ann Arbor, MI 48106. For immediate information, call (313) 761-4700.

Hayden Publishing Co., Inc., James S. Mulholland, President, printed at Brown Printing Co., Inc., Waseca, MN.

Copyright © 1977 Hayden Publishing Co., Inc., all rights reserved.

Thin-Film Mixers Team Up To Block Out Image Noise

Thin-film manufacturing techniques permit mixer pairs to be closely matched. Image can be easily separated from signal in a channelizer assembly, while intermod products are remixed for lower loss.

WHILE the goal of the digital world has been to put an entire computer system on a single semiconductor chip for fast, low-cost information processing, the goal of many RF designers has been to develop a low-cost, miniature microwave receiver that is impervious to local interference, yet has the sensitivity to receive the weakest of transmitted signals.

Designers have rightfully focused their attention on the receiver front-end to achieve this goal. It is here, in the first conversion stage, that most of the cost is incurred. And, it is here that the sensitivity, dynamic range and maximum bandwidth of the receiver is normally established. Poor reception of a distant TV station, high noise level on a long-distance telephone call or the inability to display a low-level signal on a spectrum analyzer all represent first conversion stage limitations. Future receiver performance improvements must come from new and better RF amplifiers, filters and mixers used in the microwave front-end.

Performance improvements noted

The role of the amplifier in the front end is generally to establish the noise figure, and provide enough gain to effectively mask the noise figure of the mixer and its associated IF amplifiers. The past five years have seen a strong emphasis on the GaAs FET amplifier to perform this task, and the reward has justified the investment. Noise figures at 10 GHz have plummeted from 8 dB in 1971[1] to under 3.5 dB in 1976, and are continuing to drop at a rather amazing rate as 0.5-micron devices become available (see Fig. 1).

James B. Cochrane, Manager, Relcom Dept., and **Ferenc A. Marki,** Component Section Head, R & D Dept., Watkins-Johnson Company, 3333 Hillview Avenue, Palo Alto, CA 94304.

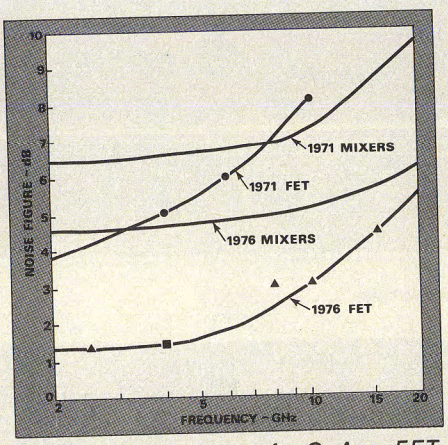

***1. Noise figures** of GaAs FET amplifiers and double-balanced mixers have improved drastically from 1971 to 1976. Triangles represent lab measurements on W-J amplifiers; box represents an NEC amplifier.*

When maximum dynamic range is required, however, it is often necessary to limit the amplifier's role or bypass it entirely and feed the received signal directly to the first mixer stage. The upper limit on dynamic range is set by the maximum input level at which linearity is preserved and nonlinear by-products, such as intermodulation signals, are held below the tangential noise level of the mixer's IF bandwidth. Thus, in most applications, there is a critical balance between RF amplifier gain and the RF input level to the mixer. In many of these applications, the burden of improved front-end performance falls on the mixer.

In the past five years, substantial progress has been made in improving the noise figure and dynamic range of microwave mixers. Higher turn-on Schottky-barrier diodes with lower series resistance and total capacitance have raised the compression point of the components, and permitted higher frequency operation. Microwave ring quads (four Schottky-barrier diodes on a monolithic substrate) have permitted designers to switch from single-balanced to double-balanced circuits without additional loss, and with the extra benefit of superior even-order harmonic suppression. Improved diodes and better matching circuits have also significantly lowered noise figures (see Fig. 1). In 1971, a mixer with 8 to 10 dB conversion loss was considered good for a double-balanced mixer in Ku-band[1]. Now, 6 to 6.5 dB is common for the same type of mixer.

Isolation has also improved dramatically. A mixer with 15-dB of LO-to-signal isolation was once considered good for a Ku-band component. Now, isolation of 30 dB is commercially available resulting in additional suppression of all even harmonics and intermodulation products at the IF port. VSWRs of double-balanced mixers have also improved from greater than 3:1 to under 2:1.

Many of these performance improvements can be traced to developments in semiconductor technology. However, refinements in thin-film circuit design have also played an important role and will continue to do so, particularly with the application of thin-film processing to mixer design. Using thin-film techniques, volume production at low-cost is a real possibility: once the original mask is cut, making a hundred copies is relatively simple. But most important, the reproducibility inherent in the thin-film manufacturing process results in units that are closely matched in terms of their electrical performance. This advantage can be put to good use in overcoming major problems in front-end design—the image frequency, image noise and noise figure.

Is it real, or an image?

A common problem for wide open ECM receivers is to differentiate be-

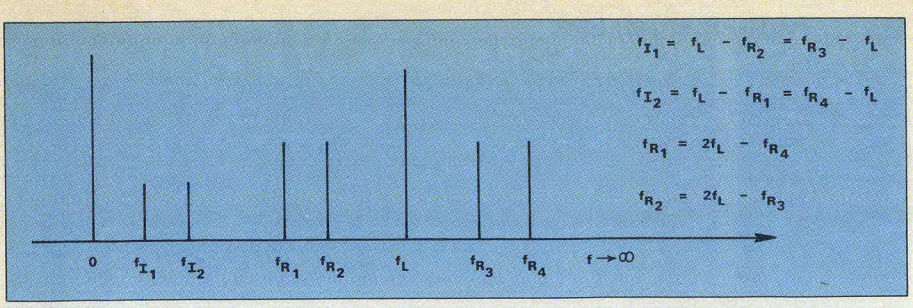

2. Image frequency *can easily be confused with a true input. For example: if f_{R1} is a desired input signal frequency, then f_{R4} is the image frequency. If f_{R4} is a desired input, then f_{R1} is its image. Likewise, if f_{R1} to f_{R2} is a desired input signal band, then an image noise band extends from f_{R3} to f_{R4}.*

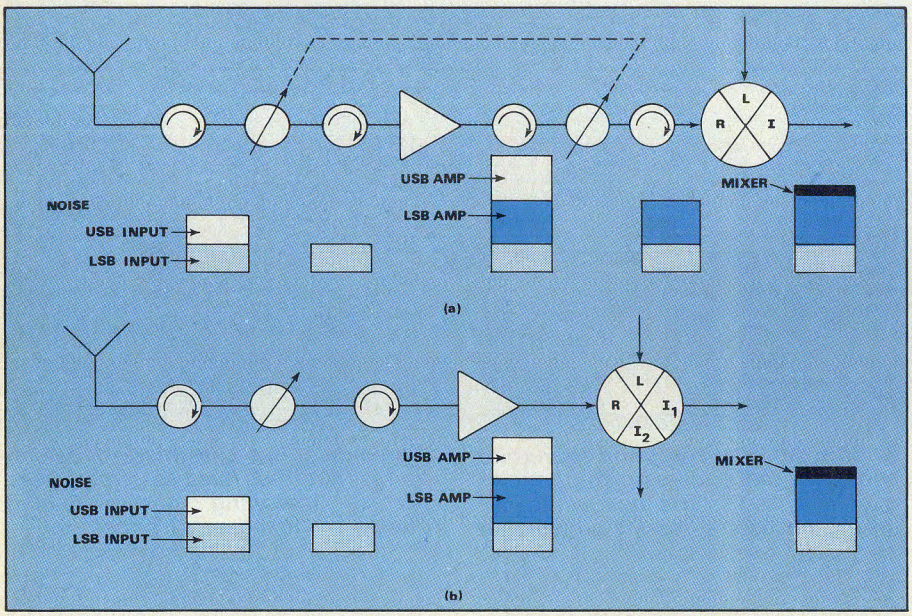

3. A normal superheterodyne front end (a) *requires tracking filters before and after the RF amplifier to suppress image noise. A design using an image channeled mixer (b) requires a simpler, smaller, less expensive tracking filter and eliminates two isolators. Amplifier image noise is channeled through port I_2, while desired IF is taken from I_1.*

tween a signal of interest and its image. The image is an input signal at a frequency that is offset from the local oscillator frequency by the intermediate frequency. Thus, on a frequency scale, it appears as the mirror *image* of the signal of interest, reflected on the opposite side of the local oscillator line (see Fig. 2). If the LO signal is sweeping, the problem is compounded, since there is always the question of whether the detected signal is on the high or low side of the LO frequency line. A receiver operator must know whether he is analyzing a real signal or its image before direction finding and frequency detection techniques can be initiated.

In narrow-band communication receivers, the obvious solution to the image problem is to insert a filter in front of the mixer. However, when the RF bandwidth stretches across several octaves only an electronically controlled preselector, such as a YIG filter[2], can be used to differentiate the image frequency. But in addition to being relatively expensive, these filters increase the receiver's noise figure and offer rather sluggish tuning speeds, making it difficult to continuously monitor frequency agile radar signals.

Perhaps the cleanest solution to the image problem is to design a mixer that inherently separates image and real frequencies. These image channelizers, although used sparingly in the past as first-stage converters, will doubtlessly play an important role in the wideband receiver of the future. The benefits of an image channelized mixer are twofold: they help a receiver operator identify whether a signal is a true threat signal or its image, and they can be used to reduce the image noise generated by an RF amplifier.

Channelization, typically 15 to 30 dB, is obtained using a pair of balanced mixers, two 90-degree quadrature hybrids, and an in-phase power divider (see "How the sideband channelizer works", p. 38). The RF input signal is split by a quadrature hybrid and fed into the two balanced mixers; the phase difference between mixer inputs is 90 degrees. The LO signal is also split, but by an in-phase power divider. Hence, both mixers are driven in phase. IF outputs are fed into a second quadrature hybrid. The down-converted image output is channeled to one IF output port, and the desired output is channeled to a second IF output port.

Image channelizing mixers, or simply sideband channelizers, are generally four-port assemblies: LO and RF inputs in addition to two IF outputs designated I_1 and I_2. The lower sideband is normally downconverted to the I_1 port, while the upper sideband is accessible at the I_2 port.

The channelizers can eliminate several expensive, lossy components in a receiver front-end, including the tracking pre-selector that normally follows an RF preamplifier. In most superheterodyne applications, the filter is necessary since the RF amplifier adds noise to both upper and lower sidebands (i.e., at real and image frequencies). Since a standard mixer cannot distinguish between the real and the image frequency or identify the sidebands, an additional 3 dB of noise is added to the system total noise figure.

With the image channelized mixer, image noise is effectively separated from the signal of interest by the output quadrature hybrid. Furthermore, since the RF input also uses a quadrature hybrid, input VSWR can be less than 1.5:1, and the isolator normally required between RF amplifier and mixer is often eliminated (see Fig. 3).

Matched components necessary

The concept of an image channelizing mixer is certainly attractive, but why has it not been more fully exploited? Part of the problem is that to obtain good image channelization, the two mixer channels must be extremely well matched. As Fig. 4 illustrates, image cancellation of 20 dB requires phase unbalance under 10 degrees and amplitude unbalance under 1.0 dB[3]. Image cancellation of 30 dB calls for phase unbalance to be under 3 degrees

(continued on p. 36)

and amplitude unbalance under 0.3 dB. In the lower microwave bands, rejection of 20 dB has been obtained using LO trimmers and painstaking matching and tweaking with the help of an automatic network analyzer. As frequency increases, however, matching becomes extremely difficult. At 18 GHz, for example, 10 degrees is equal to a line length of only 16 mils on Teflon dielectric, hardly the type of match that would be easy if the component had interconnecting transistions or required trimming.

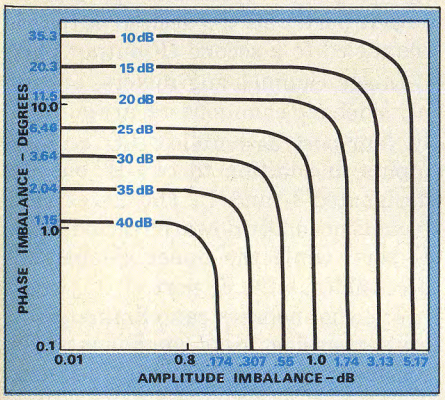

***4. Image cancellation** relies on phase and amplitude balance, as shown by this family of constant cancellation contours.*

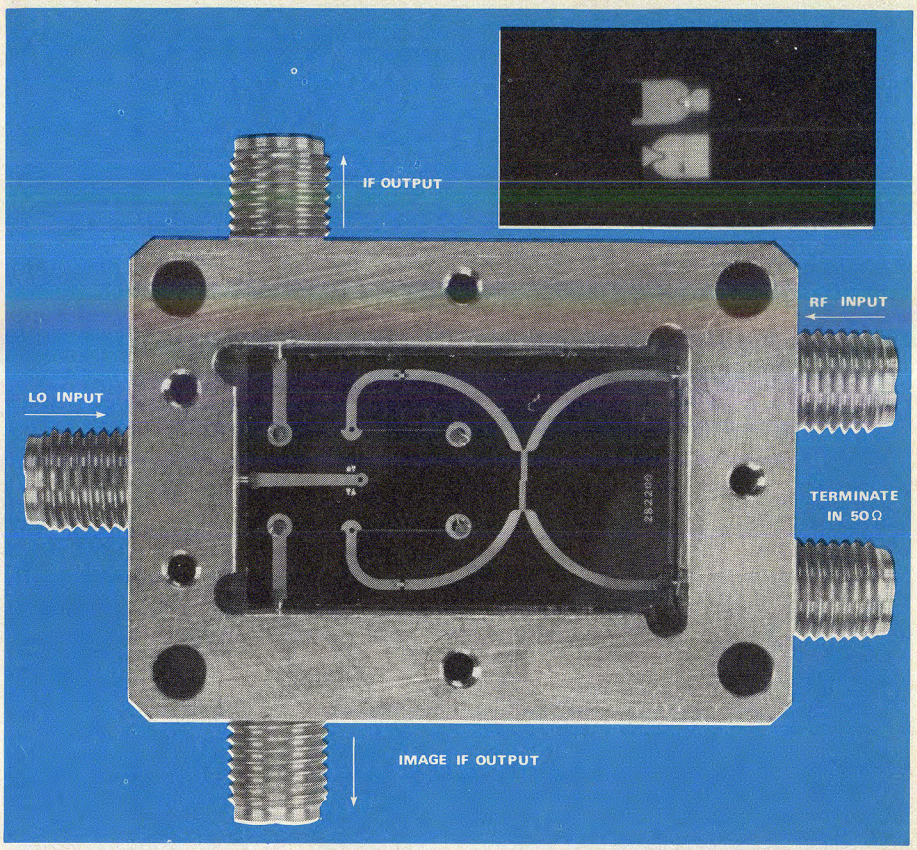

***5. This thin-film sideband channeler** separates real and image frequencies over a 7 to 18 GHz bandwidth. RF input port used depends on whether high-side or low-side image cancellation is required. Inset illustrates near perfect matching of beam-lead diodes on fused-silica substrate.*

For accuracies of this nature, the entire RF circuit must be realized on a single substrate using thin-film technology. Furthermore, a good impedance match to the ribbon of the beam-lead diode or blocking capacitor is necessary to reduce component and circuit interactions.

A good example of the thin-film fabrication techniques necessary for sideband channelizer design is shown in Fig. 5. Two virtually identical single-balanced mixers on one substrate provide image channelization of 22 to 30 dB and a noise figure of less than 7.3 dB across a full 7 to 18 GHz frequency band. The entire assembly occupies only 0.84 cubic inches.

Channelization is achieved by routing the RF input signal into a 90-degree Lange coupler, transforming it to microstrip by a sputtered-through via and applying it to the diodes from an unbalanced single coplanar line. The LO input signal is applied to the diodes through a slot line. Equal unbalanced RF signals feed the diodes from two RF coplanar lines and equal balanced LO signals feed the diodes from a slot line.

The IF signals are diplexed, routed to the basement of the subassembly by sputtered-through vias and fed into a conventional low-frequency quadrature hybrid.

Fused silica was chosen as the substrate material because of its low dielectric constant ($\epsilon_r = 3.8$) allowing the fabrication of higher impedance lines[4]. The reward is a better impedance match with beam lead diodes and capacitors that commonly require a 0.010-inch width conductor for attachment. By eliminating the lead of the diode or capacitor as a potential mismatch source, phase discontinuities are limited to the dimensional variance of the device itself. Figure 5 also illustrates how a pair of Schottky barrier diodes can be integrated into the circuit with minimum mismatch. In conjunction with the lower propagation constant for fused silica, uncontrolled beam-lead lengths were reduced from 42 degrees for an alumina substrate to 9.5 degrees for a fused silica substrate at 18 GHz.

The amplitude and phase tracking potential of such an approach is exciting. The measured phase differential of the two mixers is less than 5.5 degrees and the amplitude differential is less than 0.5 dB across a 7 to 18 GHz bandwidth. From the plot in Fig. 4, a potential image channelization of 25 dB is possible with phase imbalance being the dominant factor. If through diode matching, the phase balance

(continued on p. 38)

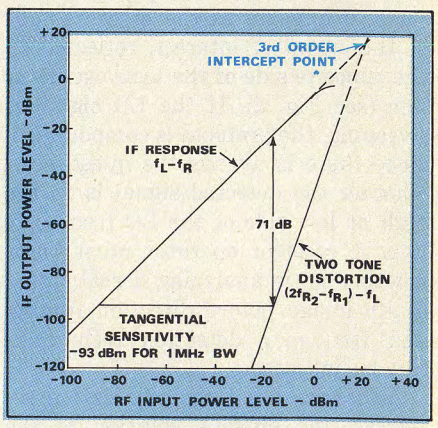

***6. Distortion-free dynamic range** depends on input level and IF bandwidth selected.*

How the sideband channelizer works

In its simplest form, the sideband channelizer is built with two single-ended (one diode) mixers using a resistive power divider (see circuit (a) in Fig. A1). Each diode (mixer) can be modeled as a current generator that obeys:

$$I(\omega_L t,\ \omega_R t) = G(\omega_L t)\ V(\omega_R t)$$

where $G(\omega_L t)$ is the diode conductance waveform and $V(\omega_R t)$ is the small signal voltage waveform that appears across the diode. It should be noted that the LO power level is much greater than the signal power level. This is then a small signal analysis.

Let us expand the functions, $G(\omega_L t)$, $V(\omega_R t)$, and $I(\omega_L t,\omega_R t)$, in the form:

$$f(x) = \sum_{n=-\infty}^{\infty} C_n\, e^{jnx} \qquad C_{-n} = \frac{1}{2}(a_n + jb_n),\ n>0$$

$$C_n = \frac{1}{2}(a_n - jb_n) \qquad C_o = \frac{1}{2}a_o$$

Then, the conductance waveform is:

$$G(\omega_L t) = \sum_{n=-\infty}^{\infty} g_n\, e^{jn\omega_L t},$$

the voltage waveform is:

$$V(\omega_R t) = \sum_{m=-\infty}^{\infty} v_m\, e^{jm\omega_R t},$$

and the diode current waveform is:

$$I(\omega_L t,\ \omega_R t) = \sum_{n=-\infty}^{\infty} g_n\, e^{jn\omega_L t} \cdot \sum_{m=-\infty}^{\infty} v_m\, e^{jm\omega_R t}$$

$$I(\omega_L t,\omega_R t) = \sum_{n,m=-\infty}^{\infty} g_n\, v_m \left\{ e^{j(n\omega_L t+m\omega_R t)} \right\}.$$

In the frequency domain,

$$F_D(f_L,f_R) = \sum_{n,m=-\infty}^{+\infty} (nf_L + mf_R)$$

$$F_D(f_L,f_R) = \sum_{\substack{nxm=\text{positive}\\ n,m=-\infty}}^{\infty} (nf_L + mf_R) + \sum_{\substack{nxm=\text{negative}\\ n,m=-\infty}}^{\infty} (nf_L + mf_R)$$

$$F_D\ (\text{sum frequencies}) = \sum_{\substack{nxm=\text{positive}\\ n,m=-\infty}}^{\infty} (nf_L + mf_R)$$

$$F_D\ (\text{diff. frequencies}) = \sum_{\substack{nxm=\text{negative}\\ n,m=-\infty}}^{\infty} (nf_L + mf_R)$$

$$I_1'\ (\omega_L t,\omega_R t) = \sum_{n,m=-\infty}^{\infty} g_n\, v_m \left\{ e^{j(n\omega_L t+m\omega_R t)} \right\}$$

$$I_2'\ (\omega_L t+\pi/2) = \sum_{n,m=-\infty}^{\infty} g_n\, v_m \left\{ e^{j(n\omega_L t+m\omega_R t+n\pi/2)} \right\}$$

Now, concentrate on the difference frequencies:

$$I_1(\omega_L t,\omega_R t) = \sum_{\substack{nxm=\text{negative}\\ n,m=-\infty}}^{\infty}$$

$$g_n\, v_m \left\{ e^{j(n\omega_L t+m\omega_R t)} + e^{j(n\omega_L t+m\omega_R t+n\pi/2+\pi/2)} \right\}$$

$$I_2(\omega_L t,\omega_R t) = \sum_{\substack{nxm=\text{negative}\\ n,m=-\infty}}^{\infty}$$

$$g_n\, v_m \left\{ e^{j(n\omega_L t+m\omega_R t+n\pi/2)} + e^{j(n\omega_L t+m\omega_R t+\pi/2)} \right\}$$

If the analysis is limited to positive IF frequencies (f_I), these equations can be solved for upper and lower sideband downconversion. For lower sideband downconversion, n = 1 and m = −1:

$$I_1(\omega_L t,\omega_R t) = 0 \rightarrow \text{Cancellation}$$

$$I_2(\omega_L t,\omega_R t) = 2g_1\, v_{-1}\, e^{j(\omega_L t-\omega_R t+\pi/2)} \rightarrow \text{Addition}$$

For upper sideband downconversion, n = −1 and m = 1:

$$I_1(\omega_L t,\omega_R t) = 2g_{-1}\, v_1\, e^{j(\omega_R t-\omega_L t)} \rightarrow \text{Addition}$$

$$I_2(\omega_L t,\omega_R t) = 0 \rightarrow \text{Cancellation}$$

Relating these results to Fig. A1, it can be seen that input frequencies above and below the LO frequency are effectively separated into two IF channels.

Expanding the analysis to the case of a double-balanced mixer reveals why the pseudo-image must be terminated by a short circuit at the RF port of the mixer. Assume that the double-balanced mixer in Fig. A2 forms half of the image-reject channelizer (circuit 1 (b) in Fig. A1). The currents flowing through the branches of the ring-type mixer are described by:

$$i_1 = I_1(\omega_L t,\omega_R t) = \sum_{n,m=-\infty}^{\infty} g_n\, v_m \left\{ e^{j(n\omega_L t+m\omega_R t)} \right\}$$

$$i_2 = I_2(\omega_L t+\pi,\omega_R t) = \sum_{n,m=-\infty}^{\infty} g_n\, v_m \left\{ e^{j(n\omega_L t+m\omega_R t+n\pi)} \right\}$$

$$i_3 = I_3(\omega_L t+\pi,\omega_R t+\pi) = \sum_{n,m=-\infty}^{\infty} g_n\, v_m \left\{ e^{j(n\omega_L t+m\omega_R t+n\pi+m\pi} \right\}$$

$$i_4 = I_4(\omega_L t,\omega_R t+\pi) = \sum_{n,m=-\infty}^{\infty} g_n\, v_m \left\{ e^{j(n\omega_L t+m\omega_R t+m\pi)} \right\}$$

Thus, in terms of branch currents, the currents flowing through the RF, LO and IF ports of the mixer can be described as:

$$i_{TL} = \frac{1}{2}(i_1 + i_4 - i_2 - i_3)$$

$$i_{TR} = \frac{1}{2}(i_1 + i_2 - i_3 - i_4)$$

$$i_{TI} = \frac{1}{2}(i_1 - i_2 + i_3 - i_4)$$

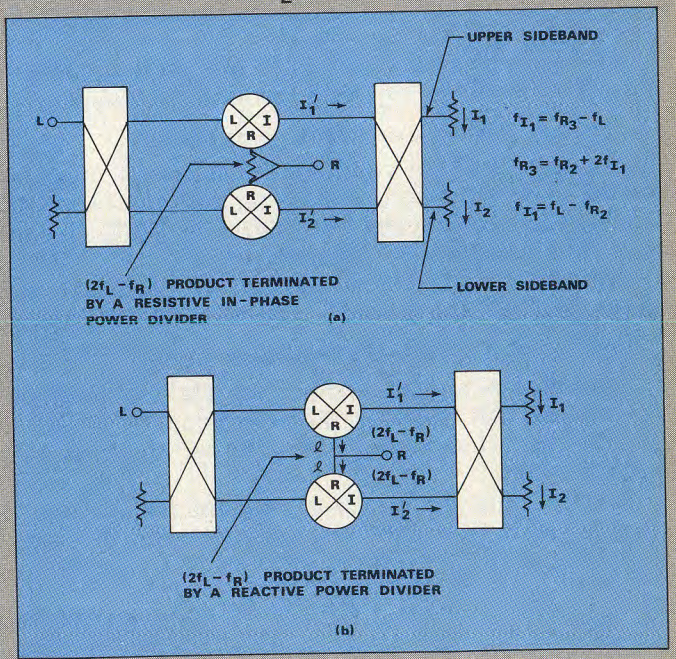

A1. LO and RF ports have been interchanged *for this analysis of sideband channelizers. RF is usually fed through the hybrid to preserve bandwidth. The $2f_L - f_R$ product may be resistively (a) or reactively (b) terminated.*

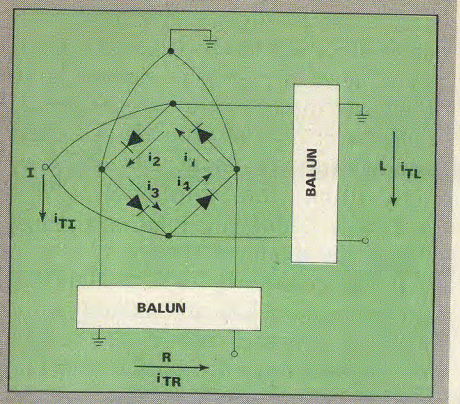

***A2. A ring-type double-balanced mixer** is used to calculate current characteristics.*

Making the necessary substitutions:

$$i_{TL} = \sum_{\substack{n=\text{all } odd \text{ integers} \\ m=0, \text{ and all } even \text{ integers}}}^{+\infty} 2g_n\, v_m\, e^{j(n\omega_L t + m\omega_R t)}$$

At the L port then, the important cancellations are:

$$f_R$$
$$f_L - f_R$$
$$f_L + f_R$$
$$2f_L - f_R$$

$$i_{TR} = \sum_{\substack{n=0, \text{ and all } even \text{ integers} \\ m=\text{all } odd \text{ integers}}}^{+\infty} 2g_n\, v_m\, e^{j(n\omega_L t + m\omega_R t)}$$

At the R port, the important cancellations are:

$$f_L$$
$$f_L - f_R$$
$$f_L + f_R$$

Note that the $(2f_L - f_R)$ pseudo-image is *not* cancelled at the R port.

$$i_{TI} = \sum_{n,m=\text{all } odd \text{ integers}}^{+\infty} 2g_n\, v_m\, e^{j(n\omega_L t + m\omega_R t)}$$

At the I port, the important cancellations are:

$$f_R$$
$$f_L$$
$$2f_L - f_R$$

Note that the $(f_L + f_R)$ is not cancelled at the I port.

In summary:

a) The $(f_L + f_R)$ is open circuited at the diode junctions by the L and R baluns.
b) The $(2f_L - f_R)$ is open circuited at the L and I ports.
c) The $(f_L + f_R)$ is resistively terminated at the I port.
d) The $(2f_L - f_R)$ is resistively terminated at the R port.

To build a low-noise *sideband channelizer* with double-balanced mixers, in addition to cancellations a) and b), the $(2f_L - f_R)$ pseudo-image must be short-circuited at the corresponding mixer R ports and the sum $(f_L + f_R)$ will have to be open-circuited at the I ports. The short circuited pseudo-image is realized when $\ell = 0$ or $n\lambda/4$, where n is an odd integer. The open-circuited sums at the I ports can be realized with properly phased low-pass filters.••

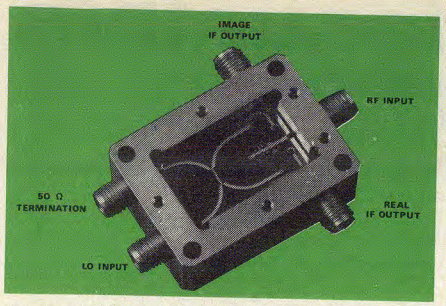

***7. Double-balanced mixers** on both sides of a fused silica substrate contribute to the performance of this recovery mixer. Intermodulation products are re-mixed to improve conversion loss. Note that the thin-film technique includes sputtered vias (see front cover).*

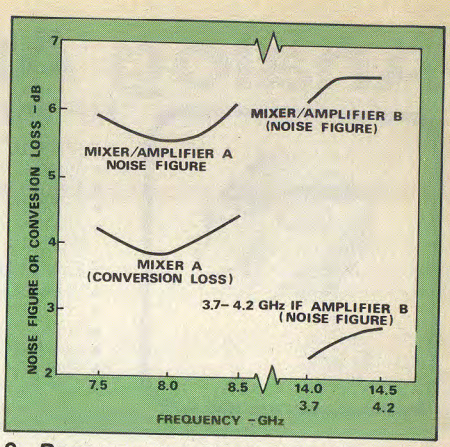

***9. Recovery-type mixer assemblies** improve conversion loss. Mixer A operates in the 7.5 to 8 GHz band. Mixer B, designed for Intelsat V, covers 14.0 to 14.5 GHz and is cascaded with a 3.7 to 4.2 GHz GaAs FET IF amplifier. Overall SSB noise figure is under 6.5 dB.*

could be improved by 3.6 degrees, the possibility of 30 dB image channelization exists.

Image versus pseudo-image

It is interesting to note how a sideband channelizer deals with intermodulation products. The mixer is a nonlinear device, thus it generates harmonics of the input signals. Without proper RF filtering, harmonics of one signal can mix with a second input signal to produce an in-band spurious IF response. Even with a single input signal, harmonics can interact with harmonics of the LO signal and produce harmonically related intermodulation products within the IF bandwidth. High-isolation, double-balanced mixers, proper IF frequency selection multiple conversion stages and IF filtering can prevent most of these intermodulation signals. However, if they do fall within the IF bandwidth, they will cause distortion and may limit the dynamic range of a receiver if they are above the tangential noise level[5].

The upper limit on dynamic range is the maximum RF power that can be inserted before compression occurs. However, in reality, since many of the spurious signals are on a 2:1 or 3:1 slope in relation to the 1:1 slope of the IF signal, the maximum upper limit is really determined by the maximum input drive before intermodulation signals appear above the noise level. In

(continued on p. 40)

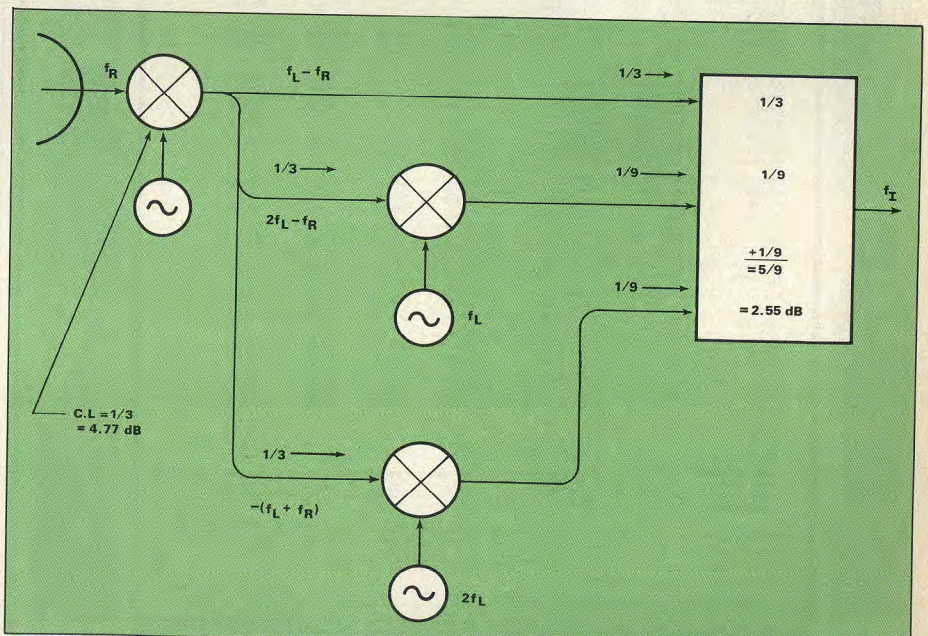

***8. A 2.55 dB conversion loss** could be achieved if the $2f_L - f_R$ and $f_L + f_R$ products could be reactively terminated and properly phased (desired output, in this case, is $f_L - f_R$). For illustration purposes, a 4.77 dB conversion loss is assumed for each mixing stage.*

Analog Attenuators

HF through UHF



APPLICATIONS

- Automatic Gain Control (AGC)
- Signal Weighting
- Automatic Level Control (ALC)
- Analog Attenuation of Signal Level
- Signal Phase Reversal
- AM Modulator
- Signal Compression and Expansion

FEATURES

- Wide Attenuation Range
- Low Insertion Loss
- Wide Bandwidth
- Low Signal Distortion
- Wide Modulation Range
- Low Phase Shift with Attenuation
- High Speed
- Precision Phase Reversal
- Matched Attenuation Characteristics
- High Rejection of Controlling Signal
- Wide Choice of Case Styles

Model No.	Characteristics	Frequency Range	Attenuation Min./Max.	Min. Atten. at Zero Current	Min. Atten. at Max. Current	Operating Time
VA-417A*/VA-418A**	HF/VHF, Phase reversible	2-150 MHz	1.5/50 dB		✓	5.0 μs
VA-419B*/VA-420B**	VHF/UHF, Phase reversible	100-350 MHz	2/45 dB		✓	0.5 μs
VA-421A*/VA-422A**	HF/VHF, Phase reversible, precise attenuation and phase tracking	20-100 MHz	1.5/50 dB		✓	0.5 μs
VA-426A*/VA-427A**	HF/VHF, In-Phase	5-100 MHz	3/38 dB	✓		5.0 μs
VA-426B*/VA-427B**	HF/VHF. In-Phase	20-200 MHz	4/35 dB	✓		0.2 μs
VA-428A*/VA-429A**	HF/VHF, In-Phase, good VSWR, broadband	5-80 MHz	3/40 dB	✓		5.0 μs
VA-428B*/VA-429B**	HF/VHF, In-Phase, good VSWR, broadband	20-180 MHz	4/30 dB	✓		0.5 μs
VA-430A*/VA-431A**	HF/VHF, In-Phase, excellent VSWR, narrowband	1.75-70 MHz (10% BW)	4/36 dB	✓		5.0 μs
VA-430B*/VA-431B**	HF/VHF, In-Phase, excellent VSWR, narrowband	30-180 MHz (10% BW)	4/34 dB	✓		0.2 μs

*PC Board Package **Connector Version

Models VA-417 through VA-421 exhibit increasing attenuation with decreasing control current, the output phase reversing with current polarity. All other models have increasing attenuation for increasing positive control current, with no phase reversal.

DIGITAL ATTENUATORS and MECHANICALLY ADJUSTABLE ATTENUATORS ARE ALSO AVAILABLE.

Send for detailed engineering information.

LORCH ELECTRONICS CORP.

105 CEDAR LANE, ENGLEWOOD, N.J. 07631
201-569-8282 • TWX: 710-991-9718

READER SERVICE NUMBER 26

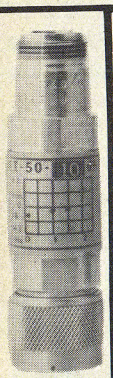





Model Number (2)	Impedance Ohms	Frequency Range	UNIT PRICE (4) BNC	TNC	N	SMA	PC
Fixed Attenuators, 1 to 20 dB:							
AT-50 (3)	50	DC-1.5 GHz	10.50	10.50	13.50	18.50	—
AT-51	50	DC-1.5 GHz	9.50	9.50	12.50	15.50	9.50
AT-53	50	DC-3.0 GHz	—	—	**18.50**	18.50	—
AT-75	75	DC-1.5 GHz	10.50	10.50	13.50	18.50	—
AT-90	93	DC-750MHz	10.50	10.50	13.50	18.50	—
Trimmer Attenuator, Range 7 to 9 dB:							
TA-8-2	50	DC-500MHz	—	—	—	39.50	—
Resistive Impedance Transformers, Minimum Loss Pads:							
RT-50/75	50 to 75	DC-1.5GHz	10.00	10.00	13.00	18.00	—
RT-50/93	50 to 93	DC-1.0GHz	10.00	10.00	13.00	18.00	—
Terminations:							
CT-50 (3)	50 (½W)	DC-4.0GHz	10.00	12.50	12.50	15.00	—
CT-51	50 (½W)	DC-4.0GHz	8.75	9.50	9.50	11.50	—
CT-52	50 (1W)	DC-2.5GHz	11.50	11.50	13.50	13.80	—
CT-53	50 (½W)	DC-4.0GHz	5.00 (10 Pc.)	—	—	5.00 (10 Pc.)	—
CT-54	50 (2W)	DC-2.0GHz	—	—	—	15.50	—
CT-75	75 (¼W)	DC-2.5GHz	10.00	10.00	10.00	15.00	—
CT-93	93 (¼W)	DC-2.5GHz	10.00	10.00	—	—	—
Feed thru Terminations, shunt resistor:							
FT-50	50	DC-1.0GHz	10.00	10.00	13.00	18.00	—
FT-75	75	DC-500MHz	10.00	10.00	13.00	18.00	—
FT-90	93	DC-150MHz	10.00	10.00	13.00	18.00	—
Resistive Decoupler, series resistor:							
RD-1000	1000	DC-1.5GHz	9.50	9.50	12.50	17.50	—
Capacitive Coupler, series capacitor:							
CC-1000	1000PF	DC-1.5GHz	9.50	9.50	12.50	17.50	—
Inductive Decouplers, series inductor:							
LD-R15	0.17uH	DC-500MHz	9.50	9.50	12.50	17.50	—
LD-6R8	6.8uH	DC-55MHz	9.50	9.50	12.50	17.50	—
Fixed Attenuator Sets, 3, 6, 10, and 20 dB, in plastic case:							
AT-50-SET (3)	50	DC-1.5GHz	40.00	40.00	52.00	72.00	—
AT-51-SET	50	DC-1.5GHz	36.00	36.00	48.00	60.00	—
Reactive Multicouplers, 2 and 4 output ports:							
TC-125-2	50	1.5-125MHz	27.00	27.00	42.00	42.00	16.00
TC-125-4	50	1.5-125MHz	35.00	35.00	60.00	60.00	24.00
Resistive Power Dividers, 3 and 4 ports:							
RC-2-30	50	DC-2.0GHz	39.50	—	—	39.50	—
RC-3-30	50	DC-500MHz	39.50	—	—	39.50	—
Double Balanced Mixers:							
DBM-500	50	2-500MHz	39.50	39.50	—	—	18.50
DBM-1000	50	5-1000MHz	39.50	39.50	49.50	49.50	—
DBM-4000	50	30-4000MHz	—	—	—	275.00	—

Note 1: Critical parameters fully tested and guaranteed. Fabricated from Mil. Spec. capacitors, High-Rel. resistors, and glass cased diodes. Mil. Spec. plated parts and connectors in nickel, silver, and gold.
2: See Catalog for complete Model Number. Specify connector sexes. Specials available.
3: Calibration marked on label of unit.
4: Price subject to change without notice. FOB Deer Park, N.Y. USA. Delivery is stock to 30 days ARO.

© 1977







Send for Free Catalog on your Letterhead.

Elcom SYSTEMS INC. 516-667-5800

127F BROOK AVENUE, DEER PARK, N. Y. 11729

READER SERVICE NUMBER 27

Fig. 6, for example, a dynamic range of 71 dB is achieved with an RF input signal level of −15 dBm. At this level, the lower limit is set by the tangential noise level of −93 dBm for a 1 MHz bandwidth. At input levels above −15 dBm, the third-order, $(2f_{R1} - f_{R2}) \pm f_L$ intermodulation product limits the dynamic range.

It has been known for some time that the conversion loss of a mixer can be made to approach zero if all the harmonic and intermodulation frequencies can be reactively terminated and properly phased. Each modulation product, $mf_L \pm nf_R$, possesses some energy and represents loss unless converted back to the IF frequency. It is practically impossible to properly control the impedances at each of the mixer terminals and at each of the frequencies, especially when the mixer is to operate over a wide frequency range. Therefore, the primary aim is to reactively terminate and properly phase the sum frequency $(f_L + f_R)$ and the $(2f_L - f_R)$ intermodulation product, often incorrectly known as the image. It is here that most of the intermodulation energy exists and the biggest recovery of energy can be obtained.

Although the $(2f_L - f_R)$ intermodulation product frequency is identical to the frequency of the image, a major distinction exists, which has not been properly observed by many authors. The *image* is a potential, or in fact, an actual input signal. The $(2f_L - f_R)$ *pseudo-image* is not, and logically, cannot be an input signal to the mixer that generated it.

Recover the sum and pseudo-image

The designer of a sideband channelizer mixer assembly is faced with two options for terminating the pseudo-image. The image reject design described earlier relies on a resistive, in-phase power divider to split the LO signal and resistively terminate the pseudo-image. Alternately, the pseudo-image can be reactively terminated by using a reactive LO power divider. This process is commonly referred to as image recovery.

The basic difference between a sideband channelizer and an image recovery design is that double-balanced mixers are substituted for single-balanced mixers and the RF and LO input circuits are reversed; the RF input signal is fed into an in-phase power divider and the LO is fed into a Lange-

(continued on p. 84)

BASIC Computer Algorithm Spots Spurious Responses

This BASIC program considers mixer and filter specs to predict spurious responses. A design example compares single-ended, single-balanced and double-balanced mixer performance in a superhet receiver.

WHAT! Another method to make receiver spurious response analysis easy? Yes, but this one has a twist: it takes the burdensome calculations off your back and places them squarely in the lap of your computer. Boiled down to a 255 line program written in BASIC language, this method should prove very useful to system designers who want a rough first cut of how a particular local oscillator, mixer and filter combination will respond to a variety of drive conditions.

In superheterodyne receivers, where a nonlinear element is used to mix an incoming signal and LO to produce an IF, undesired spurious responses can crop up within the IF bandwidth. The program, MEIXER, solves the classic problem for harmonically related distortions defined by:

$$F_{IF} = M \times F_{RF} \pm N \times F_{LO} \qquad (1)$$

where F_{IF} is the frequency of the spurious response within the IF band, M is the harmonic number of the RF input signal, F_{RF}, and N is the harmonic number of the LO input signal frequency, F_{LO}. A dictionary of input and output data to describe Eq. (1) is provided in "A user's guide to MEIXER."

Output data are printed in seven columns. Along with each spurious frequency, the program prints the corresponding signal frequency and its harmonic number, LO frequency and its harmonic number, and most importantly, the attenuation level of the spurious response relative to the required fundamental signal and LO inputs (the case of (1 × 1)). In addition, the printout indicates whether the response is a sum or difference, and if it is a difference, whether the LO frequency is above or below the signal frequency. From Eq. (1), the RF harmonic frequency can be greater than or less than the LO harmonic frequency, depending upon which sign is chosen. Therefore, it is possible to identify three spurious responses all with the same order (N × M) as follows:

order	type	$M \times F_{RF}$	printout
N × M	sum	anywhere	+
N × M	difference	above N × F_{LO}	−&+
N × M	difference	below N × F_{LO}	−&−

The algorithm used to derive the spurious response is based on two fundamental assumptions. First, for a given LO drive level, if the output level of any response is known for a given signal input frequency, then all other responses can be calculated.[1,2,3] MEIXER uses an intercept point and any level of the fundamental (1 × 1) response for these

Raymond P. Meixner, Electronic Engineer, Code 5352.1, Search Radar Branch, Naval Research Laboratory, Washington, DC 20375.

MEIXER: A program in BASIC

```
100  PAGE  60
110  REM  THIS PROGRAM CALCULATES THE LEVEL OF SPURIOUS
120  REM  RESPONSE FROM THE 1X1 RESPONSE OF A FREQUENCY
130  REM
140  REM  CONVERTER WITH AN RF PRESELECTOR AND IF FILTER
150  REM  BEFORE AND AFTER THE MIXER. KNOWLEDGE OF THE
160  REM  FILTER CHARACTERISTICS, SIGNAL, MIXER INTERCEPT
170  REM  POINTS AND SIGNAL LEVELS ARE NECESSARY.
180  REM
190  REM  SINCE THE PROGRAM ONLY READS OUT A SPUR IF IT IS
200  REM  WITHIN A CERTAIN LEVEL OF THE MAIN RESPONSE IT CAN GO
210  REM  THRU MANY ITERATIONS AND LONG CPU TIME ($) AND NEVER
220  REM  GIVE A READOUT. IN FIRST RUN MAKE L1=L2 AND SQUISH THE
230  REM  LIMITS F1 AND F2.
240  REM  BE CAREFUL IN THE RUNNING OF THE FILE.
250  REM  IN KRONOS USE COMMAND STATEMENT "SETTL, 11" TO LIMIT
260  REM  THE CPU TIME. USE "TL, 11" TO CONTINUE THE RUN
270  REM
280  REM  INPUT DATA IS READ IN
290  REM
300  READ  L1,L2,E1
310  READ  F1,F2
320  READ  I1,I2,E
330  READ  N1,M1
340  READ  F3,F4,P1
350  READ  I3,I4,P2
360  READ  H1,H2
370  READ  Q,L6,K
380  READ  S2,C,D
390  READ  Z,Y
395  REM
400  DATA  1605.01,1790.02,2
410  DATA  90.02,2200.02
420  DATA  290,490,.5
430  DATA  4,4
440  DATA  1307.5,185,30
450  DATA  390,30,30
460  DATA  10,10
470  DATA  1,7,6
480  DATA  0,60.01,60.01
490  DATA  −1,−1
500  REM
510  REM
520  LET  Q9=0
530  DEF  FNA(X9)=X9−INT(X9/2)*2
540  REM
550  PRINT  "+OR-   SPUR   SIGNAL   SIG   LO OSC   LO   ATTEN"
560  PRINT  "       FREQ   FREQ   HAR   FREQ   HAR   LEVEL"
570  PRINT
580  IF L1<>L2 THEN 610
590  LET L=L1
600  GO  TO 620
610  FOR L=L1 TO L2 STEP (L2−L1)/E1
620  LETQ9=Q9+1
630  PRINT
640  PRINT
650  PRINT  "THE LO IS ="L
660  PRINT
670  PRINT
680  REM  THE LO ORDER IS DEFINED
690  FOR  N=0 TO N1
700  REM  THE SIGNAL ORDER IS DEFINED
710  FOR  M=0 TO M1
720  REM  THIS SECTION ELIMINATES THE 0X0 RESPONSE FROM
730  REM  GOING THRU THE DO LOOP. IT ALSO SETS UP THE VARIABLE
740  REM  X FOR STEPPING THRU EACH LOOP
750  IF  N <>M THEN 770
760  REM
770  IF  N>M THEN 800
780  LET  X=M
790  GO  TO 820
800  LET  X=N
810  REM  THE (0X0) RESPONSE IS BY PASSED AT THIS STEP
```

levels. Furthermore, the LO harmonic conversion loss (N × 1) is assumed linear with N, and all signal harmonic responses (1 × M) are assumed to intersect at the intercept point. Figure 3 graphically demonstrates these assumptions.

The program has an added feature in that it checks the LO leakage to the RF port. In the example that follows, any level less than 60 dB is flagged and printed out.

Introducing a design example

Let's solve a sample problem. Suppose that a radar receiver front end will be subject to the following signal parameters in its first converter circuit:

input RF frequency:	1215 to 1400 MHz
maximum signal:	+0 dBm
dynamic range:	60 dB

The circuit is designed such that:

first IF:	390 ±15 MHz
RF or IF filter rolloff:	five poles or 30 dB/octave

In order to get a rough cut on the design, the following assumptions are made. The signal search frequencies will extend from 90 to 2200 MHz (the low end is determined so direct leakage into the IF can be checked). The IF search frequencies range from 290 to 490 MHz. A single-ended mixer is chosen so the worst case design is checked first. The intercept point is set at +10 dBm and the higher-order LO conversion loss (N × 1) is set at 10 dB/harmonic.

Response orders up to eight are initially checked so M = N = 4. Finally, Z and Y, as defined in the IF parameter section of the dictionary, must be chosen. In this case, the F_{LO} is above the R_{RF}, hence, Z = Y = −1.

(continued on p. 44)

for predicting spurious response

```
820  IF  X=0 THEN 1460
830  REM
840  REM  THE PROGRAM LOOP FOR LO AND SIGNAL FREQ STARTS
850  REM  THE LOCAL OSCILLATOR LIMITS ARE SET
860  REM  THE LO LEAKAGE IS CHECKED IN THE GO SUB ROUTINE BELOW
870  IF  M<>0 THEN 950
880  IF  (N*L)>F2 THEN 950
890  IF  (N*L)<F1 THEN 950
900  GO  SUB 2110
910  IF  B>D THEN 950
920  PRINT"LO PRESELECTOR LEAKAGE DUE TO THE";N;"HARMONIC IS";B
930  PRINT"AT A FREQUENCY OF";(N*L)
940  REM  THE PRESELECTOR LIMITS ARE SET
950  FOR  F= F1 TO F2 STEP(E*I4)/X
960  REM  THESE STEPS RECOGNIZE THAT ALL (OXM) RESPONSES HAVE
970  REM  BEEN PROCESSED IN THE FIRST L LOOP AND THE ROUTINE
980  REM  JUMPS THE PROGRAM TO THE N=1 LOOP
990  REM
1000 IF  Q9=1 THEN 1020
1010 IF  N=0 THEN 1470
1020 IF  N<>M THEN 1060
1030 REM  SORTS OUT (1X1+) SUM RESPONSE, DOES NOT PRINT IT OUT
1040 IF  N<>1 THEN 1060
1050 IF  Z>0 THEN 1250
1060 LET  I=M*F+N*L
1070 REM  THROWS OUT IF SIGNALS IF OUTSIDE THE PASSBAND
1080 IF  I>I2 THEN 1250
1090 IF  I<I1 THEN 1250
1100 GO  SUB 1630
1110 REM
1120 REM
1130 REM
1140 IF  A>C THEN 1250
1150 IF  A<.1 THEN 1250
1160 PRINT"+  ";I;"  ";F;"  ";M;"  ";L;"  ";N;"  ";A
1170 REM  THIS SECTION SORTS OUT THE ABSOLUTE VALUE OF THE (1X1−)
1180 REM  DIFFERENCE RESPONSE REQUIRED AND PERMITS THE OTHER
1190 REM  VALUE(SIG<LO OR LO<SIG) TO BE PRINTED
1200 REM  THE 1X1−,OR THE 1X1+ RESPONSES OF THE DIFFERENCE MODE
1210 REM  THIS ELIMINATES THE PRINT OUT OF ALL (0XN) & (MX0) PRODUCTS
1220 REM  SINCE THEY ARE COMPUTED AT THE I=M*F+N*L STEP
1230 IF  N=0 THEN 1440
1240 IF  M=0 THEN 1450
1250 IF  N<>M THEN 1320
1260 IF  N<>1 THEN 1320
1270 IF  Z>0 THEN 1320
1280 REM  SORTS OUT THE/1X1−/ RESPONSE THAT IS REQUIRED AND DOES
1290 REM  NOT PRINT IT OUT
1300 IF  Y<> SGN(F−L) THEN 1320
1310 GO  TO 1440
1320 LET  I=ABS(M*F−N*L)
1330 REM  DITTO AS IN 00305
1340 IF  I<I1 THEN 1440
1350 IF  I>I2 THEN 1440
1360 GO  SUB 1630
1370 IF  A>C THEN 1440
1380 IF  A <.1 THEN 1440
1390 IF  M*F>N*L THEN 1420
1400 PRINT"− & −  ";I;"  ";F;"  ";M;"  ";L;"  ";N;"  ";A
1410 GO  TO 1440
1420 PRINT"− & +  ";I;"  ";F;"  ";M;"  ";L;"  ";N;"  ";A
1430 REM  TO EXTEND THE PRINT OUT PUT A PRINT STATEMENT HERE
1440 NEXT F
1450 PRINT  M;N
1460 NEXT  M
1470 NEXT  N
1480 IF  L1<>L2 THEN 1500
1490 GO  TO 1510
1500 NEXT  L
1510 REM
1520 REM
1530 REM
1540 GO  TO 2240
1550 REM
1560 REM
1570 REM  THIS IS THE GO SUB
1580 REM  THIS SUBROUTINE CALCULATES THE LEVEL IN DB OF ANY
1590 REM  SPURIOUS RESPONSE FOUND IN THE DO LOOPS
1600 REM  THREE CASES ARE DEFINED:N=0 AND M<>0;N<>0 AND
1610 REM  M=0;N<>1,0 AND M<>1,0.
1620 REM  THE RF PRESELECTOR LOSS IS COMPUTED
1630 LET  R1 = ABS(2*(F−F3))/F4
1640 IF  R1<=1 THEN 1670
1650 LET  A1=P1*(LOG(R1)/LOG(2))
1660 GO  TO 1690
1670 LET  A1=0
1680 REM  THE ATTENUATION DUE TO THE IF FILTER IS FOUND
1690 LET R2 = ABS(2*(I−I3))/I4
1700 IF  R2<=1 THEN 1730
1710 LET  A2=P2*(LOG(R2)/LOG(2))
1720 GO  TO 1750
1730 LET  A2=0
1740 REM  ATTENUATION FOR THE THREE CASES FOLLOWS
1750 IF  M=0 THEN 2010
1760 IF  N=0 THEN 1920
1770 REM  ATTENUATION FOR ALL MXN SPURS
1780 LET  A3=H1*(N−1)+(H2−(S2−A1))*(M−1)
1790 ON  Q GO TO 1820, 1810, 1800
1800 IF  FNA(N)=0 THEN 1840
1810 IF  FNA(M)=0 THEN 1840
1820 LET  K1=0
1830 GO  TO 1850
1840 LET  K1=1
1850 LET  A3=A3+K*K1
1860 IF  (M+N)<>2 THEN 1890
1870 LET  A3=A1
1880 GO  TO 1899
1890 IF  M<>1 THEN 1899
1895 LET  A3=A3+A1
1899 LET  A=A3+A2
1900 RETURN
1910 REM  HARMONICS OF SIGNAL ONLY(N=0 AND M<>0)
1920 LET  A3=20.*.4343*LOG(M)
1930 ON  Q GO TO 1940,1935,1960
1935 IF  FNA(M)=0 THEN 1960
1940 LET  K1=0
1950 GO  TO 1970
1960 LET  K1=1
1970 LET  A3=A3+K*K1
1980 LET  A=A3+A2+A1
1990 RETURN
2000 REM  HARMONICS OF THE LO ONLY(M=0 AND N<>0)
2010 LET  A3=20.*.4343*LOG(N)
2020  :N  Q GO TO 2030, 2050, 2050
2030 LET  K1=0
2040 GO  TO 2060
2050 LET  K1=1
2060 LET  A3=A3+K*K1
2070 LET  A3=A3
2080 LET  A = A3+A2
2090 RETURN
2100 REM  ATTENUATION FROM LO TO THE "ANTENNA PORT"
2110 LET  A5=20.*.4343*LOG(N)
2120 ON Q  GO TO 2130, 2150, 2150
2130 LET  K1=0
2140 GO  TO 2160
2150 LET  K1=1
2160 LET  A5=A5+K*K1
2170 LET  A5=A5+L6
2180 LET  R4 = ABS(2*((N*L)−F3)/F4)
2190 LET  A4 = P1*(LOG(R4)/LOG(2))
2200 IF  R4>=1 THEN 2220
2210 LET  A4=0
2220 LET  B=A5+A4
2230 RETURN
2240 END
```

Lines 280 through 510 list the input data to the program for the single-ended mixer. The 0.01 numbers at the end of some of the data are merely an attempt to force the printed data to look pretty. Figures 1, 2 and 3 should be referred to along with the user's guide when preparing these data.

For discussion purposes only, the data from F_{LO} = 1605 MHz is presented. The sample computer run on p. 46 lists the spurious responses that are 60 dB or less from the required 1 × 1 response using a single-ended mixer. Notice that the local oscillator leakage radiation is 57.5 dB down from its drive level. In most radars, this is unacceptable.

It is instructive to see the response change as first a single-balanced and then a double-balanced mixer is used. Line 480 of the program is changed, and a balance of 20 dB is inserted. The abridged data print-out for the single-balanced mixer shows that only even orders of the signal frequency

(continued on p. 46)

A user's guide to MEIXER (see program, pp. 42-43)

		Units
Local oscillator parameters		
L1	lower limit of LO frequency	Hz
L2	upper limit of LO frequency	Hz
L3	controls number of LO frequencies (always ≥1)	
Mixer or frequency converter parameters		
N1	maximum harmonic of the LO	
M1	maximum harmonic of the signal	
H1	conversion loss of mixer for high orders of LO referred to (1 × 1)	dB
H2	IM intercept point for responses referred to input M terminal	dBm
L6	conversion loss of the main (1 × 1) response	dB
K	isolation loss above normal conversion loss (L6) due to balance techniques	dB
Q	defines type of mixer: 1 for single-ended 2 for single-balanced (single frequency only) 3 for double-balanced	
Filter parameters		
F1, I1	lower signal input frequency of interest	Hz
F2, I2	upper signal input frequency of interest	Hz
F3, I3	center frequency - (arithmetic or geometric mean)	Hz
F4, I4	3-dB bandwidth	Hz
P1, P2	roll-off of filters	dB/ octave
IF parameters		
C	required level of spurious down from main response	dB
Z	required response printout is skipped for mixer (+ or −): +1 for sum response −1 for difference response	
Y	determines printout for mixer above or below LO for the (−) case. Skips the right (1 × 1): +1 if LO below signal −1 if LO above	
E	A number less than one used to step the RF input frequencies through the DO loops. Usually set to 0.5 or less, to insure at least two points in the IF bandwidth.	
Signal parameters		
S1	not used	
S2	maximum signal level at input	dBm
D	required LO leakage level from LO port through the RF filter	dB
Variable parameters		
F	RF frequency	Hz
L	LO frequency	Hz
M	Signal harmonic	
N	LO harmonic	
I	IF frequency	Hz
A	value of response of any spur down from the main (1 × 1) response	dB
B	value of LO leakage at RF input port referred to LO drive level	dB
X	step loop parameter: takes the value of M or N, whichever is larger, and is used to calculate the value of the step in the L & F loops.	
R1	number of octave bandwidths (BW's) F is from F3	
R2	number of octave BW's I is from I3	
R3	not used	
R4	number of octave BW's (N*L) is from F3	
A1	RF signal attenuation	dB
A2	IF attenuation	dB
A3	RF signal attenuation due to mixer response, including A1	dB
A4	attenuation of LO harmonic through RF filter	dB
A5	level of LO harmonic at output of mixer referred to input LO drive	dB

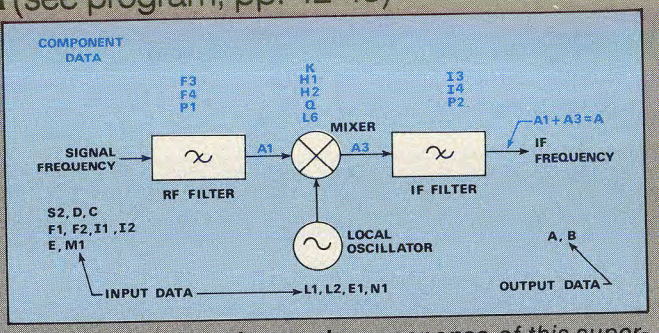

***1. MEIXER predicts the spurious response** of this superheterodyne front-end circuit. Component data describe filters and mixer. Input data characterize the RF signal and LO drive. MEIXER identifies output data A, representing spurious responses, and B, LO-to-RF leakage.*

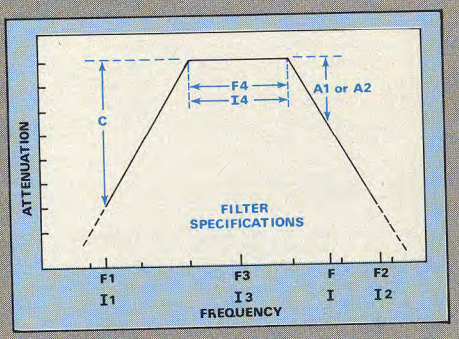

***2. Filter parameters** are important in determining the spurious response of a superheterodyne front-end. RF and IF frequency specifications are given by F and I, respectively. C represents the required suppression of spurious from the main response, in dB. A1 and A2 are RF and IF attenuation factors, respectively.*

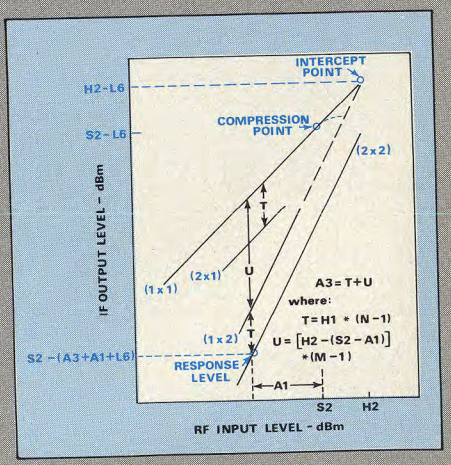

***3. Conditions** under which the MEIXER program may be applied are straightforward. LO conversion loss is assumed to be linear (see (1 × 1) and (2 × 1), for example). All signal harmonic responses intersect at the intercept point ((1 × 1) and (2 × 1) illustrate this). See adjacent text for a complete explanation of the symbols used in this graph.*

A Switch in Time....

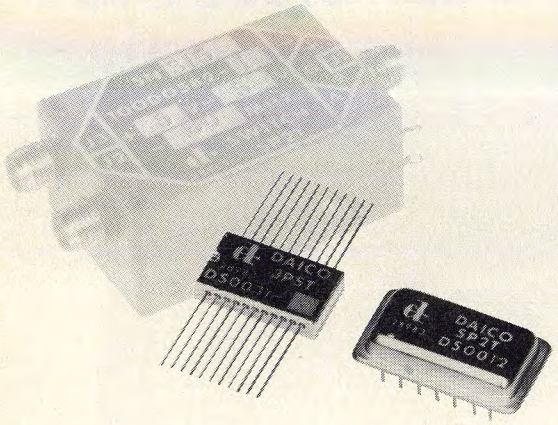

Daico high speed SP2T switches utilize thin-film circuitry. Balanced diode design allows nanosecond switching speeds with millivolt level video transients. Integral drivers provide complete T^2L compatibility. Packaging is available with conventional connectors, plug-in mount, or DIP thin-film hybrid. What are your unique switching problems? Call DAICO, we have probably already solved them.

Typical Performance	DS0042	DS0012	DS0052
Frequency (MHz)	10-200	10-500	50-1250
R.F. Power, Max. cw (dBm)	10	10	10
Impedance, nominal (ohms)	50	50	50
VSWR	1.25/1	1.10/1	1.25/1
Termination of Unused Port (ohms)	short	50	50
Insertion Loss (dB) at 160 MHz	1.0	0.4	0.5
I.L. Flatness (dB per 100 MHz)	0.5	0.1	0.05
Insertion Phase Match (deg. per 100 MHz)	0.2	0.2	0.2
Isolation (dB) at 100 MHz	50	60	75
Isolation (dB) at 500 MHz	—	48	70
Control T^2L Load Factor	2	2	2
Sw. Speed 50% Control 50% RF (nanosecond)	12	1000	500
R.F. Transition 10% to 90% (nanosecond)	6	250	250
In-Band Transients (dBm)	−50	−25	−25
Video Transients (millivolts)	50	1000	1000
3rd order Intercept Point (dBm)	+35	+30	+45

Send for Free RF Design Nomographs: Spurious Response, Noise Figure & Return Loss vs. VSWR

DAICO INDUSTRIES, INC.

2351 East Del Amo Blvd., Compton, Calif. 90220
Telephone: (213) 631-1143 · TWX 910-346-6741
©1975 Daico Industries, Inc. mp75409R

READER SERVICE NUMBER 30

—SPOT SPURIOUS RESPONSES—

Sample computer run

Output data for single-ended mixer

+OR−	SPUR FREQ	SIGNAL FREQ	SIG HAR	LO OSC FREQ	LO HAR	ATTEN LEVEL
THE LO IS = 1605.01						
1 0						
2 0						
3 0						
4 0						
LO PRESELECTOR LEAKAGE DUE TO THE 1 HARMONIC IS 57.5624 AT A FREQUENCY OF 1605.01						
0 1						
1 1						
2 1						
3 1						
4 1						
0 2						
1 2						
− & −	419.98	1395.02	2	1605.01	2	49.9711
− & −	404.98	1402.52	2	1605.01	2	21.1633
− & −	389.98	1410.02	2	1605.01	2	24.4514
− & −	374.98	1417.52	2	1605.01	2	27.5649
2 2						
− & +	375.04	1195.02	3	1605.01	2	46.9286
− & +	390.04	1200.02	3	1605.01	2	42.9926
− & +	405.04	1205.02	3	1605.01	2	38.9844
3 2						
4 2						
0 3						
1 3						
2 3						
3 3						
− & +	375.05	1297.52	4	1605.01	3	50
− & +	390.05	1301.27	4	1605.01	3	50
− & +	405.05	1305.02	4	1605.01	3	50.1442
4 3						
0 4						
1 4						
2 4						
3 4						
4 4						

Abridged output data for single-balanced mixer

0 2						
1 2						
− & −	404.98	1402.52	2	1605.01	2	41.1633
− & −	389.98	1410.02	2	1605.01	2	44.4514
− & −	374.98	1417.52	2	1605.01	2	47.5649
2 2						
− & +	375.04	1195.02	3	1605.01	2	46.9286
− & +	390.04	1200.02	3	1605.01	2	42.9926
− & +	405.04	1205.02	3	1605.01	2	38.9844
3 2						
4 2						

Abridged output data for double-balanced mixer

0 2						
1 2						
− & −	404.98	1402.52	2	1605.01	2	41.1633
− & −	389.98	1410.02	2	1605.01	2	44.4514
− & −	374.98	1417.52	2	1605.01	2	47.5649
2 2						
− & +	405.04	1205.02	3	1605.01	2	58.9844
3 2						
4 2						
0 3						

are suppressed by 20 dB. The (4 × 3) response disappears from the printout and the (2 × 2) response is reduced by 20 dB. Also, the LO leakage above −60 dB has disappeared. For the double-balanced case, all even orders are reduced, and the (3 × 2) response is now reduced by 20 dB.

Although the program is extremely helpful in preparing or evaluating proposals, like all programs MEIXER is not complete. For instance, in the single-balanced case, the assumption is made that the LO leakage is balanced and reduced at the antenna port; no provision is made for a single-balanced mixer that is not balanced for LO leakage. ••

References

1. E. W. Karpen and R. J. Mohr, "Graphing Spurious Responses In Microwave Receivers," *MicroWaves*, Vol. 9, No. 11, pp. 42-45, (November, 1966).
2. R. B. Mouw and S. M. Fukuchi, "Broadband Double Balanced Mixer/Modulators," *Microwave Journal*, Part I Vol. 12, No. 3, pp. 131-134, (March, 1969).
3. J. C. Hoeyaard, "Spurious Frequency Generation In Frequency Converters," *Microwave Journal*, Part I, Vol. 10, No. 7, pp. 61-69, (July, 1967).

Is There A Josephson Junction In Your Future?

The Josephson junction is a superconducting device with a surprising I-V characteristic. A review of device physics and experimental results reveals applications in a wide range of microwave circuits.

THE Josephson junction is a non-linear device, often lossless and active, showing great promise for low-noise, high-speed and low-power applications at millimeter and submillimeter wavelengths. The device has potential as an RF detector, mixer, parametric amplifier and upconverter, oscillator, frequency multiplier and divider, ultra-fast logic gate and switch. In addition, the junction is presently used as a magnetometer, voltmeter and voltage standard.

In each of these functions, the demonstrated performance of the Josephson junction is unexcelled.

Before exploring the many microwave applications of this exciting new super-conducting device, it's important to consider the device's DC current—voltage characteristic. Figures 1 and 2, experimental X-Y recordings of a thin-film Josephson junction fabricated by the author at the University of Southern California, clearly illustrate the startling behavior of the junction.

Notice that when driven by a current source (Fig. 1) current flows through the device *with no applied voltage.* At 3 mA, the critical current for this particular junction, voltage appears across the device, *but no DC current flows.* This voltage rapidly rises (switches) to 0.9 mV, the voltage associated with the superconducting band gap, and DC (non-Josephson) current begins to flow.

Unlike a diode, the I-V curve is symmetric about zero (in zero magnetic field). Figure 2 illustrates a sequence of I-V curves taken from the same junction when microwave fields are allowed to interact with the device. Note that current steps are created at constant voltages.

To explain why the Josephson junction behaves in this surprising (but predictable) manner, it's necessary to review the theory of superconductivity first suggested by Bardeen, Cooper and Schieffer. Their work, which captured the 1972 Nobel prize in physics, helped demonstrate that although electrons are relatively free to move within a metal, they are attracted to each other through the vibrations in the metal's crystalline lattice. If the thermal energy of the electrons is less than the energy associated with their interaction with the lattice vibration, the electrons form "bound pairs" and move together without scattering with the lattice structure. Thus below some critical temperature, T_c, which is below 23°K for all known materials, electrons flow without resistance and the metal is a superconductor.

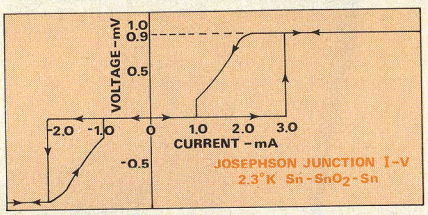

1. This actual X-Y recording was taken at the University of Southern California. *When the device current, supplied by a current source, reaches 3 milliamps, the voltage rapidly switches to 0.9 mV and non-Josephson current flows.*

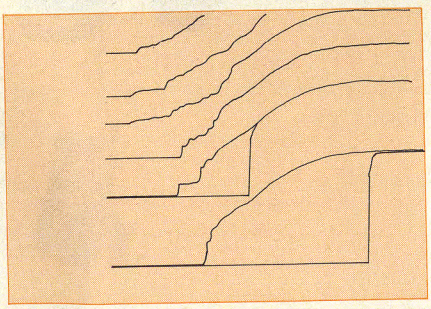

2. Superimposing microwave fields on the junction *produces discrete current steps at constant voltages.*

Since the metal lattice can transmit information over many atomic spacings, an electron, through the lattice, can interact with another electron many centimeters away. For this reason, all the electron pairs behave as if they were in one quantum mechanical state,

$$\psi = \sqrt{\rho}\, e^{i\theta} \qquad (1)$$

where ρ is the density of electrons and $\theta\left(\theta = \frac{E}{\hbar} t\right)$ is their common phase.

In addition, in the same way that a band gap is formed in a semiconductor because the electrons interact with the lattice, a small band gap (about 1 mV) is formed in a superconductor.[1]

Josephson raises a question

Brian Josephson, working at Cambridge, England, considered the interaction between two pieces of superconducting metal, each described by Eq. (1). What would happen, he wondered, if a few electron pairs flowed from piece 1 and piece 2 and "weakly linked" the two superconductors? Josephson devised a set of experiments to answer this question and describe the current flowing through the junction between the two metals. His work revealed that unusual currents flowed as a function of $\theta_1 - \theta_2$ (the electron-pair phases in metals 1 and 2) and the voltage between the superconductors. P.W. Anderson and J. Rowell at Bell Labs provided the first experimental verification.[2]

This "Josephson junction" is typically formed in one of two ways (see Fig. 3). It can be fabricated as a three-layer structure with planar integrated

Roger Davidheiser, Member of the Technical Staff, TRW Systems, One Space Park, Redondo Beach, CA 90278.

How the Josephson junction measures up

Function	Demonstrated Josephson junction performance	Competing device	Performance
Downconverter	noise temperature: 54°K, conversion gain: +1.1 dB, LO power: 10^{-4} W (36 GHz)	cooled Schottky barrier	250°K
Negative resistance amplifier	noise temperature: ≤15°K (9 GHz) broadband self-pumped	cooled paramp	45°K narrowband separate pump
Parametric amplifier	gain: 16 dB, noise temperature: 22°K, required pump power: 3×10^{-8} W		
Oscillator (low level)	frequency linear with bias voltage, 0-1000 GHz frequency range, excellent phase noise performance		
Frequency multiplier and divider	mixing with 825th harmonic of local oscillator		
Switch	delay time: 38 ps, switch power: 10^{-7} W	silicon bipolar	150 ps 10^{-3} W
Magnetometer	sensitivity: 10^{-9} G-cm²	fluxgate magnetometer	10^{-6} G-cm²
Other superconductor capabilities			
Super Schottky diode detector	NEP = 5×10^{-16} W/Hz$^{0.5}$ α = 6000 V^{-1}	room temperature Schottky diode	NEP = 4.5×10^{-13} W/Hz$^{0.5}$ a = 40 V
Super Schottky diode mixer	noise temperature 6°K (X-band)		
Superconductor microstrip resonators	Q = 100,000 (undemonstrated)	room temperature waveguide resonators	Q = 5,000 (100 GHz)

technology, using a very thin oxide, semiconductor or normal metal layer to loosely link two pieces of superconducting material. Or, the weak link can be established with a simple point contact.

Josephson used a standard equation to describe how the electron pair state in the first superconductor changes in time, then weighted this expression with a very small amount of the electron pair state of the second superconductor:

$$\frac{\partial \psi_1}{\partial t} = \left(\frac{-i}{\hbar}\right)[E_1 \psi_1 + K\psi_2] \quad (2)$$

where $\hbar$ is a constant, E_1 is the energy of the electron pairs, and $K \ll 1$, and describes the number of pairs "leaking" from superconductor 1 to 2. Likewise, for superconductor 2:

$$\frac{\partial \psi_2}{\partial t} = \left(\frac{-i}{\hbar}\right)[E_2 \psi_2 + K\psi_1] \quad (3)$$

Josephson then combined Eq. (1) with Eqs. (2) and (3) and solved for

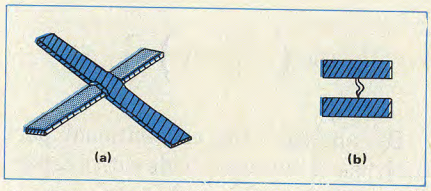

***3. Josephson junctions can be fabricated** by (a) weakly linking two superconducting pieces through a very thin oxide. A second scheme (b) links two superconducting pieces with a point contact.*

$\delta\rho/\delta t$, the current flow which we will call i. For no applied voltage, that is when $E_1 = E_2$, he found:

$$i = i_c \sin(\Theta_1 - \Theta_2) \quad (4)$$

where $i_c = \frac{2K}{\hbar}\rho$ and is called the critical current. Notice if i is greater than i_c, the equation is known as the DC Josephson effect.

Josephson went further: If a voltage, V, is applied between the two superconductors such that $E_1 - E_2 = 2$ eV (remember the electron pair charge is

(continued on p. 52)

a winning combination

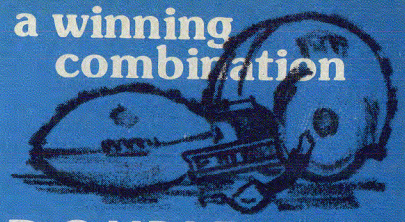

DOUBLE BALANCED MIXERS

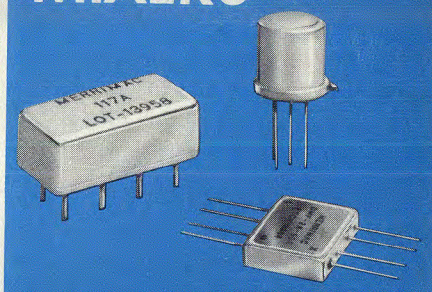

DC to 1 GHz — in TO-5, Flat Pack or Relay Header

Check our minimum performance characteristics and see for yourself why Merrimac has the winning combination for you...

DC-500 MHz MODELS				
PACKAGE	MODEL NO'S	PRICE	CONVERSION LOSS	ISOLATION (DB-MIN)
RELAY HEADER	117A	$ 9.45	5.5 dB Typ. 8.0 dB Max.	L-R 40-30 L-X 35-20
FLAT PACK	DMF-2A-250	$29.00	7.0 dB Typ. 8.0 dB Max.	L-R 40-35 L-X 30-20
TO-5 (0.3" HIGH)	M-109	$25.00	6.0 dB Typ. 8.5 dB Max.	L-R 40-25 L-X 30-18
DC-1000 MHz MODELS				
RELAY HEADER	M-119	$15.00	7.0 dB Typ. 8.0 dB Max.	L-R 30-20 L-X 25-15
FLAT PACK	DMF-2A-505	$26.00	7.5 dB Typ. 8.0 dB Max.	L-R 35-25 L-X 30-20
TO-5 (0.3" HIGH)	M-122	$39.00	6.5 dB Typ. 9.5 dB Max.	L-R 40-25 L-X 30-20

LO POWER (ALL MODELS) +7 DBM NOMINAL.

Send for complete data on the above Mixers and we will also include free MTBF data and information on our complete line of DC-3GHz "Connectorized" Single and Double Balanced Mixers.

send for our NEW '77 CATALOG OF IF SIGNAL PROCESSING COMPONENTS

Merrimac
INDUSTRIES, INCORPORATED
41 FAIRFIELD PL., W. CALDWELL, N.J. 07006
201 575-1300 • TWX 710-734-4314
now there is one...in signal processing

READER SERVICE NUMBER 36

2e), Eqs. (2) and (3) for

$$\frac{\partial}{\partial t}(\Theta_1 - \Theta_2) = \frac{1}{\hbar}\,2eV \qquad 4a$$

and from Eq. (4) the current between the superconductors is:

$$i = i_c \sin\left(\frac{2eV}{\hbar}t\right) \qquad (5)$$

where the value of $2e/\hbar$ is 483.6 MHz/μV. The frequency of current flow is proportional to the applied voltage and no DC current flows. The equation is known as the AC Josephson effect.[3] For this description, Josephson shared the 1973 Nobel prize in physics with Leo Esaki (the tunnel diode) and Ivar Giaever (single electron tunneling).

To understand how the DC I-V curve of Fig. 2 is formed, consider a DC voltage, plus some RF signal, $V = V_0 + V_1 \cos \omega t$, across the junction. The current is then described by:

$$i = i_c \sin\left[\left(\frac{2e}{\hbar}\right)V_0 t + \frac{V_1}{\omega}\sin\omega t\right]$$

$$= i_c \sum_{n=-\infty}^{\infty} J_n\left(\frac{2eV_1}{\hbar\omega}\right)$$

$$\sin\left[\frac{2eV_0}{\hbar} + n\omega\right]t \qquad (6)$$

For the correct value of V_0, DC current flows. These equations outline the unusual voltage current characteristics of the Josephson junction. Much more detailed accounts of the physics of the device are available.[4-6]

Researchers recognize applications

The years since Brian Josephson's work was first reported have been a busy period for other researchers, as they attempted to more fully explore his equations describing the current flowing through the junction between two superconductors. A review of some of the more exciting results obtained by experimenters to date reveals many possibilities for microwave component design.

For example, it was soon recognized that Eq. (5) closely resembles the classic current waveform obtained for a Schottky-barrier diode pumped with a sinusoidal local oscillator.[7] Thus, experimenters reasoned that the junction might be used as a conventional mixer or as a self-pumped (oscillating) mixer. Indeed, theoretical calculations using a model of an ideal Josephson junction with a resistive shunt predict small signal conversion gain for a junction operating as a mixer with an external local oscillator.[8]

Experimenters at the University of California at Berkeley, investigating the junction's potential as a mixer, have obtained a conversion gain of 1.3 and a noise temperature of 54° K with a local oscillator power of −60 dBm at 36 GHz.[9] In comparison, a "low-noise," room-temperature Schottky diode mixer operating with a noise figure of 5 dB has an effective noise temperature of 630° K. Thus, in this application, the Josephson junction could provide an 12 dB improvement in noise figure, in addition to conversion gain.

In another experiment, a junction oscillating near the IF has converted an RF signal to an IF of 5 MHz with an efficiency of 50 (conversion gain of 17 dB). These results are clouded, however, by an associated noise figure of about 1000°K.[10]

Further study of the equations describing current flow through a Josephson junction reveals an interesting analogy with parametric amplifier theory. Differentiating Eq. (5) with respect to time shows that the junction can be used as a variable inductance (dependent on the quantam phase difference):

$$L = V\left(\frac{\partial i}{\partial t}\right)^{-1} = \left[\left(\frac{2e}{\hbar}\right) i_c \cos\left(\frac{2e}{\hbar}Vt\right)\right]^{-1} \qquad 6a$$

By analogy, the conventional paramp uses a varactor diode with a capacitance that varies with time.

It can be shown that three of the five conditions necessary to prove the Manley-Rowe equations—which provide the basis for the study of the parametric amplifier—hold for the Josephson junction. Power flow theorems analogous to the paramp's Manley-Rowe equations have also been proven.[11]

Experimental confirmation of the Josephson junction's potential in low-noise amplifier circuits is provided by several sources. Helmut Kanter, of the Aerospace Corporation, has demonstrated a negative resistance amplifier with single idler (equivalent to the varactor diode paramp), a negative resistance amplifier with several idlers and an upconverting amplifier. His work shows that the pump mechanism is effective over a broad bandwidth, and that the junction can be operated in a self-pumped mode. A noise temperature of less than 15°K has been established for the parametric upconversion of a 115 MHz signal to 9 GHz.[12]

In other work, H. Zimmer has demonstrated parametric amplification with a Josephson junction device of approximately 16 dB with a noise temperature of 22° K. This experiment was performed with a pump power of −49 dBm and signal power of −74 dBm. Pump and signal frequencies were approximately 9.5 GHz.[13]

With its broadband nature and promise of operation to submillimeter frequencies, this Josephson circuit application is extremely attractive when compared with present parametric amplifier technology.

An exotic V-to-F converter

The voltage/frequency relationship implied by Eq. (6) points up interesting applications in fundamental oscillator circuits. If a bias voltage, V, is applied across a Josephson junction, Eq. (5) shows that microwave currents flow at $W = (2e/\hbar)V$, where $2e/\hbar$ equals 483.6 MHz/μV. The voltage-frequency relationship holds for voltages up to the superconducting band gap (typically 0.5 to 2 mV), hence currents can be made to flow between 0 and 1000 GHz.

The relationship between frequency and voltage is so linear that the value of $2e/\hbar$, an important constant for the study of quantum electronics, has been determined from the junction,[14] and the voltage generated by the junction when irradiated by a signal of known frequency is used for the US voltage standard.

Estimated power available from the Josephson junction oscillator is 10^{-8}W, but disappointing levels of 10^{-12}W are currently observed for thin-film devices and 10^{-10}W for point contact devices. The typical impedance of the Josephson junction is very low (about 10^{-4}ohm for the thin-film version) and mismatch losses with the circuit may be responsible for less than optimum performance. It is noteworthy that coupled junctions radiate coherently, thus the power delivered from two oscillators is four times that of a single oscillator.[15] Although not yet demonstrated, n junctions should radiate n^2 times single junction power. Photon shot noise and thermal voltage fluctuations across the junction determine the phase noise properties of a Josephson junction oscillator.[16]

Injection locking of a Josephson oscillator has been demonstrated[17] with frequency pulling, bandwidth narrowing and signal gain observed in accordance with the theory of Adler.

Several experiments to directly measure the frequency of infrared lasers clearly illustrate the ability of the Josephson junction to convert power in an incident signal to very high order harmonics. Workers at the National Bureau of Standards in Boulder, CO, have successfully mixed a 3800 GHz signal with the 400th harmonic of the 9.5 GHz local oscillator to produce a 9 GHz IF.[18] In addition, down-conversion of a far-infrared laser signal to 30 MHz by pumping a Josephson junction with the 825th subharmonic has been demonstrated.[19]

Another exciting conclusion of this type of experiment is that although the Josephson equations are thought to hold to only (!) 1000 GHz, Josephson-like behavior occurs at up to 45 times this frequency. In addition, a junction can produce subharmonics of signal pump frequency.

In a practical sense, the coherent multiplication properties of the junction demonstrated by NBS could have great significance to microwave designers. A Josephson junction could, for example, be used as an ultra-stable millimeter or submillimeter-wave source by phase-locking the device directly to a crystal oscillator.

Think about logic possiblities

The high operating frequency and low power consumption characteristic of the Josephson junction make it a strong competitor for tomorrow's high-density, low-power, ultra-fast logic circuits. Interest in gigabit logic has grown strongly in recent years, and demands for higher and higher switching speeds are rapidly outstripping conventional digital technologies. For example, there is presently large scale government funding for a 10 GHz (100 ps), 0.1 mW switch, a requirement that simply may be out of the reach of many established logic systems (see Fig. 4).

Workers at IBM, Zurich, Switzerland, have demonstrated Josephson switching times of 38 ps (13 GHz), power dissipations of 100 nW, and power densities of 2.5W/cm^2.[20] Switching times of 1 ps at 10 nW might eventually be possible.

More recently, Dennis Herrell, working at IBM in Yorktown Heights, NY, has demonstrated Josephson capability in the logic circuits of AND and OR gates. Using conductor line widths not less than 25 microns, he has found logic delays of 170 ps per gate and power dissipations of 28 μW. He estimates up to 100 ps of the total delay is due to propagation delay.[21]

Applications exist today

Thus far, this article has concentrated on laboratory results and potential RF applications for the Josephson junction. However, don't get the impression that the versatile superconductor is purely a laboratory curiosity. The Josephson junction is currently finding use in practical hardware in several non-microwave fields. Perhaps the most impressive application today is in magnetometer design.

When two Josephson junctions are connected in parallel with a loop of superconducting wire, the total current flowing through the pair is a strong function of the magnetic flux in the wire loop. By detecting changes in the junction pair current, relatively simple electronics can detect changes in magnetic flux of 10^{-9} G-cm^2 (or with a flux transformer 10^{-4} T/$\sqrt{\text{Hz}}$). This is three orders of magnitude smaller than that detectable by the most sensitive conventional (fluxgate) magnetometers.[22]

This sensitivity has allowed the measurement of the first magneto-cardiograms, measurement of changing rock strain along earthquake faults, and may allow the first communication system to be established with submerged submarine fleets. Because of this latter application, the Office of Naval Research (ONR) heavily funds Josephson technology development.

"Supercircuits" boost Q

Keep in mind that the Josephson junction is a superconductor; it must be cooled to temperatures below 23°K to operate. On the surface, this might seem to be an insurmountable obstacle for the device to become a practical design element. But, on second thought, it becomes apparent that the cooling requirement could be used to great advantage.

The usefulness of current microwave integrated circuitry is limited by large transmission line losses and low circuit Q. There are three contributions to microstrip losses: dielectric, radiation and metal (ohmic). Dielectric losses are

(continued on p. 54)

a winning combination



SINGLE AND DOUBLE BALANCED MICROWAVE STRIPLINE MIXERS

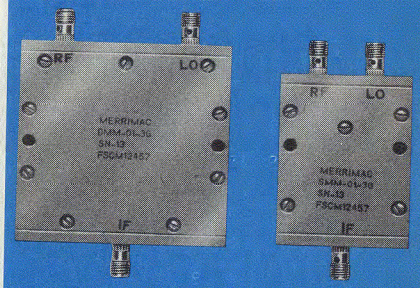

1.7-18 GHz

Check our minimum performance characteristics and see for yourself why Merrimac has the winning combination for you...

SINGLE BALANCED MICROWAVE STRIPLINE MIXERS

MODEL SMM-01-	RF & LO FREQ. (GHz)	IF BW (MHz)	ISOLAT'N dB (MIN)	NOISE FIG. dB (MAX)	CONV. LOSS dB (MAX)
2.95 G	1.7-4.2	DC-400	6	8.0	6.5
3 G	2.0-4.0	DC-400	8	7.5	6.5
3.90 G	2.6-5.2	DC-400	7	7.5	6.5
6 G	4.0-8.0	DC-400	6	8.0	7.0
10 G	8.0-12.4	DC-1000	6	8.5	7.5
15 G	12.4-18	DC-1500	6	9.0	8.0

DOUBLE BALANCED MICROWAVE STRIPLINE MIXERS

MODEL SMM-01-	RF & LO FREQ. (GHz)	IF BW (MHz)	ISOLAT'N dB (MIN)	NOISE FIG. dB (MAX)	CONV. LOSS dB (MAX)
2.95 G	1.7-4.2	DC-400	20	8.5	7.5
3 G	2.0-4.0	DC-400	20	8.0	7.0
3.90 G	2.6-5.2	DC-400	20	8.5	7.5
6 G	4.0-8.0	DC-400	20	9.0	8.0
8 G	6.0-12.4	DC-400	16	9.5	8.5
10 G	8.0-12.4	DC-700	18	9.0	8.0
15 G	12.4-18	DC-1000	15	10.0	9.0

send for our NEW '77 MICROWAVE CATALOG.

Merrimac
INDUSTRIES, INCORPORATED
41 FAIRFIELD PL., W. CALDWELL, N.J. 07006
201 575-1300 • TWX 710-734-4314

now there is one... in signal processing

READER SERVICE NUMBER 37

Divide and Conquer.

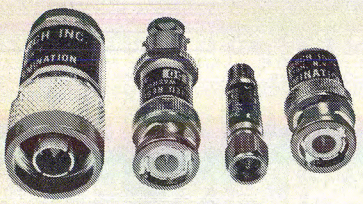

DC to 3 GHz Attenuators, Terminations, & Impedance Transformers from APPLIED RESEARCH.

For Types BNC, TNC, C, N, SMA & other connectors.

Our integrated line of fixed pad attenuators, terminations and impedance-matching transformers conquers the problem of RF measurements and system integration by providing isolation between RF components over the frequency range of DC to 3 GHz. Also provides for the matching of different impedances with minimum loss over a broad frequency band. Unit cost is practical for large and small equipment users.

GENERAL CHARACTERISTICS
Frequency Range: DC—3 GHz
VSWR: 1.25:1
Attenuation Accuracy: +0.5 dB
Impedances (nominal): 50, 75, 90 ohms
Attenuation values: 1, 2, 3, 4, 6, 10, 12, 15, 20 dB (standard)
Temp. Range: —55°C to 100°C

U.S. PAT. NO. 2,891,223/2,974,403

For details, contact: Applied Research, 76 So. Bayles Ave., Port Washington, N.Y. 11050, (516) 883-5700, TWX #510-223-0822.

Applied Research
INCORPORATED
Filters, Converters, Multicouplers, Signal Sources, Amplifiers, Multipliers

READER SERVICE NUMBER 22

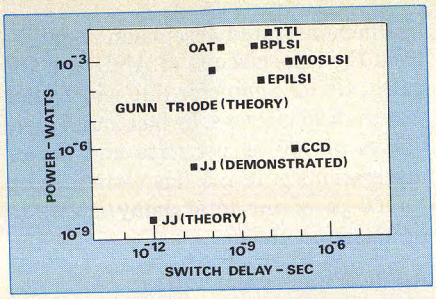

4. The Josephson junctions's impressive power-speed factor is heating up the gigabit logic race. *Maximum power and minimum switching times are illustrated for the leading contenders. Presently demonstrated Josephson junction results are about as fast as transferred-electron logic devices (TELD) but lower in power. Theory, however, predicts a 10–12 second switch delay for the junction. Other comparisons include oxide aligned transistors (OAT), bipolar large scale integrated circuits (BPLSI), transistor-to-transistor logic (TTL), metal oxide semiconductor large scale integrated circuits (MOSLSI), epitaxial large scale integrated circuits (EPILSI) and charge coupled devices (CCD).*

and X-band cavities made of these materials exhibit Qs of 10^8 to 10^{12}. [24] Thus, the superconducting microstrip circuit built on a very thin substrate could avoid radiation problems while incurring negligible ohmic losses in the metal. Circuit Qs equal to the inverse of the loss tangent of the substrate dielectric (100,000 for sapphire, 10,000 for quartz and silicon) are predicted (see Fig. 5).

Another intriguing possibility is to combine superconductor and semiconductor technologies. A team led by M. McColl at the Aerospace Corporation have recently reported a super-Schottky-barrier diode formed by electroplating a 5-micron lead (Pb) dot on heavily doped p-type GaAs substrate. In an unpublished presentation at the 1976 Applied Super-conductivity Conference, the research team reported a mixer noise temperature of 6° K at 1.1°K with an X-band signal. Diode conversion loss is approximately 7 dB with a bias of 0.6 mV and LO power of −47 dBm. When used as a detector, the diode exhibited a noise equivalent power (NEP) of 5.4×10^{-16} W/Hz$^{0.5}$ at 1.06°K with 1.0 mV bias.

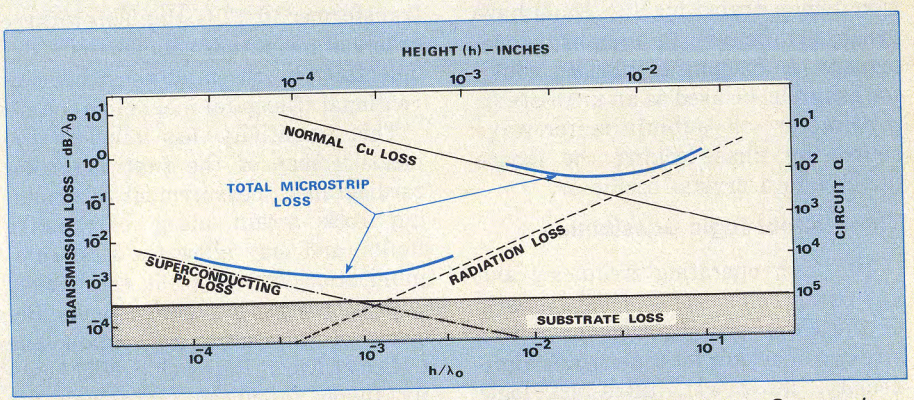

5. Superconducting lead (Pb) *typically exhibits four orders of magnitude lower transmission loss than normal copper (Cu). Comparison shown is for 50-ohm microstrip λ/2 resonators at 50 GHz.*

very small for most MIC substrates. But large radiation losses, quadratic with substrate height,[23] and ohmic losses, inversely proportional to substrate height, add to establish a high minimum transmission loss. As a result, circuit Q is limited to approximately 300 at 6 GHz and 100 at 50 GHz.

However, since planar Josephson junction devices and microstrip circuitry are clearly compatible, why not build the MIC using superconducting metals? Superconducting metals such as lead and niobium have extremely small microwave losses (as predicted by Bardeen, Cooper and Schieffer[1]),

A system of the future?

Will the helium support systems necessary for the superconducting devices discussed in this article prevent their application in future systems? This question is impossible to answer today, of course, but consider the feasibility of a rather severe system application: A relay satellite station comprised of receiver, processor and transmitter.

Present systems employ Schottky-diode mixers with about 6 dB noise figure in the receiver front end, 20 to 50 watt TWTs with redundancy in the transmitter section, and waveguide components. The RF section alone

weighs approximately 100 pounds, consumes 100 watts and needs a three-square meter solar cell generator.

It is entirely possible to imagine a superconducting satellite somewhat larger than a basketball weighing 5 pounds, including stored helium, with a life expectancy of five years. Since the total internal heat load would have to be a fraction of a milliwatt, the 1 to 2 watt FET transmitter (remember the intended superconductor receiver is 10 to 20 dB more sensitive than present receivers), SAW reference oscillators and other "high power" components would be external to the cryostat and RF information transmitted into the dewar with dielectric waveguide. Total power consumption need not be above 5 watts and a square foot of solar cells would suffice. As the receiver looks at another satellite in space, the antenna need not be cooled but only shielded from the sun. ••

References

1. P. G. DeGennes, *Superconductivity of Metals and Alloys*, W. A. Benjamin, (1966).
2. P. W. Anderson & J. Rowell, "Probable Observation of the Josephson Superconducting Tunneling Effect," Physical Review Letters, 10, 6, (1963).
3. R. P. Feynmann et al, *Lectures on Physics III*, Chap. 21, Addison-Wesley, (1965).
4. B. D. Sullivan et al, "Generation of Harmonics & Subharmonics of the Josephson Oscillation." *J. of Appl. Phys. 41, No. 12*, (November, 1970).
5. E. Burstein & S. Lindquist, *Tunneling Phenomena in Solids*, Plenum Press (1969).
6. D. N. Langenburg, D. J. Scalapino, and B. N. Taylor, "Josephson - Type Superconducting Tunnel Junctions as Generators of Microwave and Submillimeter Wave Radiation", *Proc. IEEE 54, No. 4*, pp. 560-574, (April, 1966).
7. H. C. Torrey & C. A. Whitmer, *Crystal Rectifiers, MIT RLS 15*, p. 155, McGraw-Hill (1948).
8. F. Auracher & T. Van Duzer, *Proc. of the 1972 Applied Superconductivity Conference*, p. 603, IEEE, N.Y., (1973).
9. J. H. Claasen Y. Taur, & P. L. Richards, "Noise in Josephson Effect MM-Wave Mixers," *IEEE Mag. 11, No. 2*, pp. 798-799, (March, 1975).
10. Y. Taur, J. H. Claasen & P. L. Richards "Conversion Gain in a Josephson Effect Mixer," *Appl. Phys. Let. 24, No. 2*, pp. 101-103, (January, 1974).
11. E. D. Thompson, "Power Flow for Josephson Elements," *IEEE-ED 20, No. 8*, pp. 680-683, (August, 1973).
12. H. Kanter, "Parametric Amplification With Self-Pumped Josephson Junctions," *IEEE Mag. 11, No. 12*, pp. 789-793, (March, 1975).
13. H. Zimmer, "Parametric Amplification of Microwaves In Superconducting Josephson Tunnel Junctions," *Appl. Phys. Let. 10, 7* p. 193, (April, 1967).
14. W. H. Parker et al, "Determination of E/h, Using Macroscopic Quantum Phase Coherence in Superconductors. I. Experiment", *Phys. Rev. 177, No. 2*, pp. 639-664, (January, 1969).
15. T. D. Clark, "Electromagnetic Properties of Point Contact JJ Arrays," *Phys. Rev B 8, No. 1*, pp. 137-162, (January, 1973).
16. M. J. Stephen, "Noise in the AC Josephson Effect," *Phys. Rev. 182, No. 2*, pp. 531-538, (June, 1969).
17. C. V. Stancampiano and S. Shapiro, *Appl. Phys. Let. 25*, p. 315 (1974).
18. D. McDonald, et al, "Four Hundredth-Order Harmonic Mixing of Microwave and Infrared Laser Radiation Using a Josephson Junction and A Maser," *Appl. Phys. Let. 20, No. 8*, pp. 296-299, (April, 1972).
19. T. Blaney & D. Knight, "Direct 825th Harmonic Mixing of A 1 GHz Source With A HCN Laser in A Josephson Junction," *Appl. Phys. 7, No. 14*, pp. 1882-1886, (September, 1974).
20. W. Jutzi, et al, "Josephson Junctions With 1 μm Dimensions and With Picosecond Switching Times," *Electronic Letters 8, No. 24*, pp. 589-591, (November, 1972).
21. D. J. Herrell, "Femtojoule Josephson Tunneling Logic Gates," *IEEE SC-9, No. 5*, pp. 277-282, (October, 1974).
22. J. Clarke, "Low-frequency Applications of Superconducting Quantum Interference Devices," *Proc. IEEE 61, No. 1*, pp. 8-19, (January, 1973).
23. E. J. Denlinger, "Radiation From Microstrip Resonators," *IEEE MTT-17*, pp. 235-236, (April, 1969).
24. J. P. Turneaure, "Microwave Surface Resistance of Superconducting Niobium," *J. of Appl. Phys. 39, No. 9*, pp. 4417-4427, (August, 1968).

PRODELIN OFFERS:

Copper corrugated elliptical waveguide and transitions



Spir-O-guide CC® —Copper corrugated elliptical waveguide available from stock for frequencies 3.7 GHz to 13.2 GHz. Premium or Super Premium available with VSWR values of 1.07 to 1.03 RMS.

Spir-O-guide CC Connectors—Precision matched transitions, untuned or tunable types. Attachment to waveguide is positive, pressure tight, and simple.

New catalog No. 1776 now available—write for your copy.

Prodelin®

ANTENNA AND TRANSMISSION LINE SYSTEM DESIGNERS/MANUFACTURERS/INSTALLERS

P.O. Box 131
Hightstown, N.J. 08520
(609) 448-2800
Telex: 843494

9707 South 76th Ave.
Bridgeview, Ill. 60455
(312) 598-2900
Telex: 728440

1350 Duane Ave.
Santa Clara, Calif. 95050
(408) 244-4720
Telex: 346453

READER SERVICE NUMBER 39

Low-Cost Detector Design Is Ideal For RF Monitors

The secret behind this design is to carefully trim the pigtails of two inexpensive axial-lead diodes. Bandwidth is modest, but it is possible to achieve 200 mV/mW sensitivity.

MANY applications exist for a high-sensitivity microwave detector where low cost is essential, but narrow bandwidth carries no penalty because system frequency is fixed and known. These challenges can be met inexpensively by combining a pair of 1N4454 high-conductance diodes.

Careful trimming of the axial diode leads is the key to the detector design, which has demonstrated 200 mV/mW sensitivity over a 3 to 4 per cent bandwidth. Sensitivity and bandwidth tradeoffs are possible by adding RF absorption to the design. The diodes, priced at a few cents, remain in the square-law region for inputs of many tens of mW, providing a high dynamic range. The output is a DC voltage suitable for driving instrumentation or display having an input resistance in the order of a megohm.

Combined, these characteristics make the detector attractive for many day-to-day power monitoring applications. Microwave oven maintenance comes to mind immediately. Such detectors might also be useful for monitoring purposes in connection with the radar systems used in private or commercial navigation.

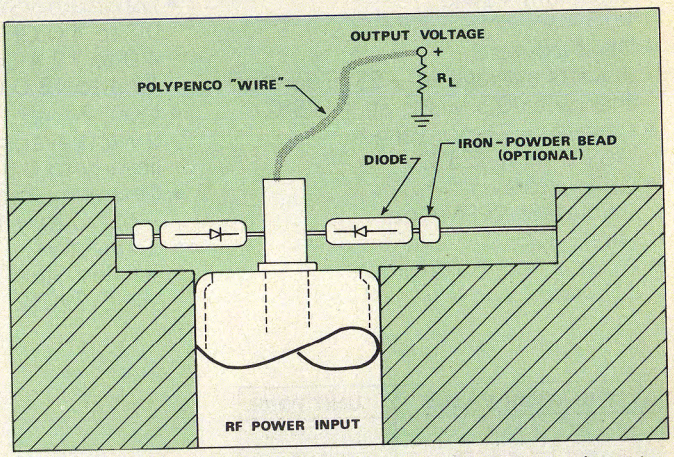

***Simple configuration and low cost** make this detector attractive for a variety of fixed-frequency applications.*

Diode leads "tweak" impedance

Details of the detector design are shown in the figure. This particular circuit is optimized for 2.45 GHz, but similar circuits should be applicable to 3 GHz. Each diode is connected directly between the RF "hot" point and ground with a length of the diode "pigtail" included. With the pigtail length minimized, the diode's impedance is expressable as $R - jX_c$, where R is approximately 3 ohms (although it increases somewhat as the absorbed RF power exceeds a few milliwatts). The value of capacitive reactance, X_c, has a slight dependence voltage developed, but can be assumed to be about 30 ohms for most 1N 4454 diodes at 2.45 GHz. As the pigtail length is increased, adding series inductance, the net reactances in series with each R can become less negative, pass through zero, and then become positive. The design objective is to make the two net diode impedances complementary: $R - jX$ where the pigtail is short and $R + jX$ where the pigtail is long. Moreover, if the relationship

$$\frac{R^2 + X^2}{2R} = R_0$$

is satisfied, the detector, as a whole, will be matched to an RF input reference impedance R_0, which would usually be 50 ohms. Unfortunately, the bandwidth of the match which is proportional to R/X, will be small because $R << R_0$. To increase the bandwidth, though always at the cost of decreasing detection sensitivity, the effective value of R may be increased by adding some RF absorption. The absorption may be added in any manner, but care must be taken not to introduce a DC path to ground. One inexpensive method is to slip an iron-powder bead (Micrometals T5-6 or T7-6, depending on the bandwidth desired) over the pigtail of each diode, and add a drop of cement to immobilize the bead.

Strictly speaking, a perfect match is not obtainable because the VSWR will always be somewhat sensitive to the RF input power level, the DC voltage developed, and changes in R_L. However, a perfect match may not be desirable because the useful bandwidth will be greater if the band-center VSWR is deliberately adjusted to be greater than unity. If the VSWR does not exceed 1.5, or even 1.75 over the needed bandwidth, the detector should be quite satisfactory for most applications.

The detector is completed by connecting a convenient length of Polypenco wire * between the diode common point and the DC output. This link has a negligible effect in the megohm-level DC circuitry, but it is a highly effective RF isolator. No bypass capacitors are needed.

Arthur Karp, Senior Research Engineer, Radio Physics Laboratory, Stanford Research Institute, 333 Ravenswood Avenue, Menlo Park, CA 94025.

Diodes operate under square law

The diode polarities (and the avoidance of DC conduction via the RF input) force any direct current flowing through either diode to return only through the large resistance R_L. The current limiting effect of R_L not only prevents component damage, but keeps the diode's forward conduction in the square-law region of the rectification characteristic. Consequently, the DC output voltage—which may reach several volts—is essentially a linear function of the RF input power over a very wide dynamic range. Although the actual limit may be higher, input powers of up to 15 milliwatts have been applied without observing any non-linearity. The only precaution necessary with regard to maximum input power (or allowable peak power in the case of pulsed signals) is that the DC voltage developed should never exceed the reverse breakdown voltage of the diode. For the lN4454, this is a comfortable 75 volts. RF input attenuators should thus be unnecessary; in fact, they're best avoided since they might introduce a DC path to ground. (In most systems, the detector would normally be appended to a short electric-field probe).

With R_L=1 megohm, and without damping beads, a detection sensitivity of roughly 200 millivolts per milliwatt has been demonstrated at the center of a frequency band 3 to 4 per cent wide at the half-efficiency points. Increasing R_L to 3 megohms increases detection sensitivity by only about 25 per cent. Including a set of T5-6 damping beads quadruples the bandwidth 15 per cent, but decreases the maximum sensitivity about 7 dB. When several units are fabricated, the actual detection efficiency will, no doubt, vary from unit to unit, but this is usually of little concern in the intended applications. Selection of diodes from a batch may be necessary if the detector cannot be "tuned" to the desired frequency or if too low or too high a detection sensitivity is observed. ••

Acknowledgement

Many thanks to H.J. Jacobs and R.C. Stenger for their efforts in fabricating and tuning a substantial number of the detector circuits described here.

*Polypenco wire is a carbon-bearing Teflon monofilament with a resistivity of about 1700 ohms per inch, manufactured by Polymer Corporation's Polypenco Division in Reading, PA. Solderable tips are easily added to the exposed ends of the sheathed plastic monofilament by applying a few turns of fine-gauge wire with a wrapping tool.

Looking for literature? MicroWaves' Catalog Update section can keep you in tune with the latest product, service and application information. To preview the latest in literature, and obtain it promptly and at no charge, turn to p.92.

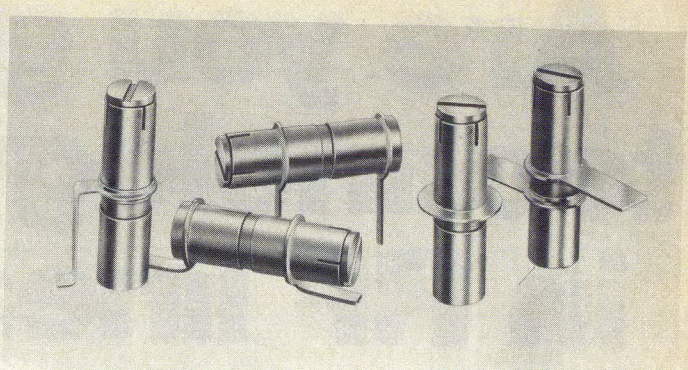

GIGA-TRIM CAPACITORS FOR MICROWAVE DESIGNERS

GIGA-TRIM (gigahertz-trimmers) are tiny variable capacitors which provide a beautifully straightforward technique to fine tune RF hybrid circuits and MIC's into proper behavior.

APPLICATIONS

- Impedance matching of GHz transistor circuits
- Series or shunt "gap trimming" of microstrips
- External tweaking of cavities

Available in 5 sizes and 5 mounting styles with capacitance ranges from .3 - 1.2 pf to 7 - 30 pf.

Johanson®

MANUFACTURING CORPORATION
Rockaway Valley Road
Boonton, N.J. 07005
(201) 334-2676 TWX 710-987-8367

READER SERVICE NUMBER 41

STANDARD MIS MATCHES

MMC

● DC-18 GHz ● PRECISION ● CALIBRATED



MISMATCH VALUE (VSWR)	MODEL NUMBER						
	TYPE N		APC7	TYPE TNC		TYPE SMA	
	Female	Male		Female	Male	Female	Male
1.05	2561A	2562A	2611A	8611A	8612A	8711A	8712A
1.10	2561B	2562B	2611B	8611B	8612B	8711B	8712B
1.20	2561C	2562C	2611C	8611C	8612C	8711C	8712C
1.30	2561D	2562D	2611D	8611D	8612D	8711D	8712D
1.50	2561E	2562E	2611E	8611E	8612E	8711E	8712E
1.75	2561F	2562F	2611F	8611F	8612F	8711F	8712F
2.00	2561G	2562G	2611G	8611G	8612G	8711G	8712G

MAURY MICROWAVE 20TH ANNIVERSARY 1957 1977

MMC produces a complete line of coaxial & Waveguide Mismatches and Terminations. Call or send for complete details. *Today!*

See our new Short Form Catalog in Microwaves 76/77 Product Data Directory.

MAURY MICROWAVE CORPORATION
CUCAMONGA, CALIFORNIA 91730, U.S.A. • TELEPHONE 714 987 4715

READER SERVICE NUMBER 42

Active Circuits Keep Systems On The Level

Whenever a constant output is needed in the presence of a varying input, some leveler circuit must be used. It turns out that an active, closed-loop leveler works best.

WHEN it comes to signal leveling, there are only two basic approaches—active or passive levelers. The simplest kind of a leveler is the familiar limiter circuit, shown in Fig. 1a. The only feedback in this circuit is that developed by the non-linear element DC current. In operation, since the bias current for the PIN diode is generated by the detector (a diode or varactor), increases in the output power level result in more DC bias that increases the PIN attenuation with the attendant decrease in the output power.

The circuit shown in Fig. 1a is simple, small and easy to build, but it works only at a given power level. To provide some control, a variable resistance can be inserted to vary the output power (see Fig. 1b). Still, this circuit has a dynamic range of only several dB since its sensitivity decreases with an increase in R.

In general, simple limiters of the kind shown in Figs. 1a and 1b suffer from being narrowband and load sensitive, offer poor correction (compared to active types), a limited dynamic range and generate harmonics. Due to these drawbacks, limiters are largely used as protective devices into a constant load, generally followed by a tuned circuit.

A more universal leveler circuit is shown in Fig. 1c. In operation, a known and constant portion of the signal is picked off by the sampler and fed to a detector. The detected output is compared to a reference and the resulting error is fed back to the voltage-variable attenuator (VVA) in proper phase to control the output. Specifications for a leveler that can be readily built on this principle are shown in Table 1. To understand how such leveler operates and can be built, let's discuss its various parts in some detail.

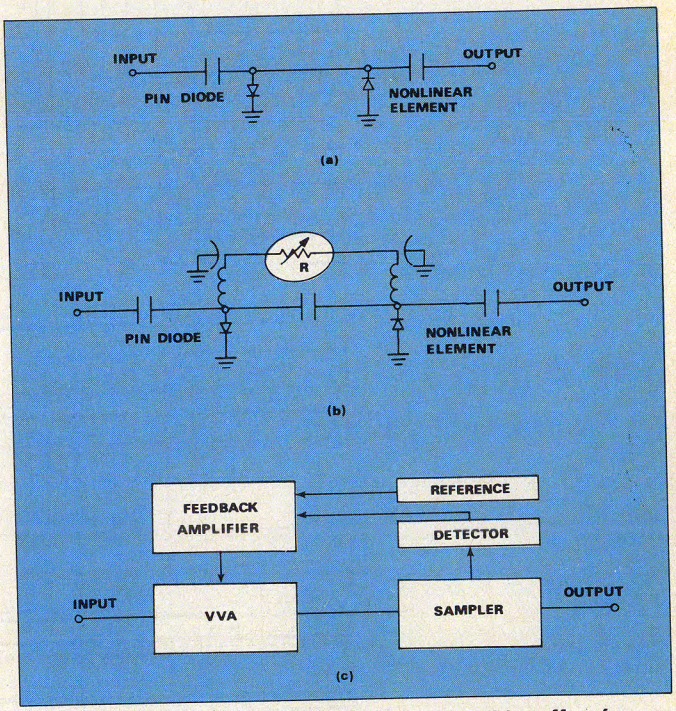

*1. **Simple limiter-type levelers (a) and (b) suffer** from a number of shortcomings that are overcome by a feedback-type leveler (c). See Table 1 for performance that can be achieved with this kind of leveler.*

Sampler is the key

Since the flatness (degree of leveling) as a function of frequency and load impedance largely depends on the sampler, it is the most critical component in the loop. The most popular leveler sampler is a flat directional coupler. To get a reasonable compromise between insertion loss and detector output voltage, its coupling value should be 10 to 20 dB (this value also depends on the desired output level). In addition to the coupling value, there are other considerations in selecting a coupler for a leveler application.

Since levelers usually must operate over a wide bandwidth, octave or multioctave band couplers are selected. Couplers of this type can have a frequency sensitivity on the order of ±0.15 dB per octave and ±0.5 dB over a 1 to 18 GHz range.

The coupled port in a "leveler-type" coupler must track the *output*. This is to ensure that the output voltage square-law detector connected to the coupled port is proportional to the coupler output power. (A "monitor-type" coupler produces an output that tracks the input). High directivity couplers generally sacrifice flatness for directivity.

When the ultimate in tracking between the detector and output ports is required, an in-phase power divider should be used. The price paid for the near-perfect tracking is insertion loss—almost 4 dB on the through line, versus less than 1 dB for a flat octave band coupler. Another advantage of a power divider is that it can be readily incorporated into a microstrip circuit.

An important function of the leveler is to effectively produce a matched source impedance at its output. This is accomplished by not responding to reflected power, i.e., this

(continued on p. 64)

Jerry Hausner, Chief Engineer, The Narda Microwave Corporation, 75 Commercial Ave., Plainview, NY 11803.

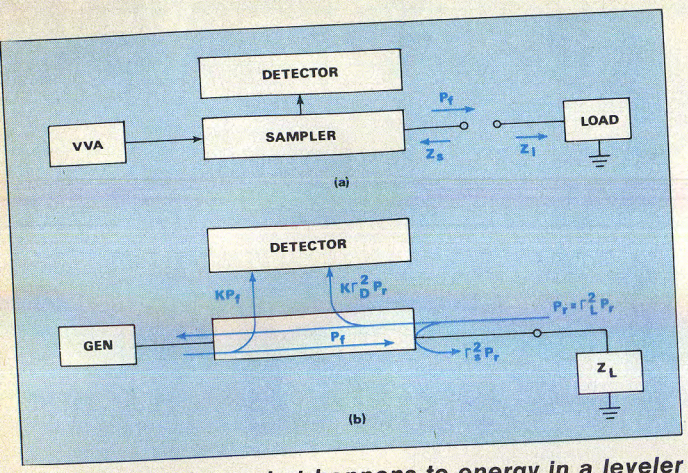

2. ***Understanding what happens to energy in a leveler*** *can be achieved with simple analysis (a). To derive the expression for the output VSWR, a more detailed diagram is used (b).*

depends on the directivity of the coupler or isolation of the power divider. Thus if the coupler had infinite directivity, none of the reflected power would reach the detector and forward power would remain constant in spite of load-impedance changes.

Ideally, the leveler will produce a constant-power signal at its output, P_f. This will only be the power absorbed by the load if the load has a zero reflection coefficient, Γ, or a VSWR of 1.0 referred to the characteristic impedance (Z_0) of the coupler, see Fig. 2a. In the case of a directional coupler, the output power is maintained constant because the coupled-arm output power is proportional to the power flowing through the main line toward the output port. A power divider produces an output to the detector that is a function of the signal entering the main junction. Excellent flatness is achieved due to the inherently good symmetry between the arms.

The forward power, P_f, consists of "new" and recycled power. The "new" power is the power passing through the VVA and is equal to the system losses plus the power absorbed by the load. The recycled power is the energy reflected by the load and then reflected again by the VVA (if the VVA is reflective rather than absorptive).

In a practical system, complete or infinite isolation is impossible and the output impedance differs from Z_0. Referring to Fig. 2b, the portion of the reflected power that reaches the detector can be defined as Γ_D. The output of a leveler is also degraded by imperfections in the transmission-line impedance and connector of the sampling device. The output VSWR of that device has an associated reflection coefficient, Γ_S.

The uncontrolled portion of the power traveling toward the load consists of $\Gamma_S P_r$ and $\Gamma_D P_r$. The combined coefficient is the vector sum $\Gamma_S + \Gamma_D = \Gamma_S'$. The output VSWR, V_S', is then

$$V_S' = \frac{(1 + |\Gamma_S'|)}{(1 - |\Gamma_S'|)} \qquad (1)$$

If the vectors add in the worst case, then

$$V_S' = \frac{(1 + |\Gamma_S| + |\Gamma_D|)}{(1 - |\Gamma_S| - |\Gamma_D|).} \qquad (2)$$

(continued on p. 66)

Table 1. Specifications achievable for a C-band leveler with octave bandwidth

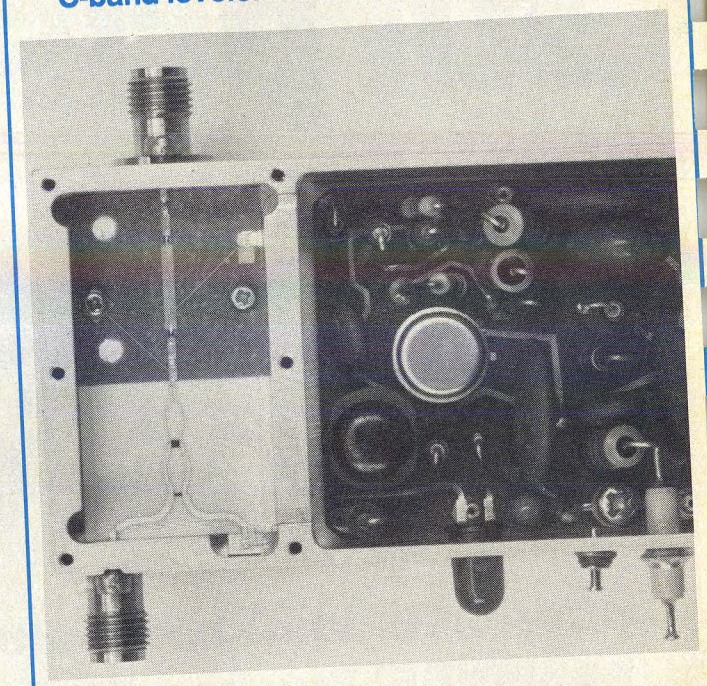

Frequency range	4.0-8.0 GHz
Power variation:	
W/ frequency	±0.25 dB
W/ input change	±0.1 dB
W/ temperature	0.005 dB/°C
Output power range (adjustable)	−10 to +20 dBm
Input power range, RF	− 5 to +30 dBm
Insertion loss (max)	5 dB
Equivalent source match (max)	1.25 VSWR
Modulation (optional)	
Output rise time (typical)	3 μs
Delay	3 μs
Input power (DC)	+15V @ 75 mA
	−15V @ 25 mA

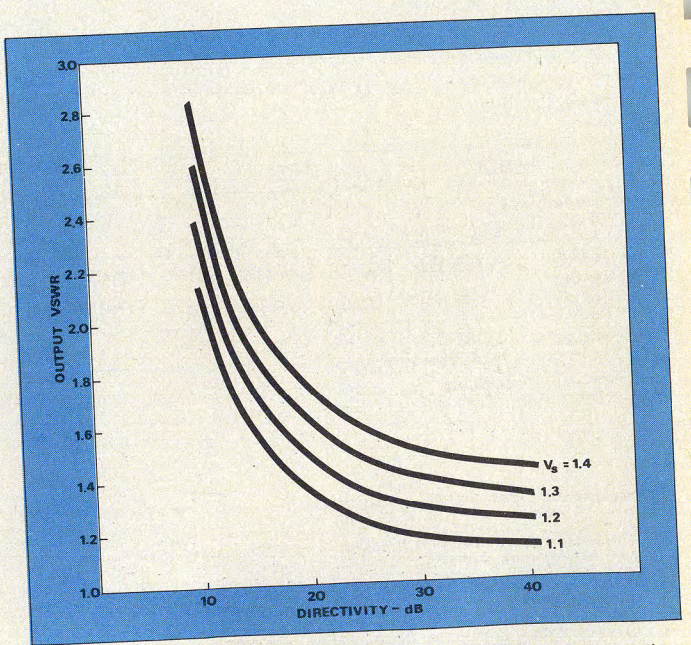

3. ***At-a-glance appraisal of leveler VSWR*** *as a function of the sampler reverse isolation for various values of sampler VSWR is obtained by plotting Eq. 5.*

Watts on your mind?

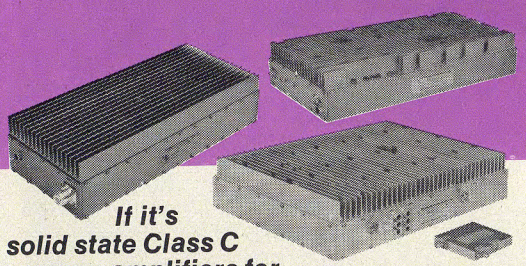

If it's solid state Class C power amplifiers for CW/FM/Pulse applications, then we've got the answers.

When your mind turns to solid state microwave power, turn toward us, because we've got the industry's most complete line-up of standard-design models in three series:

Series EWA includes 60 electronically-protected models covering frequency ranges from 2-32 MHz to 600-1000 MHz. They deliver up to 1000 watts, over a 56% bandwidth in the VHF/UHF area and decade or octave bandwidths in the HF/VHF range.

For circulator-protected units, our Series PWA offers 161 standard models spanning frequency ranges from 100-150 MHz to 3700-4200 MHz, at powers up to 1000 watts.

Series PA, with built-in load protection, is recommended for narrow band (up to 10%) high power applications requiring small size, high efficiency and maximum reliability. Models are available for frequency ranges from 2 to 4200 MHz, power outputs up to 2000 watts, and efficiency ratings as high as 80%.

And remember, these are all standard units. For your really "special" needs, or for complete amplifier systems and sub-systems, just give us a look at your specs — if we can't get the job done, it probably can't be done.

MPD

MICROWAVE POWER DEVICES, INC.

Adams Court, Plainview, N.Y. · Tel. 516-433-1400 · TWX 510-221-1862

READER SERVICE NUMBER 45

The sampler reflection coefficient is given by

$$|\Gamma_S| = \frac{(V - 1)}{(V + 1),} \quad (3)$$

where V is the output VSWR of the sampler. Since Γ_D is the numeric factor of the directivity, D ,or reverse isolation, Γ_D can be represented by the relationship:

$$|\Gamma_D| = \sqrt{10^{-D/10}}. \quad (4)$$

The output VSWR can then be written as:

$$V_S' = \frac{1 + \left|\frac{V-1}{V+1}\right| + \sqrt{10^{-D/10}}}{1 - \left|\frac{V-1}{V+1}\right| - \sqrt{10^{-D/10}}} \quad (5)$$

The above equation gives the relationship between the directivity of the sampler and output VSWR. For the sake of convenience, this equation is plotted in Fig. 3.

Detecting the output

The most common detectors used in levelers, point contact diodes, can be matched to microwave structures over broad bands with a flat sensitivity-to-frequency characteristic. They also have a fast response and good slope sensitivity, k, defined as the detector output voltage ratio to input power, i.e., $k = V_d/P_{in}$. However, they are temperature sensitive and have a high output impedance.

Schottky detectors offer relatively low output impedance but their temperature stability is insufficient in many cases. To overcome this, an approach depicted in Fig. 4 can be used. Here two Schottky detectors are used: One receives the RF signal, while the other is used as a DC reference only. If conventional Schottkys are used, equal DC bias must be supplied to both detectors. The change in forward saturation voltage of both detectors due to temperature changes is then subtracted in the differential amplifier, leaving only the variation in detector output resulting from power change.

Lately, a more popular approach has been to use a back diode detector (a back diode is a special version of a tunnel diode). In general, this diode is more difficult to handle, but it does offer temperature stability comparable to a pair of Schottkys.

The best leveling with good response time is usually achieved with the standard point-contact detector. This diode is the easiest to match over a broad band to get the flattest frequency response. Its output impedance is relatively high, typically 10k to 25k ohms. However, video bandwidths of 10 MHz are readily attainable. Consequently, negligible phase shift is introduced by this device since this is sufficiently greater than that of the closed loop.

The ultimate in leveling flatness is attained using a thermocouple or thermistor power meter mount as the detector. Their response, however, is very slow since they require RF heating of the detector element. Slow response

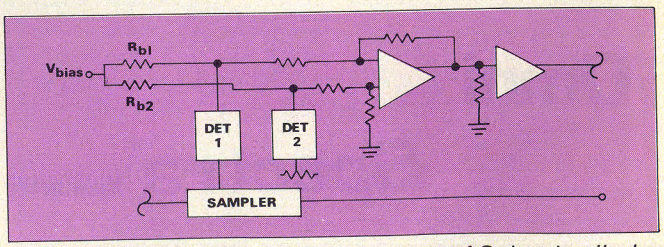

*4. **To null temperature effects,** a pair of Schottky diodes feeding into a differential amplifier are effective.*

to signal-level changes results in excessive phase shift at audio frequencies, thereby creating a pole in the closed-loop response. This, in turn, forces one to roll off the loop at low frequencies to maintain stability. The resulting narrow bandwidth (5 to 10 Hz) makes this approach unsuitable for rapidly swept systems. It can be used for swept measurements when the results are plotted on an X-Y recorder and sweep time is about 60 s per octave.

Controlling the VVA

A functional diagram of a feedback amplifier that controls the VVA is shown in Fig. 5a. Prior to discussing its operation, it is well worth it to consider the VVA.

In most self-contained systems the control element—the VVA—is usually a PIN attenuator. If a leveler is a part of a large system, the control element can be the grid of a TWT or the gate of a FET.

The PIN attenuator is selected to have a shallow attenuation versus current curve and to be as linear as possible over a wide attenuation range for stability reasons (see Fig. 5b). To avoid the generation of detrimental harmonics, the diodes should have long carrier lifetime relative to the period of the lowest operating frequency.

Turning our attention to the feedback amplifier, note that in Fig. 5a it is assumed that the reference and the detector are of opposite polarity, since most detectors have negative output. If the reference were also negative, it would be fed to the positive amplifier input.

In this circuit, the loop will adjust the weighted detector output so that it nulls out the weighted reference voltage. The term "weighted" is used because the voltages need not be equal. Thus the gain of the reference is R_4/R_3 (assuming $R_3 >> R_1$). The gain of the detected voltage, V_d, is $R_4/(R_2 + R_{dv})$, where R_{dv} is the detector video output impedance. In the case of point-contact detectors, R_{dv} is sufficiently high so that it cannot be neglected. Unequal gains from each input allow the use of a reference voltage that is much higher than V_d. This is an advantage because V_d is usually in the order of millivolts and generating such a low voltage reference is difficult from stability and noise-immunity points of view.

The amplifier output proportional to the unbalance at its input is fed to a driver circuit for the PIN attenuator via a roll-off network for controlling the loop response. Signal phasing is such that the loop will adjust the RF level so that the detector output voltage nulls out the reference at the amplifier input.

The roll-off (lead-lag) network consisting of R_5, R_6, and C_1 reduces the gain at the following frequency:

$$f = \frac{1}{2\pi\ R_5\ C_1},$$

and is necessary for the stability of the loop.

In general, stability conditions can be stated as follows. The open-loop gain must be less than unity at the frequency where the phase shift goes above 180 degrees. A convenient way to study the open-loop gain (OLG) is to plot its amplitude and phase response as a function of frequency (the Bode plot). Such a plot is shown in Fig. 5c. The first breakpoint occurs at $1/\tau_1$, where τ_1 in this case is equal to C_1R_5. The gain starts to decrease at 6 dB per octave. If this were allowed to continue uninterrupted, the phase shift due to this point would approach 90 degrees. The second breakpoint, however, enters the picture and it is due to τ_2 =

(continued on p. 68)

Our family tree of linear amplifiers.



Series LLD
Low level amplifiers, up to ½ watt.



Series LWA
High power amplifiers, up to 20 watts.



Series LAB
Laboratory instruments, up to 20 watts, leveled ±0.25 dB.



Series EWAL
Class A/B linear amplifiers up to 1000 watts.

It grows solid state Class A ultra-broadband amplifiers.

We use the industry's most advanced solid state technology and lots of in-depth experience to nourish our tree. The results are rewarding:

Series LLD includes a choice of 9 models with frequency ranges from .005-.5 GHz to 1.7-2.4 GHz, linear power outputs up to 450 milliwatts, and gain ratings up to 30 dB.

High power applications up to 20 watts call for the Series LWA, with 22 models offering frequency ranges from .005-.5 GHz to 3.7-4.2 GHz. All Series LLD and LWA units feature our exclusive replaceable module design for production uniformity and simplified field service.

For the laboratory user of RF and microwave power amplifiers, the Series LAB provides a choice of 62 models with built-in power supply, instrument case or rack mount styles, spanning the frequency spectrum from 5 MHz to 4.2 GHz. Linear power up to 20 watts, with such features as gain control, external modulation and ±0.25 dB leveled power output.

Series EWAL amplifiers deliver up to 1000 watts of Class A/B linear power. Off-the-shelf designs available for frequencies from 2 MHz to 500 MHz with wide bandwidths, up to several octaves. Ideal for applications such as TV transmitters, wideband hi-power jammers and add-on AM amplifiers.

That's our tree. All you have to do is step up and pick off the product you need. How sweet it is!

MPD

MICROWAVE POWER DEVICES, INC.

Adams Court, Plainview, N.Y. · Tel. 516-433-1400 · TWX 510-221-1862

READER SERVICE NUMBER 46

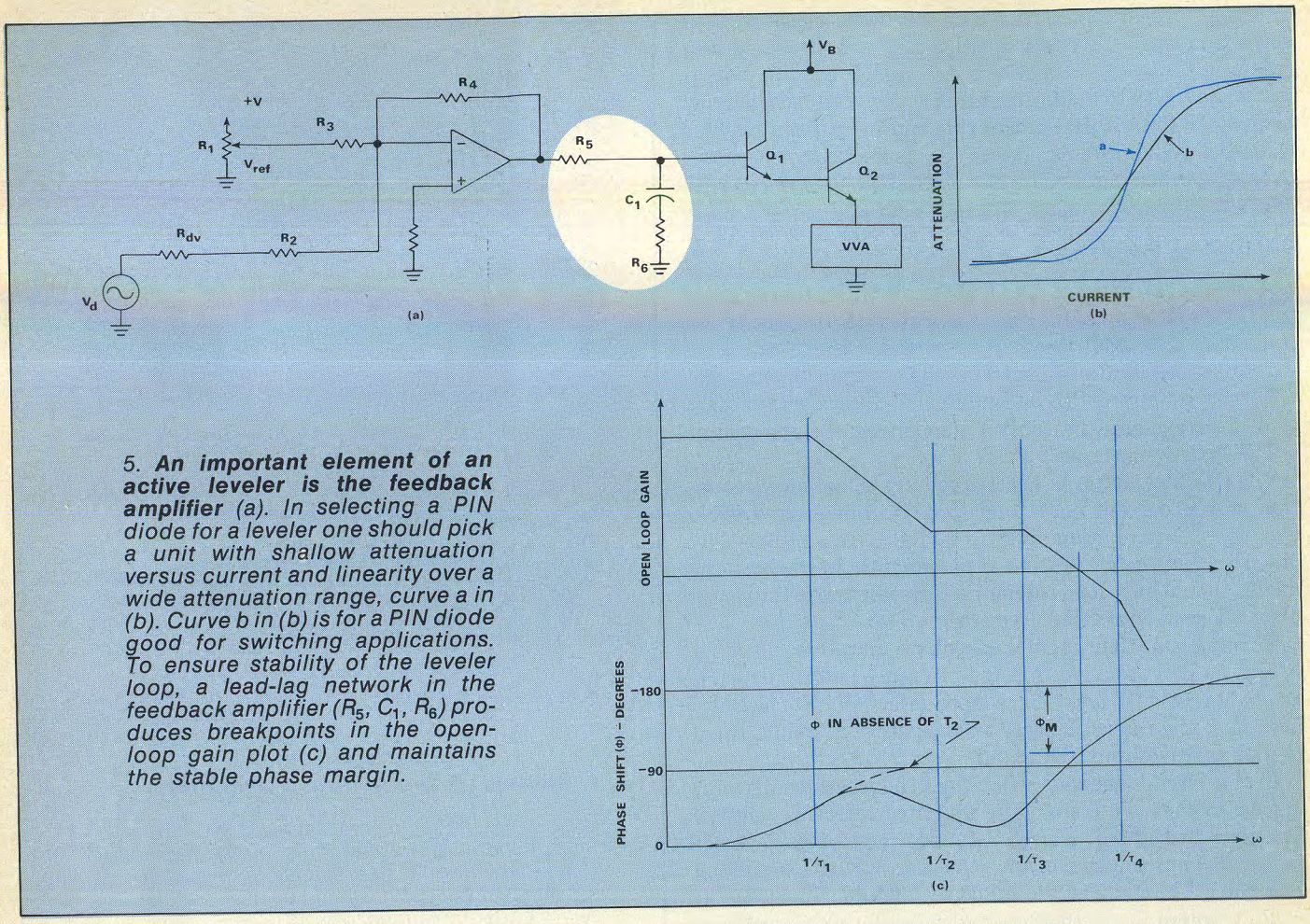

*5. **An important element of an active leveler is the feedback amplifier** (a). In selecting a PIN diode for a leveler one should pick a unit with shallow attenuation versus current and linearity over a wide attenuation range, curve a in (b). Curve b in (b) is for a PIN diode good for switching applications. To ensure stability of the leveler loop, a lead-lag network in the feedback amplifier (R_5, C_1, R_6) produces breakpoints in the open-loop gain plot (c) and maintains the stable phase margin.*

$C_1R_5 || R_6$. The zero caused by this breakpoint introduces a lead of 90 degrees, cancelling the phase shift of the first breakpoint. The two next breakpoints, $1/\tau_3$ and $1/\tau_4$, are generally caused by parasitics and are uncontrolled. Each of these will contribute a 90-degree phase shift, so that eventually there will be a 180-degree phase shift in this feedback loop. The purpose of introducing the lead-lag network was to reduce the gain in the regions of $1/\tau_3$ and $1/\tau_4$, so that there is less than 0-dB gain when 180-degree phase shift is reached. The attenuation due to this network is

$$\text{Att.} = 20 \log_{10} \left[\frac{R_6}{R_5 + R_6} \right]$$

A figure of merit for most servoloops is the phase margin, i.e., 180 degrees minus the phase shift at the point where the gain goes through unity (0 dB). A minimum phase margin of 35 degrees is considered necessary for stability. In most practical leveling loops, the slowest reacting component—and thereby the greatest contributor to the phase shift—is usually the PIN switch. This is because diodes with long carrier lifetimes are selected to ensure that harmonics are not generated under any bias conditions of the PIN diode. Typical 0-dB crossing frequency for the Bode plot is in the range of 50 to 100 kHz.

There are two other major reasons why a PIN switch contributes to the instability of the loop:

1. Since the gain vs. current curve is nonlinear, the gain of the loop changes with different power levels.
2. The speed of response is not symmetrical. That is, the PIN diode reduces power with increasing bias current much faster than it increases power with decreasing bias current. Thus the phase shift depends on the direction of level correction. To cope with this, a considerable amount of bandwidth is sacrificed when stabilizing such a loop to ensure that it will be stable under the worst-case conditions (maximum attenuation versus current) in the PIN diode and during the correction with the slowest response.

Check the dynamic range

Another parameter that should definitely be considered when designing or purchasing a leveler is the required dynamic range. It is defined as the expected peak-to-peak variation of the unleveled input plus the attenuation range desired at the leveler output. A dynamic range over 20 dB is readily achievable.

The range is usually limited by the combination of the amplifier and detector, i.e., as the output RF level is reduced, the same fractional change in output produces a smaller voltage change in the detector output than at higher levels. Reduction in output below a certain minimum level brings the detector output level below the threshold of the amplifier.

The PIN attenuator can also limit the dynamic range if the isolation minus the insertion loss is less than the detector/amplifier range. This sets the lower limit for the

(continued on p. 70)

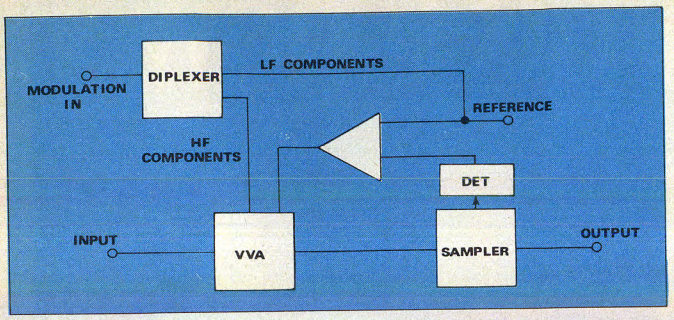

*6. **One way to modulate leveler output** might be by modulating simultaneously the VVA and the reference. This approach, so far, has not been too successful.*

dynamic range. The upper limit of the leveler dynamic range is the minimum raw input power (whether it is a function of time or frequency) less the insertion loss of the leveler.

Modulating the leveled signal

Since it is frequently desirable to amplitude modulate a leveled signal (linear audio or pulse modulation), it is well worth it to look at some approaches to this problem.

If the leveler input power does not vary rapidly with time, a narrow-band loop can be used. The modulation can then be applied directly to the VVA. If the spectrum of the modulating signal is above the loop bandwidth, then the loop will not see it. If the modulating signal has frequencies within the loop bandwidth, the loop will attempt to cancel the modulation to a degree dependent on the amount of closed loop gain existing at the modulating frequency.

In most cases, however, modulation frequencies lie within the loop bandwidth, so that the modulation must be applied through the loop. This can be done by pulsing the reference to zero or superimposing the modulating signal on the DC reference. If the detector is operating in the square-law region, the power output will vary directly as the reference voltage. If the detector is operating in its linear region, then the output voltage will vary in proportion to the reference voltage. The bandwidth of the modulation is then limited by the loop bandwidth. If this is unacceptable, an external modulator after the loop can be used.

Some attempts have been made to modulate the PIN diode simultaneously with the reference by diplexing the modulating signal so that high-frequency components bypass the loop, as shown in Fig. 6. This type of circuit, however, is difficult to adjust for proper operation due to nonlinearities and response to uncontrolled reactances at the crossover frequency. For this reason, either of the first two approaches is used with the modulation applied through or after the loop.

Modulation depth (on-off ratio) is determined by the dynamic range of the loop. Since the stability or noise during the off time is usually not too important, the depth of modulation is determined by the PIN attenuator isolation. The isolation, less the insertion loss, must be sufficient to accommodate the variation in unleveled input plus the range of control on the output plus the modulation depth. A 30-dB on-off ratio can be achieved over a broad frequency range, but not without some difficulty. ••

Acknowledgement

The author expresses his appreciation for editorial assistance to W. Camp, S. Casper, and J. Ranghelli.

Millimeter Front Ends from TRG.

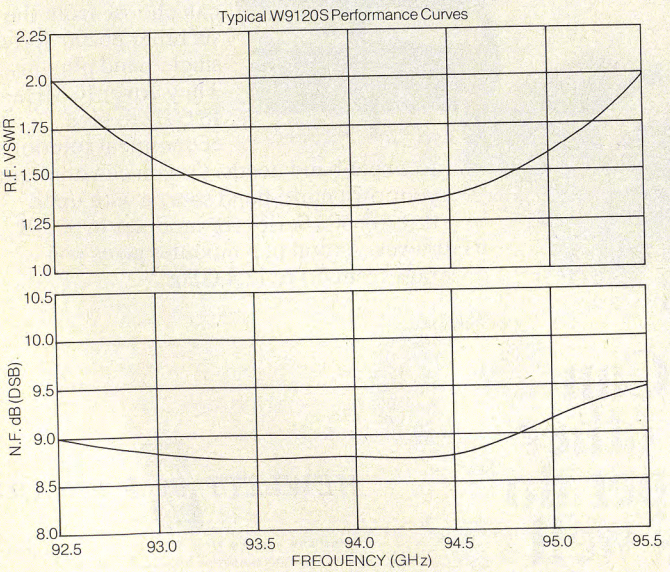

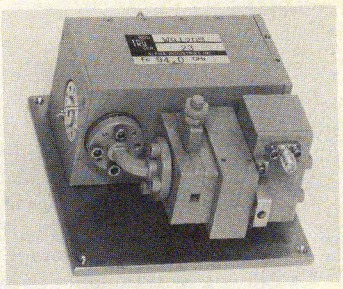

Whether you're looking for the total front end assembly or individual building blocks . . . come to TRG. We have the mixers, isolators and LO's with or without multipliers to meet your needs. For example, the receiver illustrated and known as the "quiet performer" incorporates a TRG 47GHz Gunn Oscillator, isolator and frequency doubler supplying 10mW of L.O. drive at 94GHz. So save yourself time and money at the design stage; call in the Millimeter Men or write for our catalog and data sheet.

TRG Alpha DIVISION **Our limits are your imagination.**

ALPHA INDUSTRIES, INC. • 20 Sylvan Road, Woburn, Massachusetts 01801 • (617) 935-5150 • TWX: 710-393-1236 • TELEX 949436

READER SERVICE NUMBER 48

APRIL
1977

MICROWAVES

laser technology

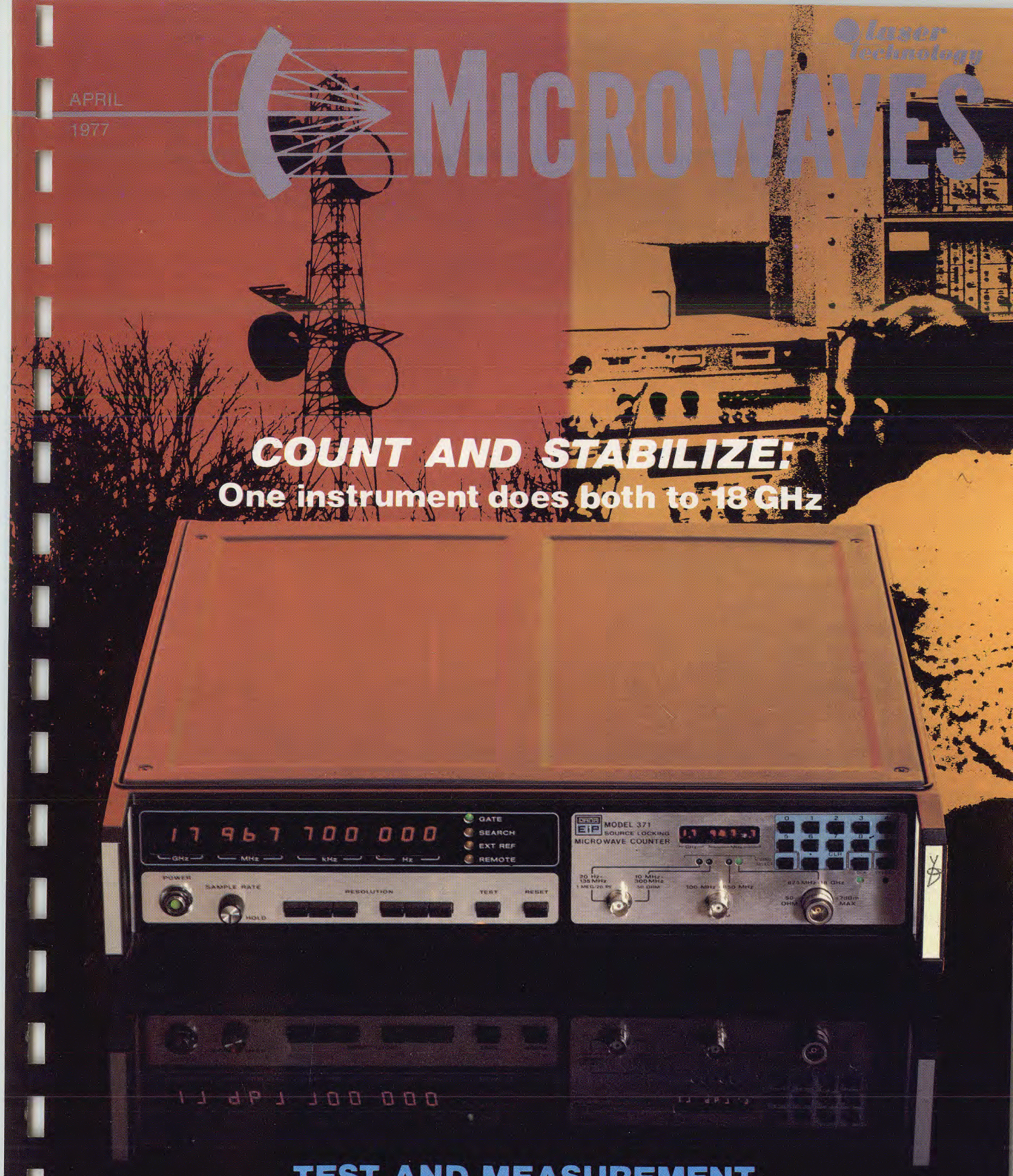

COUNT AND STABILIZE:
One instrument does both to 18 GHz

TEST AND MEASUREMENT

SWEPT MEASUREMENTS SPEED GAIN COMPRESSION TESTS

MEASUREMENT ACCURACY HINGES ON PROPER COUPLER DESIGN

CAVITY TECHNIQUE EASES COMPLEX DIELECTRIC MEASUREMENTS

ALSO: IMPATTS SURGE TO HIGHER POWERS AND FREQUENCIES

GIGABIT LOGIC: SPEED RISES, AS POWER FALLS

bipolar problems - it's MOSPOWER® FET."



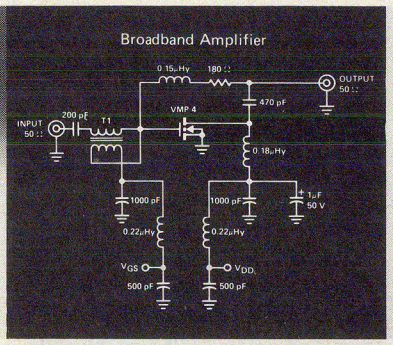

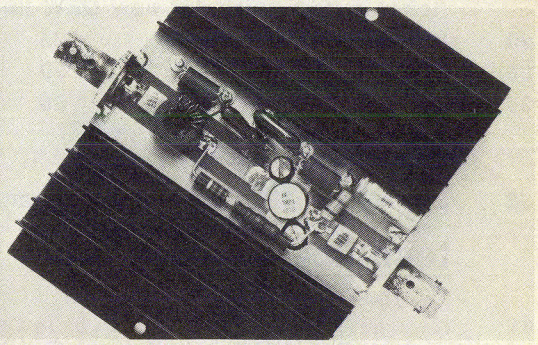

Until now, RF designers have had to live with the basic limitations of bipolar transistors that complicated VHF/UHF transmitter and transceiver design. You had to build costly stages, with careful load matching and extra components to prevent thermal runaway and load mismatch failures.

Our new VMP 4 MOSPOWER FET changes all that. It's the first commercially available FET to operate at high power at radio frequencies offering better than 10W class C at 150 MHz. It's also the first with ideal characteristics for small-signal applications as well as linear power and switching amplifiers. So you can use it at any VHF transceiver stage, achieving new economies in design, production and maintenance.

The VMP 4 is, first of all, a high reliability, high performance power transistor offering input impedances that are easier to match over broad bands and capable of unsaturated gain of as much as 18 dB at 200 MHz. It can operate under the most adverse RF loads—short circuit to open circuit. So it eliminates mismatch burnout and loss of available output power.

Now efficient class D, E and F switch mode designs are practical with the VMP 4. Since the VMP 4 is MOSFET, it's a majority carrier device, with no minority carrier storage time. So it can, for example, switch 2A in less than four nanoseconds, or 10A in less than six. That's 10 to 200 times faster than bipolars.

As a front end in VHF transceivers, the VMP 4 offers low noise figure as well as high dynamic range due to its small-signal linearity. It's minimum gain is 15 dB at 150 MHz, with a typical small-signal noise figure of 2.5 dB at 150 MHz. Two tone intermodulation intercept point is a high + 46 dBm.

Siliconix has the VMP 4 in stock now, for as low as $13.97 in 100-up quantities. To encourage you to see how the VMP 4 can improve your RF design, we're offering a single VMP 4 plus applications notes and data sheet at the 100-up price.

To place an order, or for more information, contact our franchised distributors: Components Plus, Elmar, Future, Hamilton/Avnet, Pioneer, Quality Components, Semiconductor Specialists, Wilshire or RAE. Siliconix Incorporated, 2201 Laurelwood Road, Santa Clara, CA 95054 (408) 246-8000.

Siliconix incorporated

READER SERVICE NUMBER 6

MICROWAVES

April 1977
Vol. 16, No. 4

news

9 **Impatts surge to higher powers and frequencies**
12 **Gigabit logic: Speed rises as power falls**
14 **NBS study focuses on SMA connectors**
Robot radars eyed for new DEW line
20 **Industry** 23 **Washington**
28 **International** 30 **Meetings**
35 **R & D** 36 **For Your Personal Interest...**

editorial

38 Engineering: Still a white man's game

technical

Test and Measurement

41 **Measurement Accuracy Hinges On Coupler Design.** Christian Staeger and Dr. Peter Kartaschoff of the Swiss Post Office, zero in on the role of the directional coupler in a variety of swept measurement systems ranging from a simple reflectometer to a computer-controlled analyzer.

48 **Swept Measurements Speed Gain Compression Tests.** Thomas R. Brinkoetter of Hewlett-Packard Company, offers several swept-measurement methods for characterizing broadband, linear amplifiers.

56 **Vector Voltmeters Perk Up With High-Speed Sampling.** Don Stock of the PRD Division of Harris Corp., explains how the high-speed sampling techniques used in modern vector voltmeters can be put to use for a wide range of RF measurements.

64 **Simple Setup Measures Complex Dielectric Data.** Ashish K. Tagore of the Advanced Center for Electronic Systems and Dr. Chinmoy Das Gupta of the Indian Institute of Technology, describe a coax-line resonator that simplifies the measurement of a material's complex dielectric constants.

departments

66 **Cover Feature:** Count and stabilize: One instrument does both to 18 GHz
69 **New Products** 80 **Application Notes**
81 **New Literature** 83 **Advertisers' Index**
84 **Product Index**

About the cover: EIP's new model 371 enjoys a split personality: In addition to being an automatic frequency counter, the instrument provides an ultra-stable locking circuit to improve the output of almost any signal generator. For details on this double-duty source-locking counter, see page 66. Cover photo by Tycer-Fultz, Palo Alto, CA; composition by Art Director Robert Meehan.

coming next month: Electronic Warfare

ECM Systems: Internal or Pod? Before the Vietnam-era Soviet EW systems stunned US defense planners, the issue was whether or not ECM protection for aircraft was needed. Now that its importance has been recognized, industry has split down two paths: pod-mounted and internal systems. In a staff-written report, we'll examine the particular requirements each approach places on the RF design engineer.

Design GaAs FET Amplifiers For Multi-Octave Performance. Broadband is the key word in EW, and the key feature of the GaAs FET. Guidelines are presented in a highly design-oriented article for designing low-noise amps over bandwidths of 5:1 or greater. Performance examples include a 1.5 to 8 GHz amplifier module that offers 7.5 ±1 dB gain, 4.5-dB noise figure and +10 dBm output power.

Publisher
Howard Bierman

Editor-in-Chief
Stacy V. Bearse

Associate Editor
Frank G. Lynn

Contributing Editor
George R. Davis

Washington Editor
Paul Harris
Snyder Associates
1050 Potomac St. NW
Washington, DC 20007
(202) 965-3700

Editorial Assistant
Gail Murphy

Production Editor
Sherry Lynne Karpen

Art Director
Robert Meehan

Art Illustrator
Janice Tapp

Production
Dollie S. Viebig, Mgr.
Anne Molfetas

Circulation
Barbara Freundlich, Dir.
Sherry Karpen,
Reader Service

Directory Coordinator
Janice Tapp

Editorial Office
50 Essex St.,
Rochelle Park, NJ 07662
Phone (201) 843-0550
TWX 710-990-5071

A Hayden Publication
James S. Mulholland, Jr.,
President

MICROWAVES is sent free to individuals actively engaged in microwave work. Prices for non-qualified subscribers:

	1 Yr.	2 Yr.	3 Yr.	Single Copy
U.S.	$25	$40	$ 60	$3.00
Foreign	$40	$70	$100	$4.00

Additional Product Data Directory reference issue, $15.00 each (U.S), $27.00, (Foreign). POSTMASTER, please send Form 3579 to Fulfillment Manager, MicroWaves, P.O. Box 13801, Philadelphia, PA. 19101.

Back Issues of MicroWaves are available on microfilm, microfiche, 16mm or 35mm roll film. They can be ordered from Xerox University Microfilms, 300 North Zeeb Road, Ann Arbor, MI 48106. For immediate information, call (313) 761-4700.

Hayden Publishing Co., Inc., James S. Mulholland, President, printed at Brown Printing Co., Inc., Waseca, MN.

Copyright © 1977 Hayden Publishing Co., Inc., all rights reserved.

Measurement Accuracy Hinges On Coupler Design

The accuracy of a swept measurement system depends largely on the directional coupler used. Here is a design with 50-dB directivity that allows simple measurement setups to handle precision chores.

WHILE improved waveguide and waveguide components have helped the modern system designer reach new levels of performance, they have created new challenges for the engineer charged with evaluating reflection coefficient, VSWR and return loss.

The classical methods of measurement using slotted lines and traveling detectors no longer fulfill the requirements of rapid and thorough system checkout during installation and maintenance. Swept frequency reflection measurement techniques have gained wide acceptance, but commercially available measuring equipment barely meets—and often fails—to fulfill the accuracy requirements for components with very low reflection coefficients.

Upon inspection, it becomes clear that the accuracy of the swept-frequency test set rests on one of the less elaborate instruments used in the system—the directional coupler. Commercially available couplers typically exhibit directivities of 40 dB or less, severely limiting the usefulness of simple scalar reflectometer test setups. A new high-directivity coupler introduced here, boosts directivity to more than 50 dB, making complex computer-controlled test systems even more precise and extending the applications of simple setups. For instance, using the new 50-dB components, a computer-controlled network analyzer should be capable of making measurements accurate to ±2 dB at 45 dB. Likewise, a simple reflectometer built for field use can achieve an accuracy of ±2.5 dB at 35 dB.

Christian Staeger, Chief Engineer, Microwave Research Group and **Dr. Peter Kartaschoff,** Head, General Radio Technology Section, Swiss Post Office, Telecommunications Research and Development Division, CH 3000 BERN 29, Switzerland.

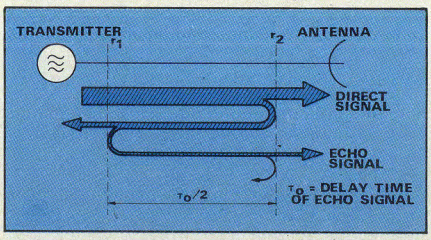

***1. Echo signal path in an antenna feeder** is due to two reflection points, r_1 and r_2. Note that the delayed echo creates added baseband noise.*

A look at the problem

To appreciate the measurement problems posed by today's high performance waveguide systems, consider the antenna feeder line of a high capacity microwave radio link using frequency division multiplex on a frequency modulated microwave carrier signal (FM/FDM system). The transmitted signal in such a system is very complex and occupies a microwave bandwidth of several tens of MHz. The effect of reflections in the RF path linking the transmitter output to the antenna via combining filters and feeder guides (Fig. 1) shows up in all individual speech channels as an increase of intermodulation noise. Total baseband noise actually depends on four parameters:

- system baseband width and FM deviation,
- amplitude of the echo signal created by reflections r_1 and r_2,
- echo delay, τ_o, with respect to the main signal, and
- waveguide attenuation between r_1 and r_2.

Similar conditions also apply to a receiver feed line. In today's broadband systems, 2,700 telephone channels for example, two single discontinuities causing small reflection factors ($|r_1| + |r_2| \approx 0.04$) may cause as much as 1 pW additional baseband noise power.

High-quality communications waveguide components exhibit typical return loss figures of about 36 dB, which is in the same order as high-quality laboratory equipment. Reflectometer circuits with directivities of 40 to 46 dB are simply not accurate enough for measuring components at these high return loss values, since the inherent measurement setup error approaches the return loss to be measured. This situation is best illustrated by the examples shown in Figs. 2 and 3, which demonstrate that even some recently proposed methods for broadband reflectometry—swept slotted line and coaxial offset reflectometer techniques—have weaknesses. While both are broadband techniques, neither is well suited to measurements on subsystems such as antenna feeds where the sum reflection factor shows rapid variations as a function of frequency. Com-

(continued on p. 42)

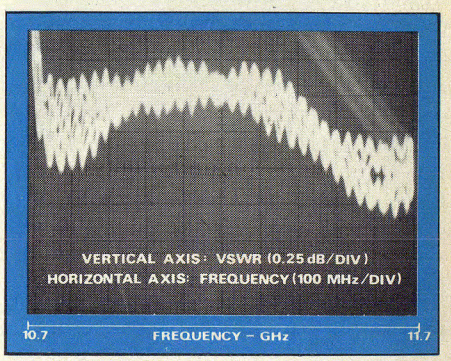

***2. Actual data of a swept slotted line VSWR on an antenna feed system** shows how the reflection minima are masked by the residual slotted line reflections. The 13.1-meter feeder system tested here is made of R100 (WR90) waveguide. The need to make at least six slow sweeps causes the measurement to be rather slow.*

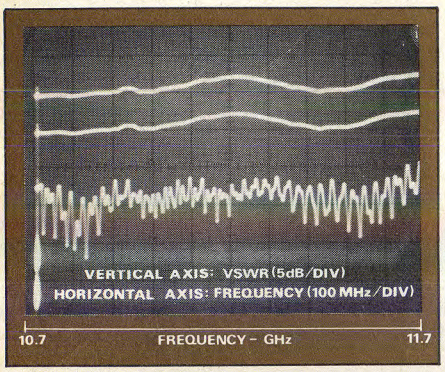

***3. Superposition of several minimum and maximum ripples** takes place even when the same system described in Fig. 2 is measured with an offset technique, making it difficult to interpret the response.*

paring the result of measurements on the same test device, obtained by means of a directional coupler reflectometer circuit to be detailed later, shows some of the problems.

Data from the swept-slotted line method, shown in Fig. 2, are difficult to read due to insufficient tracking between the detector probes. Furthermore, the residual reflection of a good slotted line is in the order of $\rho \leq 0.015$ and cannot be separated from the reflection to be measured. This can cause large measurement errors.

The offset reflectometer measurement method, on the other hand, is only well-suited for measuring devices with flat response of ρ versus frequency. As Fig. 3 indicates, however, superposition of several minimum and maximum ripples masks the ρ versus frequency fine structure. Better results can be obtained by an extension of conventional methods using multi-hole directional couplers. In fact, accuracy can be improved to the limits set by the state-of-the-art of waveguide and flange manufacturing technology. A set of straightforward methods equally applicable to field or laboratory measurements is possible.

Pinpointing error sources

The principle of swept measurements can be conveniently reviewed using the scalar reflectometer circuit shown in Fig. 4. The unknown component or subsystem is connected to the forward outport port (B) of a directional coupler. The input port (A) is driven by a swept frequency gener-

Four ways to make

Four different measurement systems can be used to obtain swept frequency data, depending upon the degree of accuracy required. Although they range from simple to complex, in all cases a signal generator must be carefully selected to avoid impairment of accuracy due to harmonics or spurious signals. In some cases, appropriate low-pass filters or band-limited detectors are required.

The most basic setup is a simple scalar reflectometer. This setup (Fig. A) requires an adjustable known standard reflection. The best procedure is to first record the response of the tested device and later correct the results with a calibration run. Calibration is performed by substituting a standard reflection for the device.

The advantages of this reflectometer are its simplicity, independence from generator and detector frequency response, calibration at similar levels as the measurement and negligible effects due to multiple reflections. Its main drawback is accuracy that is limited to that of the standard reflection (roughly 10 per cent of the measured value) which adds directly to the directivity error (see curve A in Fig. 7).

Another convenient measurement scheme is a scalar reflectometer using one or two couplers and a calibrated attenuator. As shown in the block diagram of Fig. B, this setup calls for a calibrated attenuator, leveled generator power and ratiometer.

To calibrate the system, the test port is closed by a short circuit plate (total reflection) and the calibrated attenuator is set to a value above the expected return loss of the tested device, usually at A = 40 dB. The response for this setting is recorded with a X-Y recorder or storage scope connected to the detector (option A). The device to be tested is connected to the test port and the setting of A is changed until the response is equal to the previous calibrated value at the desired frequency. For an attenuator setting of x dB, the measured return loss is equal to:

$A_r = 40 - x$ (dB)

Since most devices have a frequency response different from the rest of the

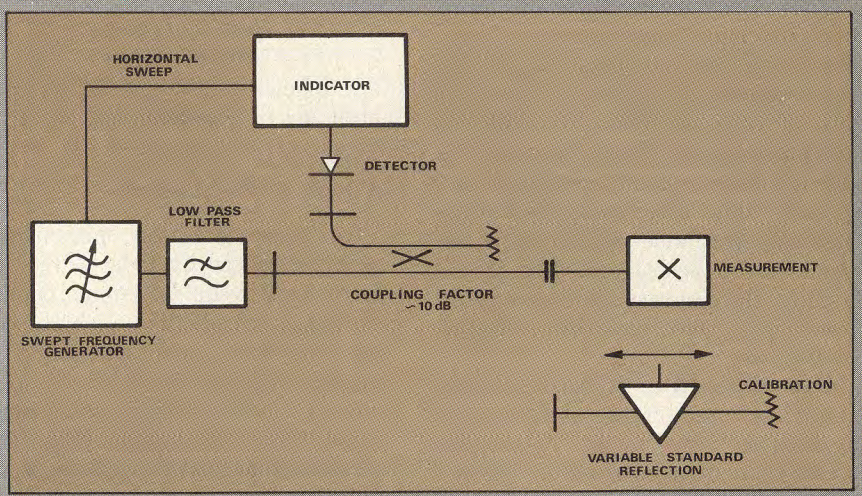

***A. Single coupler reflectometer** uses a substitution for calibration.*

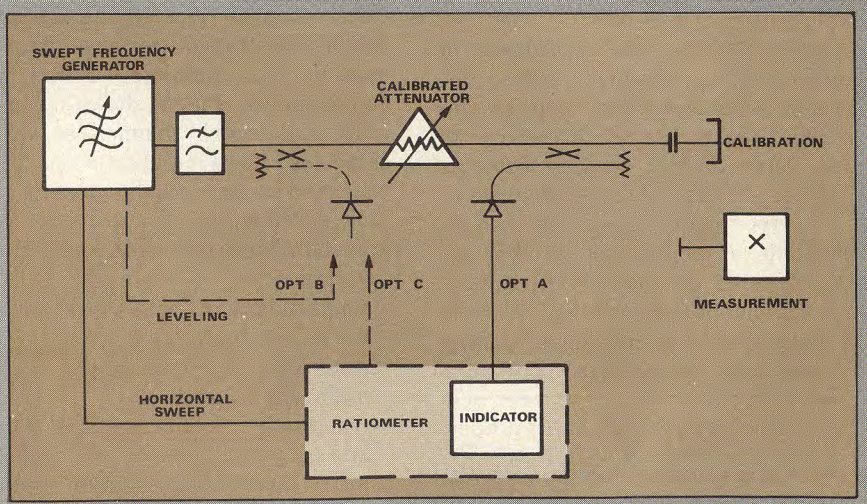

***B. One or two couplers** can be used in the scalar reflectometer method. Options include an X-Y recorder or storage scope, power leveling and a ratiometer.*

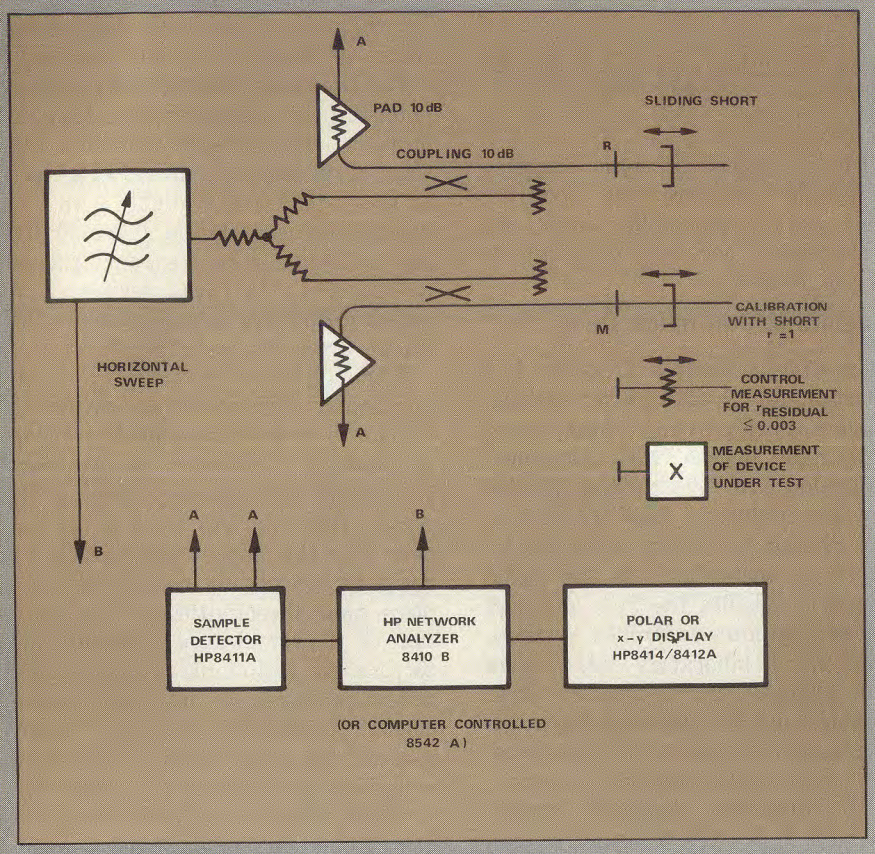

***C. The complex reflectometer system** uses a bridge to measure the magnitude and phase of reflection factors.*

circuit, the two tracks coincide at few frequencies. The evaluation of a swept frequency recording, therefore, requires a calibrated detector and display. The output of the signal generator may be externally leveled by wiring in option B in Fig. B to reduce level variations as a function of frequency. The ratiometer connection, option C, offers the best calibrated display system. The flatness of the response during calibration is then only limited by the tracking error of the couplers and detectors, a distinct advantage. But the technique requires a well-matched attenuator, otherwise noticeable errors will occur during calibration. An attenuator reflection factor will reduce this error below that due to the uncertainty of relative attenuator settings ($\rho \approx 0.025$).

The third swept measurement setup is a complex reflectometer bridge. Figure C shows a bridge circuit using two precision couplers and an accurate power divider for measuring the complex reflection factor (magnitude and phase). A network analyzer system such as the Hewlett-Packard Model 8410 serves as detector and calibrated (X-Y or polar) display unit. The bridge is driven by means of a power-leveled swept frequency signal generator.

Two calibrations are necessary for this system. Connecting a shorting plate to test port M provides data for $\rho = 1$. Displays are centered or zeroed at $\rho < 0.003$ by varying the position of a sliding termination connected to test port M.

The device to be tested is connected to test port M and polar or X-Y diagrams are displayed for the set frequency range. The sliding short at reference port R allows adjustment of the reference plane. In some cases, it may be convenient to replace the short by a sliding standard reflection. The bridge network shown masks residual reflections during the calibration for $\rho = 1$. For the sampler detector head, this is obtained with the 10-dB pads shown and for the power divider mismatch via the 10-dB coupling factors of the couplers. Thus, the open-short ratio of the network is optimized.

The worst case amplitude uncertainties of this circuit are the same as those of the previous setup (see curves B and C, Fig. 7).

The final system suggested is similar to the setup in Fig. C, but substitutes an automatic network analyzer for the manual version. Comparative measurements and error analysis have been made with this bridge and with the coaxial reflection/transmission test unit HP 8743 A supplied with the analyzer. The procedure was performed as described previously and according to the calibration routine described in the network analyzer operating manual. This system when used with a high directivity bridge circuit is responsible for a 16 dB improvement in isolation: a level that will satisfy even the most exacting requirements presently known.••

ator. A detector and signal display (oscilloscope or X-Y recorder) is connected to the output port (C) coupled to the reverse wave reflected from the device under test. The principle of the measurement is based on substitution: system calibration is followed by device measurement.

The reflectometer is first calibrated by connecting a short circuit to the output port. The totally reflected wave produces an output power, P_o, at the detector. This indication corresponds to a voltage reflection factor of $\rho = 1$, or a return loss $A_r = 0$ dB (see Fig. 4(a)).

An unknown component is measured by replacing the short as shown in Fig. 4(b). The output power in this case, P_2, is smaller than P_o and the scalar, or absolute value $|P|$, is given by

$$|\rho| = \sqrt{\frac{P_2}{P_o}} \quad \text{for the unknown device.}$$

Obviously, the equivalent return loss, A_r, is

$$A_r = 10 \log \frac{P_o}{P_2} (\text{dB})$$

Manageable error sources in the scalar reflectometer test setup include detector and generator mismatches, which can be kept small by proper padding, and detector/indicator nonlinearity. But three other error sources are inherent to the directional coupler measurement system, and are not so easily handled. *(continued on p. 44)*

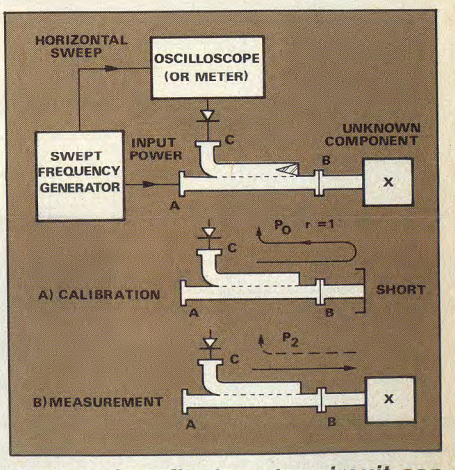

***4. A basic reflectometer circuit** can be made even simpler by replacing the scope with a meter and the sweeper with a signal generator.*

The first is directivity error. Directivity is the ratio of the total forward coupled power, P_o, to the total backscattered power, P_c (see Fig. 5). In a waveguide coupler, these powers are due to the superposition of all wave components generated individually by the coupling holes. Thus, directivity depends strongly on the geometrical layout of the coupling network structure. A second error source is termination mismatch. The return loss of the internal termination, R, in the coupler results in a reflected power P_T. Finally, there is a test port error, where the flange connection at the test port produces a reflected power P_F.

These powers add arithmetically since the phase angles of the corresponding field vectors have a random distribution. The overall directivity of the coupler system then is:

$$D_{overall} = 10 \log \frac{P_o}{P_C + P_T + P_F} (dB)$$

If we take as an example a coupler having a coupling structure directivity, D = 46 dB, a termination return loss A_{rT} = 50 dB and a test port flange return loss A_{rF} = 50 dB, and assume a coupled driving power of P_o = 1 W, the reflected powers are:

$$P_c = 0.25 \times 10^{-4} \text{ W}$$
$$P_T = 0.1 \times 10^{-4} \text{ W}$$
$$P_F = 0.1 \times 10^{-4} \text{ W}$$

And the overall directivity is:

$$D_{overall} = 10 \log \frac{1}{0.45 \times 10^{-4}} = 43.5 \text{ dB}$$

which is typical of most precision waveguide measurement couplers. This overall directivity limits the measurement accuracy of small reflection factors.

Computerization helps some

The effect of limited directivity in a reflectometer circuit with conventional couplers or bridges can be compensated to a high degree with automatic calibration in computer-controlled network analyzers. The precision is then limited by system noise and by frequency instabilities in the signal generator. Besides the bulk and high cost of computer-controlled systems, which favor laboratory rather than field applications, automated error compensation by computing has a major drawback compared to systems using a continuous frequency sweep.

The computer controlled system measures at discrete frequency points. If the properties of a continuous sweep are to be approximated over a wide frequency range, the frequency step increments must be made small. Thus, the number of points required is very large, and even with a fast computer the system is operating relatively slow.

If, for the sake of speed, the frequency increments are increased, sharp resonance phenomena can go unnoticed.

For the same reasons, narrowband point-to-point measurements that require retuning at each frequency fall short of the requirements. E-H bridges or magic-tee's are available with low internal error (isolation above 50 dB) but only for narrow frequency ranges (about 1.2:1). In these devices, mismatch errors due to reflections in the bridge arms can be large.

Although it is possible to build broadband high-precision waveguide bridges, extreme mechanical precision is required. Difficulty of manufacturing and high cost are probably the reason these devices have never appeared on the market. Conventionally designed waveguide directional couplers have directivities of not more than 46 dB over a waveguide band. This corresponds to an inherent error in the reflection factor of less than about 0.005. Considering the other error sources, the uncertainty of measured reflection factors is in the order of $\rho \leq \pm 0.01$, thus the probable error of a measurement on a test device matched to $\rho \approx 0.01$ is 100 per cent.

With conventional couplers having directivity of less than 40 dB, only computer-controlled network analyzers allow accurate measurements of low reflection factors with $\rho \leq 0.01$, whereas the less elaborate systems fail to yield useful results.

Coupler design reduces error

A major requirement for a truly precision reflection measurement technique then, is a highly directive waveguide coupler with a directivity of at least 50 dB. Such couplers have been developed resulting in vastly improved accuracies. Advancing the state-of-the-art directivity of conventional couplers from 40 to 50 dB reduces the errors to be compensated for in a computer measurement system between test runs and allows simple measurement setups to be used.

Designing waveguide couplers with directivity of greater than 50 dB is not at all difficult once the design principles are fully examined. Conventional coupling network designs are based on coupling hole arrays spaced one quarter wavelength apart, and augmented at each end by corresponding matching networks. The disadvan-

(continued on p. 46)

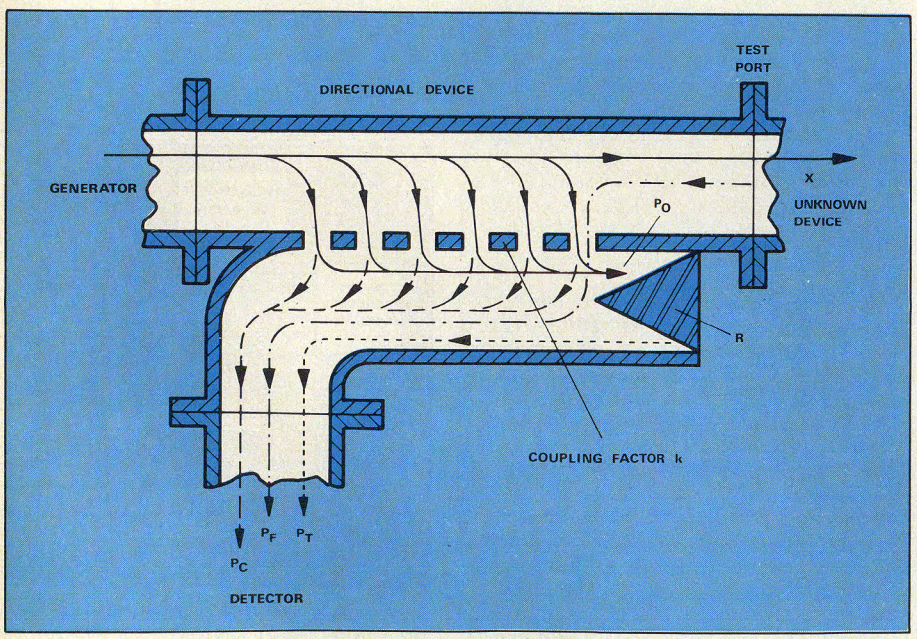

5. Directivity error in a waveguide coupler is due to backscattered power P_c, termination reflected power P_T, and test port reflected power P_F.

tages of these designs, however, are well known. The number of coupling holes in any overall length is limited. For coupling coefficients of 10 to 20 dB, large holes are required which cause field distortions and second order perturbations making computed designs somewhat unpredictable. This, and limited mechanical precision cause measured directivities to be about 25 dB less than the theoretical values.

Several possibilities do exist, however, for achieving high directivity over a full waveguide bandwidth. Additional holes, that is longer $\lambda/4$ arrays inserted between networks, superposition of two or more different $\lambda/4$ arrays or an increased number of coupling holes with reduced spacing in the array are three such methods.

If the overall design length of the coupler is limited, as practical considerations may dictate, then only the closely spaced array remains as a possible solution. One advantage appears immediately: if in an otherwise identical array the number of holes is quadrupled, a directivity increase of 12 dB is obtained. Such a close-spaced array can be well-matched over the entire waveguide band using the following design principle.

At both ends of a close-spaced ($\Delta << \lambda/4$) array (Fig. 6(a)), a computer-optimized matching network is added. The unterminated regular array produces a reflected wave which is represented by the vector sum of the individual components generated by each coupling hole as detailed in Fig. 6(b). Amplitude and phase angle of this vector are frequency dependent as is the circle defined by the individual components. The purpose of the matching network is to shift the center of the circle to the origin of the complex plane seen in Fig. 6(c). This is best obtained by spacing the coupling holes at both ends of the array differently so that the vector end points are located on a spiral originating at and returning to the origin.

Ideally, the vector polygon obtained would remain closed at the origin, whatever the frequency. In practice, however, a small residual vector remains which represents the back-scattered wave. This residual is minimized by computer optimization.

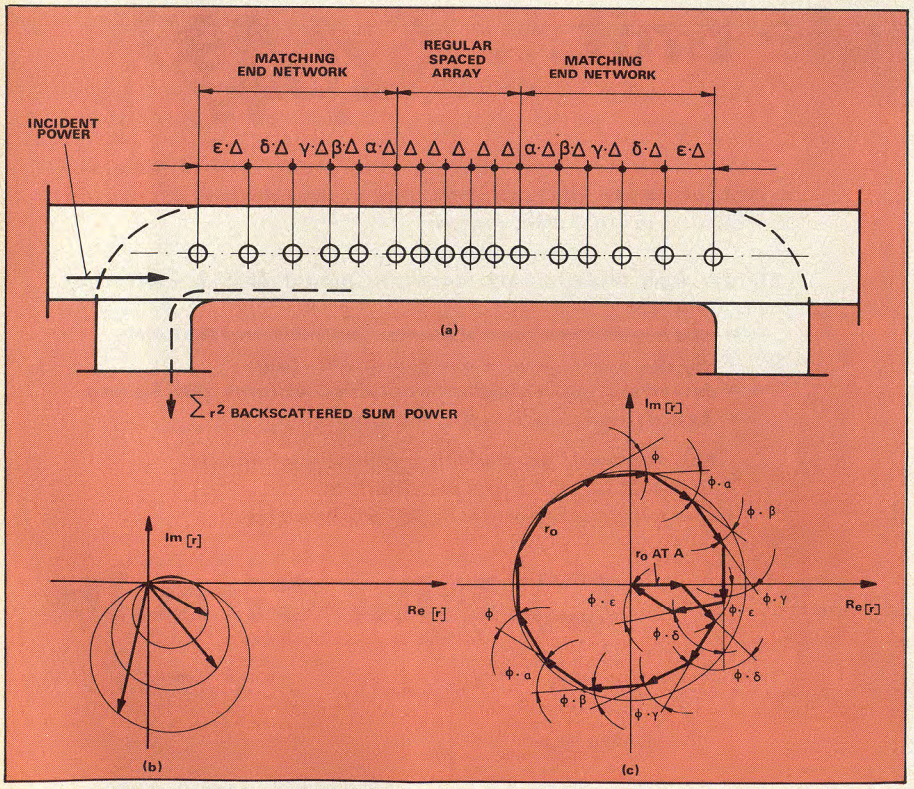

6. *The high-directivity coupler design procedure adds* *matching networks to the array (a) to overcome the reflected wave (b). The networks shift the impedance to the origin of the complex plane (c).*

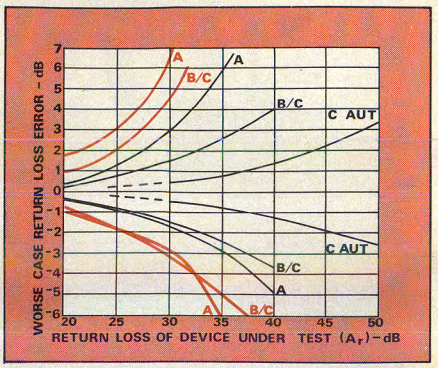

7. *A 10-dB improvement in coupler directivity* *drastically improves the accuracy of single-coupler (A) and scalar (B/C) reflectometer systems. Curves in color represent uncertainty associated with 40-dB coupler. Curves in black correspond to a 50-dB component. Accuracy curves for an automatic network analyzer system with 50-dB directivity couplers are labeled* C_{aut}.

This technique allows an array directivity of more than 60 dB. Combined with a well-designed internal termination having a return loss of greater than 60 dB and a precision test port flange with return loss greater than 54 dB, an overall directivity of more than 52 dB can be realized. At least 20 couplers with a coupling factor of 10 dB and directivity of greater than 50 dB have been built for various laboratory applications in WR 229 (3.6 to 4.9 GHz), WR 137 (5.3 to 8.2 GHz), WR 90 (8.2 to 12.4 GHz), WR 75 (10 to 15 GHz) and WR 62 (12.4 to 18 GHz) waveguide.

The error diagrams of Fig. 7 show that in all cases discussed, the directivity improvement of couplers and bridges from 40 to more than 50 dB results in a major improvement in the accuracy of return loss measurements. The greatest impact of the high-directivity components should be felt in the simple test setups described as A and B in "Four ways to make swept measurements." With conventional couplers having directivity of 40 dB or less, only computer-controlled network analyzers allow accurate measurement of components with reflection factors of less than 0.01. But the improved coupler design allows inexpensive test setups to perform return loss and reflection measurements to accuracy requirements hitherto impossible to meet, but necessary to the satisfactory operation of wideband microwave systems.••

Swept Measurements Speed Gain Compression Tests

CW measurements are fine for narrow-band tests, but use a swept frequency method for characterizing broadband linear amplifiers. Here are three solutions to the problem of comparing gain traces.

GAIN compression measurements are a standard part of amplifier characterization for both linear and nonlinear applications. For linear service, the third-order intermodulation distortion can be directly related to the amplifier's gain-compression point. For nonlinear service, amplifiers can be characterized and compared for power capability by measuring the gain at a particular level of gain compression, usually 1 dB.

A number of fixed-frequency, CW techniques have traditionally been used to measure gain compression points. While these methods are fine for narrow-band components, they become time consuming and potentially inaccurate when characterizing a broadband amplifier. Point-by-point CW tests must be repeated at a number of closely spaced frequencies to fully characterize the amplifier over a wide operating bandwidth. As this article demonstrates, 1-dB gain compression can occur anywhere in the amplifier's operating bandwidth; as bandwidths grow to several octaves, the likelihood of missing the frequency at which compression occurs becomes greater. The alternative is to measure gain compression on a swept-frequency basis.

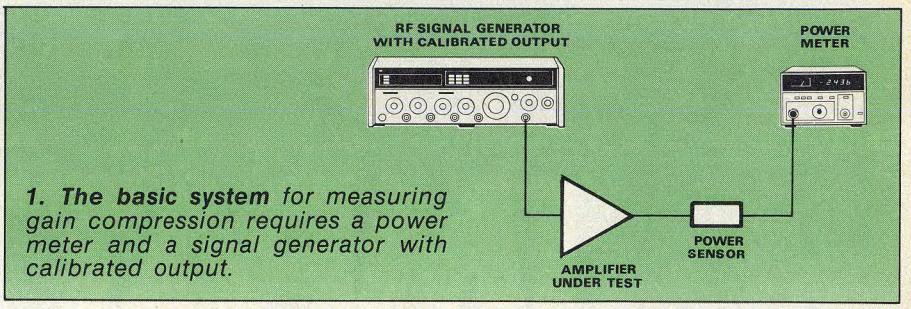

*1. **The basic system** for measuring gain compression requires a power meter and a signal generator with calibrated output.*

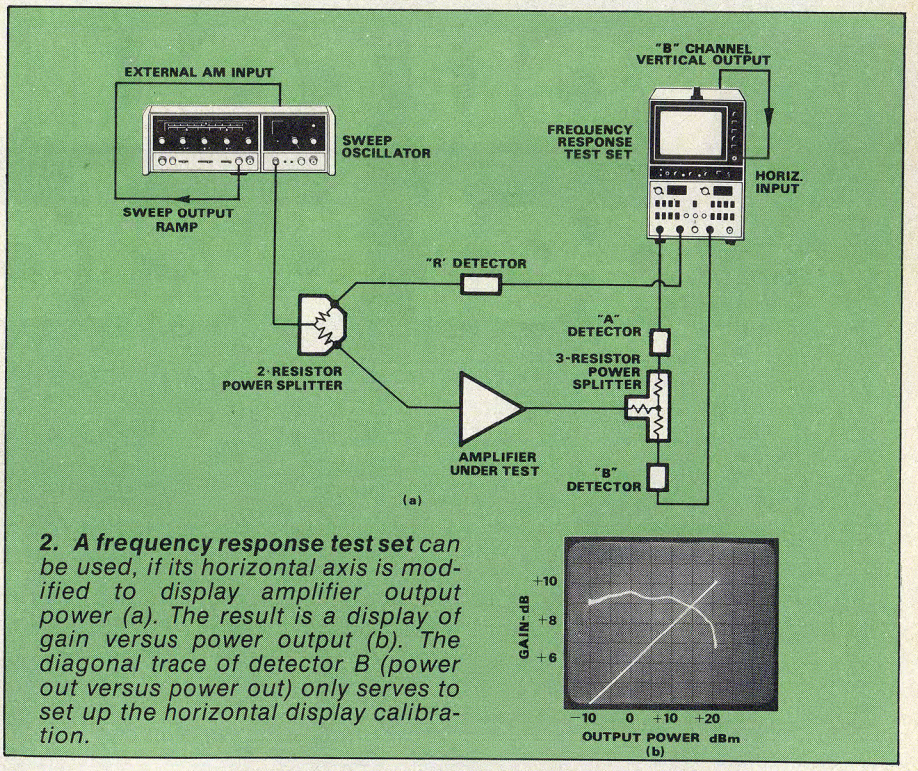

*2. **A frequency response test set** can be used, if its horizontal axis is modified to display amplifier output power (a). The result is a display of gain versus power output (b). The diagonal trace of detector B (power out versus power out) only serves to set up the horizontal display calibration.*

Consider CW techniques

The basic CW measurement requires a signal generator with calibrated RF output level and a power meter, as shown in Fig. 1. Amplifier gain is calculated by subtracting the generator output power from the power meter reading. Input power to the amplifier is increased from a small-signal level, and gain is recalculated until it is 1 dB below the initial value: the power meter then indicates the output power for 1-dB gain compression.

A more sophisticated CW measurement technique, shown in Fig. 2, relies on a sweep generator and frequency response test set. The test set, however, does not provide its normal amplitude versus frequency display: the horizontal display axis is reconfigured to indicate power, while the vertical axis displays gain by comparing the ratio of power sampled before and after the amplifier (detectors R and A, respectively, in Fig. 2).

Wiring the horizontal axis to indicate power is a bit tricky. A portion of the output power from the amplifier is detected and fed to channel 2 of the analyzer (detector B in Fig. 2). The rear panel output of channel 2 (typically 0.5 volt per division) is brought to the front

(continued on p. 51)

Thomas R. Brinkoetter, Applications Engineer, Hewlett-Packard Company, 1400 Fountain Grove Parkway, Santa Rosa, CA 95404.

of the instrument to drive the horizontal input. The gain of the horizontal input amplifier is then adjusted so the channel 2 is a 45-degree diagonal line (one division horizontal deflection for one division vertical deflection). Thus, the need to have a linear relationship between the RF output power and the DC modulator drive voltage is eliminated. Nonlinearities in the modulator are translated to intensity variations, and not horizontal axis inaccuracies.

Power input to the amplifier is varied by modulating the output of the sweep oscillator with a DC ramp voltage, which can be derived from the sweeper by placing it in the CW/ΔF mode with ΔF set to zero. Gain compression is indicated by a downward slope of the gain display as the output power increases (see Fig. 2 (b)).

Tackling broadband measurements

For wideband linear amplifiers, the 1-dB gain-compression point defines the first frequency over the entire bandwidth of the amplifier at which the gain is compressed 1 dB with the output power level held constant. This assures the user that a particular level of output power can be obtained without worry of intermodulation distortion.

Swept-frequency gain compression measurements have a great advantage when the bandwidth of interest is very wide. Using a CW technique, many measurements must be made to insure that excessive gain compression does not occur at any frequency within the amplifier's bandwidth. A swept measurement, on the other hand, provides a picture of the entire band, identifying all points of gain compression.

Swept-frequency gain compression measurements basically involve standard gain measurement techniques, but with two additional requirements. First, a method for comparing compressed gain displays must be devised because the system is basically set up to measure gain, while the end result must be gain compression or *changes* in gain. Second, the *output* power of the amplifier-under-test must be leveled to be certain that a particular level of output power can be obtained anywhere within the operating bandwidth without 1-dB gain compression.

Compressed and uncompressed gain displays can be compared in three ways. The three techniques share a common RF test setup, but differ in how the display is presented and in the time frame of the information. The first technique relies on a storage oscilloscope. Although it involves the least amount of equipment, it does not provide real-time information or a direct view of the display in dB. The second method modulates the RF with a square wave at one-half the sweep speed rate, so both the uncompressed and compressed displays are presented as real-time information. The final approach uses digital normalization to provide a direct view of gain compression in dB.

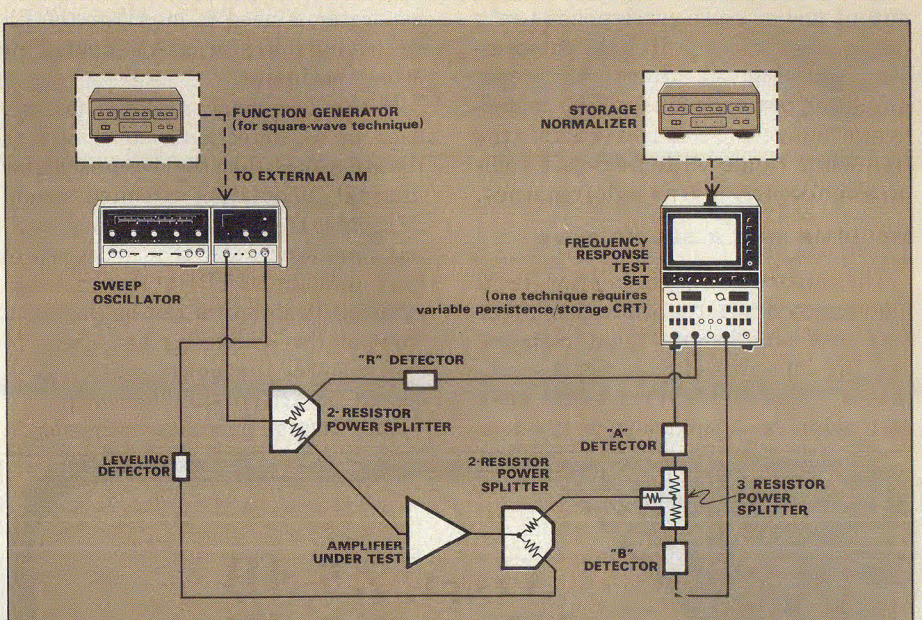

***3. Swept-frequency measurements** require a leveling loop and a way to compare compressed and small-signal gain displays. Channel 1 of the test set displays gain, while channel 2 displays output power.*

Figure 3 illustrates the basic configuration for the three measurement techniques. Channel 1 of the frequency response test set displays gain (the ratio of detectors A and R), while channel 2 displays the output power of the amplifier (detector B). Note that power and gain levels are displayed on the vertical axis and frequency is represented on the horizontal axis.

The external leveling capabilities of the sweeper can usually be used to meet the second measurement requirement, maintaining a constant amplifier output. The leveling loop gain should be adjusted to hold the output power constant with frequency while being varied from a small-signal level to a fully compressed level. A two-resistor power splitter, such as the Hewlett-Packard 11667A, should be used to sample the amplifier output because this type gives the best leveling and source match. Note that a three-resistor power splitter, such as the Weinschel 1506A, should be used to feed detectors A and B because it maintains system impedance to minimize mismatches.

Use a storage scope

The storage oscilloscope swept-frequency gain compression technique provides a series of gain displays, whose total trace width is proportional to gain compression. This is done by increasing the persistence of the storage oscilloscope once a small-signal gain display is obtained. As the output power is increased, successively compressed gain displays are stored alongside the small signal display.

When the gain trace becomes 1-dB wide at any frequency, the uppermost

(continued from p. 52)

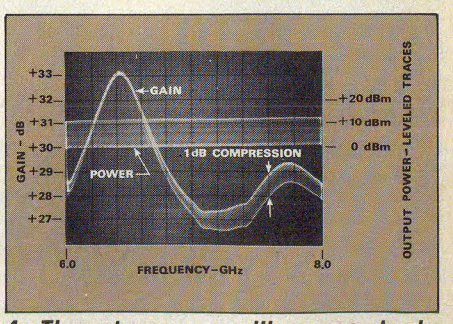

***4. The storage oscilloscope technique** produces a trace width proportional to gain compression. Here, 1-dB compression of a 6 to 8 GHz amplifier occurs at about 7.6 GHz.*

◄ READER SERVICE NUMBER 41

output power trace corresponds to the output power for 1-dB gain compression (see Fig. 4). Since the output amplifier power is leveled, the component is delivering this power across the frequency range with 1-dB gain compression occurring at a single frequency.

Modulate with a square wave

The square-wave modulation technique provides a real-time display of both the small-signal gain response and the compressed gain response, allowing adjustments that would alter both displays. A square-wave function generator is used to modulate the RF by driving the external AM input of the sweep oscillator.

If the frequency response test set uses an AC detection system, such as the HP 8755B, then the sweep oscillator internal modulation circuitry should be capable of AM modulation and leveling simultaneously. If it is desired to have unmodulated RF at the amplifier, external modulators can be placed in front of the R detector and ahead of the three-resistor power splitter. Both should be driven simultaneously.

The function generator frequency is set to approximately half that of the sweep speed, while the amplitude and DC offset are adjusted to obtain two absolute power displays and two gain displays, as shown in Fig. 5. Since the upper gain display corresponds to the small-signal, or uncompressed condition, the difference between the two gain displays is the gain compression. This difference can be increased to 1 dB by increasing the amplitude of the square-wave modulation signal.

The final method is digital normalization. Here, a small-signal, uncompressed gain display is digitized and stored. This characteristic is later subtracted from successively compressed gain displays. Changes in gain or gain compression are viewed directly in dB as the amplifier output power level is increased by changing the power level control on the sweep oscillator. Once the gain is compressed by 1 dB at any frequency on the display, the output power indicated by the B detector is the output power of the amplifier for 1-dB gain compression (see Fig. 6). The initial storage process should be repeated if adjustments are made on the amplifier that would alter the small signal gain response. ••

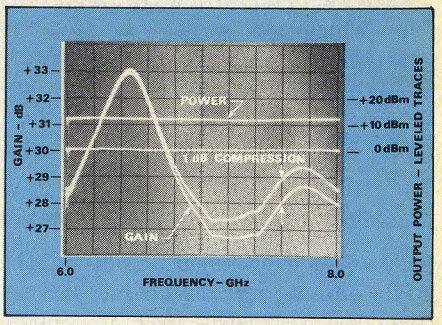

***5. The square-wave modulation method** produces two traces (same amplifier tested as in Fig. 4). One dB separation of gain traces at 7.6 GHz indicates a gain compression point at about +10 dBm.*

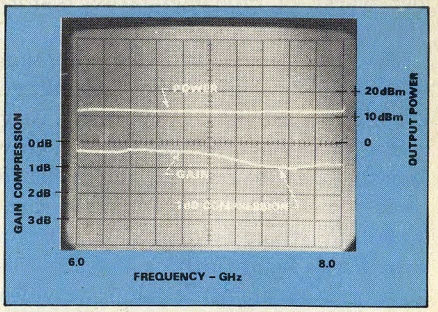

***6. Digital normalization** compares compressed gain with a stored small-signal characteristic; power and gain compression appear as single traces. This measurement of the 6 to 8 GHz amp cited earlier, again shows 1-dB compression at 7.6 GHz.*

No. 1 IN A SERIES
LOW NOISE MICROWAVE TRANSISTOR UPDATES FROM AVANTEK

G_{NF}: 7.5 dB
NF_{opt}: 3.5 dB
Frequency: 4.0 GHz
Avantek AT-4641

Guaranteed Specifications

Type	NF_{opt} dB (max)	G_{NF} dB (typ)	I_C mA	G_{max} dB (min)	I_C mA	f_{Test} GHz	f_T GHz (typ)
AT-4641	3.5	7.5	5	8	15	4.0	8.0

OUTLINE DRAWING

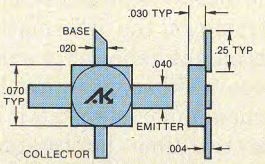

Built-In Reliability
The AT-4641 features a superior gold metallization system and hermetic packaging. All Avantek transistors are manufactured under the most stringent quality controls, assuring the designer of high MTBF's.

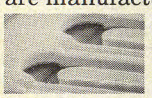

***Fast* Delivery**
Concerned about a supplier located halfway around the globe? Avantek is just a phone call away. Orders placed by noon will normally ship the *same day*.



Dependable Performance
The AT-4641 is a proven performer in critical military *and* space applications with HI REL screening available as a *standard* option. It features a very high dynamic range among its impressive specifications. Reliability, performance, and immediate availability —Avantek's AT-4641 is your solid choice.

NOISE FIGURE vs FREQUENCY

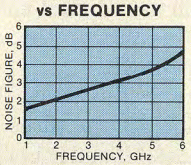

Contact: Avantek Transistor Applications Engineering (408) 249-0700
3175 Bowers Ave., Santa Clara, CA 95051
TWX 910-339-9274 Cable: AVANTEK

SEM photo of AT-4641 (1000X magnification).

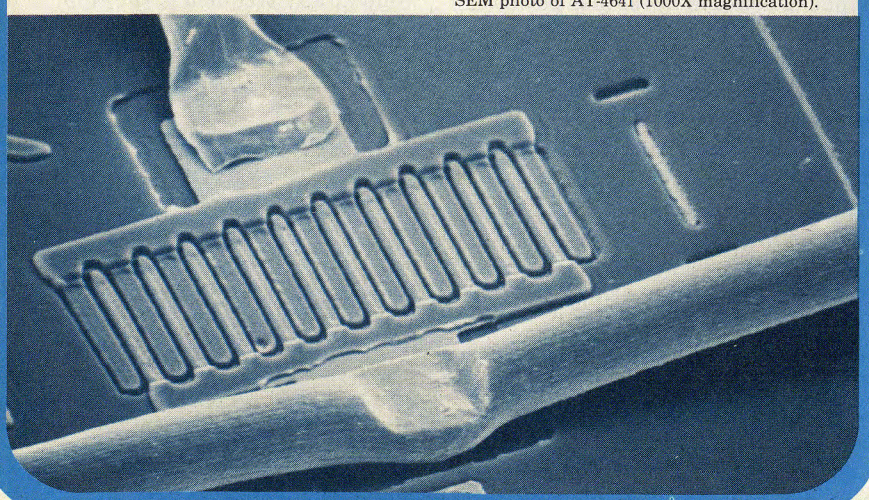

READER SERVICE NUMBER 42

Vector Voltmeters Perk Up With High-Speed Sampling

Today's vector voltmeter can directly measure phase and voltage at frequencies above 2 GHz. Here's how to take advantage of improved sampling circuitry to measure a variety of important RF parameters.

THE vector voltmeter has become a powerful tool in the measurement arsenal of the microwave engineer, thanks to the introduction of "fast" detector diodes and speedy sampling techniques.

Direct measurements of s-parameters, insertion loss, phase shift, amplifier gain, power and group delay at frequencies ranging to more than 2 GHz are well within the capabilities of modern vector voltmeters. In addition, the RF-to-IF conversion inherent to the meters can be used to convert a low-speed scope into a high-speed sampling instrument.

The heart of today's vector voltmeter is the front-end sampling head. Basically, it is a very wideband, dual-channel, automatically tuned superheterodyne receiver (Fig. 1). Two input signals (channel A and B) are coherently sampled and translated into IF signals, typically at 20 kHz. Channel A functions as a reference channel and is used to achieve phase lock, while channel B responds only to signals of the same frequency applied to channel A. It requires only −50 dBm to achieve phase lock in most instruments.

Each channel of the vector voltmeter presents a matched 50-ohm load to an external circuit equipped with coaxial ports. These 50-ohm loads can be considered as isolating pads to which two Schottky-barrier diodes are connected. When a signal is applied to either channel, the diode, driven by an internal pulse generator, closes for a short time, charging a capacitor. The switch then closes again, perhaps many cycles of the signal later, giving the capacitor an added charge.

If there is no correlation between the signal and the switching pulse, samples are taken randomly and consequently, all phase information is lost. To avoid this, a phase-lock loop is introduced to "lock" the pulse to the signal. Of course, this merely causes the same point on the signal to be sampled during each pulse; therefore, a voltage-tunable oscillator is used to time the pulse and "strobe" it along the signal. The capacitor then charges to a low-frequency, IF replica of the signal.

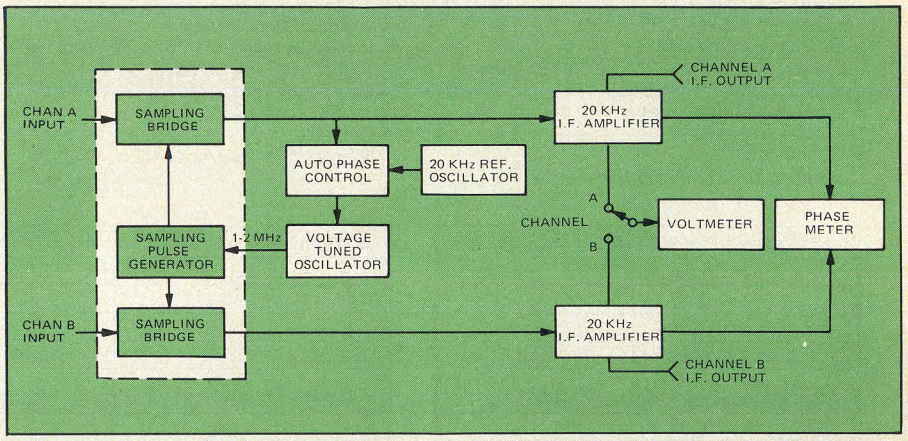

1. The diode bridges used in the front-end sampling head typically provide linearity better than ±2 per cent over a dynamic range that approaches 80 dB.

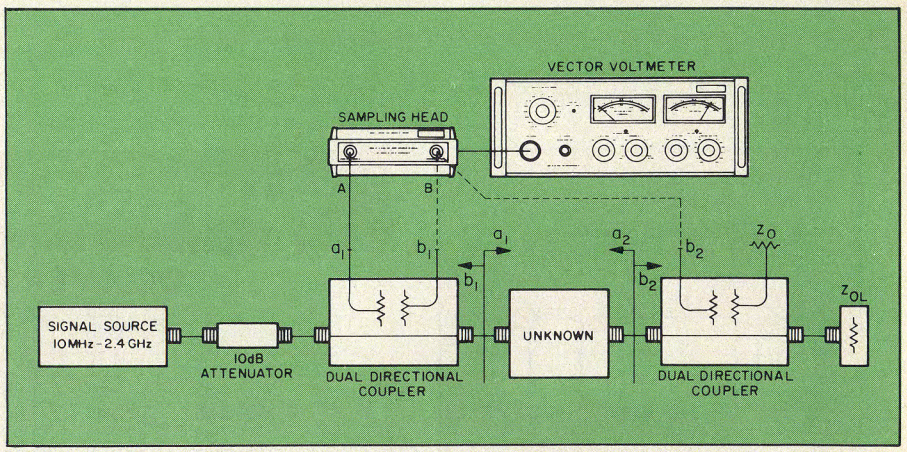

2. By measuring the phase difference between two signals, angles of scattering coefficients are readily determined, while amplitudes are measured by transmission methods.

The two IF signals produced are exact replicas of the original RF signals and conventional low-frequency circuitry can be employed to measure the amplitude of each IF signal and their phase relationship. These quantities are conveniently displayed on two front-panel meters.

Measure s-parameters

Since the vector voltmeter measures the phase difference between two sig-

(continued on p. 58)

Don Stock, Project Engineer, Harris Corporation, PRD Electronics Division, 6801 Jericho Turnpike, Syosset, NY 11791.

nals, angles of scattering coefficients can be readily determined, while amplitudes are measured using transmission methods.

The vector voltmeter can be used to quickly measure the scattering parameters of a device with 50-ohm characteristic impedance using the setup shown in Fig. 2. In this circuit, two dual directional couplers, CP_1 and CP_2, are assembled between a well-matched generator and a precision load, Z_{OL}.

Initially, the two couplers are joined together and, with channel A connected to a_1, channel B is connected to b_2 to observe the relative phase. This channel should be set to zero with a line stretcher inserted before channel B. The phase at b_1 should be noted. This establishes the reference planes for the angles of S_{11} and S_{21}.

The directional couplers are now separated and the unknown unit is inserted between them. With a_1 applied to channel A as the reference signal, measurements of b_1 and b_2 are made and the phase meter indications are recorded (see Table 1). Measurement of S_{22} and S_{12} may be obtained by interchanging the generator and Z_{OL}.

Since the technique described is a reflectometer method, the measurements are subject to the same errors as reflectometer readings. Therefore, the directional couplers should have high directivity, the generator should be close to an ideal match, and coupling variations should track closely between couplers. The detector VSWR is adequately low, but connectors should be kept clean and free of damage. Since this method provides phase in addition to the magnitude readings given by conventional reflectometers, connector mating should be electrically "smooth" at the frequencies used.

In the calibration measurement, the phase of b_1 should differ from that at b_2 by the length of line between them. The mating connector pair must be of low reflectance for this measurement. If greater accuracy is required in measuring the angle of S_{11}, replace Z_{OL} with a short circuit for calibration, then replace the short with the unit under test terminated by Z_{OL}.

Loss measurements simplified

A simple method of making insertion loss measurements with the vector voltmeter takes advantage of the arrangement shown in Fig. 3. For reciprocal devices ($S_{12} = S_{21}$), insertion

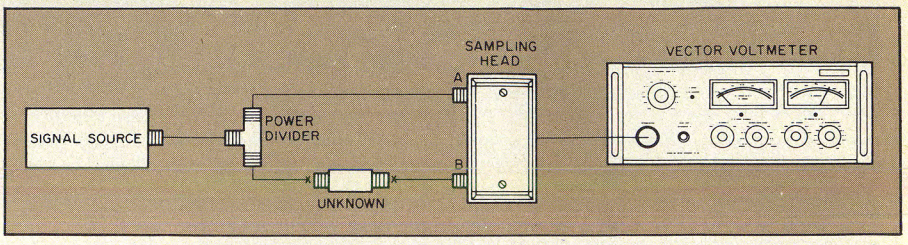

3. Sample setup for measuring insertion loss. The same results can be obtained by using setup of Fig. 2 and measuring dissipation and reflection losses separately.

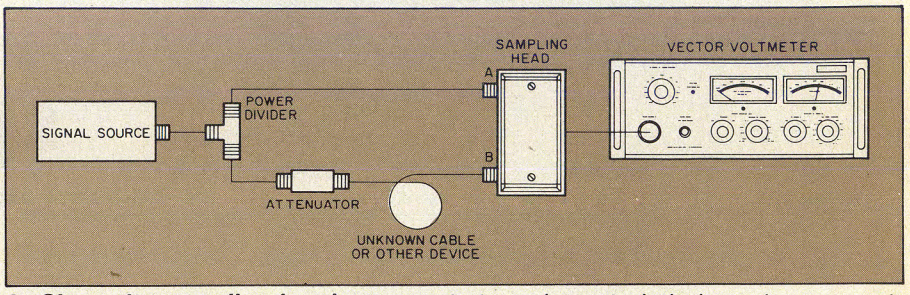

4. Since the sampling head represents two characteristic impedance terminations for 50-ohm systems, the transmission phases of the devices may be compared.

Table 1: Scattering parameter measurement

Parameter	Amplitude meter (ch. A) indicates	Phase meter indicates	Amplitude meter (ch. B) indicates
$S_{11} = \frac{b_1}{a_1}$ $a_2 = 0$	a_1	ϕ_{11}	b_1
$S_{21} = \frac{b_2}{a_1}$ $a_2 = 0$	a_1	ϕ_{12}	b_2
interchange generator and Z_{OL}			
$S_{22} = \frac{b_2}{a_2}$ $a_1 = 0$	a_2	ϕ_{22}	b_2
$S_{12} = \frac{b_1}{a_2}$ $a_1 = 0$	a_2	ϕ_{12}	b_1

loss may be expressed in terms of scattering parameters as:

$$\text{I.L.} = 10 \log \frac{1}{|S_{21}|^2}$$

$$\text{I.L.} = 10 \log \frac{1}{|S_{12}|^2}$$

This loss may be broken up into a dissipative loss

$$10 \log \frac{1 - |S_{11}|^2}{|S_{21}|^2}$$

and a reflective loss

$$10 \log \frac{1}{(1 - |S_{11}|^2)}.$$

The former is commonly referred to as attenuation. It may be measured separately by the methods of the previous section if the unknown device is placed between tuners to match out the reflections at ports 1 and 2. This matching may be accomplished at port 1, for example, with reference to Fig. 2, by adjusting tuners at ports 1 and 2 for b_1 as small as possible.

A few things should be kept in mind when using the setup in Fig. 3 to measure insertion loss. Both cables should be initially connected directly to the sampling head to assure that equal amplitudes are available from each. Two 10-dB pads may be used for isolation at the power divider. However, the difference in attenuation between the two should be determined before inserting the unknown.

Determine phase shift

Since the sampling head represents two characteristic impedance terminations for 50-ohm systems, the transmission phases of two devices may be compared using a vector voltmeter. Suppose it is desired to determine the length of a cable required to *produce*

(continued on p. 60)

phase shift ø at frequency f. A signal generator of frequency f, with power set at a convenient level, say 0 dBm, is connected to channels A and B through nearly identical paths as shown in Fig. 4.

The cable of unknown length is inserted into channel B and ø is read directly on the phase meter. If the cable is more than λ/2 in length at f, phase shift must first be approximated from the equation:

$$ø = \frac{Lf}{3\times10^2} 360$$

where:

ø = phase of cable length in free space (degrees)
L = length of cable in meters
f = frequency in MHz.

Since the sampling head presents a good match to 50 ohms, it is normally not necessary to assure a good source match for the measurement of ø. Above 1 GHz, an attenuator may be inserted just before the unknown cable to prevent connector mismatch from affecting the measurement.

Gauge amplifier gain

Microwave transistor amplifiers constructed in 50-ohm stripline are directly compatible with the vector voltmeter sampling head. Since the VSWR of the head is low, accurate, gain measurements can be made with the configuration of Fig. 2. The gain for negligible $|S_{11}|$ and $|S_{22}|$ is S_{21} $(j\omega)^2$, while the phase shift is the angle measured for S_{21}. If the amplifier exhibits mismatch at its input and output ports, the gain must be computed as:

$$\left|\frac{b_2}{a_1}\right|^2$$

It should be noted, however, that since it is impossible to match a lossless tee at all three ports, errors may be expected where S_{11} and S_{22} are not negligible. In addition, if the amplifier output exceeds the input limit of the voltmeter (typically +13 dBm), the signal from the amplifier must be attenuated. In this case, it is suggested that a low VSWR attenuator of proper value be first calibrated with the vector voltmeter and then inserted at the amplifier output.

Hunt for harmonics

When checking RF power source for the number and amplitude of its harmonics, the arrangement shown in Fig. 5 can be used.

Since the purpose of this system is to measure harmonics, it is necessary to limit the fundamental frequency from the RF source to at least one-half the vector voltmeter bandwidth. The harmonic generator produces strong harmonics of the RF signal for phase-locking the vector voltmeter. The frequency meter assures that only one harmonic is available at any time to which the vector voltmeter can lock and also provides an approximate reading of the frequency. Since the phase-locking loop acts like a very narrow-band tracking filter, an accurate amplitude reading is obtained which is unaffected by noise or adjacent spurious responses.

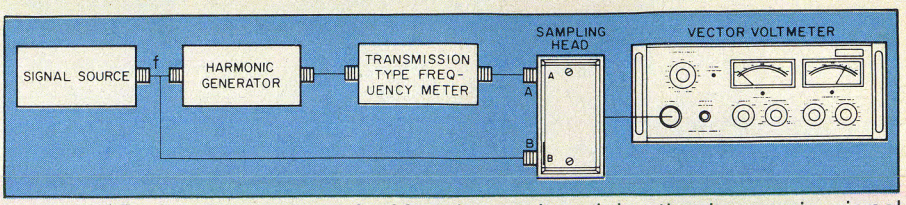

5. The RF signal for phase-locking is produced by the harmonic signal generator.

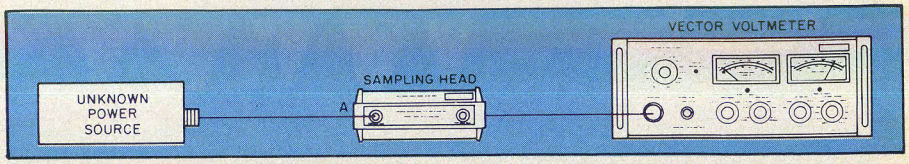

6. Unknown RF power levels above the phase-lock threshold can be easily measured by connecting the unknown power source to channel A.

Extend the range of scopes

Since the vector voltmeter produces an IF output which closely tracks an RF input, it can be used to convert a low-frequency oscilloscope to a high-frequency sampling instrument in applications where pulses are not to be examined. Thus, the vector voltmeter can be used to measure per cent modulation of microwave signals.

For amplitude-modulated signal, the vector voltmeter locks to carrier frequency f_c, and sidebands $f_c \pm \Delta f$ are reproduced at the IF output as $f_{IF} \pm \Delta f$. If the IF signal is observed on a low-frequency scope, modulation percentage can be calculated from:

$$\% \text{ Modulation} = \frac{M-1}{M+1}$$

$$\text{where } M = \frac{\text{Crest}}{\text{Trough}}$$

By applying the IF output to a low-frequency spectrum analyzer, the spectral content of the signal can also be observed. The Δf should be limited to prevent distortion in the IF section of the vector voltmeter.

Power measurement is easy

CW and modulated RF power levels can be measured by the setup of Fig. 6. However, modulation levels must not reduce the signal level below the phase-locking level of channel A, which is typically in the order of −50 dBm.

It should be noted here that since the measuring technique used in this case is equivalent to linear detection or mixing, the accuracy is dependent upon the predictability of the detector, be it square law or linear.

Measuring RF power levels below the phase-lock threshold requires a second signal of the same frequency, but at a higher power level to lock the vector voltmeter. Unless both sources are extremely stable, a phase-lock loop must be established, as indicated in Fig. 7. In operation, the signal generator is tuned to the approximate frequency of the unknown power source and then fine-tuned to obtain a 0-degree indication on the phase meter. At this point, the phase-lock loop is closed and the phase meter settles at one value.

Determine group delay

Group delay, the transit time of a signal through a device, has become an extremely important phenomena to designers interested in pulsed compression radars, phased array antenna systems, data and voice communications, CATV and computers.

Group delay is related to the slope of the phase vs. frequency curve and can be defined by:

$$t_D = \frac{d\phi}{d\omega} \qquad (1)$$

If the phase vs. frequency curve is linear, t_D will not be constant and distortion will take place.

Both single and swept frequency group delay measurements can be easily accomplished from 1.5 GHz to 2.4 GHz, and up to 18 GHz by using mod-

(continued on p. 62)

ulation techniques.

Figure 8 is the test setup for the single frequency group delay measurement. The measurement procedure is as follows:

1. Set the signal generator to the lower frequency starting point with the unit under test not in the circuit.
2. Zero-out the phase difference in the two measurement arms with the zero offset control on the vector voltmeter.
3. Insert the unit under test.
4. Change the frequency of the signal generator to the next higher frequency and note the change in phase reading.
5. Calculate the group delay as:

$$t_D \text{ (sec)} = \frac{\Delta\phi}{360\ f}$$

This gives the average group delay over the range that the frequency is changed. Frequency increments of 2.778 are the most convenient to use since:

$$t_D = \frac{1}{360} \times \frac{\Delta\phi}{2.778\ \text{MHz}}$$

$$t_D = \Delta\phi \quad \text{ns}$$

yields phase meter indications which can be read directly as nanoseconds of group delay. To increase accuracy, a frequency counter can be used to monitor the signal generator.

Figure 9 is the test setup for making swept frequency group delay measurements. A sample of the modulated swept RF signal is taken with the 10-dB directional coupler, detected and applied to the reference channel A. The output of the unit under test is detected and applied to channel B. In this way, the unit under test is swept with the RF signal, but the vector voltmeter measures the phase of CW modulating signal. The phase shift of the modulating signal is directly proportional to the group delay of the RF signal and may be calculated from:

$$t_D = \frac{\phi}{360\ f_m}.$$

Here again, if a modulation frequency of 2.778 MHz is used, the phase meter indications can be read directly as nanoseconds of group delay.

Testing discrete components

The measurement of a single component over its frequency range represents a special case of testing a two-port network. To illustrate this, consider a single resistor mounted in series with the center conductor of a coaxial line. The two-port circuit thus formed

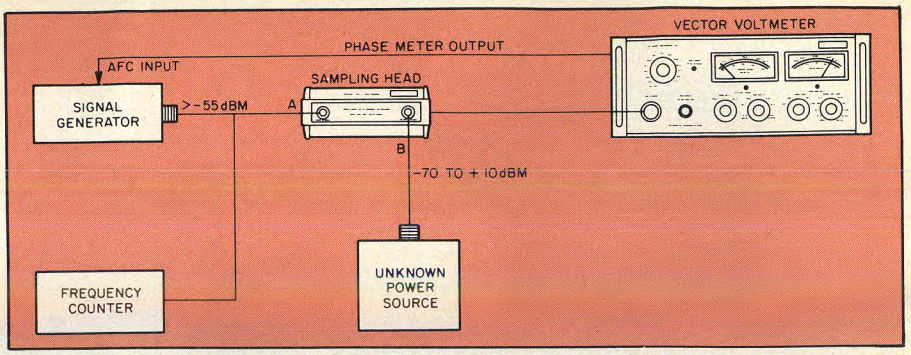

7. An additional source of the same frequency is required for measuring RF power levels below phase-lock threshold.

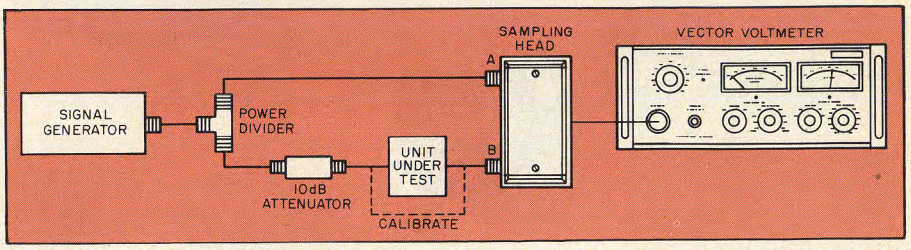

8. By changing the frequency and noting the change in phase reading, single-frequency group measurements can be made with this simple arrangement.

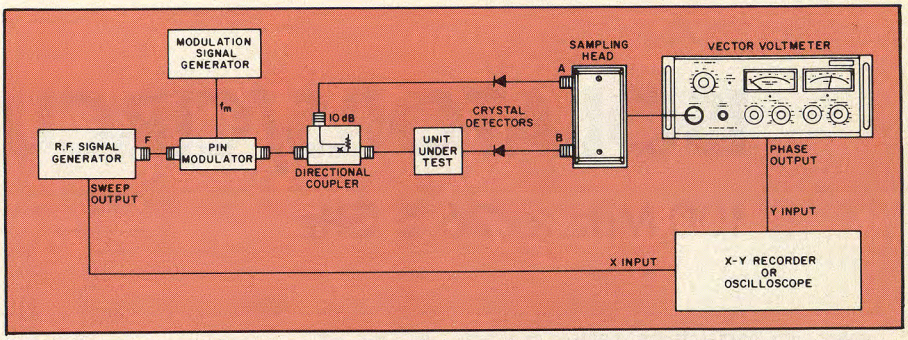

9. When the unit under test is swept with RF signal, the vector voltmeter measures the phase of CW modulating signal.

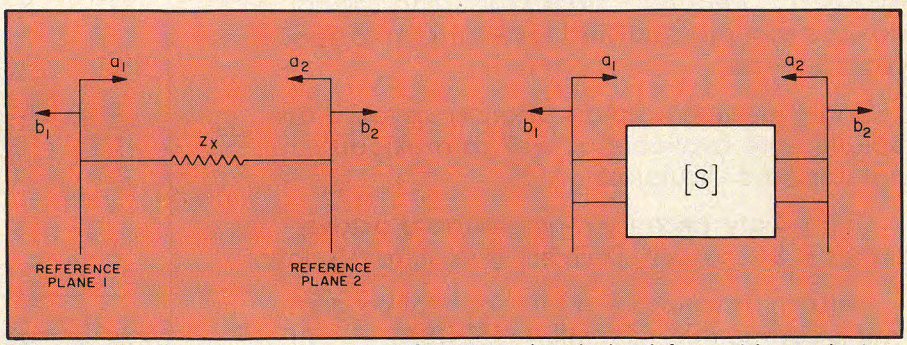

10. The two-port scattering equations can be derived from this equivalent circuit showing a single resistor mounted in series with the center conductor of a coaxial line.

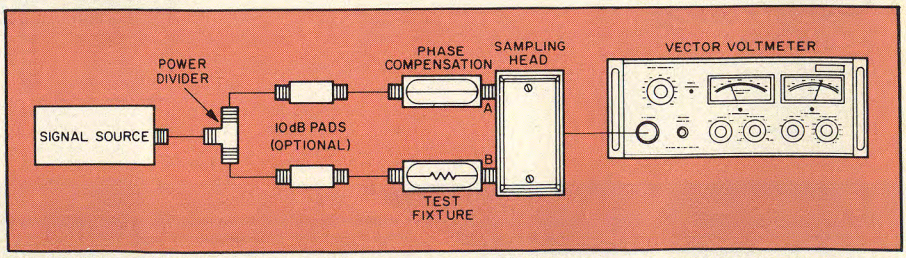

11. In this arrangement for testing a two-port device, signal generator output should be adjusted between 0 and −10 dBm.

is shown in Fig. 10.

The two-port scattering equations for this case may be written as:

$$b_1 = \frac{z}{2+Z} a_1 + \frac{2 a_2}{2+z}$$

$$b_2 = \frac{2}{2+z} a_1 + \frac{z}{2+z} a_2$$

where $z = \frac{Z_x}{Z_o} = \frac{R_x \pm jX_x}{Z_o}$

The setup for this measurement is shown in Fig. 11. Z_x is mounted in an insertion unit, such as the GR 874-X, and inserted into channel B. To preserve the phase equality of the paths, a length of line, such as the GR 874-LR, or another GR 874-X insertion unit with a proper center conductor is inserted into the channel A path. The signal generator output should be adjusted for a convenient reading on channel A; for example, 0 dBm, or −10 dBm if pads are used for isolation. This reference reading is proportional to a_1 in the above equations.

Since the sampling head is matched to 50 ohms, $a_2=0$ and the channel B reading is proportional to b_2 from:

$$b_2 = \frac{2}{2+z} a_1$$

Thus, the measurement procedure at each frequency is: read channel A, channel B and phase.

The magnitude of S_{21} is:

$$\left|\frac{b_2}{a_1}\right| = \frac{\text{channel B reading}}{\text{channel A reading}}$$

and the phase of S_{21} is ø, the phase meter reading. Thus:

$$Z_x = 2 Z_o \frac{(1 - S_{21})}{S_2}$$

This may be computed, where:

$$S_{21} = \frac{b_2}{a_1} \epsilon^{J\phi}$$

For example, an RN55D 49.9-ohm resistor is mounted in the insertion unit and the following readings are taken at 20 MHz:

A = 223 mV
B = 150 mV
ø = 0°

Thus,

$$S_{21} = 0.67 \epsilon^{J\phi}$$

$$Z = \frac{49.3}{50} \text{ ohms}$$

Theoretically, for a 50-ohm resistor, z = 50/50; therefore,

$$\left|S_{21}\right| = \frac{2}{3} = 0.667$$

••

This simple equation solves all your RF power amplifier needs:

5X=ar

Here's how! Don't consider five different sources when AR can satisfy all your RF power requirements. It's basic. Of the five major manufacturers of broadband amplifiers in the United States today, only Amplifier Research offers a full line of RF power amplifiers —— from DC to 1000 MHz and up to 5000 watts. With these capabilities, our amplifiers are ideally suited for a wide variety of applications, including general laboratory use, EMI susceptibility testing, laser modulation, NMR spectroscopy and ultrasonics.

Write now for free short form catalog. Your basic formula for RF power.

ar AMPLIFIER RESEARCH
Amplifier Research
160 School House Road
Souderton, PA 18964
215-723-8181

YOUR BEST SOURCE FOR RF POWER AMPLIFIERS

READER SERVICE NUMBER 48

Inside Anzac Amplifiers

are the patented designs which make ANZAC the leader in high technology/high reliability RF components... plus the quality of workmanship you can expect from our MIL-Q-9858A approved facility.

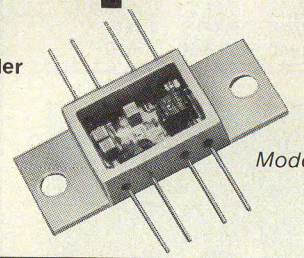

Model AM-123

10 dB Gain, Wide Dynamic Range
5 - 500 MHz

Noise Figure	4 dB typical
Power Output	+22 dBm (1 dB compression)
3rd Order Intercept	+40 dBm
Bias Power	1 watt typical

Call or write for the latest ANZAC Full Line Catalog.

All Amplifiers Available from Stock

anzac ELECTRONICS
Division of Adams-Russell

39 Green Street • Waltham, MA 02154 • Tel. (617) 899-1900 • TWX 710 324-6484

READER SERVICE NUMBER 49

Simple Setup Measures Complex Dielectric Data

A basic coax-line resonator is the heart of this dielectric measurement setup. Complex dielectric constant and loss tangent can be calculated by measuring tuning displacement and circuit Q.

MEASUREMENTS of loss tangent and complex dielectric constant on low-permittivity materials usually involve tedious, time consuming procedures. But these tests can be accelerated by an unusual microwave method[1] proposed by Russian scientist, C. L. Cubin. Cubin's method relies on a simple coaxial resonator to speed measurements without sacrificing accuracy. Simple mathematics, fast results and easy verification make the technique suitable for a multitude of materials.

Ashish K. Tagore, Research Engineer, Advanced Center for Electronic System, and **Dr. Chinmoy Das Gupta,** Assistant Professor, Department of Electrical Engineering, Indian Institute of Technology Kanpur, 11T Post Office, Kanpur-16, U. P. (India).

Briefly, the experimental sample is formed into a disk with the same diameter as the center conductor of the tunable, coaxial-line resonator shown in Fig. 1. Calculating the ratio of the tunable conductor's length, with and without the sample, leads to the material's complex dielectric constant (ϵ'). The sample's loss tangent ($\tan \delta$) is easily determined from the difference in the circuit's Q before and after the sample is installed.

Experimental investigations have proven Cubin's method to be simple, fast and highly effective. The effectiveness, in fact, is best illustrated in Table 1, which lists ϵ' and $\tan \delta$ of four different materials. It can be seen that Cubin's method yields results comparable to those produced by a far more rigorous procedure proposed by this author in 1974.[2].

First find the loss tangent

The largest advantage of this method is the simplicity of the working equations and the speed with which the parameters can be determined. If a

Table 1: Comparison of dielectric measurement methods

Material	Cubin's Method		Rigorous Method	
	ϵ'	$\tan \delta$	ϵ'	$\tan \delta$
Viniplast	3.8-4.0	65×10^{-2}	3.43-4.0	$(5\text{-}6)\times10^{-2}$
Transparent Plastic	3.0-3.3	5.5×10^{-2}	3.31-3.6	$(4.5\text{-}6)\times10^{-2}$
Sital	8.8-9.0	3.0×10^{-3}	9.3-9.5	4.1×10^{-3}
Ceramic	20	4.0×10^{-3}	18.5-20	5.5×10^{-3}

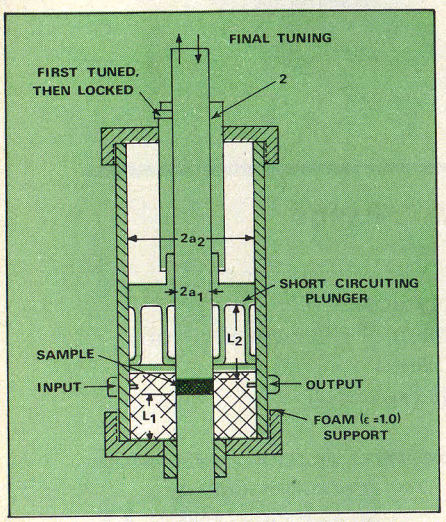

1. Cubin's method relies on substitution. *The coax line resonator is measured with and without a material sample. The difference determines the sample's dielectric properties.*

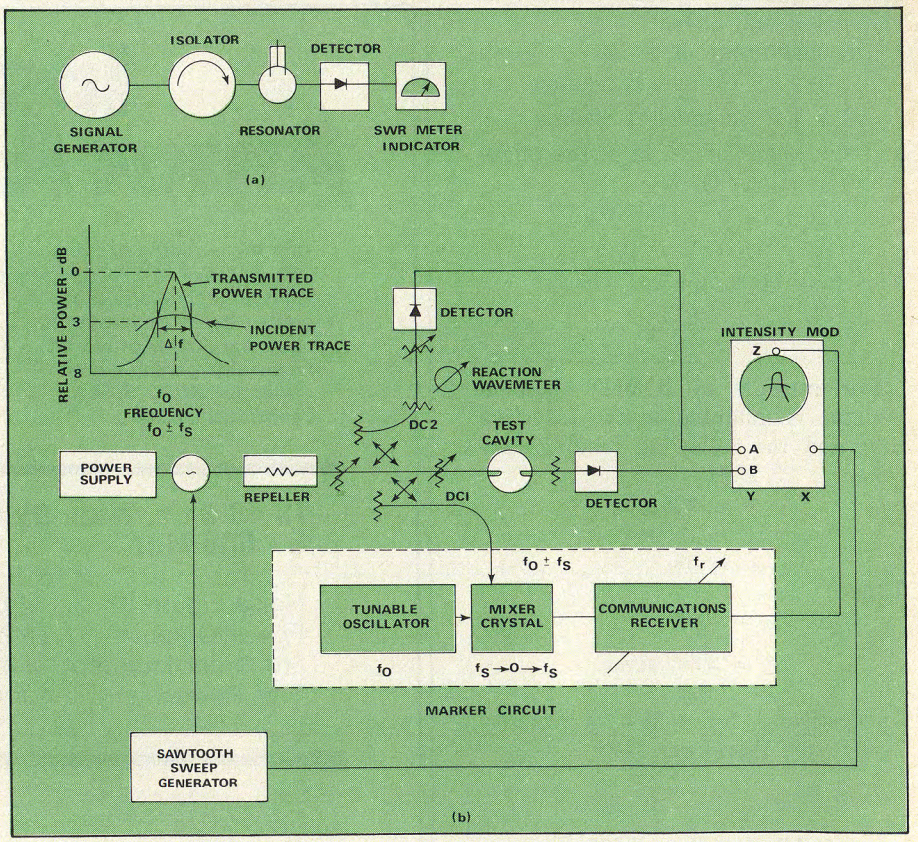

2. Resonance (a) and Q (b) tests are necessary *to determine a material's dielectric constant and loss tangents. Both tests sets use equipment on hand in most labs.*

sample's quasi-stationary field satisfies:[3]

$$\frac{2a_1}{\sqrt{\epsilon}} << \lambda/2 \qquad (1)$$

(where 2a is the diameter of the center conductor) and higher order modes are not excited within the resonator by maintaining:[3]

$$\lambda >> \pi (a_2 + a_1) \qquad (2)$$

then, the system's initial resonance with the sample in place can be achieved by adjusting length L_2 with plunger 2.

The sample's loss tangent can then be determined from:

$$\tan \delta = \frac{W}{W_E}\left\{\frac{1}{Q_x} - \frac{1}{Q_o}\right\} \qquad (3)$$

where: W = system's maximum stored energy
W_E = dielectric's maximum stored energy
Q_0 = resonator's Q with a hypothetical dielectric
Q_x = resonator's loaded Q with the sample

Thus, for the TEM mode, the system's stored energy—when L_1 and L_2 are equal to one-half wavelength—can be expressed:[1]

$$\frac{W}{W_E} = \frac{k^2 d^2}{2} \ln\left\{\frac{a_2}{a_1} \cdot \frac{L_1}{2}\right\} + \left\{\frac{k^2 a_1^2}{2\cos kL_2}\left\{\frac{L_2}{2} + \frac{\sin 2kL_2}{4k}\right\}\right\} \qquad (4)$$

where d = sample thickness,
a_2 = internal radius of the external conductor,
a_1 = radius of the internal conductor,
$k = \frac{2\pi}{\lambda}$, the wave number,
and L_1, L_2 are the lengths shown in Fig. 1.

After the experimental sample is removed, a new resonance condition is set up by tuning the center conductor with plunger 2 bolted to it.

ϵ' is just an equation away

The sample's complex dielectric constant is quickly determined using:

$$\epsilon' = \frac{d_s}{d_o}$$

where d_s = the thickness of the sample corresponding to L_1 and L_2 for resonance condition
d_o = the resonant gap width between center conductors without the experimental sample for the same resonant lengths as L_1 and L_2.

The first two equations, along with the condition for maximum Q of the resonator when $a_2/a_1 = 3.6$, dictate the necessary design criteria for the coax-line resonator. The probe's input and output coupling positions can be determined with a waveguide handbook.[4] It should be pointed out that while effectivness could be increased by tailoring the sample's diameter to avoid exciting higher order modes, the working equations become more complex, due to the presence of an air gap around the material.

A word about accuracy and limits

Although theoretical accuracy requires further analysis, particularly taking higher order modes into account, the technique yields practical accuracies of 2 to 3 per cent for ϵ' measurements. For tan δ measurements between 10^{-3} and 10^{-2}, a 10 per cent accuracy is possible. This falls off to about 25 per cent, however, for loss tangents of 10^{-4}. The complex dielectric accuracy holds to a full ϵ' value of 20.

As noted earlier, good agreement was achieved measuring a number of materials with Cubin's and this author's methods. In order to make these comparisons, convenient test methods were designed to extract the material's resonances and Qs. A quick measurement of the resonance point can be achieved with the circuit detailed in Fig. 2(a). Finding Q—necessary to evaluate tan δ—is somewhat more complicated. The circuit[5] in Fig. 2(b) was chosen for this purpose using an S-band resonator. The method's frequency range, however, is limited to the range that satisfies the two conditions necessary to suppress high-order modes.••

Acknowledgement

Many thanks to Professor O. G. Vendick of the Leningrad Institute of Electrical Engineering for his guidance and many works in this field.

References

1. C. L. Cubin, *Proceedings of Leningrad Polytechnic Institute*, No. 194, pp. 166-174, (1958).
2. C. Das Gupta, "Microwave Measurements Of A Complex Dielectric Constant Over A Wide Range Of Values By Means Of A Waveguide-Resonator Method," *IEEE Trans. on Microwave Theory and Techniques*, MTT-22, No. 4, pp. 365-371, (April, 1974).
3. A. L. Feldstein, L. P. Iavitch and V. P. Smirnov, *Waveguide Handbook*, Soviet Radio Moscow, (1967).
4. N. Marcuvitz, *Waveguide Handbook*, MIT Radiation Laboratory Series, Vol. 10.
5. M. Sucher and J. Fox, *Handbook of Microwave Measurements*, Vol. II, Polytechnic Press of Brooklyn.

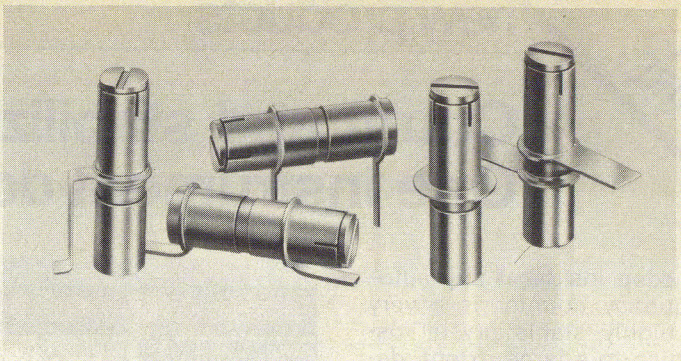

GIGA-TRIM CAPACITORS
FOR MICROWAVE DESIGNERS

GIGA-TRIM (gigahertz-trimmers) are tiny variable capacitors which provide a beautifully straightforward technique to fine tune RF hybrid circuits and MIC's into proper behavior.

APPLICATIONS

- Impedance matching of GHz transistor circuits
- Series or shunt "gap trimming" of microstrips
- External tweaking of cavities

Available in 5 sizes and 5 mounting styles with capacitance ranges from .3 - 1.2 pf to 7 - 30 pf.

Johanson®

MANUFACTURING CORPORATION
Rockaway Valley Road
Boonton, N.J. 07005
(201) 334-2676 TWX 710-987-8367

READER SERVICE NUMBER 67

COVER FEATURE

Count and stabilize: One instrument does both to 18 GHz

Hidden deep inside of any automatic frequency counter is a very accurate, highly stable crystal oscillator, which to a large extent, determines the accuracy of the instrument. Similarly, expensive signal generators designed for precise laboratory chores employ a crystal reference oscillator to phase-lock the output for good accuracy and stability.

Wouldn't it be handy to be able to get inside the counter's circuitry and use the instrument's crystal time base to improve the output characteristics of your run-of-the-mill signal generators?

Well, with EIP's new model 371 source-locking counter you can do that and more. In addition to its normal capability of automatic frequency counting from 20 Hz to 18 GHz, model 371 allows you to lock any swept source within the range of 10 MHz to 18 GHz to the same long-term accuracy and stability as the time-base oscillator in the counter. The only requirements are that the source must have an FM input and be manually set to within 20 MHz of the desired output frequency.

Two cables connect the source-locking counter to a signal generator. The counter measures the output frequency of the generator in the normal manner, however, a second hookup is necessary to transmit a correction signal from the counter to the FM input port of the generator.

Operation is straightforward. Manually tune the source to within 20 MHz of the desired output, using the counter's 11-digit sectionalized LED display to check the exact frequency (see Fig. 1). Once within this range, simply enter the desired frequency on the front-panel keyboard provided by the counter (see Fig. 2). This number will register on a separate LED for future reference. Frequency steps of 100 kHz are possible (400 kHz from 300 to 850 MHz). Finally, press the LOCK button. To be sure that the lock has indeed occurred, check the output frequency of the signal generator by reading the main display of the counter.

Once locked, the source will have the same long-term accuracy and stability as the time-base oscillator in the counter. Standard worse-case specifications for the 10 MHz clock used in model 371 include 3 x 10^{-7}/month aging rate, 2 x 10^{-6} temperature sensitivity over a range of 0 to 50°C and 1 x 10^{-7} frequency shift with ±10 per cent change in line voltage. Three time-base options offer even better performance since they include a porportional control oven. The top-of-the-line time base (option 05) offers a worse-case aging rate of 5 x 10^{-10}/day, temperature stability of 3 x 10^{-8} over a range of 0 to 50°C and sensitivity to a ± 10 per cent line-voltage fluctuation of 2 x 10^{-10}.

The phase-lock loop bandwidth of model 371 in combination with a signal generator is approximately 2 kHz. The manufacturer claims that this helps to eliminate residual FM at 60 Hz and its harmonics.

One of the unique features of the source-locking counter is automatic bandwidth and polarity control. The FM inputs of sweepers and sources have different modulation sensitivities and polarities depending upon the specific model and manufacturer. The 371 automatically provides the correct output for sources of either polarity with modulation sensitivities between 2 and 200 MHz/volt; no adjustments are necessary.

In its role as an automatic frequency counter, model 371 offers performance equal to that of the EIP model 351D. Specifications over the counting range of 20 Hz to 18 GHz include sensitivity to −30 dBm, 40-MHz FM tolerance and 2-W burnout protection. YIG preset, an option on earlier counters, is standard with model 371. This allows the operator to begin a search at any selected frequency using keyboard control, thus speeding acquisition time and providing selectivity with multiple inputs.

System oriented options include provisions for BCD output and programming, or general purpose interface bus (GPIB) operation. P&A: model 371: $6,800; option 05: $550; 90 to 120 days. **EIP, Inc., 3230 Scott Blvd., Santa Clara, CA 95050 (408) 244-7975 (Electro Booth No. 1223).**

CIRCLE NO. 109

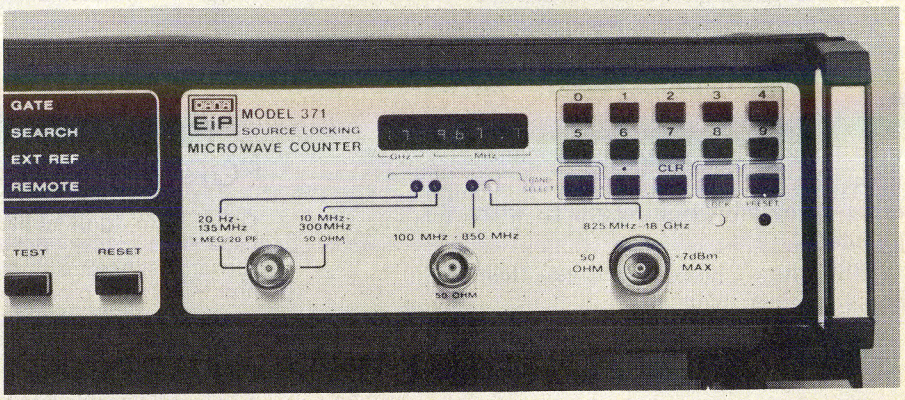

2. The microprocessor-controlled source locker features keyboard control. A separate LED display records the desired output frequency



1. Source locking capability is added to a frequency counter without any increase in size. Cost is about $1,000 more than the counter alone.

laser technology

MICROWAVES

MAY 1977

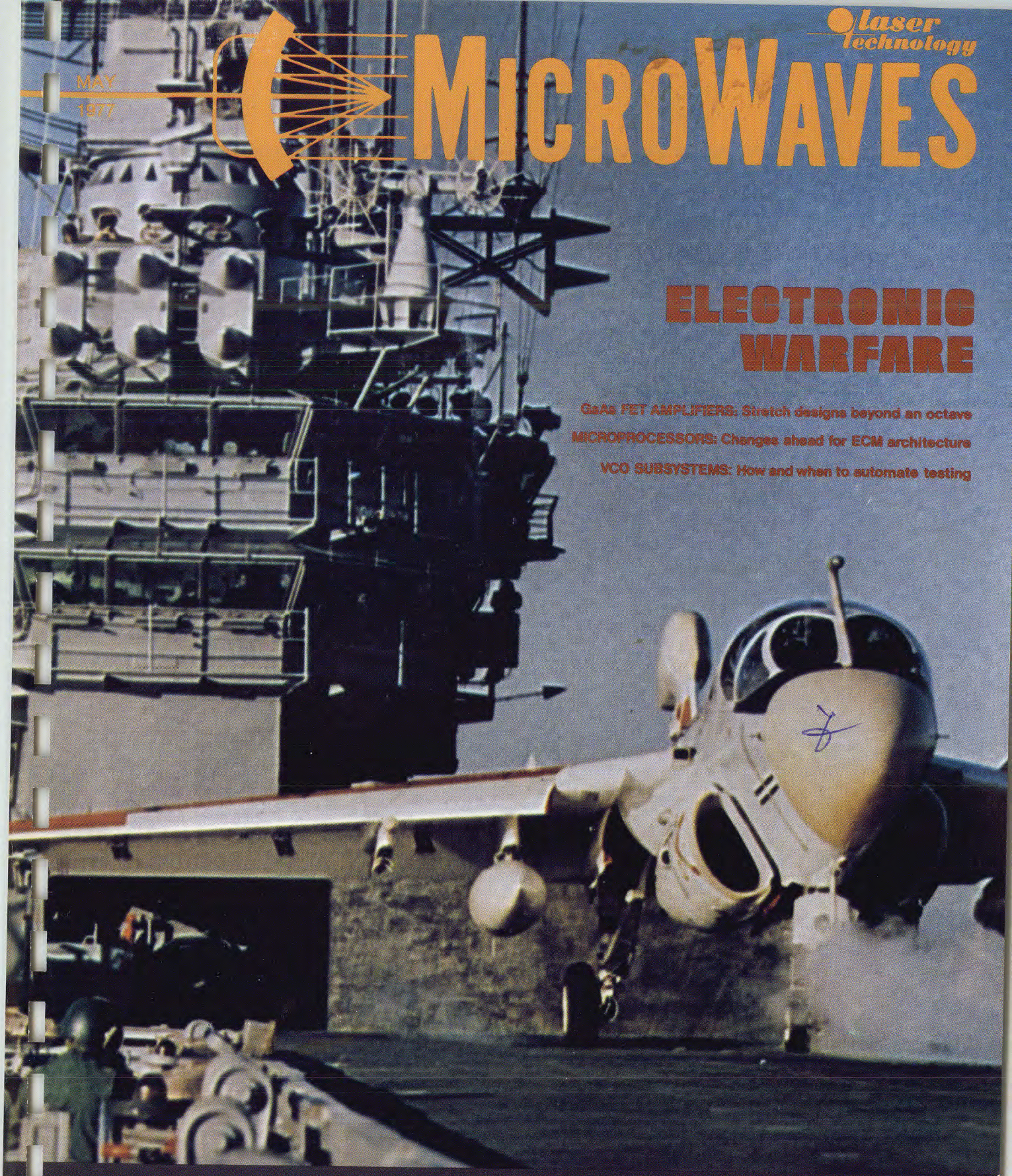

ELECTRONIC WARFARE

GaAs FET AMPLIFIERS: Stretch designs beyond an octave

MICROPROCESSORS: Changes ahead for ECM architecture

VCO SUBSYSTEMS: How and when to automate testing

Also:

A Designer's Guide To Microstrip

Dealing With T-Junction Discontinuities

Calculator Program Predicts Waveguide Moding

RENEW YOUR SUBSCRIPTION NOW
See card inside front cover.

RF devices are prevented by TRW's use of gold metallized die, gold wire bonds and gold package metal. Gold wire bonding does not work-harden and is thousands of times more resistant to fatigue than is the more brittle aluminum wire alternative. TRW's gold thermal-compression bonding technique provides you with bond-to-pad mechanical integrity, not possible with aluminum or ultrasonic bonding systems.

RF POWER TRANSISTORS & HYBRIDS—BUILT-IN RELIABILITY

Performance And Reliability

Take advantage of TRW Semiconductors' performance and reliability in your next circuit design. Check our chart. We have RF devices for every circuit requirement. More details are available in our Product Selection Guide.

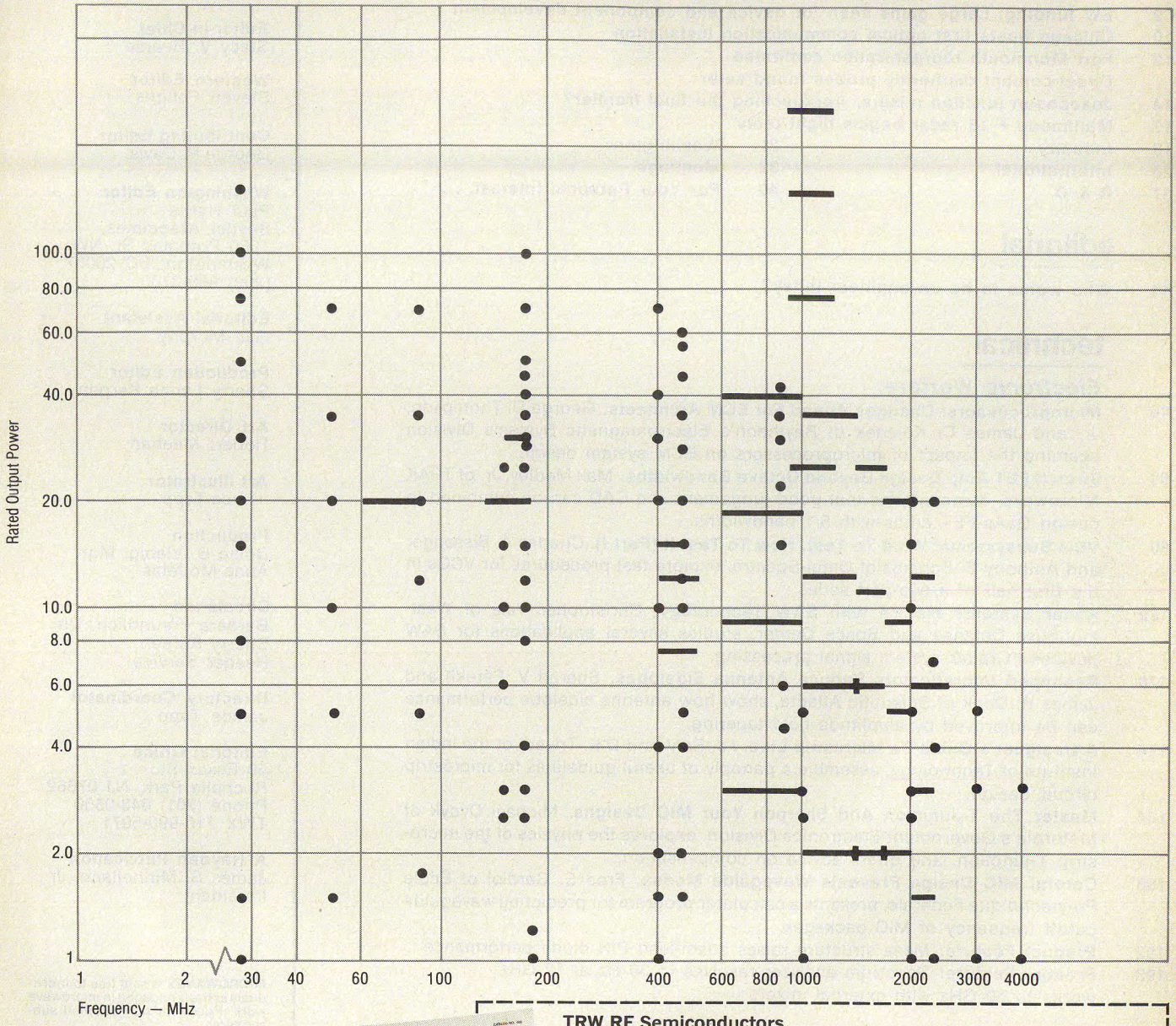

Aren't they worth checking out?

Use this coupon, or call Warren Gould at (213) 679-4561 for complete specs and samples of TRW RF discretes and hybrids—milliwatts to kilowatts, 1MHz to 4GHz. When it comes to RF semiconductors, we're ready to help.

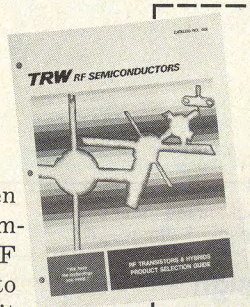

TRW RF Semiconductors
An Electronic Components Division of TRW Inc.
14520 Aviation Blvd., Lawndale, California 90260

☐ Please send me your new RF Product Selection Guide.
☐ Please have an applications engineer contact me: _____ (PHONE)

NAME _____

POSITION _____

COMPANY NAME _____

ADDRESS _____

CITY _____ STATE _____ ZIP _____ M

TRW RF SEMICONDUCTORS

ANOTHER PRODUCT OF A COMPANY CALLED TRW

READER SERVICE NUMBER 5

MICROWAVES

May 1977
Vol. 16, No. 5

news

9 EW funding: Large gains seen for device and component development
10 Chicago hosts first optical communication installation
12 Fort Monmouth reorganization confirmed
Direct-contact diathermy probes found safer
14 Josephson junction mixers: Approaching the final frontier?
17 Multimode F-16 radar begins flight tests
18 Industry
21 Washington
28 International
32 Meetings
37 R & D
40 For Your Personal Interest. . .

editorial

44 Who wants to be an engineer today?

technical

Electronic Warfare:

46 **Microprocessors: Changes Ahead For ECM Architects.** George D. Thompson, Jr. and James C. Kolanek of Raytheon's Electromagnetic Systems Division examine the impact of microprocessors on ECM system design.
54 **Stretch FET Amp Design Beyond Octave Bandwidths.** Max Medley, Jr. of TRAK Microwave, demonstrates that good judgement and CAD can be combined to design GaAs FET amps with 5:1 bandwidths.
60 **VCO Subsystems: What To Test, How To Test It (Part I).** Charles A. Bissegger and Anthony E. Schlenz of Omni-Spectra, explore test procedures for VCOs in the first half of a two-part series.
162 **Radar Systems Mature With SAW Technology.** Christopher Vale of Westinghouse Defense and Space Center, studies several applications for SAW devices in radar system signal processing.
170 **Reshaped Subreflectors Reduce Antenna Sidelobes.** Sharad V. Parekh and James H. Cook of Scientific Atlanta, show how antenna sidelobe performance can be improved by amplitude field tapering.
174 **A Designer's Guide To Microstrip Line.** I.J. Bahl and D.K. Trivedi of the Indian Institute of Technology, assemble a panoply of useful guidelines for microstrip circuit design.
184 **Master The T-Junction And Sharpen Your MIC Designs.** Michael Dydyk of Motorola's Government Electronics Division, explores the physics of the microstrip T-junction, and offers advice on compensation.
188 **Careful MIC Design Prevents Waveguide Modes.** Fred E. Gardiol of École Polytechnique Fédérale, presents a calculator program for predicting waveguide cutoff frequency of MIC packages.
192 **Product Feature:** Mesa structure raises beam-lead PIN diode performance
193 **Product Feature:** Spectrum analyzer resolves to 30 Hz at 12 GHz, works to 60 GHz with external mixers

departments

193 New Products
206 New Literature
212 Application Notes
214 Bookshelf
215 Advertisers' Index
216 Product Index

About the cover: The EA-6B Prowler, caught here catapulting off a carrier deck, is the focal point of many Navy airborne ECM programs. Photo courtesty of Grumman Aerospace, Bethpage, NY.

coming next month- Computer-Aided Design

June's issue examines the growing role of computer-aided design in many sectors of the microwave industry. CAD, once a luxury, is now a near necessity for the firm that wants to stay atop a competitive market. Staff reports and articles delve into the measurement, characterization, synthesis and optimization issues involved with this revolutionary trend. **Plus:** An exclusive cover story reveals a new concept in power transistor design which provides a four-fold increase in input and output impedances. Performance of 100 W CW over a bandwidth of 90 to 500 MHz, and 75 W CW in the 750 to 1000 MHz range is typical. This radically new transistor demands equally novel RF circuit design. Dont't miss the details in June!

Publisher
Howard Bierman

Editor-in-Chief
Stacy V. Bearse

Western Editor
Steven Peliotis

Contributing Editor
George R. Davis

Washington Editor
Paul Harris
Snyder Associates
1050 Potomac St. NW
Washington, DC 20007
(202) 965-3700

Editorial Assistant
Gail Murphy

Production Editor
Sherry Lynne Karpen

Art Director
Robert Meehan

Art Illustrator
Janice Tapp

Production
Dollie S. Viebig, Mgr.
Anne Molfetas

Circulation
Barbara Freundlich, Dir.
Sherry Karpen,
Reader Service

Directory Coordinator
Janice Tapp

Editorial Office
50 Essex St.,
Rochelle Park, NJ 07662
Phone (201) 843-0550
TWX 710-990-5071

A Hayden Publication
James S. Mulholland, Jr.,
President

MICROWAVES is sent free to individuals actively engaged in microwave work. Prices for non-qualified subscribers:

	1 Yr.	2 Yr.	3 Yr.	Single Copy
U.S.	$25	$40	$ 60	$3.00
Foreign	$40	$70	$100	$4.00

Additional Product Data Directory reference issue, $15.00 each (U.S), $27.00, (Foreign). POSTMASTER, please send Form 3579 to Fulfillment Manager, MicroWaves, P.O. Box 13801, Philadelphia, PA. 19101.

Back Issues of MicroWaves are available on microfilm, microfiche, 16mm or 35mm roll film. They can be ordered from Xerox University Microfilms, 300 North Zeeb Road, Ann Arbor, MI 48106. For immediate information, call (313) 761-4700.

Hayden Publishing Co., Inc., James S. Mulholland, President, printed at Brown Printing Co., Inc., Waseca, MN. Copyright © 1977 Hayden Publishing Co., Inc., all rights reserved.

Microprocessors: Changes Ahead for ECM Architects

Microprocessors will play a key role in the dense, complex signal environment forecast for the future. Low-cost units will change the makeup of the ECM system, placing new demands on the RF designer.

ELECTRONIC countermeasure (ECM) systems have evolved over the past several decades from manually operated receiver and transmitter sets to integrated systems which provide fully automatic operation. Today's systems process vast amounts of data to assess the signal environment and to control complex and interrelated resources. Requirements have been generated which specify extremely dense emitter environments and the analysis of complex signals. Together, these requirements indicate the need for both increased processing speed and more sophisticated algorithms.

The advent of low-cost, compact microprocessors has produced a quantum jump in the capacity of ECM systems to meet present and projected system requirements. Microprocessors have revived interest in the development of multiple processor architectures which provide parallel processing capability and the decentralization of processing to several points in the system. Multiple processors can provide an order of magnitude increase in performance for the same hardware package as a centralized mini-computer design.

The implications for the RF and microwave designer are many and varied. Microprocessors will find their way into parts of the ECM system never associated with digital interfaces before. "Smart" antennas will be controlled by microprocessors in spatial scanning applications. Design criteria for components will change as microprocessors are used to compensate for non-ideal characteristics. Overall, microprocessors will present new and interesting challenges for the RF designer.

Threats grow in number and complexity

Depending upon system sensitivity, it has been estimated that future systems may encounter between 400 and 1,000 emitters within the dynamic range of the receiver. The expected environment may include CW in combination with 250-thousand to 1-million pulses per second. In processing such an environment, each received signal must be compared with established emitter tracks. Direct comparison would require between 100-million and 1-billion comparisons per second. Obviously, high-speed and clever sorting techniques must be applied to reduce this number to realizable proportions. Increased spatial and spectral resolutions are one way of reducing the number of comparisons that must be made. One-degree beamwidths and 1-MHz frequency bins will be typical operating parameters for sorting and association.

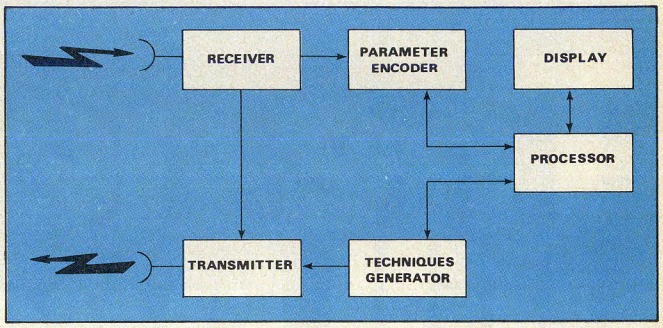

***1. Automatic ECM systems** must receive, assess and respond in increasingly complex signal environments.*

It will be necessary to correlate colocated search and acquisition radars with terminal threats for identification purposes. This will increase sensitivity and intercept probability requirements. System sensitivities of −60 to −80 dBm with intercept probabilities exceeding 90 per cent will be typical. Whether this will be realized with systems that are wide-open or fast-scanning will be determined by the RF designer.

The transmitting portion of the system will be required to respond to up to 100 emitters during any given time interval. Increased effective radiated power (ERP) is likely because overlapping signals and directional responses will require power management algorithms to be used. Look-through capability for the receiver will be required either by increased isolation, cancellation techniques or rapid gating of responses.

Even in the future, the bulk of the environment will undoubtedly be handled by the main receiver system. But the special cases of exotic emitters, such as parameter agility and coded pulses, will be handled by special receiving systems using dedicated microprocessors.

How will the microprocessor enter the picture?

The current trend in ECM system design is being directed to incorporate "smart" subsystems which include microprocessors as part of their basic design. This approach has evolved naturally from a desire to partition a system design into identifiable units which are dedicated to performing specific tasks within a well-defined interface organization. As the management and processing requirements for these units became more complex, it became desirable to incorporate the capabilities that are afforded by programmable general-purpose processors. And, as low-cost and compact microprocessors became available, the processors themselves were placed within the units.

George D. Thompson, Jr., Principal Engineer, and **James C. Kolanek**, Senior Engineer, Raytheon Company, P.O. Box 1542, Goleta, CA 93017.

Once this situation occurs, subsystem performance requirements expand to include more, if not all, of the real time management responsibilities, while executive communication takes place via the interface organization.

To understand how the processor relates to the system, consider the block diagram in Fig. 1, showing the major functional elements which may be found in any of several designs of a generic class of ECM systems which require automatic response.

The receiving assembly acquires raw signals from the environment. A parameter encoder interfaces the receiver to the processor by converting the analog output of the receiver to a digital format. This digitally encoded data is referred to as a signal descriptor word (SDW), and generally includes such parameters as signal amplitude, carrier frequency, direction of arrival, and time of arrival.

The processor operates on these SDWs to assess the environment, then initiates a response by a series of commands sent to a techniques generator. The techniques generator provides the low-level RF signal to the transmitter as well as switch commands for the signal path. The processor may also be required to provide data to a situation display which includes provisions for operator interaction.

Two system architectures emerge

The microprocessors can be interconnected in any one of several architectures to perform the processing. However, architectures fall into two general categories: federated and multiprocessor.

In the federated architecture, each processor performs its own dedicated job. Each microprocessor has its own simple executive, and interprocessor communication takes place, except for interrupts, only at the beginning and end of tasks. The individual processors are loosely coupled and operate, to a large extent, independently of one another. However, there is a static allocation of jobs with no capability for a lightly loaded processor to assist a heavily loaded unit.

In contrast, a multiprocessor architecture operates under the central control of an executive processor which allocates jobs to whichever processor is not busy; each processor has access to all of the memory. The overall processing load can be evenly distributed and the flexibility of job assignment gives graceful degradation in case of processor failure. This type of architecture requires a complicated executive and must resolve conflicts for memory access.

Multiprocessor architectures are usually more complicated and do not accommodate the modular software checkout inherent in federated architectures. Because microprocessors are such a recent development, multiprocessor architectures have not yet appeared in operational ECM systems. However, an example of a federated architecture can be found in an ECM system intended for use in tactical aircraft. In this system, all software related processing is performed by a total of six microprocessors as shown in Fig. 2. The track-correlator processor is a special-purpose array component which performs simple pulse-to-pulse tracking by comparing received frequency and azimuth to the contents of track files contained in content-addressable memories.

The six microprocessors perform the following functions:

- New emitter start processor—analyzes pulse data stored by azimuth and frequency to determine the type of emitter file to establish.
- Track management processor—performs smoothing and analysis of data to track changing emitter parameters and to update track files.
- Classification processor—compares emitter parameters between limits with parameters of known emitters to perform an identification function.
- SDW analysis processor—performs detailed PRI and scan analyses on real-time data to assist the CP in the identification process.
- Resource management processor—allocates resources, adapts system operating parameters and continually reassesses emitter lethality to manage available resources.
- Techniques generator processor—calculates parameter ranges, sets up technique generators and manages real-time technique generation.

The architecture shown in Fig. 2 is flexible and expandable, since microprocessors and memory can be added as required to accommodate new requirements. For example, a microprocessor for a display can be added to format data, to sense control inputs and to control displays and indicators. The use of microprocessors has allowed an increase in processing capability with hardware comparable to a single minicomputer.

In addition, the distribution of functions allows multiple input/output channels that can operate on a non-interfering

(continued on p. 48)

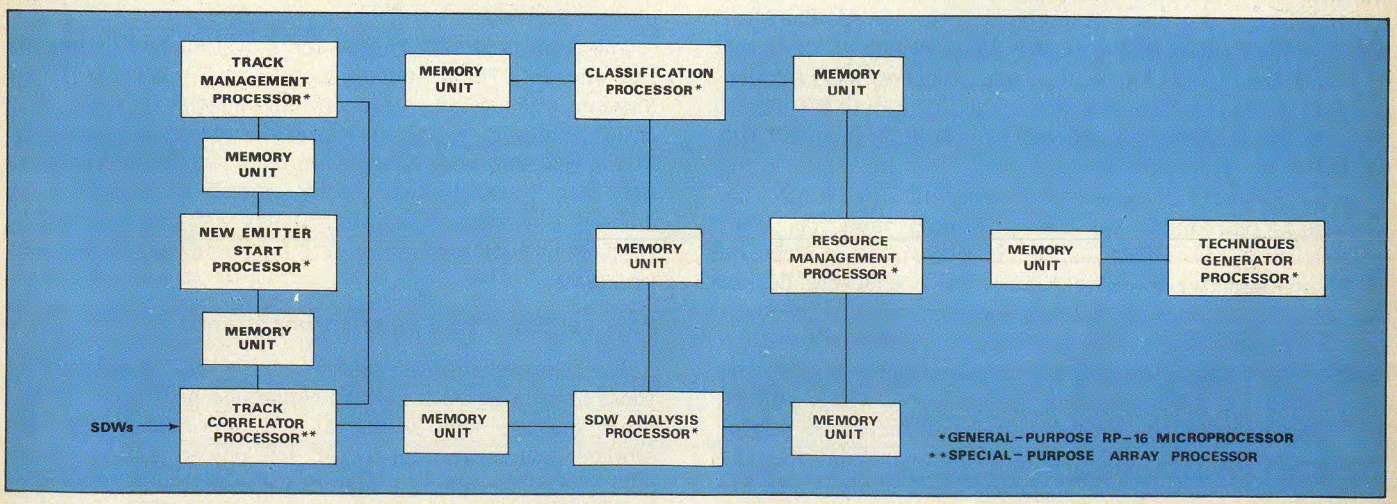

2. *Six microprocessors* *control this tactical ECM system. Since it uses a federated architecture, each processor performs one function.*

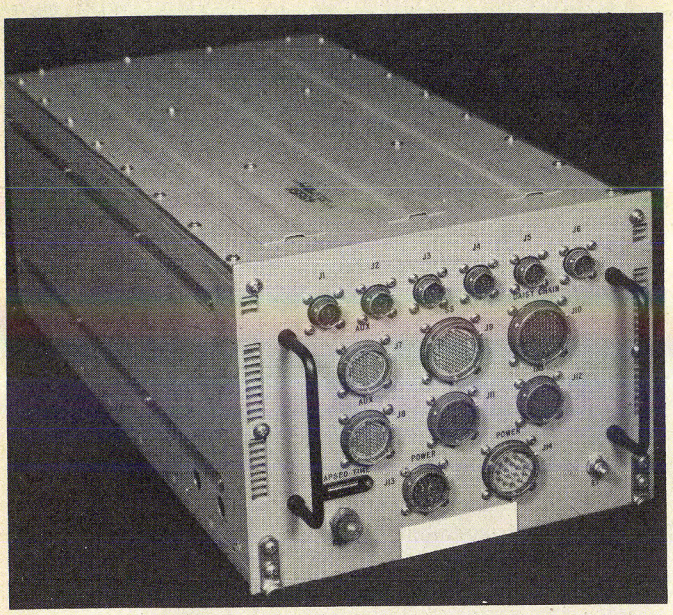

***3. A single ATR case** contains three microprocessors, a 49K memory, six serial input/output channels and three parallel data bases.*

basis. For example, the full ATR case shown in Fig. 3 contains an ECM system controller consisting of three Raytheon microprocessors (model RP-16), 49K of memory, six serial input/output channels, and three parallel data bases. The processing capability of the system controller is in excess of one-million operations per second.

The processor architecture presented represents a first step toward multiple processor architectures using microprocessors for total system processing. However, even greater dispersion of microprocessors throughout the ECM system will occur. Control functions for antennas, receivers and transmitters will be implemented with microprocessors. The devices will also be used to analyze exotic signals.

Although the vast majority of received signals will be associated with "standard" emitters having single beams and stable parameters, increasing numbers of exotic emitters having frequency agility, PRI agility and coded pulses are becoming of concern. While the main processing system handles the standard emitters, special-purpose receivers using microprocessors will analyze exotic signals. The situation is illustrated in Fig. 4. As the presence of an exotic signal is detected, the special-purpose receiver will be called upon to gather data and to do the detailed analyses necessary to allow the main processing system to identify the signal.

It is evident that microprocessors will provide greater processing capability for ECM systems than has been realized thus far. This is especially significant in airborne ECM systems where weight and size are severe design constraints. As microprocessors become scattered throughout the ECM system, loosely federated processor architectures will result. Central processing functions may be performed by multiprocessor architectures which will be just one part of the larger system of federated microprocessors. But a key question still remains: What does the trend toward "smarter" ECM systems with a larger number of "thought centers" mean to the RF designer?

Traditional constraints on RF design may be relaxed as microprocessors are used to compensate for deviation from ideal parameter values. However, increased performance in other areas will be required as, for example, increased bandwidth is traded for allowing greater in-band amplitude variations. The dividing line between the analog and digital portions of a system will become less distinct as more units in the system incorporate microprocessors into their design.

The RF designer will find that his design requirements will:

- be more stringent in the areas of greater sensitivity, greater frequency coverage, more ERP and fast-switching sources,
- change in emphasis for different design criteria as microprocessors are used to compensate for parameter variations, and
- include an interface to a microprocessor for control, processing, compensation or switching functions.

Let's examine the impact on receivers, signal sources and transmitter from a system viewpoint.

Receiving antennas must improve

Because of greater emitter density and the need for emitter-to-emitter correlation, the receiver subsystem must provide improvements over existing designs in the areas of resolution, sensitivity, and interference suppression. Increased spatial and frequency resolution will be needed to separate signals so that they can be tracked and identified. Dense environments and increased sensitivity will make it a necessity to encode the parameters of overlapping signals. Even in the absence of high duty cycle emitters, the percentage of overlapping pulses with Poisson arrival times will approach 40 per cent for the pulse rates of 10^6 pps. High duty cycle emitters further complicate the overlap problem and will require suppression techniques to reduce the interference.

The receiver antenna provides perhaps the first item to be investigated for performance gains. A large aperture not only provides gain for increased signal sensitivity but also provides spatial filtering to resolve signals in dense environments. Since essentially a first pulse intercept must be maintained, large aperture arrays will require either multibeam organization or intrapulse scanning. Signal processing arrays of one form or another may be incorporated for interference suppression of high duty cycle signals, such as standoff jammers, which may be operating in the vicinity of the receiver.

The receiver design chosen for a system will be heavily influenced by the associated antenna or vice versa. If the antenna provides adequate gain and spatial filtering, then crystal video receivers may provide adequate sensitivity. Microprocessor controlled, frequency selective receivers may also be required to resolve signals in the frequency domain. For example, multifrequency transmissions can be resolved only by processing with frequency-selective measurements.

Fast settling VCOs become important

The requirements for signal sources will be confined to those associated with voltage-controlled oscillators. While other sources, such as digital and microwave delay line storage devices are important, low-power microwave oscillators are becoming a significant component in current ECM designs.

Generally, each signal that is to be transmitted by the

(continued on p. 50)

We'll bring you down softly.

60,000 MHz
40,000 MHz
20,000 MHz



SpaceKom is at home at high microwave frequencies.

If your existing receiving system goes up to only 12 or 18 GHz, and you would like to extend its frequency coverage to 40 or 60 GHz, SpaceKom low noise mm-wave mixer-preamplifiers or downconverters should be your choice.

For swept LO receiving systems, only four fixed-tuned mixer-preamplifiers (connected to the IF input of your receiver) will extend the frequency coverage of a 0.1-12.4 GHz receiver to 60 GHz. For swept IF or channelized receivers, SpaceKom downconverters with up to 10 GHz instantaneous RF/IF bandwidth will provide 12 to 40 GHz frequency coverage and assure the highest detection probability.

Mixer-Preamplifiers
For Swept LO Receivers

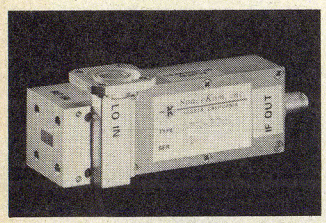

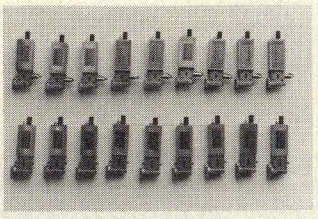

RF and LO* Input GHZ	IF Output MHz	Max. DSB Noise Figure	RF-IF Gain	Model No.
12.4-18	10-500	4.0db	25db	FKu-U
18-26.5	10-500	5.0db	25db	FK-U
26.5-40	10-500	6.5db	25db	FKa-U
40-60	10-500	7.5db	25db	FQ-U

* LO power 2-10mW

Mixer-Preamplifiers and Downconverters
For Swept IF or Channelized Receivers

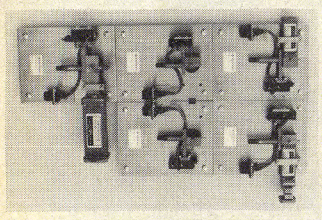

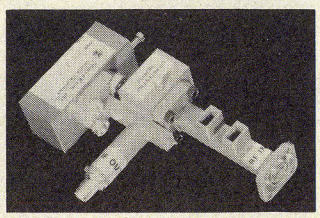

RF Input GHz	IF Output GHz	Max. SSB Noise Figure	Image Rejection Min.	RF-IF Gain	LO Freq.** GHz	Model No.†
18-22	4-8	10db	25db	15db	26	F20-6
22-26	4-8	10db	25db	15db	30	F24-6
26-30	4-8	10db	25db	15db	34	F28-6
30-34	4-8	10db	50db	15db	26	F32-6
34-38	4-8	10db	50db	15db	30	F36-6
38-42	4-8	11db	50db	15db	34	F40-6

** All units available with integrated Gunn-diode LO source or integrated LO frequency doubler. With integrated LO frequency doubler, external LO source must deliver 40mWmin. at ½ of the LO frequencies given in the table.

† Up to 10 GHz RF/IF bandwidth available without IF preamplifier.

SpaceKom, inc.

212 East Gutierrez Street, Santa Barbara, California 93101 (805)965-1013

READER SERVICE NUMBER 41

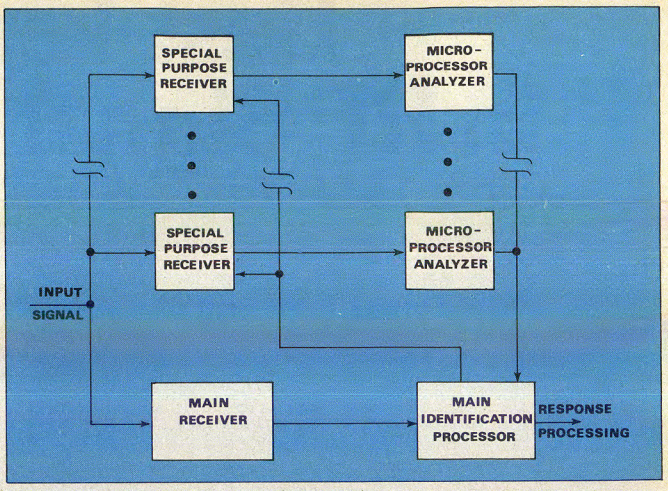

***4. Special purpose receivers** such as this will augment normal equipment to handle exotic signals.*

ECM system varies from CW to relatively low duty cycle waveforms (0.1 to 10 per cent). This implies that, except for CW, one VCO can be time shared among several responses. Effective time sharing requires that the VCO be capable of being tuned between any two points within its operating range and settle to within the radar bandwidth in less than the interpulse spacing.

If time sharing is incorporated, the design must take into account the fact that each response occurs independently from one another. Microprocessors will provide the means to handle overlapping requests for the VCO. Performance requirements may restrict the number of pulses dropped; therefore, a multichannel structure will be required. The number of channels depend on the number of signals handled simultaneously as well as the assignment philosophy. Typically, one may expect the number of VCO channels to extend from 5 to 20. If the design frequency range covers five octaves, this implies 25 to 100 octave-bandwidth VCOs per system. The potential for the proliferation of microprocessors for the control of signal sources will be evident.

Transmitter power to be managed

Current transmitter designs provide adequate ERP in low-density environments. However, future generations of ECM systems will demand high duty-cycle, multiple-signal capability. At the present time, two design approaches are being pursued to meet these requirements: dual-mode and distributed amplifiers. The former design uses high-power TWTs, which can operate either as low duty cycle, high-power amplifiers or as high duty cycle amplifiers at reduced power levels. The latter design uses low power CW amplifiers distributed throughout an antenna array or throughout a power combiner before input to the antenna.

Distributed amplifiers imply a large aperture with resultant beam steering requirements. Dense environments where multiple transmissions are required demand both spatial and power management disciplines to be implemented. A microprocessor located within the transmitter subsystem will likely be tasked to perform this function. It should be relatively straightforward to develop programs which account for variations from nominal design parameters such as boresite shift with frequency or amplifier gain changes with frequency. ••

Stretch FET Amp Design Beyond Octave Bandwidths

Broadband GaAs FET amplifiers continue to improve EW systems. This approach to multi-octave design illustrates that although CAD is necessary, it's not a substitute for good engineering judgement.

PRUDENT selection of load and source impedances are insuring the "off-the-shelf" status of GaAs FET low-noise amplifiers with bandwidth ratios greater than 5:1. In fact, the limiting factors of these designs are now the hybrid couplers rather than the amplifier stage. Using today's computer-aided design programs like COMPACT[1], it is conceivable that 1-to-18 GHz solid-state low-noise amplifiers will be a phone call away in the near future.

Several different amplifiers have been constructed and reproduced with remarkable agreement between the measured and calculated gain, VSWR, noise figure and power response. To verify the design procedure, three single-ended gain modules were designed around a one-micron gate-length GaAs FET with the following results: A 2 to 4 GHz design with 11.1±0.5 dB gain, 2.6-dB maximum noise figure and +8 to +10 dBm output power at the 1-dB gain compression point; a 2 to 6 GHz design shows 8.5±1 dB gain, maximum noise figure of 3.6 dB and minimum output power of +8 dBm; while a 1.5 to 8.0 GHz design has 7.5±1 dB gain, 4.5-dB noise figure and +10-dBm output power.

Weigh the design goals

Since a good deal of any amplifier design is compromise, especially when multi-octave goals are to be achieved, an important first step in designing low-noise GaAs FET amplifiers is a careful listing of design goals in order of decreasing priority.

Although this may seem a trivial first step, it does have a significant effect on the resulting amplifier. For example, if noise figure is most important, the amplifier input and perhaps the output, must be mismatched to achieve the best noise figure and gain flatness. This results in an overall network with a good noise figure, but with high input and output VSWRs. To correct this, a balanced amplifier approach using two identical stages connected to the conjugate ports of two hybrid couplers may be required. When the maximum amplifier width and height necessary to prevent undesired waveguide modes is calculated, the designer may find that he must design two identical amplifiers which will be side-by-side on a very small substrate without interacting. This constraint alone dictates that matching networks requiring large widths will not be suitable for the design.

Once the goals have been properly weighed, the design can proceed by:

- selecting the circuit material,
- characterizing the GaAs FET,
- synthesizing the matching network, and
- modeling the amplifier.

To illustrate the technique, let's choose the 2 to 6 GHz low-noise amplifier. The most important objective is reasonable gain and gain flatness. Second on the priority list is lowest noise figure and highest output power. Additional, though less significant emphasis is placed on the input and output VSWR, stability and physical makeup.

Material is crucial

Choosing microstrip as the design medium, because of the ease with which transmission lines, lumped components and active devices can be interconnected, the designer is left with a choice of materials. For the design being examined, fused silica was initially selected because the high-impedance lines required to match the FET could be easily realized. However, this material has several disadvantages when compared to alumina: The lower dielectric constant causes the matching network to be physically larger, stress induced in the metalization limits the thickness of the conductors below that required for lower frequency operation, longer delivery lead times, and greater expense.

Consequently, 25-mil alumina was finally selected as the best overall material. Thicker material allows higher impedance lines, since the width-to-height ratio determines the line impedance, and circuit Q is improved. But dispersion (the frequency dependence of microstrip) and radiation losses become significant.

Calculations of the maximum width and height required to suppress undesired waveguide modes and reduce cover effects to a minimum, show that a standard one-half-inch-wide substrate with the cover mounted 10 substrates high (250 mils) places the lowest waveguide mode above 10 GHz, while causing minimum interaction between the circuit and cover.

Characteristics of the microstrip lines are well documented and past experience with lumped elements such as bonding inductance, along with coupling and bypass capacitors, give the designer a good feel as to what parasitics should be included to insure accurate modeling. This leaves the FET as the single item to be measured.

Unpackaged device used

Although the s-parameters for various packaged and chip GaAs FETs are published by manufacturers, they are usually not measured with the same size enclosure, bias scheme or mounting technique used in an amplifier design. Since all of these will affect the s-parameters, they must be measured as accurately as possible in a fixture

Max W. Medley, Jr., Member of the Technical Staff, Trak Microwave Corp., 4726 Eisenhower Blvd., Tampa, FL 33614.

and with a bias network approximating the final amplifier.

The GaAs FET poses a much more difficult broadband matching problem than the bipolar because of its higher "Q" at the input and output. Another serious problem is low frequency stability. Although this problem is found with bipolar transistors, it is heightened in the FET because of higher low-frequency gain and an input and output reflection coefficient that approaches unity. The matching problem can be reduced somewhat by using an unpackaged FET which removes package parasitics and allows the matching network to be placed closer to the device. Low frequency stability can be improved slightly by the proper choice of the source bypass capacitors and resistors used for self bias. At frequencies where the capacitors no longer provide adequate RF bypass, the bias resistor acts as series resistive feedback which reduces the gain. However, the in-band stability problem is significant and has a pronounced effect on the selection of the matching topology.

Published parameters should be used as a first approximation to determine performance in the band of interest. On this basis, a test fixture can be constructed to simulate the final amplifier.

Which noise measurement?

Noise figure is an important consideration in the amplifier design and must be accurately measured. The basic method is to place a tuner at the input, tune for minimum noise, measure the gain, then using the system noise figure and Friis' formula

$$F = F_1 + \frac{F_2 - 1}{G_1}$$

where: F is the overall noise figure,
F_1 is first-stage noise figure,
F_2 is second-stage noise figure and
G_1 is first-stage gain,

calculate the FET noise figure without the second-stage contribution. The tuner is then removed and the impedance tuner-test fixture interface measured. The optimum source impedance is now determined by moving the measured impedance into the

(continued on p. 56)

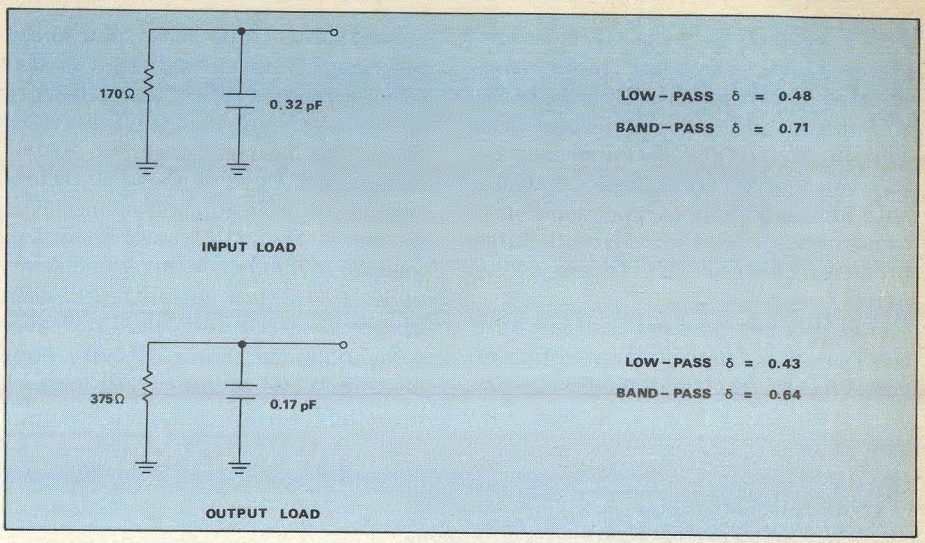

2. The load decrement *(δ) equivalent circuits actually detail the network Q.*

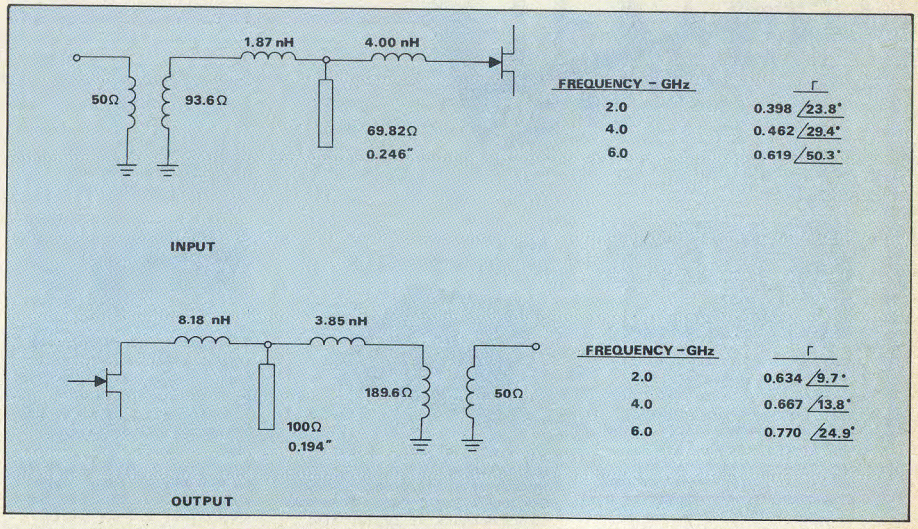

3. The input and output networks *are both low-pass circuits, necessitating a transformer to be included.*

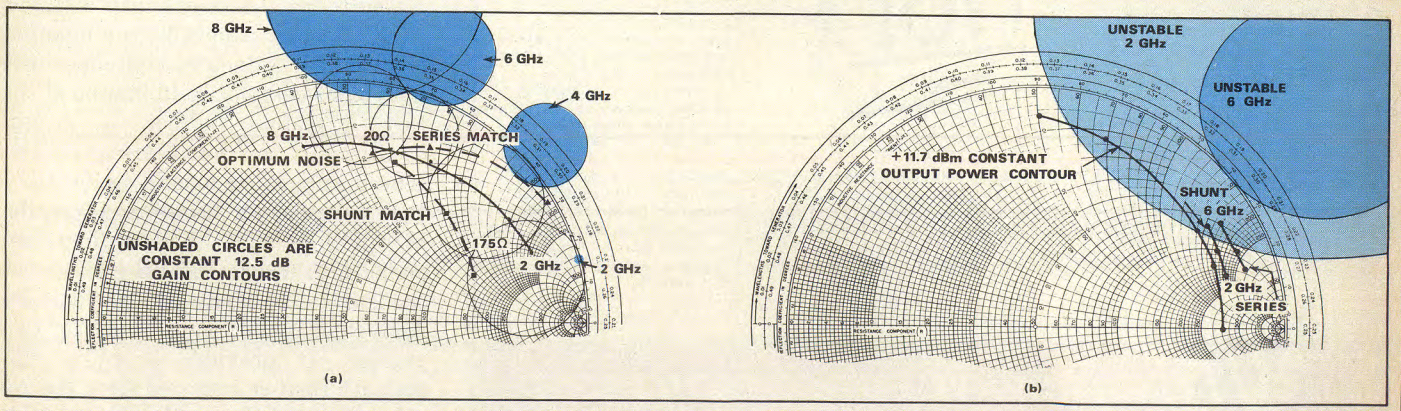

1. Series and shunt networks *(a) represent two possible source impedances plotted on the source plane from 2-to-8 GHz. On the load plane (b), the networks are plotted from 2-to-6 GHz.*

FET's reference plane. This measurement is somewhat more complicated than it appears. Because of the effects gain and the second-stage noise contribution, a false optimum may result. To further complicate matters, both input and output reflection coefficients approach unity, and it is possible to cause either or both to be larger than unity.

A far better technique[2] is to calculate the four noise parameters—optimum noise figure, real and imaginary optimum source impedance and the noise resistance from measurement at four different source reflection coefficients, by solving four simultaneous equations. This method has several distinct advantages. First, it allows the source impedance to be adjusted so the device is stable. Secondly, more than four measurements can be made and several solutions, each with different combinations of the data, used to reduce measurement errors. These noise measurements are also used to check the validity of the measured s-parameters by comparing the calculated transducer gain at the known source impedance with the measured gain through the tuner-test fixture.

The most difficult task facing the amplifier designer is synthesizing input and output networks which have a predetermined frequency response and yet can be physically realized. One of the better techniques is to plot the most important amplifier parameters on the load and source planes.[6] This enables the designer to immediately determine what effect a particular impedance has on the amplifier response.

The s-parameters are then used to determine the maximum available gain at several frequencies in the band. This analysis shows that the stability factor is less than one, which means the maximum stable gain (MSG) must be used. The MSG decreases from approximately 20 dB at 2.0 GHz to 15 dB at 6 GHz for the NEC-244 transistor used in this particular design. Since the maximum stable gain is the maximum possible gain before instability occurs, it is not a good idea to design for this value; a reduction of several dB from the MSG will provide a comfortable margin. The required gain reduction versus frequency can be realized either by reactive mismatch or dissipative absorption using resistors. Since the lowest possible wideband noise figure and highest output power are desirable for this amplifier, reactive mismatch will be used. As long as the input and output must be mismatched, it might as well be in the direction of low noise and maximum output power.

Series or parallel networks?

The FET's stability circles, optimum noise location, and contours of constant gain (12.5 dB from 2 to 8 GHz) are detailed in Fig. 1(a). It is easier to match to an equivalent load which is either a series or parallel combination of resistors, inductors and capacitors than some complex combination of the two; therefore, either a series-equivalent or parallel-equivalent source impedance should be found.

Although both series and parallel networks provide the required impedance to insure 12.5-dB gain across the 2 to 6 GHz bandwidth, the parallel equivalent is the better choice for two reasons. It provides a source impedance further removed from the regions of instability and has better noise figures at lower frequencies (contours

SOLID STATE POWER TECH NOTES

TECH NOTES No. 2

Highlights of interesting new prototypes, special-purpose designs and recent R&D activities.

SPACE-QUALIFIED AMPLIFIERS

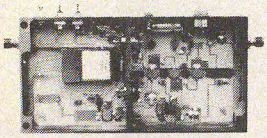

Engineered, fabricated, inspected and tested in accordance with Hi-Rel specifications, including complete space qualification and screening of all components, materials and production processes. Shown above is a power amplifier built for TIROS N Weather Satellite. L and S-band, with 5.5 watts min. power output.

LOS & FM TV BOOSTER AMPLIFIERS

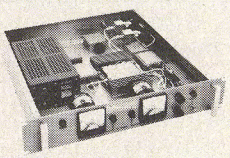

For existing radio and TV relay links, in frequency ranges of 1.7-2.0 GHz, 1.9-2.1 GHz and 2.0-2.3 GHz. Standard power outputs of 10, 20 and 50 watts. Transparent for NPR distortion. Typical unit shown above is telecommunication booster amplifier with 10-watt power output, 1.7-2.0 GHz frequency range. Includes forward and reverse power alarms. Circulator input/output for lower return loss.

HIGH POWER BOOSTER AMPLIFIERS FOR UHF AM/FM TRANSCEIVERS

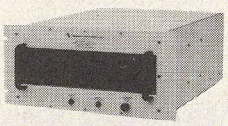

Designed to increase power output of AM transmitters with 20-watt carrier output, or FM transmitters with 20-watt output, such as UHF air/ground transceivers. Typical model shown is all solid state, operates in 225 to 400 MHz frequency band, delivers 400 watts PEP for AM systems and 400 watts CW for FM systems. Includes self-contained forced air cooling. Standard rack-mountable cabinet.

TACAN/DME MODULATOR/AMPLIFIERS

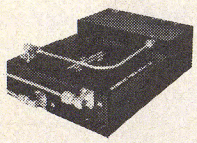

Broad band solid state TACAN modulator/amplifier, 100 watt peak power (other models up to 1000 watts peak RF power output). For airborne applications in 960-1215 MHz frequency range. Weighs only 2½ lbs. Gaussian shape RF output per MIL-STD-291B. Requires no tuning or shaping adjustments over entire frequency range. Cooling by forced air or conduction. Fully qualified per MIL-E-5400.

TROPOSCATTER AMPLIFIERS

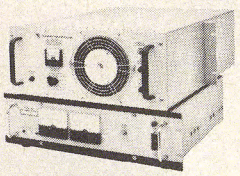

Up to 1000 watts at 755-985 MHz, up to 100 watts at 2.1-2.3 GHz. Features include circulator load protection, B+ reversal protection, thermal overload protection. Transparent to NPR/BINR (CCIR noise loading specification). Rack-mounted, self-cooled, with built-in test equipment.

SUB-SYSTEM ASSEMBLIES

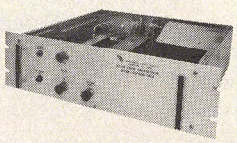

Now available from MPD is the custom-design and construction of sub-system equipments where high power solid state amplifiers represent a major portion of the electronics. Typical sub-system shown above is a Transceiver UP/DOWN Converter for L-band operation from 960 to 1215 MHz, with 100 watts power output. 70 MHz RF input and 70 MHz IF output to feed external modem. Includes diplexer and built-in T/R switch.

MPD MICROWAVE POWER DEVICES, INC.
Adams Court, Plainview, N.Y. 11803 • Tel. 516-433-1400 • TWX 510-221-1862

READER SERVICE NUMBER 44

of constant noise figure can be generated on the source plane which show that these circles compress as the reflection coefficient increases). Before the input network can be synthesized, however, additional investigation is required. An unrealistic number of sections may be required, or the characteristics of the associated output matching network may be undesirable.

Figure 1(b) maps the required load impedance for both prospective input networks (the input constant gain contours assume conjugate output match), the stability circles and maximum output power contours. A good first approximation[5] of the maximum output power is to use the load conductance determined by the quiescent bias point of 3 volts and 10 mA, or approximately 3.3 mmho. Unlike the input, both candidates for the output load are parallel equivalents since their conductance rather than resistance is constant with frequency. The impedance due to the parallel input network is a better choice because it is further from the region of instability, closer to the maximum output power contour, and has a lower impedance which will be easier to realize.

Synthesize the networks

Once the device has been characterized and impedances mapped, the matching networks can be synthesized.[3] Both loads are approximated, the load decrement (a measure of the Q of the load) and the required number of sections determined, and the element values calculated. Both models used to determine the load decrement, δ, are seen in Fig. 2. The desired source and load impedance (Fig. 1) cannot be exactly represented by these models but a calculator program can be written to curve-fit the data and reduce the error to a minimum (see "Calculator aids design and reduces error").

Since the load does not pass through resonance within the band of interest and each model is in the form of a low-pass structure, the matching network can be either bandpass or low pass. A bandpass structure yields a better match since the load decrement is higher but may be more difficult to realize. These networks generally use J-inverters (admittance transformers with constant phase shift at all frequencies) that require negative elements for wide bandwidths. The negative elements can sometimes be absorbed in part of the load or within the matching structure, but not always.

The low-pass structure has several distinct advantages for this application. If the shunt capacitors and series inductors are not too large, they can be realized with open shunt transmission lines and short lengths of bonding wire. Also, as the frequency decreases, the impedance into these networks will degenerate into the 50-ohm termination resistance where the FET is stable. The disadvantage is that the designer has no control over the required termination impedance and a low-pass broadband transformer is necessary. The calculated load decrements in Fig. 2 are used to calculate the maximum mismatch loss for various orders of matching networks; typical results for the 2 to 6 GHz design are shown in Fig. 3. The maximum calculated mismatch losses for a four-section network are 0.38 dB (input) and 0.60 dB (output). These networks actually represent three matching ele-

SOLID STATE POWER TECH NOTES

TECH NOTES No.3

Update report on the development and production of RF/microwave amplifiers in the "KILOWATT+" power range.

KILOWATT POWER BREAK-THRU

- COMBINATION COMMUNICATION & JAMMER SYSTEMS
- ELECTRONIC WARFARE JAMMING SIMULATOR SYSTEMS
- POWER CALIBRATION SYSTEMS
- RFI TESTING SYSTEMS

Since it was founded in 1967, MPD has achieved considerable technological progress .... to a point where we are now widely recognized as a principal leader in the field of solid state RF/microwave high power amplifiers.

Particular emphasis has been placed on raising the "state-of-the-art" in power levels obtainable with transistorized amplifier systems. For some time, 1000 watts had been considered a major "milestone" to be attained. That important goal was recently reached with the delivery of several MPD equipment systems for applications requiring power levels of 1000 watts or greater. Some of these are described below.

For additional information about these systems, or about the unique concepts and techniques we've developed for high power solid state amplifiers, call your local MPD representative or contact the factory.

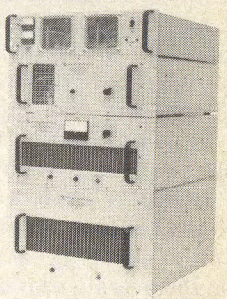

30-80 MHz, 1000-WATT LINEAR AMPLIFIER SUBSYSTEM

Special systems available to meet a variety of custom requirements such as frequency range, harmonic rejection, switchable output filters and high efficiency power supplies for minimum energy consumption.

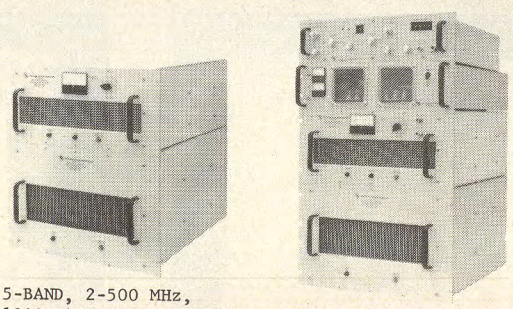

5-BAND, 2-500 MHz, 1000-WATT LINEAR OUTPUT AMPLIFIER SYSTEM

Designed for broadband communication, this system finds application in many military requirements for high power transmitters.

1000-WATT, 225-400 MHz POWER AMPLIFIER

System includes synthesizer, pulse generators and function generators. Class A/B operation permits all types of input signals to be amplified to 1000 watts.

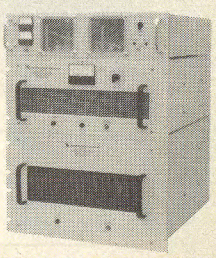

MULTI-BAND KILOWATT POWER METER CALIBRATION SYSTEM

High power stable signals for the accurate calibration of power meters at 1000 watts or less. Broadband untuned amplifiers simplify calibration procedures while requiring a minimum of units.

MPD MICROWAVE POWER DEVICES, INC.

Adams Court, Plainview, N.Y. 11803 • Tel. 516-433-1400 • TWX 510-221-1862

READER SERVICE NUMBER 45

ments since the first is part of the load. The transducer gain is calculated from the load and source reflection coefficients (Fig. 3) and found to vary from a maximum of 10.8 dB at 4.0 GHz, to a minimum of 10.1 dB at 6.0 GHz. It would appear from these calculations that the design goal should be set at 10.0 dB per stage.

Calculation of the element values for the 50-to-100 ohm input transformer and the 50-to-150 ohm output transformer completes the synthesis of the matching networks.

Model step-by-step

The final step is to precisely model the amplifier using a computer-aided program like COMPACT. The computer model must include as much information about the circuit and components as possible. Microstrip losses, junction effects and component losses must all be included. A step-by-step procedure is best, starting with the simplest amplifier form and progressing to the most complete. Fixed parasitics should be included in the early models, but those due to physical dimensions, like microstrip step and junction discontinuities, must only be added after they are finalized.

COMPACT uses a gradient optimization technique which computes the result of changing each variable element on the overall, user defined, error function. The error function is the weighted difference between the calculated circuit response and specified target response and may be specified to place more emphasis on certain parameters such as gain and noise figure, and less on others such as input and output match. The magnitude of the gradient provides a measure of the sensitivity of the various elements to the overall circuit response and can be used by the designer to reduce optimization time and help insure a reproducible design.

A sensitivity analysis (gradient calculation) of all matching elements included in the initial simplified amplifier model reveals which elements have the most effect on the desired performance; these should be used for the first optimization. The most important parameter in the design of this amplifier, for instance, was 10-dB gain across a frequency band from 1.5 to 6.5 GHz, which was slightly increased from the 2.0 to 6.0 GHz design goal in order to provide some margin for component error. The input and output match were not weighed because a hybrid coupler could be used to provide a good match.

Following the initial optimization, several simple bias schemes should be included and optimized for minimum interaction, then the entire amplifier can be modeled and optimized. This final model will include the parasitics and losses along with the physical length of the microstrip lines and effective dielectric constant. During the final optimization, only the lengths of the microstrip lines should be allowed to vary because the losses and effective dielectric constant are a function of the impedance or line width. A final sensitivity analysis of all elements should reveal that no single element is more sensitive than any other.

The overall amplifier stability should be investigated at all frequencies using the completed computer model. The matching networks are usually designed such that the amplifier is stable when terminated in 50 ohms; however, unconditional stability implies that there are no combinations of passive load or source terminations that will cause instability. Fortunately, the same mechanism that enables the hybrid coupler to provide a good input match when the conjugate ports are mismatched also improves the stability. The input reflection coefficient is the difference of the reflection coefficients at the conjugate ports with each multiplied by a different frequency dependent coupling factor. At center frequency for a 3-dB coupler, the input is one-half the difference of the two terminations (assuming perfect isolation); therefore, the maximum reflection that either amplifier stage will see due to all possible real loads is 0.5. During the synthesis of the matching networks, the load and source planes must be mapped through the coupler and matching networks to verify amplifier stability. However, the best test for stability is to analyze the balanced amplifier at as many frequencies as possible. All the balanced amplifiers described in this paper are unconditionally stable.

The final design consists of series transmission lines, open shunt stubs, series inductors and the bias networks. The open shunt stubs simplify tuning, if required, and clean up the circuit layout.

Continuing computer optimizations may also allow the same substrate to be used for other low-noise amplifiers operating at different frequencies, if

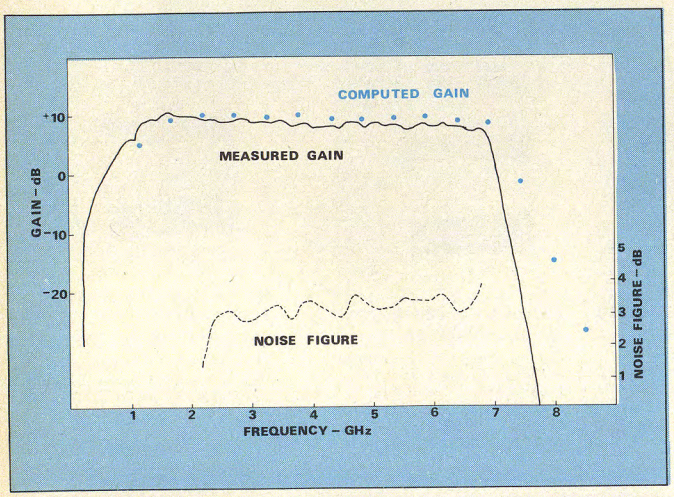

4. Calculated and measured gain *indicate close agreement for the 2-to-6 GHz amplifier module. Note that noise figure remains well under 4dB over the entire amplifier bandwidth.*

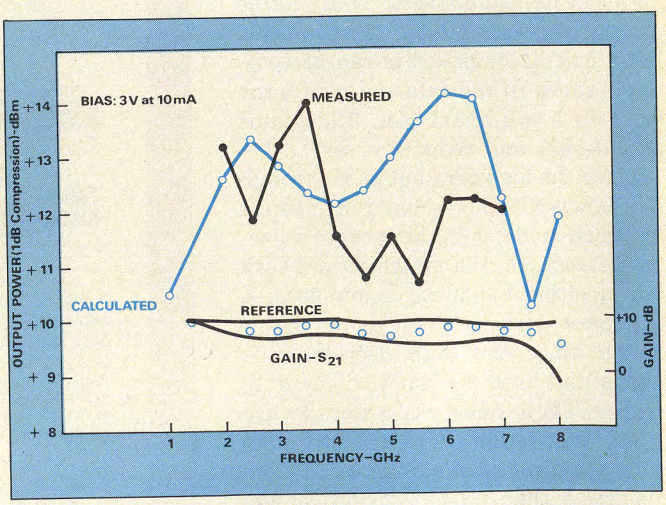

5. The same 1-dB difference *exists for the 2-to-7 GHz module while the output power at 1-dB compression is different by as much as 3 dB this, however, can easily be tuned to within 1 dB.*

Calculator aids design and reduces error

Although there is no substitute for a computer-aided design process for designing low-noise microwave amplifiers, a programmable pocket calculator, like the HP-67, can be indispensable in the early stages.

A complete set of microwave programs written using s-parameters allows the designer to analyze most active and passive circuits. The programs require minimum entry and use familiar units.

To use these programs, first store the frequency (which does not change throughout the analysis) and load a program card containing the first circuit element. Then enter the required values for the element and push the appropriate key for that element. The calculator calculates the "S" matrix and stores it as two-port "A". The next element is calculated in the same manner except it is stored as two-port "B". You may interconnect the two ports using the desired interconnection card: cascade, series, parallel, series-parallel, parallel-series or hybrid coupled. The results of the interconnection are stored as two-port "A" ready for the next element to be entered as two-port "B" and interconnected.

The HP-67 reads and writes data, as well as the program, from cards which allow the s-parameters for an active device to be stored on a data card and read when required. This capability also allows intermediate results to be saved. For instance, the cascaded s-matrix can be saved on a card while a complex shunt network such as the bias is cascaded and converted from a one port to a two port. The data can then be reloaded and cascaded with the resultant two port.

Although a computer is preferred for the full design task, the calculator is often more convenient for intermediate calculations during the procedure. Two and three-port mapping procedures, for example, are solved simply and quickly on the HP-67.

Simply enter a constant resistance or reactance (either positive or negative) and the calculator computes a center and radius for this value and is ready for a new entry. Series or shunt feedback or mapping of the load and source plane can be accomplished in less time than it would take to enter the program into a computer. Additional programs that calculate "K", MSG or G_a max, matched load, matched source, S_{11}', S_{22}', transducer gain stability circles, constant gain circles, constant noise figure circles and mismatch circles are also useful.

The HP-67 can be programmed to provide a simple optimization scheme as well. A program written for ladder network analysis enables the user to store the circuit file in an unused portion of program memory and element values in an unused portion of data memory. A start, stop and step frequency is entered and program execution started. The calculator then computes the input impedance or reflection coefficient at the first frequency and stops. A restart causes the frequency to be increased by the specified step and a new input calculated without additional entry. During optimization, the register number of the variable element is entered. At each program stop, the user enters the desired target value of input impedance or reflection coefficient, unless it is constant over frequency and can be programmed. The calculator changes the desired element, computes the error function over the frequency range, compares this value to the initial error function to calculate the gradient and changes the element back to its original value. Another gradient can be calculated by entering another register number and starting program execution. The calculated gradients and error functions can be used to determine step size and direction for each variable element in order to minimize the error function.

only elements which are easy to adjust are optimized. For example, in this particular design, small bonding pad islands were used to vary the open stub length and series inductance.

The complete 2 to 6 GHz amplifier was constructed as a single-ended design on two one-half-inch square substrates. The input and output networks each occupy an area approximately 350 mils long by 170 mils wide, leaving room for the hybrid couplers.

Tuning the single-ended design to cover 2.0 to 4.0 GHz naturally improves the performance since the load decrement is higher. The amplifier provides 11.1±0.5 dB gain, 1.7-to-2.6 dB noise figure and minimum output power at the 1-dB gain compression point of +8 to +10 dBm. Figure 4 compares measured data and the computer model from 1 to 8 GHz for the 2 to 6 GHz amplifier design. The data indicates that the measured in-band gain is approximately 1-dB below the predicted value; however, the maximum noise figure is 3.6 dB and the minimum output power is +8 dBm, which is in good agreement with calculations.

A 2 to 6 GHz hybrid coupler was designed and fabricated for the balanced amplifier. The measured response for the original design indicates a coupling value of −2.18 dB and center frequency of 4.2 GHz. When compared with the design values of −2.25 dB and 4.0 GHz, this design shows excellent agreement with theory.[4] Other measured parameters include an insertion loss of approximately 0.3 dB (which includes both connectors and a microstrip line 500 mils long), isolation ranging from −38 to −17 dB, and an input return loss of less than −25 dB (VSWR of 1.12) across the 2-to-6 GHz band.

The same design technique was applied to a slightly broader band version of the low-noise amplifier (2 to 7 GHz) with approximately the same agreement between calculated and measured results (Fig. 5). As with other designs, the gain is approximately 1 dB lower than calculated at 7.0 dB, but the flatness is within ±1 dB. Input and output VSWR is under 2.0:1 except for the input at 2.0 GHz which can easily be tuned to achieve a better match. Figure 5 also points out the worst case error between the measured and calculated 1-dB gain compression point is 2.8 dB at 5.5 GHz and approximately 1 dB at all other frequencies. Output power curve can be improved by tuning without degrading the other parameters.

Other 2 to 7 GHz gain modules exhibit gains between 7 and 8 dB, flatness of ±1 dB, and input and output VSWRs less than 2.0:1. Three modules were cascaded without any associated problems to form a single 21-dB gain, 2 to 7 GHz amplifier. This amplifier shows an overall gain flatness of ±1.5 dB, VSWRs less than 2.0:1, output power of +10 dBm minimum, and noise figure of 5.0 dB at 25°C.••

Acknowledgement

The author would like to express his appreciation to Edwin Kyte and Larry Miller for their valuable technical contributions during this project, and especially to Laura Hudson for her exacting assembly work.

References

1. Les Besser, *Compact*, Compact Engineering, Inc., 1651 Jolly Court, Los Altos, CA 94022.
2. Karl Hartman, "Noise Characterization of Linear Circuits," *IEEE Transactions on Circuits and Systems*, Vol. CAS-23, No. 10, pp. 581-590, (October, 1976).
3. Matthaei, Young and Jones, *Microwave Filters, Impedance Matching Networks and Structures*, McGraw-Hill, (1964).
4. Donald D. Paolino, "Design More Accurate Interdigitated Couplers," *MicroWaves*, Vol. 15, No. 5, pp. 34-38, (May, 1976).
5. Kenneth Richter, "Predicting Linear Power Amplifier Performance," *MicroWaves*, Vol. 13, No. 2, pp. 56-59, (February, 1974).
6. Hewlett-Packard Application Note 95, (September, 1968).

Part I

VCO Subsystems: What To Test, How To Test It

A number of measurement techniques are needed to fully define VCO subsystem performance. The first half of this two-part article defines basic parameters and introduces an automated test bench.

THE heartbeat of the modern electronic warfare system is the voltage-controlled oscillator. But testing this sophisticated microwave subsystem can be as complex a task as designing it initially.

VCO testing is usually undertaken for three reasons. Obviously, the VCO designer must rely on accurate testing during the conceptual and breadboard phases of a new design. In this case, the testing is done to establish benchmarks against which design improvements may be compared. The emphasis here is on accuracy.

Secondly, the performance of a VCO must be verified to its severest critic —the user. Qualification procedures and tests, jointly agreed upon by both the manufacturer and user and performed at the manufacturer's test facility, are usually the best testing methods. Emphasis in this test situation must be on understandable measurements, procedures and reports yielding clear, unambiguous data outputs.

Finally, once the VCO subsystem has gone into production, it must be tested quickly, fully and economically. Obviously, some compromises are made on acceptance tests and procedures at this point. Emphasis is on sufficient testing at a reasonable cost to insure that the VCO subsystem meets all requirements. Automated testing should certainly be considered here as a tradeoff against test labor time. Again, concise testing, procedures and reports are required.

Charles A. Bissegger, Manager, Special Programs and **Anthony E. Schlenz,** Engineering Aide and Computer Programming Specialist, Special Programs, Microwave Subsystems Division, Omni Spectra, Inc., 2626 South Hardy Drive, Tempe, AZ 85282.

Note that the three basic testing situations do not generally involve similar tests, and therefore, similar equipment. The following rules of thumb have been found to apply:

- If the test requires a large amount of data accumulation and processing—automate. The overall cost of the test equipment will be paid for in labor savings, with the additional benefits of more data and improved data accuracy.
- If the test requires a great deal of operator analysis of interpretation —beware. When this problem arises, get your best test engineers to put their heads together and come up with other approaches. A little brainstorming usually pays off.

Defining important tests

Now that we've established why VCOs must be tested, the next logical

(continued on p. 62)

Standard definitions for VCO parameters

AM noise: The random and/or systematic variations in output power amplitude. Usually expressed in terms of dBc in a specified video bandwidth at a specified frequency removed from the carrier.

Barometric effects: Maximum frequency change of the unmodulated carrier at any point in the tunable frequency range by a specified change in altitude. The test must be performed in a manner which will avoid coincidental thermal effects.

FM noise: The short-term frequency variations in the output frequency which appear as energy at frequencies other than the carrier. It is usually expressed in terms of dBc or as a RMS frequency deviation in a specified video bandwidth at a specified frequency removed from the carrier.

Frequency accuracy: The maximum output frequency deviation from a specified tuning function under specified conditions.

Frequency drift with temperature: The maximum change in output frequency as a result of a specified change in operating temperature.

Frequency pulling: The difference between the maximum and minimum values of the oscillator frequency when the phase angle of the load impedance reflection coefficient varies through 360 degrees.

Frequency pushing: The incremental output frequency change produced by an incremental change in supply voltage (Δ MHz/ΔV). If supply voltage ripple, frequency range and amplitude are not specified, measurements are conducted at a DC rate.

Frequency range: The mechanically or electronically tunable bandwidth over which the oscillator meets all specifications.

Harmonic signals: Signals which are coherently related to the output frequency. In general, these signals are integer multiples of the output frequency except for doubling oscillators which have harmonic signals at fractional multiples of the output frequency ($Nf_o/2$).

Modulation response bandwidth: The modulation frequency range where, for a reference deviation bandwidth, all included modulation frequencies of equal amplitude will result in no less than a ratio of 1.414 (3-dB) of minimum to maximum deviation. The type of modulation should be specified.

Non-harmonic signals: Signals which are not coherently related to the output frequency.

Operating temperature: The temperature as measured on the oscillator mounting surface or heat sink if different from the mounting surface.

Incidental FM: The peak-to-peak variations of the carrier frequency due to external variations with the unit operating at a fixed frequency at any point in the tunable frequency range.

Integrated spurious output power: The total power of all spurious outputs in and out of the frequency range.

Linearity: The maximum output frequency deviation forms a best fit straight line approximation of the tuning circuit under specified load and constant temperature conditions.

Maximum output power: The maximum RF output power at all output frequencies within the oscillator's tunable bandwidth under all specified conditions.

Minimum output power: The minimum RF output power at all output frequencies within the oscillator's tunable bandwidth under all specified conditions.

Modulation or tuning sensitivity: The slope or first derivative of the tuning curve (Δ

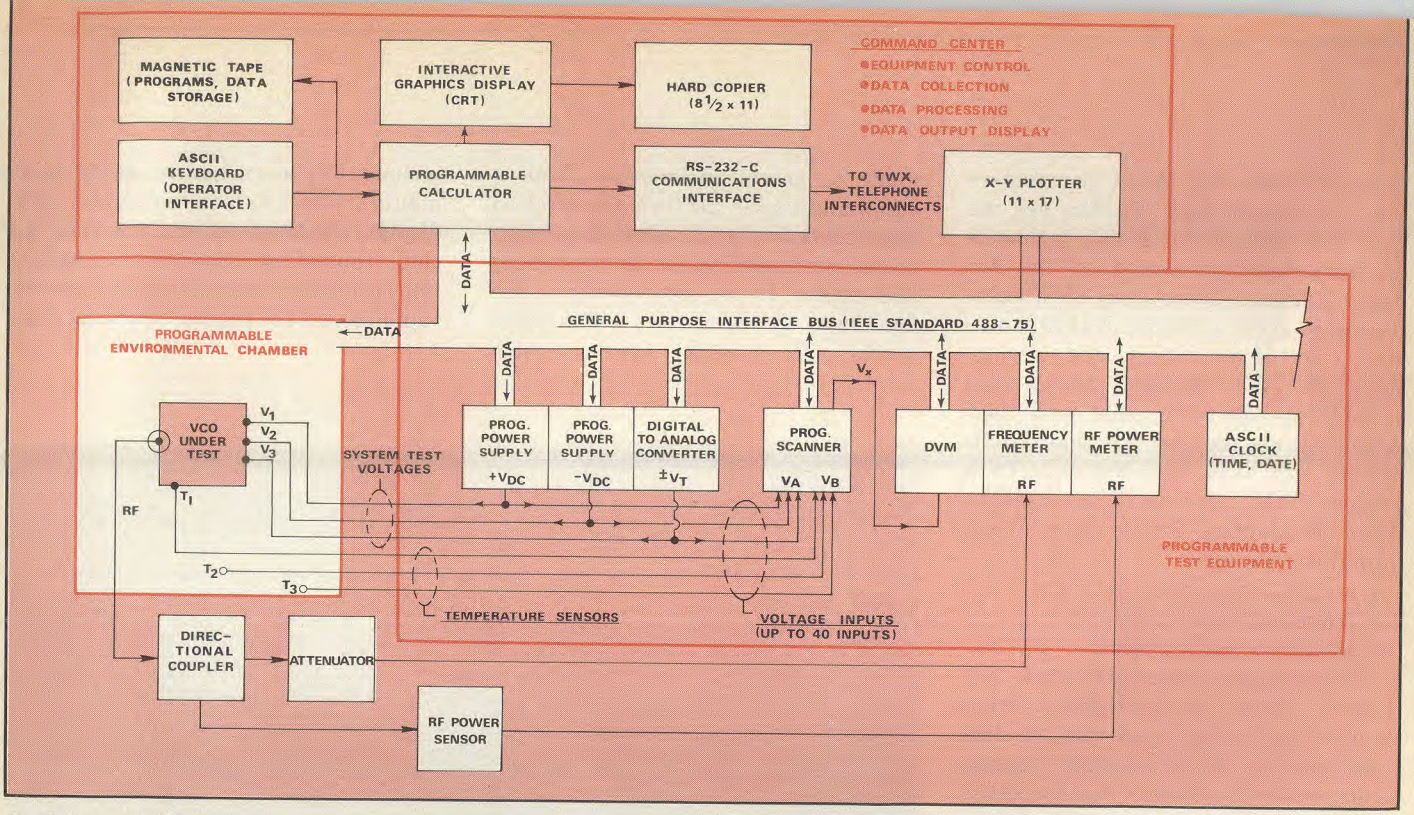

***1. Automated test setup for steady-state measurements** is built with equipment interacting through the general purpose interface bus. Command center controls the instrumentation and collects, processes and displays data.*

MHz/ΔV). Where necessary, the fine grain or incremental slopes and the ratio of the slope should be specified over the frequency range.

Modulator or tuning sensitivity variation: The change in the first derivative as a function of tuning voltage and/or frequency. Usually specified as per cent change of the first derivative over an incremental frequency range. Direction of tuning for measurement should be specified.

Oscillator load: The maximum VSWR seen by the oscillator at the ouput port, referenced to 50 ohms.

Output frequency: Of all the frequency components which may be present at the oscillator output port, the output frequency is defined as the frequency of the desired output of the oscillator.

Per cent bandwidth: $2(f_2 - f_1)/(f_2 + f_1) \times 100$ where f_1 and f_2 are the lower and upper endpoints, respectively, of the frequency range.

Post-tuning drift (PTD): The maximum change in frequency (Δf_{PTD}) from the frequency measured at the beginning of the time interval (t_1). The time interval ($t_1 - t_2$) shall be referenced to the application of a tuning command (t_0). The period of measurement ends at t_2 (see figure).

Power output variation or flatness: The maximum peak-to-peak power variation at all output frequencies in the tunable frequency range under all specified conditions.

Settling time: The time (t_{ST}) required for the output frequency f_1 to enter and stay within a specified error band ($\pm\Delta f_{ST}$) centered around a reference frequency (f_r) after application of a step input voltage. The time (t_r) shall be specified for determining the reference frequency (f_r). The period of measurement ends at the reference time (see figure).

Slew rate: The rate which the VCO frequency can change in response to a step input on the tuning port. The step input waveforms should be specified.

Spurious outputs: Spurious outputs are both harmonically and non-harmonically related signals. Their tolerable amplitude should be specified within and outside of the frequency range of the VCO.

Spurious output power: Power of each spurious output, in dBc or dBm measured in a specified bandwidth.

Tuning input impedance: The small-signal impedance seen at the tuning input port at a specified modulation frequency or frequencies.

Tuning monotonicity (decreasing): Continuously decreasing output frequency for a continuously increasing tuning voltage $f(V_1) > f(V_2)$ for $V_1 < V_2$.

Tuning monotonicity (increasing): Continuously increasing output frequency for a continuously increasing tuning voltage $f(V_1) < f(V_2)$ for $V_1 < V_2$.

Tuning repeatability: The ability of the oscillator to repeat a frequency within specified limits when the original command voltage is reapplied after having been commanded through an arbitrary tuning history. The repeated frequency (f_a) is defined at the specified reference time and time interval ($f_a = f(V) \pm f$ from t_1 to f_2). Temperature stability and dwell time are to be specified.

Warm-up time: The minimum time required for the unit to meet all specified operating parameters. The heater and bias power program must be specified.••

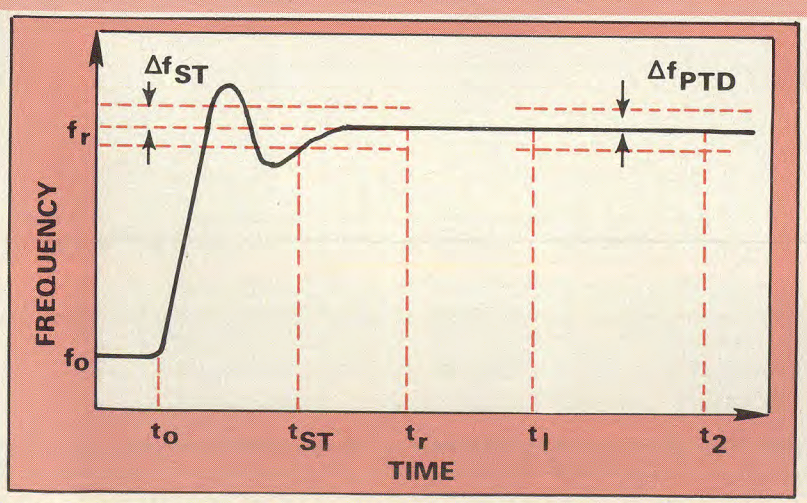

***Settling time and post tuning drift** describe the behavior of a VCO after command voltage is applied at time t_0.*

questions are: (1) What parameters must be tested? and (2) How are the tests best performed? A VCO technology workshop[1] sponsored by the Air Force Avionics Laboratory of Wright-Patterson AFB in March of 1975 generated a set of definitions and descriptions of VCO terminology to help standardize the terms that were then in general useage (see, "Standard definitions for VCO parameters"). In a modern VCO, the tests to measure these parameters break down nicely into three groups:

- steady-state measurements
- transient measurements
- quality measurements

Steady-state measurements are those in which the oscillator is being exercised at a very slow rate by electrical and/or environmental inputs. Examples of this class of measurement include:

- Frequency output (f_o) as a function of tuning voltage (V_t) or digital word command.
- RF power output (P_o) as a function of V_t or digital command.
- Small variations of f_o as a function of supply voltage variation (frequency "pushing") or load VSWR variation (frequency "pulling").
- Variations of f_o and P_o as a function of ambient temperature.
- "Fine grain" or differential linearity. This characteristic of the VCO is computed by automatic test equipment from the data of an output frequency vs. tuning voltage test; it is a measure of the variation of the modulation sensitivity (df_o/dV_t) of the VCO at all points of the f_o/V_t curve. A second derivative of the tuning curve, d^2f_o/d^2V_t, may also be calculated and is useful in determining monotonicity of the tuning curve.
- Deviation of the f_o/V_t curve from a best straight line fit. Again, this is a computed characteristic.

Lots of data? Automate!

A typical test equipment block diagram for automated steady-state measurements is shown in Fig. 1. The test equipment is automated for data collection and processing via the general purpose interface bus (GP-IB per IEEE Standard 488-1975) for digitally programmable instrumentation. By use of the GP-IB, a number of varied types of testing instruments can be made to accept instructions from a command center, perform the required data collection and return these data to the command center for processing and output. In the setup of Fig. 1, the command instrument is a Tektronix model 4051 graphics system, which includes keyboard and magnetic tape inputs and an interactive graphics CRT display. Instruments on the bus include those that only receive instructions, such as the programmable power supplies and the digital-to-analog con-

(continued on p. 64)

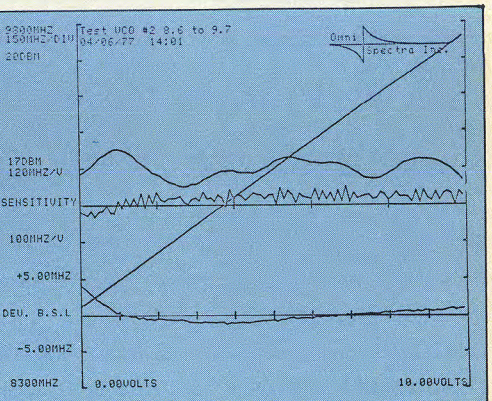

Test VCO #2 8.6 to 9.7 04/06/77 14:01 FILE -1 PAGE 1

VOLTS	FREQ.	DBM	MHZ/V	VOLTS	FREQ.	DBM	MHZ/V
0.00	8636.540	16.82		5.00	9191.759	17.13	112.836
0.10	8647.342	16.89	108.111	5.10	9202.767	17.20	110.190
0.20	8658.031	16.97	106.956	5.20	9214.184	17.23	114.399
0.30	8668.851	17.04	108.168	5.30	9225.356	17.26	111.608
0.40	8679.486	17.14	106.649	5.40	9236.694	17.28	113.721
0.50	8690.300	17.26	108.118	5.50	9247.959	17.28	112.650
0.60	8701.143	17.33	108.311	5.60	9259.017	17.25	110.470
0.70	8712.154	17.39	109.868	5.70	9270.339	17.23	112.881
0.80	8722.776	17.46	107.695	5.80	9281.403	17.20	112.211
0.90	8733.538	17.50	107.609	5.90	9292.600	17.17	111.858
1.00	8744.863	17.50	110.964	6.00	9303.952	17.14	111.622
1.10	8755.758	17.48	109.081	6.10	9315.353	17.13	114.238
1.20	8766.915	17.44	111.749	6.20	9326.454	17.12	111.121
1.30	8777.897	17.38	109.666	6.30	9337.807	17.11	113.530
1.40	8789.031	17.30	111.720	6.40	9348.927	17.12	111.423
1.50	8800.022	17.19	109.855	6.50	9360.237	17.13	113.100
1.60	8811.334	17.12	113.086	6.60	9371.337	17.12	110.889
1.70	8822.289	17.04	109.331	6.70	9382.741	17.12	113.926
1.80	8833.424	16.95	112.817	6.80	9393.699	17.09	110.911
1.90	8844.466	16.87	110.420	6.90	9405.198	17.05	114.990
2.00	8856.005	16.83	113.461	7.00	9416.506	16.99	110.754
2.10	8867.146	16.77	111.522	7.10	9427.809	16.92	113.143
2.20	8878.226	16.69	111.022	7.20	9438.986	16.86	111.770
2.30	8889.420	16.62	111.717	7.30	9450.201	16.79	112.150
2.40	8900.548	16.58	111.727	7.40	9461.408	16.73	112.520
2.50	8911.746	16.55	111.868	7.50	9472.681	16.71	112.617
2.60	8922.988	16.51	112.420	7.60	9483.842	16.70	111.499
2.70	8934.093	16.49	110.718	7.70	9495.053	16.70	111.775
2.80	8944.957	16.51	110.071	7.80	9506.228	16.73	113.337
2.90	8956.102	16.55	111.450	7.90	9517.514	16.77	112.747
3.00	8967.516	16.55	111.792	8.00	9528.817	16.84	111.247
3.10	8978.616	16.59	111.111	8.10	9540.006	16.90	112.121
3.20	8989.948	16.67	113.433	8.20	9551.329	16.96	113.340
3.30	9001.102	16.72	111.652	8.30	9562.559	17.06	112.189
3.40	9012.268	16.77	111.884	8.40	9573.748	17.13	112.225
3.50	9023.369	16.83	111.010	8.50	9584.981	17.16	112.213
3.60	9034.643	16.87	112.622	8.60	9596.055	17.20	110.745
3.70	9045.839	16.90	111.849	8.70	9607.462	17.23	113.729
3.80	9056.662	16.90	109.546	8.80	9618.377	17.24	110.588
3.90	9068.048	16.91	113.861	8.90	9629.763	17.23	113.860
4.00	9079.279	16.91	111.308	9.00	9641.114	17.22	111.833
4.10	9090.538	16.88	112.819	9.10	9652.269	17.21	111.061
4.20	9101.773	16.86	112.349	9.20	9663.541	17.19	113.433
4.30	9112.898	16.87	111.258	9.30	9674.659	17.15	111.180
4.40	9124.080	16.86	112.156	9.40	9685.938	17.08	113.016
4.50	9135.392	16.85	113.120	9.50	9697.294	17.03	113.560
4.60	9146.698	16.89	112.834	9.60	9708.619	16.97	113.024
4.70	9157.987	16.94	112.665	9.70	9719.631	16.86	110.010
4.80	9168.991	16.99	111.602	9.80	9730.843	16.77	113.482
4.90	9180.261	17.05	112.700	9.90	9742.097	16.68	112.540

***2. Versatility** is a major asset of automated systems. Here, data is presented in tabular and graphical formats.*

verter used for incrementing V_t; those that both receive instructions and retransmit data, such as the frequency counter, the power meter and the digital voltmeter; and those that input data only, such as the ASCII clock.

Preprogrammed test sequences stored on the 4051's tape memory are transferred into the calculator's temporary memory when the test is prepared for a run (programs available from the author upon request). This onboard RAM will also store the accumulated data for processing later. As the program runs, the various voltage inputs required by the unit under test (UUT) are set in. In a typical test where f_o and P_o versus V_t are being run, the tuning voltage is incremented, via the digital to analog converter, in voltage steps as small as ten millivolts over the range of V_t desired. At each V_t increment, the calculator asks and receives data on f_o and P_o from the frequency counter and power meter, as well as an accurate reading of V_t from the DVM. Since data per increment only requires several hundred milliseconds, a 100 point run can be taken in less than a minute; a 1,000 point run, in about six minutes. Additional inputs of interest, such as titling of the test, are entered by the operator at the keyboard, while time of day and date are automatically inputed via the ASCII clock. When a number of voltage readings and temperature readings are to be inputed, a programmable scanner is added to the system. This instrument will sample a large number of voltage readings in sequence, upon command and output the readings to the calculator for display.

On the output side, the 4051 will display the accumulated and processed data for review on the CRT. This can be tabular data or graphic data, such as shown by Fig. 2. If required, a permanent copy of the CRT display is made using either the 8 1/2 x 11-inch hard copier or the X-Y plotter. If desired, the data can be put into a format suitable for relaying over teletype lines via the RS-232 interface. This interface also allows data from another test location to be transferred over telephone lines to this test station.

Extensive testing can be performed at a low cost; temperature measurements can be performed without an operator in attendance. Changes in performance can be monitored as any one of the several variables, temperature, for example, is automatically varied.

Steady-state measurements are ideally suited for automated testing. Output data is clear, concise and permanent. Test programs are relatively easy to create, offer tremendous flexibility for special variations and make test procedures repeatable and operator simple. The entire automated system of Fig. 2 will fit into a 60" high x 40" wide x 34" deep console, including the environmental chamber. Cost of this equipment is not excessive, ranging from $40,000 to $50,000 depending on choice of manufacturer.

The second part of this examination of VCO subsystem testing will focus on the rigorous requirements of transient measurements, with special attention paid to limits and error expectancies. ••

Reference

1. AFAL-TR-75-187, "VCO Definition Workshop," Wright-Patterson AFB, OH, (Mar. 18-20, 1975).

WANTED

★★★★★★★★★★★★★★★

★ **APPLICATION NOTES** ★

Want those new microwave application notes just finished by your company read by the sharpest people in the field? Looking for good response from an interested readership? If so, this is the place!

If your application notes are:

- Sufficiently general to enable others to use them in their applications
- Sufficiently detailed to give specific methods and procedures for obtaining the desired results
- Available in sufficient quantities for distribution

Then don't delay—send them to: **Stacy V. Bearse, Editor-in-Chief MicroWaves, 50 Essex Street, Rochelle Park, NJ 07662**

If the Mini-Circuits' *Mixer Applications Handbook* to the right has been removed, Circle Reader-Service No. 100 to receive your personal copy.

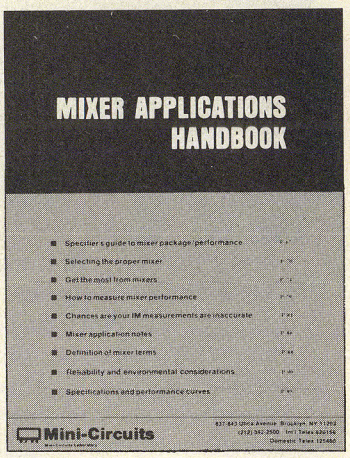

Contents of this 96-page handbook include:

- **Specifier's guide**
- **How to select the proper mixer**
- **How to measure mixer performance**
- **Mixer application notes**
- **Definition of mixer terms**
- **Specifications and performance curves**

READER SERVICE NUMBER 100

Radar Systems Mature With SAW Technology

SAW components are improving the performance of radar components while reducing their size and cost. Here, filter, quadraphase code generator and stable local oscillator circuits are examined.

WHENEVER multiple functions are performed on the surface of a single substrate, considerable cost savings, volume reductions and reliability increases can be obtained. Surface acoustic wave (SAW) technology can bring these advantages to radar signal processing, where tediously matched, lumped components have traditionally been used, and to oscillator design, where fundamental oscillators operating at a gigahertz with crystal stability are now within reach.

A notable example of how SAW technology is changing the complexion of radar circuits is the Barker code correlator shown in Fig. 1. In the foreground is the surface-wave model, dwarfed by a commercial bulk-wave model. In the SAW device, the delays, phase shifts and summing are all combined on the surface of a quartz platelet with trimming required only for the matching networks. Opposing this, the bulk-wave model requires 13 separate bulky delay lines with a separate summing network and reactive and resistive trimming required on each line.

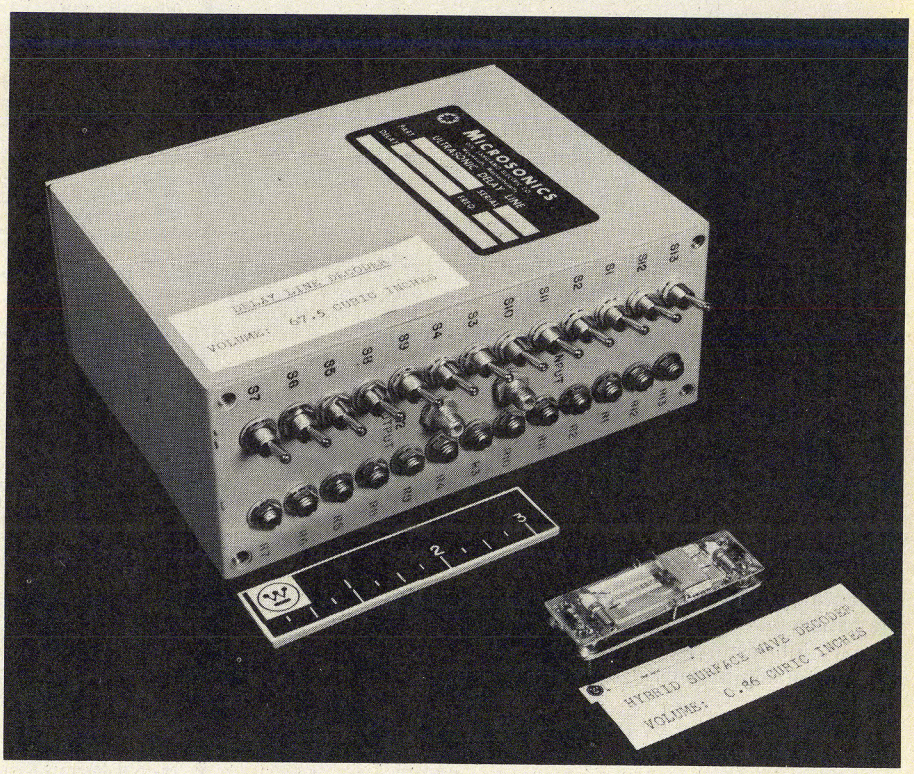

***1. Large reductions in cost and volume** are possible with SAW (surface acoustic wave) delay lines.*

Saving phase

A major application for compact, temperature insensitive SAW devices is in monopulse radar systems. Monopulse radars interrogate the relative phase between a single return in a pair of receivers separated by a known distance. This phase information eventually is used to determine the angular position of the target, thus the two receivers must not introduce a phase difference of their own.

In the past, the relative phase between a pair of radar signals was preserved by means of pairs of ovenized crystal filters. These filter pairs are quite expensive, requiring intricate tuning procedures for matching bandwidth and center frequency. In addition, a typical pair occupies approximately 12 cubic inches.

More importantly, the narrow-band crystal filters are designed for Gaussian impulse response, stretching the input signal in time by a factor of 100 in order to give adequate digital processing time at the peak of the pulse. Digital processing is performed only at the flat top of the Gaussian response, and the build-up and decay periods of the pulse are wasted.

A more desirable response in time would be a rectangle of voltage which exists for a processing period, and then ceases to exist beyond that time region. Fourier transform theory shows that only a device whose frequency response is (sinx/x) will exhibit this desirable time response.

SAW technology provides a straightforward way to design two nearly identical filters with this rectangular frequency response on a single quartz substrate. Not only are size, cost and complexity smaller (no ovens are needed), but these filter pairs can be matched much more closely in production than their crystal counterparts. The desired rectangular shape is obtained by using uniform finger overlap. The time length of the pulse is achieved by laying down as many finger pairs as there are sine waves in the desired

Christopher Vale, Senior Engineer, Westinghouse Electric Corporation, Defense and Space Center, P.O. Box 1897, Baltimore, MD 21203.

time length. The risetime is controllable by varying the number of finger pairs in the launching array. Figure 3 compares the time response of the SAW device to that of a dual-crystal filter. Clearly, the SAW filter can be interrogated for another target within a short period of time, while the crystal filter is "down" for several hundred microseconds.

One important question remains: "What is the phase equality between a pair of SAW filters realized on a single substrate?" Measurements performed at Westinghouse with a carefully calibrated detector show that the phase difference between the two filters is less than 0.7 degrees over the entire 6.5 μs length of the rectangular pulse. Thus, SAW filter pairs have been shown to be eminently suitable for monopulse applications.

More than two phase

New regulations regarding the spectral output of radars will eventually limit the utility of the biphase code; consequently, decoders for these signals (Fig. 1) will find declining use.

J.W. Taylor of Westinghouse has shown the advantage of quadraphase codes for limiting radar spectral splatter. This approach is much more attractive than the bi-phase decoders now used, since the 180-degree phase changes called for require a very wideband energy spectrum. Accordingly, it was decided to try whether or not four phases (0, 90, 180 and 270 degrees) could be accurately represented on a surface wave pattern.

Figure 4 shows an interdigital pattern for generating the Taylor 26 code. It consists of two interleaved 13-bit Barker bi-phase codes that are summed in such a manner that one of the codes is in quadrature with the other. By taking two bi-phase decoder patterns and shifting one with respect to the other by 1/2 bit and then shifting it again by 1/4 cycle, the essential elements of the Taylor 26 code are realized. Now, they must only be summed. In this instance we ignored the amplitude-weighting requirements assuming that finite bandwidth matching networks will provide gradual rise and fall times.

Two devices were made with launching transducers at either end of the quadraphase pattern. One end was coherently impulsed to generate the code. This was amplified and fed into the other device from the opposite end to perform decoding. The generated code was viewed on a spectrum

(continued on p. 165)

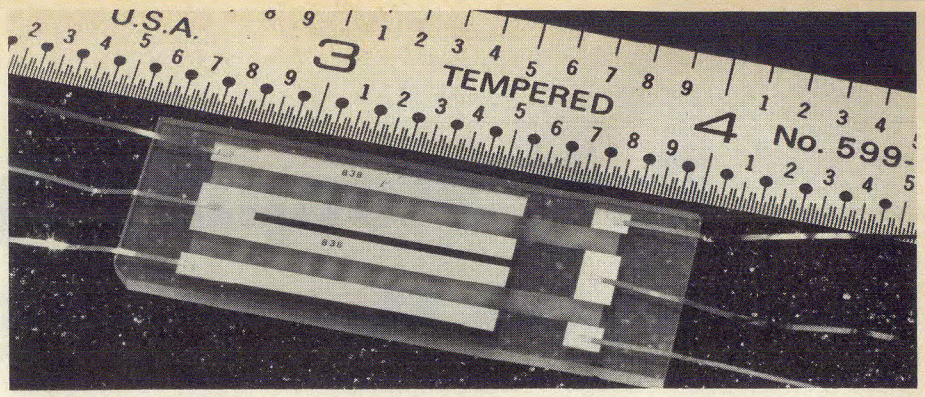

***2. Zero phase difference exits** between these two filters assembled on a single substrate and used in a monopulse radar.*

SAW devices: Getting back to basics

A Rayleigh wave is an elastic surface wave that propagates along the plane surface of an elastic solid, with most particle displacement occurring within one wavelength of the surface. This physical characteristic allows surface delay lines to have two distinct advantages over the conventional delay lines: (1) Most energy is concentrated at the surface and can be easily coupled out of the device, and (2) since the signal is propagating on the surface, it can be sampled at more than one point.

These surface waves can be produced in a piezoelectric substrate with a deposited metallic interdigital transducer. A fluctuating electrical signal applied across the finger pairs of such a transducer will launch an elastic wave along the surface of the substrate with wavefronts parallel to the finger length and propagation direction perpendicular to the finger length.

A transducer pattern is generated on a Gerber plotter at 20 times the actual size. It is then photoreduced and the resulting mask is used to expose aluminum (coated with photoresist) approximately 2000Å thick. Conventional photomasking techniques can be used to do this with good results.

The most sensible choice of substrate is quartz. It is quite stable with time, humidity and even temperature. Furthermore, it is easily available from many vendors who manufacture quartz-crystal resonator. Schultz and Holland have shown that there is a quartz cut with a zero temperature coefficient, the so-called ST cut or +42.75-degree rotated Y-cut. The temperature coefficient of frequency change of ST quartz is not a constant but rather changes with temperature. Even so, the measured change is less than 8 kHz over a range of −60 to +100°C and 5 kHz for −40 to +85°C, relative to 30 MHz. ••

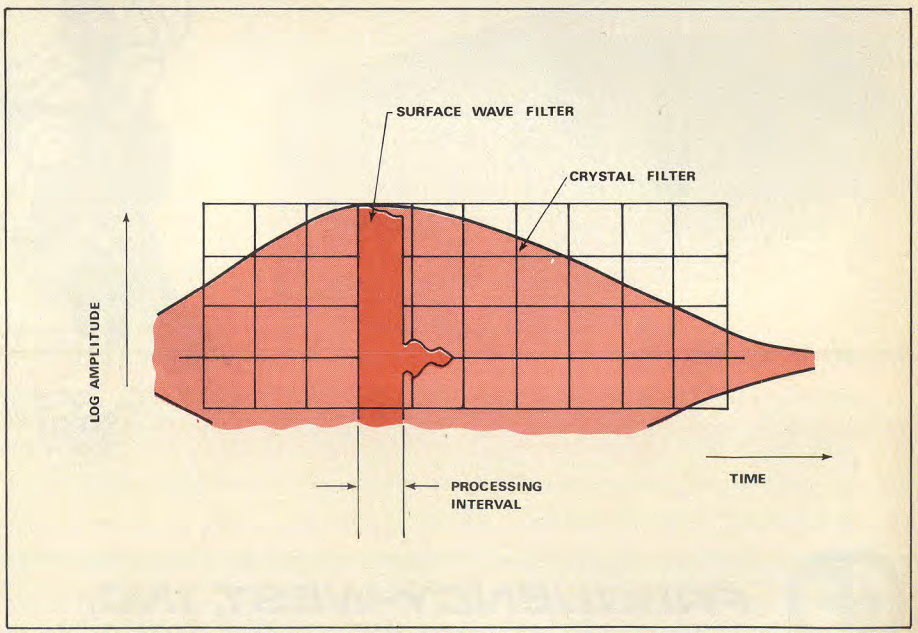

***3. Superior time response is obtained** with a surface-wave filter.*

analyzer and compared to a similarly generated Barker bi-phase code. In addition, the quadraphase code that was generated in coherence with a 30-MHz sine wave was fed into the R port of a phase detector at the same time as the 30-MHz signal was fed into the L port. The resulting phase versus time signal confirmed the existence of the four phases in correct sequence.

The spectrum of the Taylor 26 code is shown in Fig. 5a, while the output from the phase detector when the code is compared to a coherent sine appears in Fig. 5b. The theoretical code sequence is

1 j−1; −j 1 j; −1 −j 1; 0 1 j; −1 −j −1; −j 1 j; 1 j 1; j 1 j; 1 j. At either +j or −j the phase detector should indicate zero volts. There are hesitations in the phase detector at each j value where the phase detector tries to indicate 0 volts. Thus the sequence shown in Fig. 5b matches the theoretical sequence if j's are substituted for zeros. Also it can be seen that there are two ordinary reverse bi-phase Barker codes generated—one real, and the other imaginary—by counting every other bit.

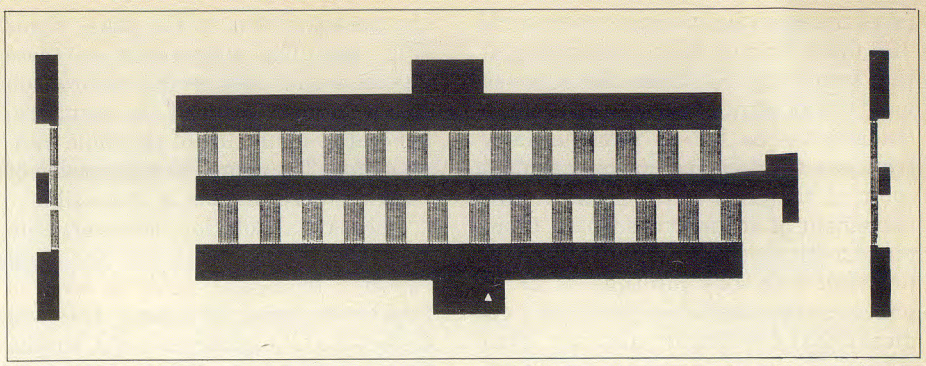

4. Taylor 26 code is generated and decoded *by this interdigital pattern.*

This shows that a good quadraphase code can be generated by coherently impulsing a surface-wave delay line, which represents a considerable simplification over the present method of generating Taylor codes electronically. Furthermore, such a device will be small, compact and inexpensive.

Using the pattern of Fig. 4 that has launching transducers on both ends of the encoding pattern allows the decoding to be performed in the same device. Impulsing the left transducer generates the code; impressing the encoded signal (after transmitting, receiving, and mixing) on the right-hand side transducer allows the decoded signal to be picked off by the encoding pattern.

Building a SAW oscillator

A SAW delay line for an oscillator application has different design considerations than one to be used as a filter. Out-of-band rejection, for instance, is of a secondary consideration, but reduction of passband ripple is of prime importance. The highest phase slope will yield the highest Q, and thus the highest stability. The relationship

$Q = \pi\tau f_0$

(continued on p. 166)

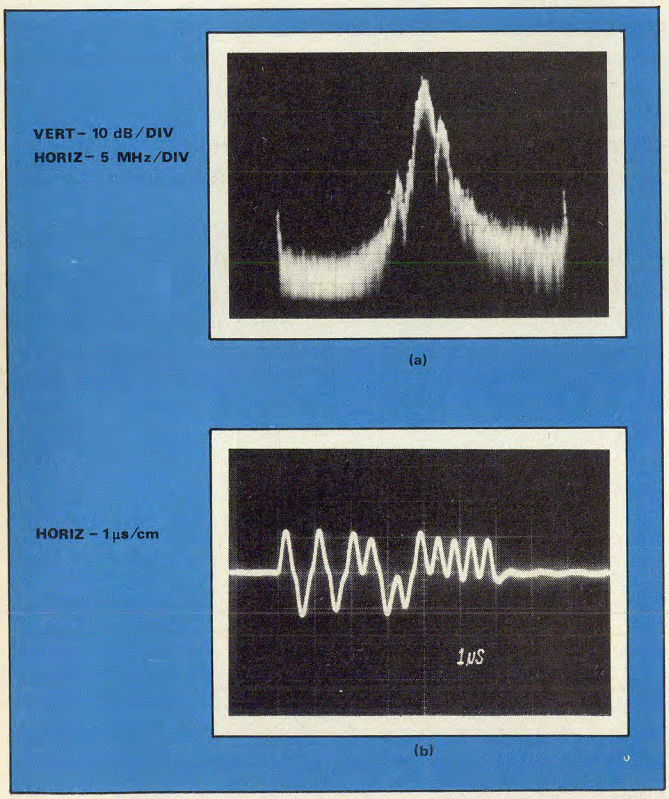

5. Note the characteristic dissymmetry of polyphase codes in the Taylor 26 code spectrum (a). Phase detector output when the code is compared to a coherent sine wave is 10-101010-10-101010101010 (b), demonstrating quadraphase codes can be generated by SAW devices.

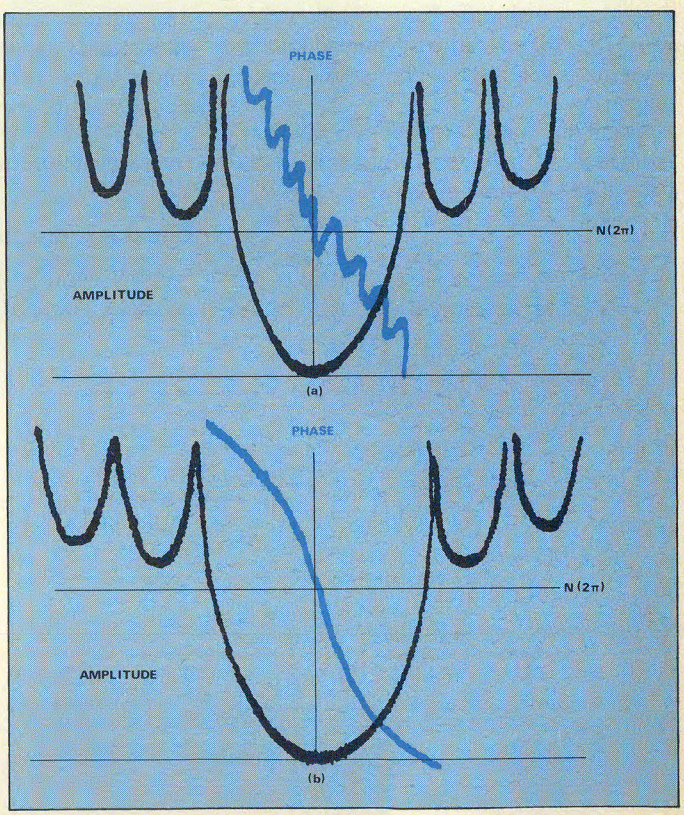

***6. Multiples of 2π will occur at several frequencies** in the presence of high-rate-of-occurrence ripple (a). Low-rate-of-occurrence phase ripple can be obtained by adding the prime regenerated signal and the triple transit signal back into the main expected triangular pulse (b).*

gives the equivalent single-resonator Q of a delay line of delay τ operating at the frequency f_0. Thus for a given length of substrate one should place the transducers as far as possible away from one another, leaving only enough room at the ends of the substrate for placement of acoustic absorbers. Combined with this, however, is the need to select only one multiple of 2π in phase for the oscillator operation. This means that few finger pairs (say, 10 to 20) would not have enough amplitude selectivity for a practical oscillator since these transducers would be broadband. Therefore, the best oscillator surface-wave delay line would fill the useable area of the substrate with finger pairs.

An obvious division would be to assign half of these finger pairs to the input and the other half to the output transducer. The impulse response of such an arrangement would be a triangular envelope on the center-frequency sine wave in time; the frequency response would be $(\sin x/x)^2$. This would have the desirable property of identical input and output impedances for matching to the required active feedback network. Furthermore, the frequency response would offer possible spurious passbands 26.5 dB below the main passband—more than adequate rejection for assuring single-frequency operation.

Much surface-wave work in the past has resulted in large-amplitude, high-rate-of-occurrence phase ripples in the passband, especially at the center frequency. This is not acceptable in oscillator applications, since multiples of 2π can occur at several frequencies in the passband due to the phase ripple (Fig. 6a). The suppression of these ripples would require the suppression in the time domain of the prime regenerated signal and of the triple transit signal. The complete suppression of both of these signals is impossible.

One partial solution, however, is to add these signals back into the main expected triangular pulse as soon as feasible in time. Of course, this will distort the triangular envelope, but the frequency response will be improved. According to the theory of paired echoes, the higher the rate of occurrence of spurious time signals, the lower the rate of occurrence of amplitude and phase ripples in the frequency domain (Fig. 6b). Thus by placing the input and output transducers within $\lambda_s/4$ of each other, the prime regenerated signal and the triple transit will add to the main signal and will do so at the maximum rate of occurrence.

Figure 7a depicts the calculated amplitude and phase characteristics of a surface-wave delay line designed on the basis of the above principles. There are 312 finger pairs, each finger and each separating space 4-μm wide. Identical arrays are assigned to the input and output transducers. Assuming a sinusoidal phase ripple about some linear slope, the zero crossover of the phase would occur at the center frequency and at ± 1.25 MHz, thus effectively assuring single-frequency operation.

Checking the theory

After completing all theoretical calculations, a delay line was built on an ST-cut quartz substrate. The interdigital pattern was generated on the David Mann mask generator; 312 finger pairs with no apodization are separated from an identical array only by a $\lambda_s/4$ gap. Aluminum deposition and metal-lift-off procedures ensure a clean pattern. Gold leads were thermocompression bonded and the final device was mounted on a plate with RTV and connected to BNC chassis-mounted connector. The input and output impedance was characterized at 196.656 MHz, the measured center frequency. The resistance was 120 ohms, but the reactance was -30 pF, due to the long leads to the R-X meter. The steady-state attentuation and phase measured between 50 ohms are shown in Fig. 7b.

Note that the transducer design attains the goal of stretching out the phase ripples because only one multiple of 2π occurs in the passband. The large amplitude ripple is probably due to finger reflections, since when the same pattern is generated with split fingers, a perfectly smooth passband is obtained exhibiting a response shape that is very close to the theoretical response of $(\sin x/x)^2$. Nevertheless, the response shape of Fig. 7b is certainly useful for oscillators. Even the undesirable peak at +500 kHz does not present a problem, for it was learned experimentally that this network in the feedback path of an amplifier does not hesitate to operate at 196.656 MHz, completely ignoring the other possible modes.

It is remarkable how low the electromagnetic feedthrough has been maintained, since in both the simple

(continued on p. 168)

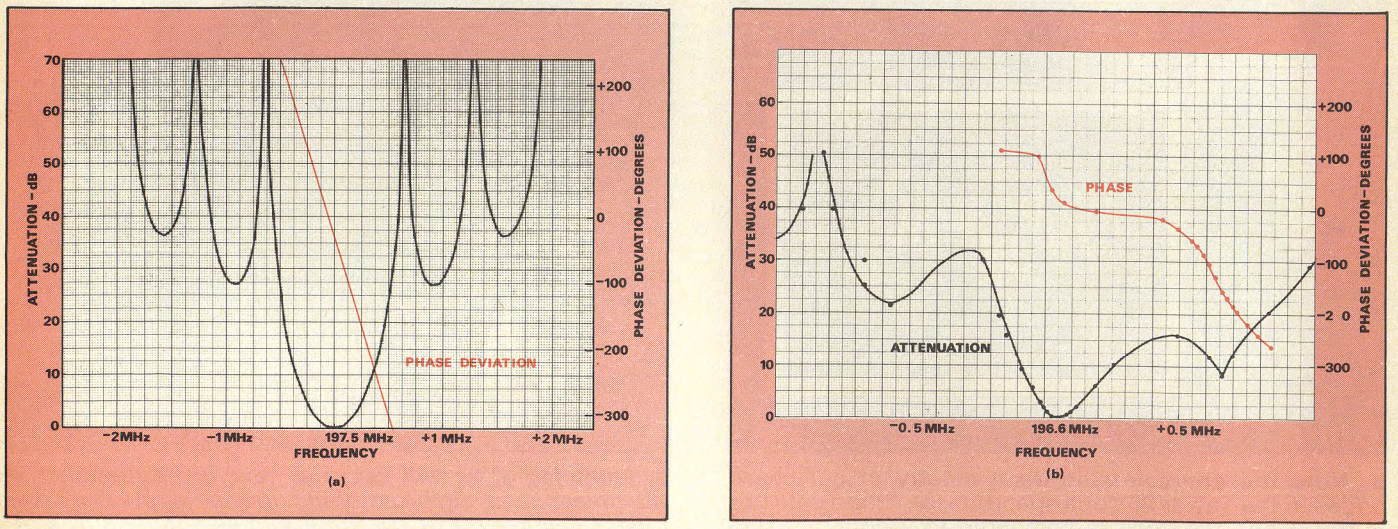

7. Good agreement is obtained *between calculated and experimental data for surface wave oscillator delay line, (a) and (b), respectively. Note that only one multiple of 2 π occurs in the passband.*

finger model of Fig. 7b and the split-finger model, ripple identifiable with high level of feedthrough has not been found. This is at least partially due to grounding those portions of the input and output transducers that are connected to the closely adjacent fingers in the center of the delay line. Thus the electrically "hot" portions of the transducers are diagonally opposed and are automatically shielded by two grounding fingers. The low insertion loss (14-dB in a 50-ohm measuring system) is due to a partial series coil-matching effect due to moderately long input and output leads. A mere 20 nH would have provided tuning for these large 100-wavelength aperture grids.

Figure 8 illustrates the noise performance in 1-kHz and 1-Hz bandwidths. This performance does not quite match that of our latest bulk-mode 30-MHz oscillators. However, more attention can be paid to the active portion of the oscillator, and the pattern can be extended to improve the Q. In addition, the operating frequency can be raised to L-band, eliminating all noise contribution due to multipliers and all the hardware associated with multiplication. There appears to be a drift of less than 4 ppm per decade of minutes, that is almost entirely accounted for by the temperature drift over the measuring period. This temperature drift is larger than normal because the substrate does not perform like a true ST-cut: The zero turnover point occurs at +5°C instead of +28°C. Taking this error into account lets the surface wave oscillator drift compare favorably with that of ordinary quartz-crystal bulk oscillators that operate at lower frequencies.

Figure 9 shows the operation of the oscillator over a temperature range. The offset in the turnover point mentioned above can be noted in the figure. Due to the open breadboard, the oscillator stopped oscillating at −30°C when a heavy frost deposit covered the propagating surface.

All these measurements have been taken using a rough, open breadboard. It is expected that cleaning up the active network will improve its noise performance. To provide double protection for the delay line, it is proposed that the delay line be packaged in a hermetically-sealed container and then the resulting oscillator be packaged in another hermetically-sealed container.

More recent data indicate that large metallized arrays of fingers tend to shift the location of the turnover temperature on ST-cut quartz substrates. Once experimentally determined, the shift is easily compensated by using a substrate face orientation that departs slightly from the true ST location. Presuming we require an unloaded substrate turnover temperature located 23° above room temperature, this would be achieved with a +36-degree rotated Y-cut, or just a little more than a standard AT-cut resonator. The effective oscillator turnover temperature would then finally be shifted to the desired room temperature by the mechanism that caused the shift of Fig. 9.

This performance demonstrates that SAW oscillators are attractive alternatives for radar stable local oscillator (stalo) applications. Quartz stability will soon be available in fundamental frequency sources in the vicinity of 1 GHz. ••

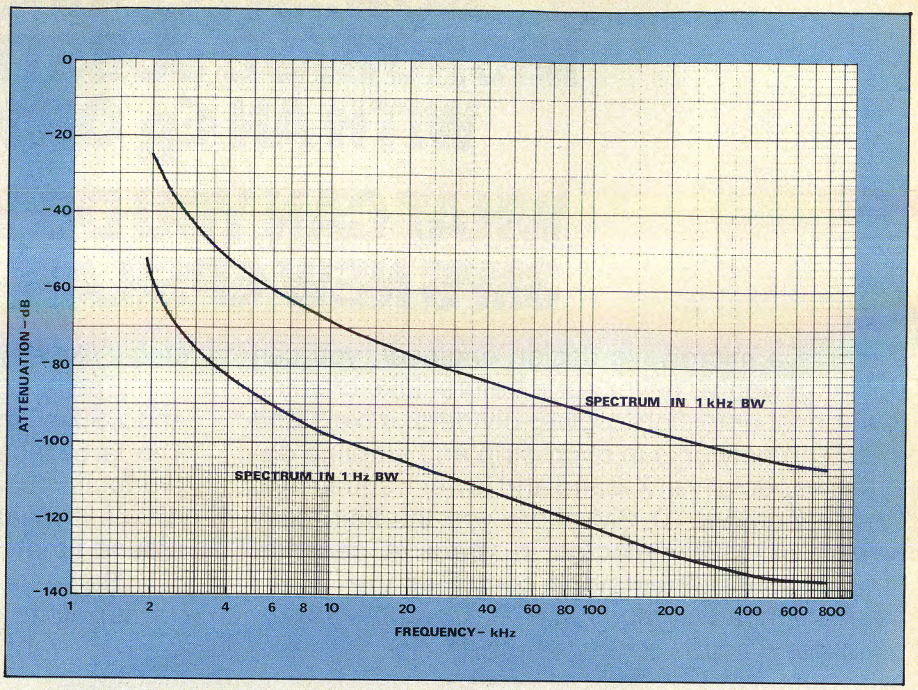

8. Acceptable noise performance is obtained *from a SAW delay line. Improvements are expected by cleaning up the breadboard.*

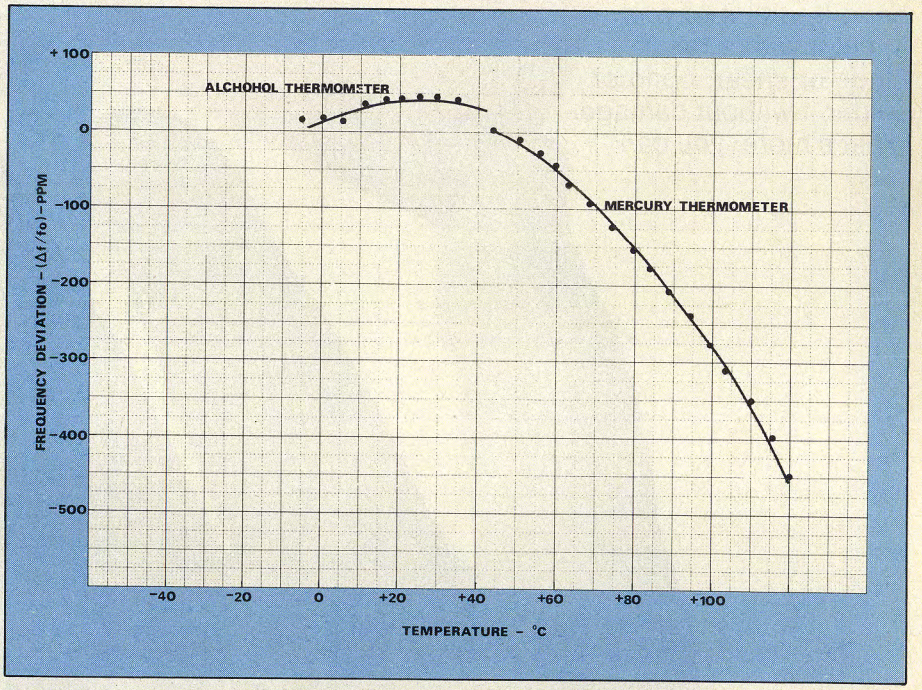

9. Slight temperature drift can be corrected *by selecting a quartz crystal with a face orientation that departs from the true ST-cut location.*

Reshaped Subreflectors Reduce Antenna Sidelobes

Improve the sidelobe performance of dual-reflector, high-efficiency antennas by tapering the amplitude field across the secondary aperture. A modified subreflector will do the trick.

THE main and secondary reflectors of dual-reflector, high-efficiency earth station antennas are generally shaped to achieve uniform field amplitude and phase distributions across the secondary aperture.[1,2] Although such distributions may result in the highest possible gain performance, uniform field amplitude across the secondary aperture may not be the best distribution in terms of sidelobe performance.

Interference from adjacent satellites or nearby terrestrial microwave links can degrade the performance of the antenna unless the total sidelobe envelope is below a certain level. For example, FCC regulations currently require that at an angle, θ, from the center of the main lobe, gain sidelobes from any transmitting antenna used in a satellite communications system be less than $32 - 25 \log \theta$ dBi, for $1° \leq \theta \leq 48°$, and -10 dBi for $48° \leq \theta \leq 180°$.[3] As more and more operational satellites line up in geosynchronous equitorial orbit, interference specifications such as these will become more important to the antenna designer.

Edge diffraction from the main reflector edge and spillover beyond this edge caused by the subreflector edge diffraction may substantially increase the level of some of the sidelobes in older antennas designed with the uniform field amplitude criteria. In order to achieve an acceptable tradeoff between far-out sidelobe levels and gain —and upgrade the antennas to contemporary sidelobe specifications—an amplitude field taper across the secondary aperture is required.

Sharad V. Parekh, Senior Antenna Engineer and **James H. Cook,** Manager, Antenna and Microwave Department, Scientific-Atlanta, Inc., 3845 Pleasantdale Road, Atlanta, GA 30340.



***1. The sidelobe performance** of dual-reflector earth terminal antennas is largely determined by the shape of the subreflector.*

This field taper can be achieved in a number of ways. Obviously, the shape of the two reflectors could be modified. However, such a modification is extremely expensive since it requires the replacement of the large, main reflector. More economical approaches include, (1) replacing the horn in the feed with another horn, whose primary pattern yields the desired secondary field amplitude taper, or (2) replacing the subreflector with a new design shaped to redistribute energy over the surface of the main reflector while maintaining constant phase distribution over the aperture.

This article concentrates on the latter of these two approaches. A simple technique is presented to describe the shape of a subreflector once the feed horn primary pattern, horn phase center position, and the shape of the main reflector are known. A required constant is uniform phase distribution across the secondary aperture.

A look at the optics

Consider a system where the main reflector and the sub-reflector are shaped to provide a uniform phase and a uniform amplitude field distribution across the secondary aperture (Fig. 2). Here, O is the feed phase center position and OP = X_0. The radii of the main and subreflectors are r_2 and h_1, respectively. The angle subtended by the edge of the subreflector to the feed phase center position is θ_{1m} and the angle

subtended by the main reflector edge from the edge of the subreflector (in the plane of the paper) is θ_{2m}.

For a uniform phase condition across the secondary aperture, the rays leaving the feed at angles θ ($\theta \leq \theta_{1m}$) will suffer reflections from both the subreflector and main reflector surfaces, and will emerge parallel to the central axis. As mentioned previously, the field amplitude taper across the secondary aperture is uniform. For some other field amplitude taper (where the field amplitude at the edge of the aperture is down with respect to the peak at the center) the subreflector radius must be greater than h_1 (call this h_2, where $B'C' = h_2$). The position of the new subreflector must satisfy:

$$PC' = (r_2 - h_2) \cot(\theta_{2m}) \quad (1)$$

This equation meets the requirement that the edge fray from the feed (at angle θ'_{1m} where $\angle B'OC' = \theta'_{1m}$ and $\theta'_{1m} > \theta_{1m}$) strike the edges of the main and the subreflectors and emerge parallel to the central axis to satisfy the uniform phase condition. Hence the subreflector, apart from having a larger radius, is also moved closed to the feed by $OC - OC'$.

For a more tapered aperture field, the new subreflector must also be shallower than the original subreflector, since more of the incident feed energy needs to be concentrated toward the center of the secondary aperture. This can be demonstrated by considering the tangents to the surface at points B and B′ of the two subreflectors. The tangent to the surface at point B makes an angle $(\theta_{2m} - \theta_{1m})/2$ with the vertical. Since the main reflector coordinates remain the same, the same conditions apply for any other ray, thus indicating a shallower subreflector.

The total path length with the new subreflector for any ray is equal to $(OB' + B'A)$, where

$$OB' + B'A = h_2 \operatorname{cosec}(\theta'_{1m}) + (r_2 - h_2) \operatorname{cosec}(\theta_{2m}) \quad (2)$$

In the above equation, θ'_{1m} is given by

$$\theta'_{1m} = \tan^{-1}\{h_2/(X_0 + PC')\} \quad (3)$$

where PC is given by Eq. 1.

Expanding the analysis

For any other point on the main reflector, consider Fig. 3. The main reflector coordinates are known, therefore, for any position (X_2, Y_2) on the main reflector we also know the angle (θ_2) between the path MN and the horizontal for the final ray to emerge parallel. Hence, the path length this ray travels must equal the total path length. That is,

$$ON + MN + MK = AB' + OB' \quad (4)$$

where the right-hand side of this equation is represented by Eq. 2, and the terms of the left-hand side are given by the following:

$$ON = \{Y_1^2 + (X_0 PC' - X_1^2)\}^{1/2} \quad (5)$$

$$MK = X_2 \quad (6)$$

and

$$MN = \{(Y_2 - Y_1)^2 + (X_2 + PC' - X_1)^2\}^{1/2} \quad (7)$$

Finally, θ_2 is given by

$$\theta_2 = \tan^{-1}\left\{\frac{(Y_2 - Y_1)}{(X_2 + PC' - X_1)}\right\} \quad (8)$$

Once X_2, Y_2, θ_2, PC and X_0 are known, Eqs. 4 and 8 can be used to solve for the unknowns X_1 and Y_1. In this manner, the coordinates can be determined for the entire subreflector. Thus, the optics for the modified system are known, and with the knowledge of the feed pattern (with the feed phase center at position O), the secondary amplitude distribution across the main aperture can be calculated. It is an easy matter to study different size subreflectors and associated amplitude tapers numerically, and select the desired result. An example will best demonstrate the use of this technique.

Consider a design example

Using the standard procedure for shaped dual reflector antennas,[1,2] first determine the coordinates of the two reflectors assuming the requirement for uniform amplitude and phase distribution across the secondary aperture. For this example, the feed was assumed to have a $\cos^{100}(\theta)$ circularly symmetric power pattern and its phase center was positioned 0.5-inch behind the secondary aperture plane. The subreflector to main reflector radii ratio (h_1/r_2) was chosen to be 0.085.

A computer analysis provided the coordinates of the two reflectors as well as the angle θ_2 for all the coordinate positions. Next, with the same main reflector coordinates (and associated θ_2 angles) and assuming the same phase center position of the feed we determined, using the principles outlined in this paper, the coordinates of a subreflector which was 13 per cent larger than the original subreflector $(h_2/r_2 = 0.096)$.

The resulting geometric-optics am-

(continued on p. 173)

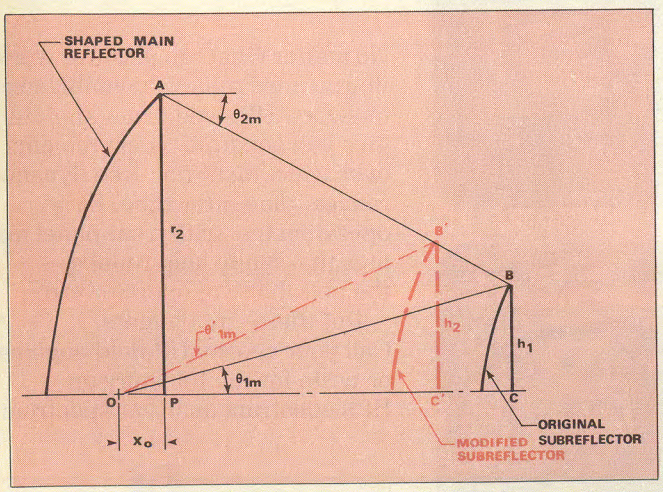

2. The modified subreflector *is located closer to the main reflector. This acts to taper illumination near the edge of the large dish, reducing diffraction and spillover.*

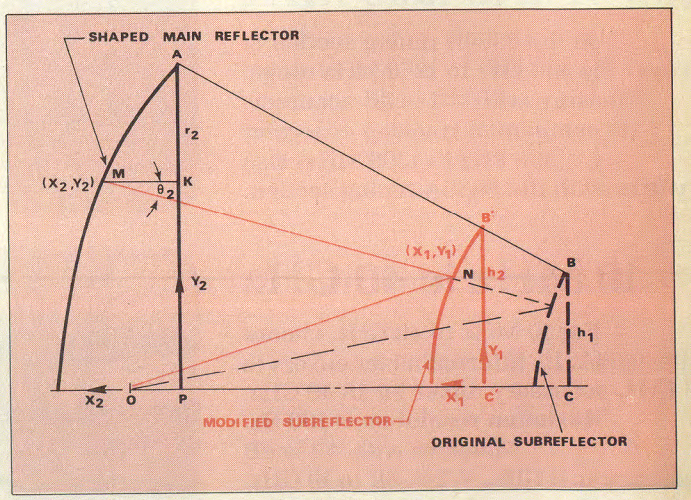

***3. The analysis correlates points** on the surface of the main reflector (X_2, Y_2) with points on the modified subreflector surface (X_1, Y_1).*

RESHAPED SUBREFLECTOR

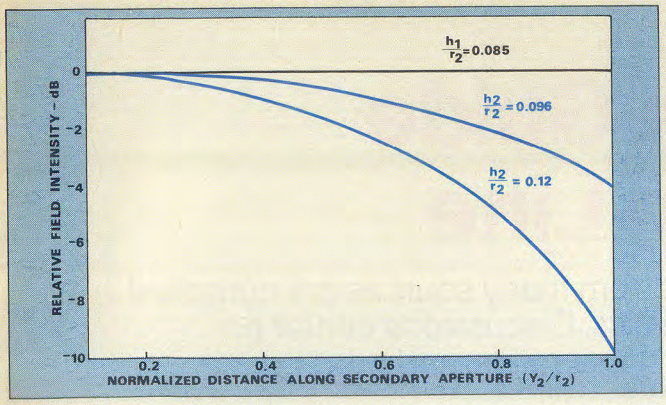

***4. Field intensity is tailored** by changing the ratio of main-to-subreflector diameter.*

plitude taper on the secondary aperture was computed and this is plotted in Fig. 4. The amplitude distribution is no longer uniform but has a taper with the edge field down by 4 dB. The back of the subreflector moved 0.93-inch towards the main reflector. With a 42 per cent larger subreflector (h_2/r_2 = 0.12), the computed field distribution showed the edge field down by 10 dB.••

References

1. W.F. Williams, "High Efficiency Antenna Reflector," *Microwave Journal*, Vol. 8, No. 7, pp. 79-82, (July, 1965).

2. V. Galindo, "Design Of Dual-Reflector Antennas With Arbitrary Phase and Amplitude Distribution," *IEEE Transactions on Antennas and Propagation*, Vol. AP-12, pp. 403-408, (July, 1964).

3. FCC Rules and Regulations, Part 25.209, Antenna Performance Standards.

END LAUNCH

WAVEGUIDE TO COAXIAL

ADAPTERS

MAURY MICROWAVE 20TH ANNIVERSARY 1957 1977

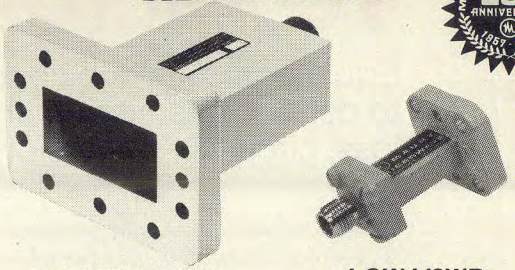

• 1.7 TO 40 GHz • LOW VSWR

• ALL CONNECTOR TYPES

MMC produces a complete line of *End Launch* waveguide to coaxial adapters from 1.7 to 40 GHz. Models are available with SMA (to 40 GHz), N, APC7, TNC, GR900, MPC8 (OSSM equiv. to 40 GHz), MPC2, 7/8 EIA, etc. coaxial connectors. VSWR is less than 1.25 max., with 1.10 max. VSWR options and better available in most bands. Convenient compact configuration ideal for EW/ECM system applications.

See our new Short Form Catalog in Microwaves Product Data Directory.

Call or send for full details. ***Today!***

MAURY MICROWAVE CORPORATION

CUCAMONGA CALIFORNIA 91730 U.S.A. • TELEPHONE 714 987 4715

READER SERVICE NUMBER 52

HP's Small Wonders

for microwave detection to 26.5 GHz



• 10 to 26,500 MHz (8473C); 10 to 18,000 MHz (8473B)

• ±0.6dB flatness, <1.5 SWR to 18,000 MHz

• New APC 3.5 connector is fully SMA compatible

• Prices: 8473B, $235*; 8473C, $275.*

More than 300 other microwave measurement items are described in our Microwave Test Catalog. Call your nearby HP office or write. *Domestic prices only.

HEWLETT hp PACKARD

1507 Page Mill Road, Palo Alto, California 94304

For assistance call: Washington (301) 948-6370, Chicago (312) 255-9800, Atlanta (404) 955-1500, Los Angeles (213) 877-1282

04705

CIRCLE READER SERVICE NUMBER 80 FOR PRODUCT DATA

CIRCLE READER SERVICE NUMBER 81 FOR CATALOG

A Designer's Guide To Microstrip Line

Equations, data and conclusions from many sources are compiled to define transmission characteristics. Discussions center on loss, circuit Q, dispersion, dimensional ratios, and moding.

THIS is not an announcement of a revolutionary *new idea* for microstrip circuit design. It is, however, a compendium of the *best ideas* presented over the past several years on design considerations for this ubiquitous transmission medium.

Microstrip technology is quite mature, offering a superior blend of performance characteristics[1] to the designer of microwave integrated circuits (Table 1). Nearly 50 references at the end of this article attest to the number of investigators who have published design formulas for microstrip. So today, the problem is not that the circuit designer lacks information concerning this transmission medium, but that too much information is available, scattered throughout too many journals. What follows is an attempt to review the most useful formulas and conclusions, and arrange them in a logical, easy-to-follow order.

But first, understand the difference between microstrip and other forms of MIC transmission line that are often erroneously referred to as "microstrip." By definition, a microstrip transmission line consists of a strip conductor and a ground plane separated by a dielectric medium (Fig. 1a). The dielectric material serves as a structural substrate upon which the thin-film metal conductors are deposited. Conductors are usually gold or copper.

Since field lines between the strip and the ground plane are not contained entirely in the substrate (Fig. 1b), the propagating mode along the strip is not purely transverse electromagnetic (TEM) but quasi-TEM. Assuming the quasi-TEM mode of propagation, the phase velocity in microstrip is given by

$$V_p = \frac{c}{\sqrt{\epsilon_{eff}}} \qquad (1)$$

where c is the velocity of light, and ϵ_{eff} is the effective dielectric constant of the substrate material. The effective dielectric constant is lower than the relative dielectric constant, ϵ_r, of the substrate, and takes into account external fields.

The wavelength, λ_g, in microstrip line is given by

$$\lambda_g = \frac{V_p}{f} \qquad (2)$$

where V_p is given by Eq. 1 and f is frequency.

The characteristic impedance of the transmission line is given by

$$Z_o = \frac{1}{V_p C} \qquad (3)$$

where C is the capacitance per unit length of the line.

The analysis for the evaluation of ϵ_{eff} and C based on quasi-TEM mode is fairly accurate at lower microwave frequencies. At higher frequencies, the ratio of longitudinal-to-transverse electric field components becomes significant and the propagating mode can no longer be considered quasi-TEM. Analysis of this "hybrid mode" is far more rigorous.

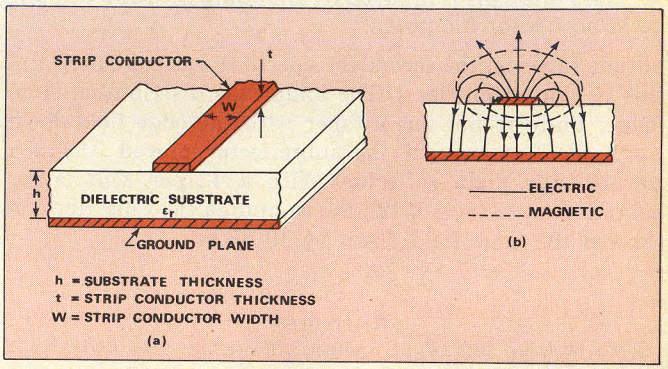

***1. Microstrip** is separated from a ground plane by a dielectric substrate (a). Since not all field lines pass through the substrate (b), a quasi-TEM analysis is used.*

Table 1: Comparison of popular transmission media

Characteristic	Microstrip	Stripline	Coaxial	Waveguide
Line losses	high	high	medium	low
Unloaded Q	low	low	medium	high
Power capability	low	low	medium	high
Isolation between neighboring circuits	poor	fair	very good	very good
Bandwidth	large	large	large	small
Miniaturization	excellent	very good	poor	poor
Volume and weight	small	medium	large	large
Realization of passive circuits	very easy	very easy	easy	easy
Integration				
with chip devices	very good	fair	poor	poor
with ferrites	good	good	poor	good
with lumped elements	very good	very good	good	poor

Dr. I. J. Bahl, and **D. K. Trivedi,** Research Engineers, Indian Institute of Technology, Advanced Centre For Electronic Systems, Department of Electrical Engineering, Kanpur-208016, India.

Closed-form expressions are vital

Early attempts to charactercize the performance of microstrip line were based on the quasi-TEM model. Various electrostatic approximations such as conformal map-

ping[2, 3], relaxation methods[5], variation techniques,[6,7] the method of Green's function[8, 9, 10] and the moment method[11] are generally used. During the last few years, a number of papers using a hybrid-mode model of microstrip line have appeared, but these involve extensive computations. Closed-form expressions are absolutely necessary for optimization and computer-aided design of a microstrip circuit.

The closed form expressions for Z_0 and ϵ_{eff} have been reported by Wheeler[3], Schneider[1] and Hammerstad.[4] Wheeler and Hammerstad have also given an expression for W/h in terms of Z_0 and ϵ_r. For a practical range of microstrip lines ($0.05 \leq W/h \leq 20$ and $\epsilon_r \leq 16$) Hammerstad reported that his expressions are more accurate than earlier work, and fall within ±1 per cent of Wheeler's numerical results. His expressions, which are based on the work of Wheeler and Schneider, include useful relationships defining both characteristic impedance and effective dielectric constant:

For $W/h \leq 1$,

$$Z_0 = \frac{60}{\sqrt{\epsilon_{eff}}} \ln (8\ h/W + 0.25\ W/h) \qquad (4)$$

where:

$$\epsilon_{eff} = \frac{\epsilon_r+1}{2} + \frac{\epsilon_r-1}{2} [(1 + 12\ h/W)^{-1/2} + 0.04(1-W/h)^2] \qquad (5)$$

For $W/h \geq 1$,

$$Z_0 = \frac{120\ \pi/\sqrt{\epsilon_{eff}}}{W/h + 1.393 + 0.667 \ln (W/h+1.444)} \qquad (6)$$

where:

$$\epsilon_{eff} = \frac{\epsilon_r+1}{2} + \frac{\epsilon_r-1}{2}(1 + 12\ h/W)^{-1/2} \qquad (7)$$

Hammerstad notes that the maximum relative error in ϵ_{eff} and Z_0 is less than ±0.5 per cent and 0.8 per cent, respectively, for $0.05 \leq W/h \leq 20$ and $\epsilon_r \leq 16$. His expressions for W/h in terms of Z_0 and ϵ_r are:

For $W/h \leq 2$,

$$W/h = \frac{8\ \exp(A)}{\exp(2A)-2} \qquad (8)$$

For $W/h \geq 2$,

$$W/h = \frac{2}{\pi} [B-1-\ln(2B-1) + \frac{\epsilon_r-1}{2\ \epsilon_r} \left\{ \ln(B-1)+0.39 - \frac{0.61}{\epsilon_r} \right\}] \qquad (9)$$

where:

$$A = \frac{Z_0}{60} \sqrt{\frac{\epsilon_r+1}{2}} + \frac{\epsilon_r-1}{\epsilon_r+1} (0.23 + 0.11/\epsilon_r)$$

$$B = \frac{377\ \pi}{2\ Z_0\sqrt{\epsilon_r}}$$

These expressions provide the same accuracy as Eqs. 4, 5, 6 and 7.

The results discussed above assume a two-dimensional strip conductor. But in practice, the strip is three-dimensional—its thickness (t) must be considered. However, when $t/h \leq 0.005$, $2 \leq \epsilon_r \leq 10$, and $0.1 \leq W/h \leq 5$, the agreement between experimental and theoretical (t/h=0) results is excellent.[12]

The zero-thickness (t/h=0) formulas given above can also be modified to consider the thickness of the strip[1, 3] when the strip width, W, is replaced by an effective strip width, W_e. Expressions for W_e are:

For $W/h \geq 1/2\pi$,

$$\frac{W_e}{h} = \frac{W}{h} + \frac{t}{\pi h} (1+\ln \frac{2h}{t}) \qquad (10)$$

For $W/h \leq 1/2\ \pi$,

$$\frac{W_e}{h} = \frac{W}{h} + \frac{t}{\pi h} (1+\ln \frac{4\ \pi W}{t}) \qquad (11)$$

Additional restrictions for applying Eqs. 10 and 11 are $t \leq h$ and $t < W/2$. Typical strip thickness varies from 0.0002 to 0.0005 inch for metalized alumina substrate, and from 0.001 to 0.003 inch for low-dielectric substrates.

Most microwave integrated circuit applications require a metallic enclosure for hermetic sealing, strength, electromagnetic shielding and ease of handling. The effect of the top and side walls on the microstrip characteristics has been studied using numerical methods.[5, 7, 13, 14] The conclusion: packaging tends to lower impedance and effective dielectric constant. This is because the fringing flux lines are prematurely terminated, which increases the density of field lines in air. But when the ratio of the distance between the lower and upper walls to substrate thickness is larger than five, and the side wall spacing is five times the strip width, the effect of enclosure is negligible on microstrip characteristics.

Consider dispersion at higher frequencies

The formulas for characteristic impedance and effective dielectric constant presented thus far have been based on a quasi-TEM mode of propagation. At lower frequencies, this is a good static approximation of a dynamic structure. However, at higher frequencies the effective dielectric constant and characteristic impedance of a microstrip line begins to change as frequency, increases making the transmission line dispersive.[15, 16] This dispersive characteristic is due to propagation of hybrid modes.

(continued on p. 176)

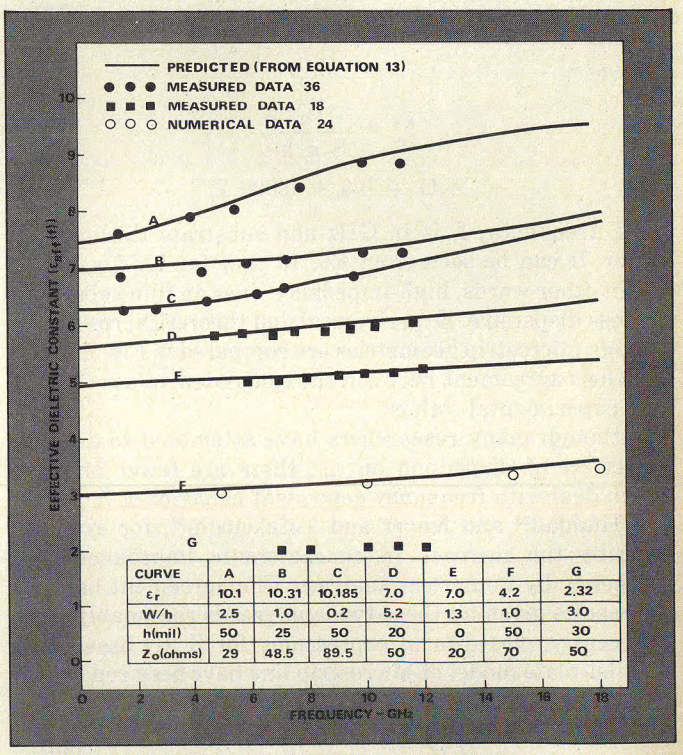

CURVE	A	B	C	D	E	F	G
ϵ_r	10.1	10.31	10.185	7.0	7.0	4.2	2.32
W/h	2.5	1.0	0.2	5.2	1.3	1.0	3.0
h(mil)	50	25	50	20	0	50	30
Z_0(ohms)	29	48.5	89.5	50	20	70	50

2. Dispersive effects *raise the effecive dielectric constant (ϵ_{eff}) slightly as frequency is increased.*

The frequency dependence of the effective dielectric constant describes the influence of dispersion on the phase velocity, whereas the frequency dependence of the effective width describes the influence of the dispersion on the characteristic impedance.[17] The phase velocity in microstrip line decreases with increasing frequency, hence ϵ_{eff} increases with frequency. The characteristic impedance of microstrip line increases with frequency, so the effective width must decrease with frequency.

Fortunately, changes in ϵ_{eff} and Z_o with frequency are very small. However, the frequency below which dispersion effects may be neglected is given by the relation[18]

$$f_o\ (GHz) = 0.3\sqrt{\frac{Z_o}{h\sqrt{\epsilon_r}-1}} \quad (h \text{ in cm}) \quad (12)$$

Equation 12 shows that f_o is higher for high-impedance lines on thin substrates.

The numerical analysis for dispersion in shielded as well as open microstrip transmission lines has been treated extensively.[19–29] These analyses, however, require extensive computations and fail to provide insight into the dominant physical phenomenon at work. For these reasons, the numerical approach is not convenient for microstrip circuit design and therefore, not discussed in this paper.

Both experimental and empirical attempts to describe microstrip dispersion have also been reported.[15, 16, 30–37] The empirical expressions reported for dispersion are limited in terms of applicability and suffer from inadequate theoretical foundation. Analytical formulas for dispersion which agree closely with experimental and numerical results have appeared just recently.

These analytical expressions, by Getsinger[36] and Carlin[37], are very similar. But the results given by Getsinger are closer to experimental as well as numerical results. The dispersion in ϵ_{eff} is given by

$$\epsilon_{eff}(f) = \epsilon_r - \frac{\epsilon_r - \epsilon_{eff}}{1+G(f/f_p)^2} \quad (13)$$

where:

$$f_p = \frac{Z_o}{8\ \pi\ h}$$

$$G = 0.6 + 0.009\ Z_o$$

Here, frequency, f, is in GHz and substrate thickness, h, in cm. It can be seen from Eq. 13 that for $f_p \gg f$, $\epsilon_{eff}\ (f) = \epsilon_{eff}$. In other words, high-impedance lines on thin substrates are less dispersive. Experimental and theoretical results for various microstrip geometries are compared in Fig. 2. There is a close agreement between the calculated values (Eq. 13) and experimental values.

Although many researchers have attempted to describe the effect of dispersion on ϵ_{eff}, there are fewer analyses which deal with frequency dependent behavior of Z_o. Krage and Haddad[25] and Knorr and Tufekcioglu[29], for example, describe the increase in characteristic impedance with frequency by numerical analyses. The agreement between the results given by these two analyses is reasonably good.

Recently, closed-form expressions for $Z_o\ (f)$ based on a parallel-plate model of microstrip line have been reported.[38] These expressions are:

$$Z_o(f) = \frac{377\ h}{W_{eff}(f)\ \sqrt{\epsilon_{eff}\ (f)}} \quad (14)$$

The effective width, $W_{eff}\ (f)$, is given by

$$W_{eff}\ (f) = W + \frac{W_{eff}\ (0) - W}{1 + (f/f_p)^2} \quad (15)$$

where $W_{eff}\ (0)$ is obtained from Eq. 14 when $f = 0$.

The variation in characteristic impedance with frequency is shown in Fig. 3. The solid curve is arrived at using Eqs. 14 and 15, while the dotted curve is the one reported by Knorr and Tufekcioglu.[29] The increase in $Z_o\ (f)$ (for $\epsilon_r = 10$ and $W/h = 1$) is only 4 per cent from DC to 10 GHz, which is quite small. This change cannot be confirmed experimentally since, at 10 GHz, transitions pose a considerable problem in accurate measurement. Therefore, the effect of dispersion on Z_o can be generally neglected.

Two mechanisms contribute to loss

Attenuation constant, α, is one of the most important characteristics of any transmission line. There are two sources of dissipative losses in a microstrip circuit: conductor loss and substrate dielectric loss.

Assuming a uniform current distribution across strip width and ground plane, conductor loss may be approximated as:

$$\alpha_c = \frac{8.68}{Z_o\ W} R_s \text{ dB/cm} \quad (16)$$

The surface resistivity, R_s, for the conductor is given by

$$R_s = \sqrt{\pi\ f\ \mu_o/\sigma}$$

where μ_o is the free space permeability and σ is the conductivity of the microstrip material.

It should be noted that this simple expression for conductor loss is valid only for very wide strip widths ($W/h \to \infty$): There is a very large discrepancy between the experimental data and this expression at practical values of W/h. However, Eq. 16 can be brought closer to reality by considering nonuniform current distribution. Expressions for the conductor loss derived by Pucel[39] in this manner are very accurate.

For $W/h \leq 1/2\ \pi$,

$$\alpha_c = \frac{8.68\ R_s}{2\ \pi\ Z_o h} \cdot P \cdot \left[1 + \frac{h}{W_e} + \frac{h}{\pi\ W_e}\left(\ln\frac{4\ \pi W}{t} + \frac{t}{W}\right)\right] \quad (17a)$$

(Continued on p. 178)

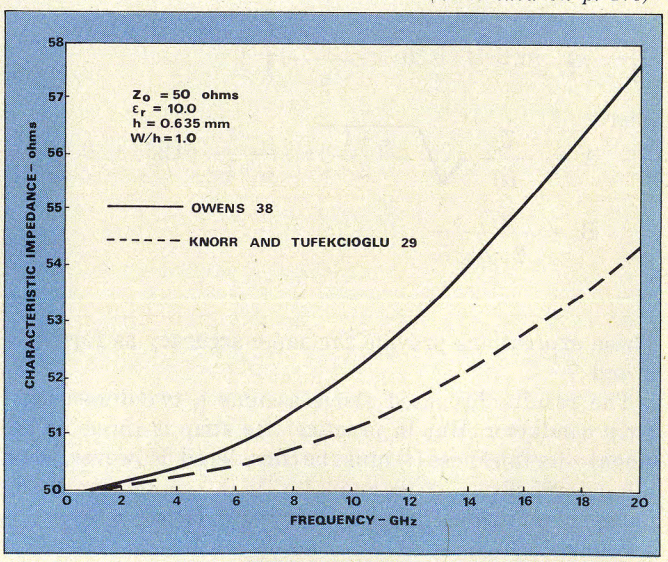

3. Characteristic impedance *increases somewhat with frequency. But note that there is only a 4 per cent change from DC to 10 GHz.*

For $1/2\ \pi < W/h \leq 2$,

$$\alpha_c = \frac{8.68\ R_s}{2\ \pi\ Z_o h} \cdot P \cdot Q \qquad (17b)$$

For $W/h \geq 2$,

$$\alpha_c = \frac{8.68\ R_s}{Z_o h} \cdot Q \cdot \left[\frac{W_e}{h} + \frac{2}{\pi} \ln\left\{2\pi e\left(\frac{W_e}{2h} + 0.94\right)\right\}\right]^{-2}\left[\frac{W_e}{h} + \frac{W_e/\pi h}{\frac{W_e}{2h} + 0.94}\right] \qquad (17c)$$

where:

$$P = 1 - \left(\frac{W_e}{4h}\right)^2$$

$$Q = 1 + \frac{h}{W_e} + \frac{h}{\pi\ W_e}\left(\ln\frac{2h}{t} - \frac{t}{h}\right)$$

For a fixed characteristic impedance, conductor loss decreases inversely with substrate thickness and increases with the square root of frequency.

The dielectric loss in microstrip line is an important parameter when microwave circuits requiring small attenuation are considered. Welch and Pratt[40] and Schneider[41] derived the expressions for the attenuation constant for a dielectric with loss tangent, tanδ, given below:

$$\alpha_d = 27.3 \frac{\epsilon_r}{(\epsilon_{eff})^{1/2}} \cdot \frac{\epsilon_{eff}-1}{\epsilon_r - 1} \cdot \frac{\tan\ \delta}{\lambda_o}\ \text{dB/cm}$$

where λ_o is the free space wavelength.

For $\sigma \neq 0$,

$$\alpha_d = 4.34 \frac{\epsilon_{eff}-1}{\sqrt{\epsilon_{eff}}(\epsilon_r - 1)}\left(\frac{\mu_o}{\epsilon_o}\right)^{1/2} \sigma\ \text{dB/cm} \qquad (18b)$$

where ϵ_o is the free space permittivity.

Dielectric losses are normally very small compared with conductor losses for dielectric substrate. Dielectric losses in silicon substrates, however, are usually in the same order as, or larger than conductor losses. The reason for this is that resistivities higher than few hundred ohm-cm are difficult to maintain for Si. However, higher resistivity can be maintained in GaAs, and hence the losses are less for this material.

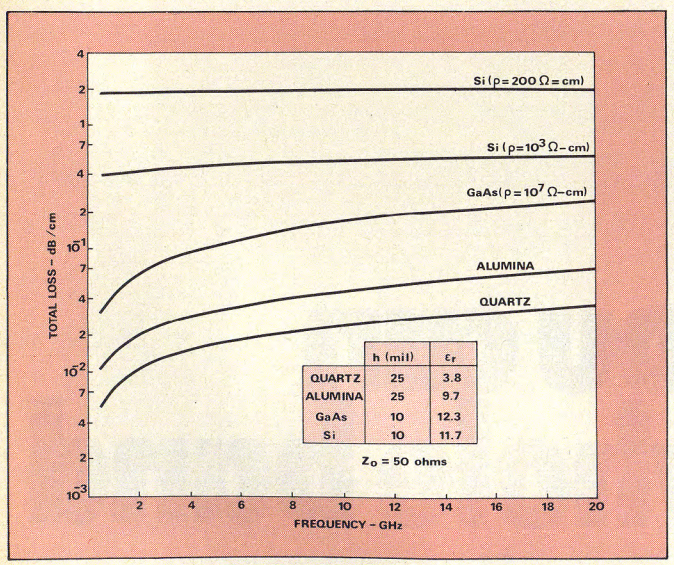

***4. Losses in semiconductor substrates** are substantially higher than those in ceramic or quartz material. Silicon introduces high losses due to the difficulty of growing high resistivity material.*

Figure 4 compares the total loss for 50-ohm microstrip lines on silicon, GaAs, alumina and quartz substrates. It is obvious from the figure that silicon MICs are more lossy. GaAs circuits will have more loss than ceramic circuits because the semiconductor substrates are thinner. Lines on quartz have the least loss.

Quality factor depends on substrate

The quality factor, Q, of a microstrip line can be related to the total losses in the line by[42]

$$Q_T = \frac{\beta}{2\ \alpha_T} \qquad (19)$$

where Q_T is the total resonator Q, α_T is the total loss in the resonator and $\beta = 2\pi/\lambda_g$. Microstrip line Qs are lower than the Qs of coaxial or waveguide transmission lines.

When the losses in a resonant line are considered (such as $\lambda_g/2$ or $\lambda_g/4$ resonators) another loss factor, α_r, due to radiation at the discontinuities must also be considered. The corresponding radiation Q-factor is given by[43]:

$$Q_r = \frac{Z_o}{480\ \pi(h/\lambda_o)^2 F} \qquad (20)$$

where

$$F = \frac{\epsilon_{eff}(f) + 1}{\epsilon_{eff}(f)} - \frac{(\epsilon_{eff}(f) - 1)^2}{2\ (\epsilon_{eff}(f))^{2/3}} \cdot \ln\frac{\sqrt{\epsilon_{eff}\ (f)} + 1}{\sqrt{\epsilon_{eff}(f)} - 1}$$

Note that the effect of dispersion is considered, as described by Eq. 13. The total Q of the resonator can be expressed by

$$\frac{1}{Q_T} = \frac{1}{Q_c} + \frac{1}{Q_d} + \frac{1}{Q_r} \qquad (21)$$

Here, Q_c, Q_d and Q_r are the quality factors corresponding to conductor, dielectric and radiation losses, respectively. Finally, the circuit quality factor, Q_o, can be defined as

$$\frac{1}{Q_o} = \frac{1}{Q_c} + \frac{1}{Q_d} = \frac{\lambda_o\ (\alpha_c + \alpha_d)}{\pi\sqrt{\epsilon_{eff}}} \qquad (22)$$

The variation of Q_o, Q_r and Q_T with frequency for a quarter-wave resonator on GaAs, alumina and quartz substrates is shown in Fig. 5. A quarter-wave, 50-ohm resonator on 25-mil-thick alumina substrate has a Q_o of about 240 at 2 GHz and 550 at 10 GHz, whereas Q_T is 230 at 2 GHz and nearly 160 at 10 GHz. This is due to the fact that radiation losses are higher than conductor and dielectric losses at higher frequencies. A quarter-wave, 50-ohm resonator on 10-mil GaAs substrate has Q_o of about 82 at 2 GHz and 160 at 10 GHz, whereas Q_T is 82 at 2 GHz and nearly 145 at 10 GHz. This is due to the fact that radiation losses are smaller than conductor and dielectric losses for thin substrates at higher frequencies. Thus, the commonly accepted rule for high-Q microstrip circuits using thick substrates does not apply due to high radiation losses incurred under this condition.

Moding limits high-frequency operation

Maximum frequency of operation in microstrip line is limited by the excitation of spurious modes in the form of

(Continued on p. 180)

surface waves and transverse resonances. Surface waves are TM and TE modes which propagate across a dielectric substrate with ground plane. The frequency at which significant coupling occurs between the quasi-TEM mode and the lowest-order surface wave mode is given by[44]

$$f_T = \frac{c}{2\pi h}\sqrt{\frac{2}{\epsilon_r - 1}} \bullet \tan^{-1}(\epsilon_r) \qquad (23)$$

For $\epsilon_r > 10$, Eq. 23 reduces to[45]

$$f_T\ (\text{GHz}) = \frac{10.6}{h\sqrt{\epsilon_r}}\ (\text{h is in cm}) \qquad (24)$$

Cutoff frequency, f_T, decreases when either the substrate thickness or dielectric constant is increased.

Thus three limitations—maximum substrate thickness, minimum Q and surface wave excitation—define a region of useful microstrip line operation (see Fig. 6). From the usable region of Fig. 6, one obtains a range of substrate thickness which should be used for microstrip line circuits. For $\epsilon_r = 9.7$, this range is:

$0.23 \leq h \leq 1.8$ cm @ 2 GHz
$0.01 < h \leq 0.36$ cm @ 10 GHz
$0.01 < h \leq 0.17$ cm @ 20 GHz

In addition to the conductor and dielectric losses (Q_o), the maximum Q of microstrip is also limited by radiation losses from discontinuities. When radiation losses are taken into account for calculation of maximum Q, the plots in Fig. 6 are slightly modified. But, if packaging and circuit design techniques are employed to reduce radiation losses, the curves in Fig. 6 will remain valid.

Relate fabrication tolerances to properties

High-impedance lines, or lines on thin substrates of high dielectric constant material require very narrow conducting

(Continued on p. 182)

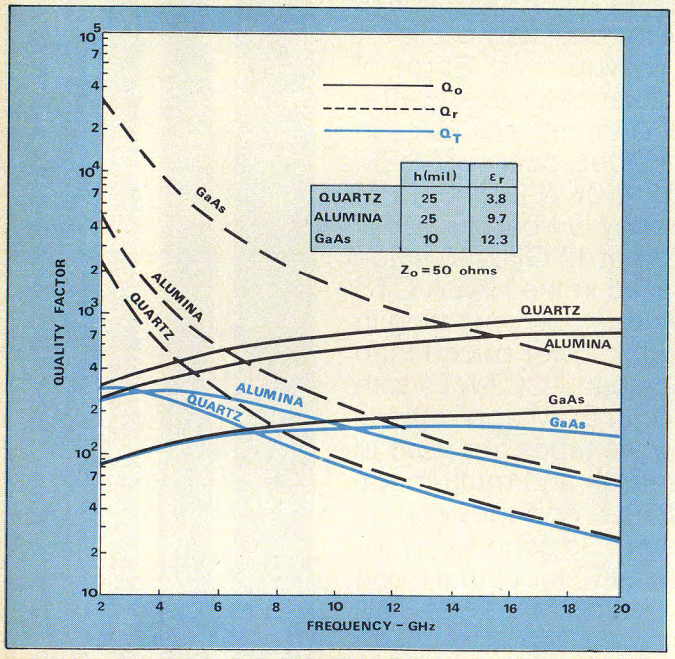

***5. The total Q of a resonator** is determined by considering circuit (Q_o) and radiation (Q_r) quality factors.*

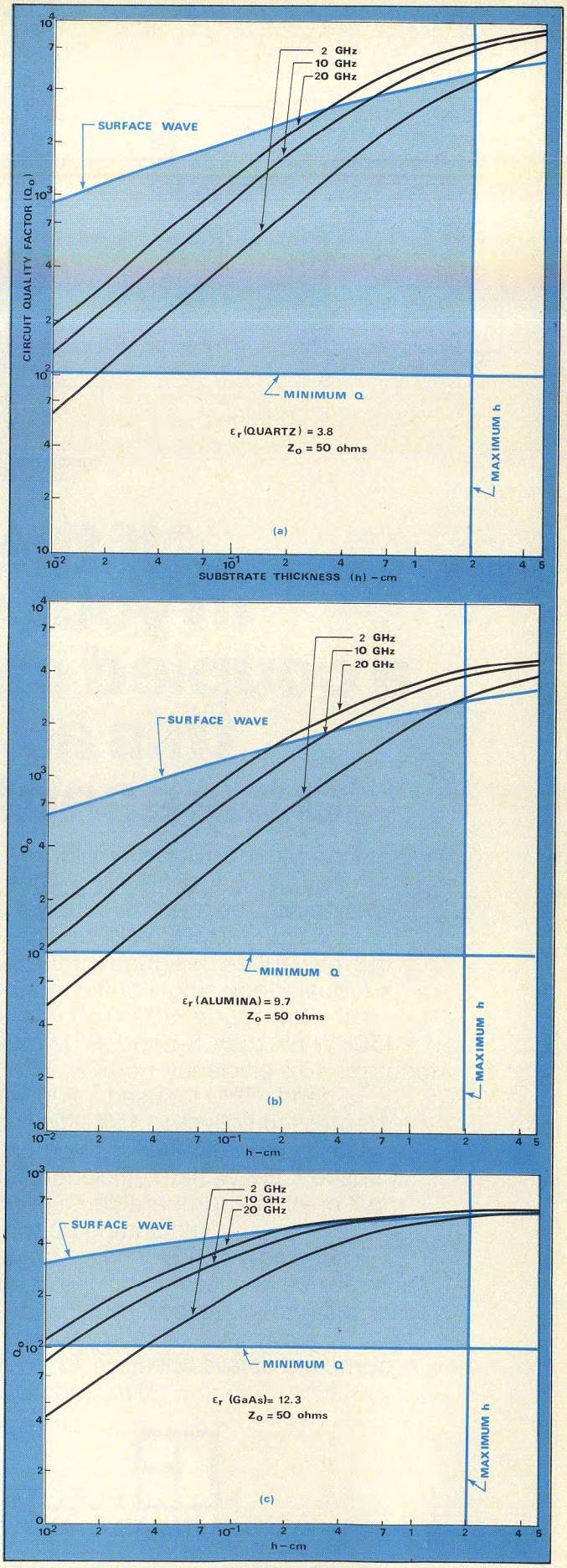

***6. Maximum substrate thickness, minimum Q and surface-wave modes** border a useful operating region.*

strips. Fabrication tolerances naturally impose a limit on the accuracy of such lines. Bahl and Trivedi[46], for example, have studied the effect of dimensional tolerances on ϵ_{eff} and Z_0 with the conclusion that the maximum per cent error in ϵ_{eff} is $0.16\ \Delta X/X$ for $\epsilon_r \leq 16$ and $0.05 \leq X \leq 10$, where ΔX is the deviation in aspect ratio ($X = W/h$). A 5 per cent deviation in strip width of a 50-ohm line on alumina substrate gives rise to ± 0.4 per cent change in ϵ_{eff}, which introduces a maximum error of ± 0.2 per cent in phase velocity as well as characteristic impedance.

The variation of $(\Delta Z_0/Z_0)/(\Delta X/X)$ with X is plotted in Fig. 7. Note that the error increases with X: for $X \leq 1$ the percentage error in Z_0 is less than $-0.5\ \Delta X/X$ whereas for $1 < X \leq 10$, the error is less than $-0.9\ \Delta X/X$. Microstrip lines on semiconductor substrates use substrate thicknesses of 10 mil or less. Since a 50-ohm line on silicon substrate ($\epsilon_r = 12.0$) requires a W/h ratio of 0.74, W is 7.4 mil for a typical substrate thickness of 10 mil. When the deviation in the strip width is 0.5 mil, the error in Z_0 is about ± 3 per cent. This indicates that 50-ohm microstrip lines on semiconductor substrates ($h \geq 10$ mil) require dimensional tolerances in the order of 0.5 mil for satisfactory performance (i.e, VSWR$= 1 + \Delta Z_0/Z_0 \simeq 1.03$).

Some final notes on power handling

The peak power handling capability of microstrip line is poor. Although it is limited primarily by the sharp edges of the strip conductor, in some cases, connectors or launchers decide the power handling capability of the microstrip line. One additional factor which may significantly reduce the power handling capability is the effect of internal mismatches. Howe[47] has reported successful operation up to 10kW at S-band and 4kW at X-band. Peak power data is not readily available and difficult to calculate accurately.

The average power capability of microstrip line is influenced by the temperature rise of the strip conductor and the supporting substrate. It is, therefore, related to the loss tangent and thermal conductivity of the substrate (low loss tangent and large thermal conductivity will increase the average power capability of microstrip lines). It has been reported[48] that a 50-ohm alumina line (50-mil) can easily handle 100 W of CW power. ••

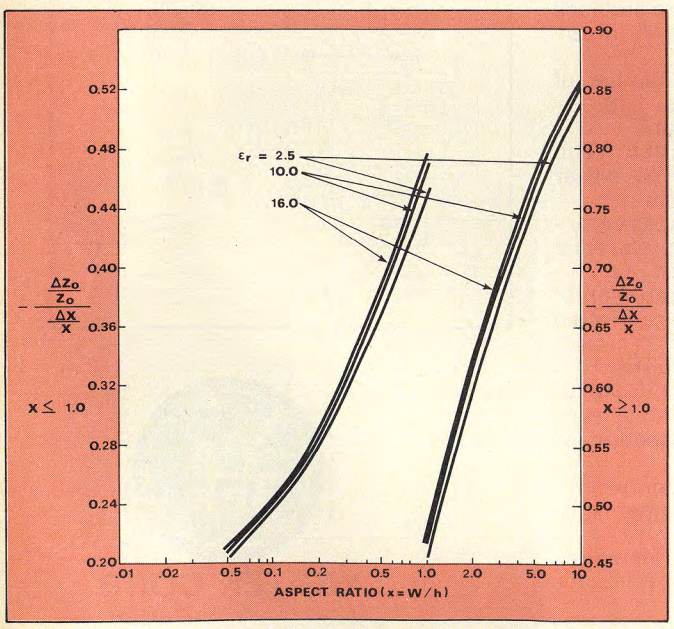

***7. Fabrication tolerances** become more important as the aspect ratio grows larger.*

Acknowledgement

The authors wish to thank Mr. Bh. A. R. B. Raju for going through the final manuscript.

References

1 M.V. Schneider, "Microstrip Lines For Microwave Integrated circuits," *Bell Syst. Tech. J.*, Vol. 48, pp 1421-1444, (May-June, 1969).
2 H.A. Wheeler, "Transmission Line Properties of Parallel Wide Strips By A Conformal Mapping Approximation," *IEEE Trans. Microwave Theory Tech.*, Vol. MTT-12, pp. 280-288, (May, 1964).
3 "Transmission Line Properties Of Parallel Strips Separated By A Dielectric Sheet," *IEEE Trans. Microwave Theory Tech.*, Vol. MTT-13, pp. 172-185, (March, 1965).
4 E.O. Hammerstad, "Equations For Microstrip Circuit Design," *Proc. European Microwave Conference*, Hamburg (Germany), pp. 268-272, (September, 1975).
5 H.E. Stinehelfer, Sr., "An Accurate Calculation Of Uniform Microstrip Transmission Lines," *IEEE Trans. Microwave Theory Tech.*, Vol. MTT-16, pp. 439-444, (July, 1968).
6 E. Yamashita and R. Mittra, "Variation Method For The Analysis Of Microstrip Lines," *IEEE Trans. Microwave Theory Tech.*, Vol. MTT-16, pp. 251-256, (April, 1968).
7 E. Yamashita, "Variation Method For The Analysis Of Microstrip Like Transmission Lines," *IEEE Trans. Microwave Theory Tech.*, Vol. MTT-16, pp. 529-539, (August, 1968).
8 P. Silvester, "TEM Wave Properties Of Microstrip Transmission Lines," *Proc. IEE.* Vol. 115 pp. 43-48, (January, 1968).
9 T.G. Bryant and J.A. Weiss, "Parameters Of Microstrip Transmission Lines and Of Coupled Pairs Of Microstrip Lines," *IEEE Trans, Microwave Theory Tech.*, Vol. MTT-16, pp. 1021-1027, (December, 1968).
10 A. Farrar and A.T. Adams, "A Potential Theory Method For Covered Microstrip," *IEEE Trans. Microwave Theory Tech.*, Vol. MTT-21, pp. 494-496, (July, 1973).
11 "Characteristic Impedance Of Microstrip By The Method Of Moments," *IEEE Trans. Microwave Theory Tech.*, Vol. MTT-18, pp. 65-66, (January, 1970).
12 M.A.R. Gunston and J.R. Weale, "Variation Of Microstrip Impedance With Strip Thickness," *Electron. Lett.*, Vol. 5, pp. 697-698, (Dec. 27, 1969).
13 J.A. Weiss, *Advances in Microwave*, Vol. 8, L. Young and H. Sobol (Eds), Academic Press, pp. 308-309 (1974).
14 D.L. Gish and O. Graham, 'Characteristic Impedance and Phase Velocity Of A Dielectric—Supported Air Strip Transmission Line With Side Walls', *IEEE Trans. Microwave Theory, Tech.*, Vol. MTT-18, pp. 131-148, (March, 1970).
15 C.P. Hartwig, et al., "Frequency Dependent Behavior Of Microstrip," *G-MTT Int. Micro. Symp.*, Detroit, Michigan, pp. 110-116, (May, 1968).
16 L.S. Napoli and J.J. Hughes, "High Frequency Behaviour of Microstrip Transmission." *RCA Review*, Vol. 30, No. 2, pp. 268-276, (June, 1969).
17 I. Wolff and W. Menzel, "A Universal Method To Calculate The Dynamical Properties Of Microstrip Discontinuities," *Proc. Europe. Micro. Conf.*, Hamburg (Germany), pp. 263-267, (September, 1975).
18 W.J. Chudobiak, et al., "Dispersion In Microstrip," *IEEE Trans. Microwave Theory Tech.*, Vol. MTT-19, pp. 783-784, (September, 1971).
19 J.S. Hornsby and A. Gopinath, "Numerical Solutions Of Inhomogeneously Filled Guides With Symmetrical Microstrip Line," *Proc. Euro., Micro. Conf.* London (England), pp. 114-117, (September, 1969).
20 J.S. Hornsby and A. Gopinath, "Fourier Analysis Of A Dielectric Loaded Waveguide With A Microstrip Line," *Electron. Lett.*, Vol. 5, pp. 265-267, (June 12, 1969).
21. P. Daly, "Hybrid-Mode Analysis Of Microstrip By Finite Element Methods," *IEEE Trans. Microwave Theory Tech.*, Vol. MTT-19. pp. 19-25, (January, 1971).
22 G.K. Grunberger, et al., "Longitudinal Field Components and Frequency Dependent Phase Velocity In The Microstrip Line," *Electron. Lett.*, Vol. 3 pp. 683-685 (Oct. 15, 1970).
23 E.J. Denlinger, "A Frequency Dependent Solution For Microstrip Transmission Lines," *IEEE Trans. Microwave Theory Tech.*, Vol. MTT-19, pp. 19-25, (January, 1971).
24 R. Mittra and T. Itoh, "A New Technique For The Analysis Of The Dispersion Characteristics Of Microstrip Line," Ibid, pp. 47-56.
25 M.K. Krage and G.I. Haddad, "Frequency Dependent Characteristics Of Microstrip Transmission Lines," *IEEE Trans. Microwave Theory Tech.*, Vol. MTT-20, pp. 618-688, (October, 1972).
26 T. Itoh and R. Mittra, "Spectral Domain Approach For Calculating The Dispersion Characteristics Of Microstrip Lines," *IEEE Trans. Microwave Theory Tech.*, Vol. MTT-21, pp. 496-499, (July, 1973).
27 "A Technique For Computing Dispersion Characteristics Of Shielded Microstrip Lines," *IEEE Trans. Microwave Theory Tech.*, Vol. MTT-22, pp. 896-898, (October, 1974).
28 A. Kimura and J. Frey, "Calculation and Measurement Of The Frequency Dependence Of Effective Dielectric Constant Of Microstrip Lines," *Microwave Integrated Circuits*, J. Frey (Ed.), Arteh House, Inc., (1975).
29 J.B. Knorr and A. Tufekcioglu, "Spectral Domain Calculation Of Microstrip Characteristic Impedance," *IEEE Trans. Microwave Theory Tech.*, Vol. MTT-23, pp. 725-728, (September, 1975).
30 P. Troughton, "Measurement Techniques In Microstrip," *Electron. Lett.*, Vol. 5, pp. 25-26, (Jan. 23, 1969).
31 "The Evaluation Of Alumina Substrate For Use In Microstrip Microwave Integrated Circuits," *Proc. Euro. Micro. Conf.* London (England), pp. 49-52, (September, 1969).
32 G.I. Zysman and D. Varon, "Wave Propagation In Microstrip Transmission Lines," *G-MTT Int. Micro. Symp.*, Dallas, Texas, pp. 3-9, (May, 1969).
33 S. Arnold, "Dispersive Effects In Microstrip On Alumina Substrates," *Electron. Lett.*, Vol. 5, pp. 673-674, (Dec. 27, 1969).
34 O.P. Jain, et al., "Coupled Mode Model Of Dispersion In Microstrip," *Electron. Lett.*, Vol. 7, pp. 405-407, (July 15, 1971).
35 M.V. Schneider, "Microstrip Dispersion," *Proc. IEEE*, Vol. 60, pp. 144-146, (January, 1972).
36 W.J. Getsinger, "Microstrip Dispersion Model," *IEEE Trans. Microwave Theory Tech.*, Vol. MTT-21, pp. 34-39, (January, 1973).
37 H.J. Carlin, "A Simplified Circuit Model For Microstrip," Ibid, pp. 589-591, (September, 1973).
38 R.P. Owens, "Predicted Frequency Dependence Of Microstrip Characteristic Impedance Using The Planar—Waveguide Model," *Electron. Lett.*, Vol. 12, pp. 269-270, (May 27, 1976).
39 R.A. Pucel, D.J. Masse and C.P. Hartwing, "Losses In Microstrip," *IEEE Trans. Microwave Theory Tech.*, Vol. MTT-16, pp. 342-350, (June, 1968). "Correction To 'Losses In Microstrip,' Ibid., (Correspo.), Vol. MTT-16, pp. 1064, (December, 1968).
40 J.D. Welch and H.J. Pratt, "Losses In Microstrip Transmission Systems For Integrated Microwave Circuits," *NEREM Rec.* Vol. 8, pp. 100-101, (1966).
41 M.V. Schneider, "Dielectric Loss In Integrated Microwave Circuits," *Bell Syst. Tech. J. 48, No. 7, pp. 2325-2332*, (September, 1969).
42 V. Buontempo, and M. Reggiani, "Determinations Of Transmission Line and Discontinuity Characteristics In Microwave Integrated Circuits," *Rev. Tecnica Selenia*, Vol. 2(2), pp. 33-52, (1975).
43 E. Belohoubek and E. Denlinger, "Loss Considerations For Microstrip Resonators," *IEEE Trans. Microwave Theory Tech., Vol. MTT-23, pp. 522-526*, (June, 1975).
44 George D. Vendelin, "Limitations On Stripline," *Microwave Journal*, Vol. 13, No. 5, pp. 63-69, (May, 1970).
45 H. Sobol, "A Review Of The Technological and Electromagnetic Limitations Of Hybrid Circuits For Microwave Applications," *IEEE Trans. Parts Hybrids, Packag.* Vol. PHP-8, pp. 59-66, (June, 1972).
46 I.J. Bahl and D.K. Trivedi, "Effect Of Dimensional Tolerances On Microstrip Line Characteristics," Communicated.
47 H. Howe, Jr., "Stripline Is Alive and Well....," *Microwave Journal*, p. 25, (July, 1971).
48 S.D. Choi and J.F. Boreham, "High Power Microstrip RF Switches," *G-MTT Int. Micro. Symposium*, pp. 52-54, (May, 1972).

Master The T-Junction And Sharpen Your MIC Designs

Neglecting high frequency T-junction discontinuities may be a costly error. Once understood, junction effects can be easily compensated for in a variety of microwave circuits.

LOOK into the hearts of a vast array of microwave circuits, and you will find a T-junction; branch-line and rat-race couplers, SPDT switches and power dividers are just a few examples. The junctions—treated as right-angle transmission-line interconnections—are usually ignored for low frequency applications where their size is negligible compared to a wavelength. Step up into higher X and Ku bands, however, and T-junction discontinuities must be dealt with. The challenges then become, (1) how to best describe the junction's effects, and more importantly, (2) how to compensate for them.

However ominous they seem, T-junction effects do obey the laws of physics and, therefore, can be modeled. Some mathematical manipulations are required, but the results are worth it.

Look inside the T-junction

Before deriving a few simple equations which will take T-junction effects into account, let's examine a basic T-junction.[1,2] Interestingly, the symmetrical microstrip T-junction equivalent detailed in Fig. 1 contains no allowance for radiation loss. This is valid because calculations[3] have shown that the junction's effective radiation has little effect except to add insertion loss.† Consequently, radiation loss need not play a role in the analysis of high frequency T-junction discontinuities.

But how does the T-junction affect a microwave circuit? To answer the question, let's add the T-junction to a two branch-line coupler[4] (Fig. 2). Fortunately, the coupler has a line of symmetry, permitting only half the circuit to be included in the analysis.[5]

The circuit is best analyzed using Reed and Wheeler's method, which, although quite complex, does yield a complete four-port solution by breaking the circuit into three sections and operating on each independently as shown in Fig. 3.

Develop branch-line equations

The ABCD matrix of the first section, (Fig. 3a) is:

$$\begin{bmatrix} A & B \\ C & D \end{bmatrix} = \qquad (1)$$

$$\begin{bmatrix} \cos\theta_x + X_A Y_x \sin\theta_x & -j2X_A\cos\theta_x + j\,\sin\theta_x(Z_x - X_A{}^2 Y_x) \\ jY_x\,\sin\theta_x & \cos\theta_x + X_A Y_x\,\sin\theta_x \end{bmatrix}$$

Michael Dydyk, Principal Staff Engineer, Motorola, Inc., 8201 E. McDowell Road, Scottsdale, AZ 85252.

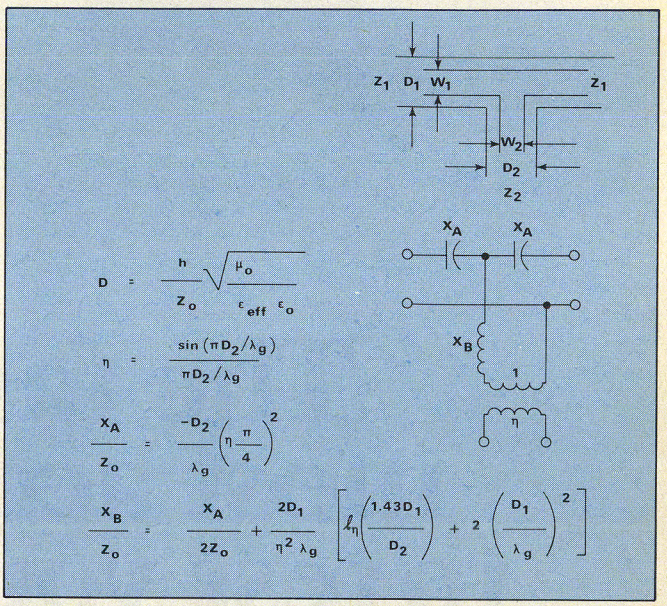

***1. The basic MIC T-junction** is characterized by expressions relating design parameters to line impedance, dielectric constant and frequency. Note that equations describing radiation effects are not included.*

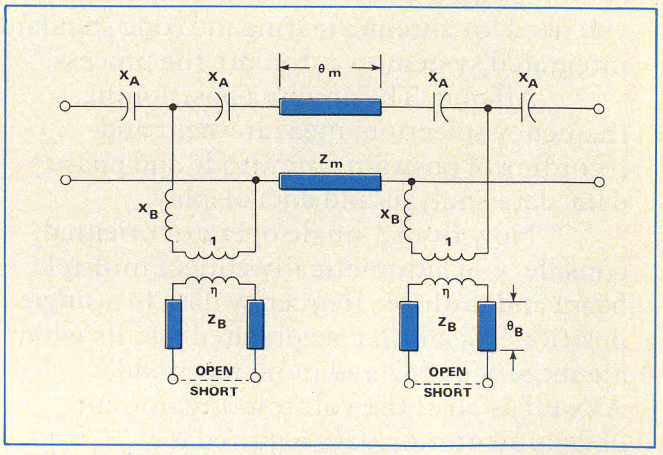

***2. The symmetrical makeup** of the two branch-line coupler and its junction effects permit only half the circuit to be analyzed.*

† Although Lewin[3] calculated radiation losses in stripline, his approximations are valid for microstrip if the correct value of effective line width, D, is used.

where $\theta_x = (2\pi/\lambda_g)\,\ell_x$.

and λ_g = wavelength in microstrip medium.

The ABCD matrix of a length of line which this circuit should represent is:

$$\begin{bmatrix} A & B \\ C & D \end{bmatrix}_m = \begin{bmatrix} \cos\theta_m & jZ_m \sin\theta_m \\ jY_m \sin\theta_m & \cos\theta_m \end{bmatrix} \quad (2)$$

Equating the A and B terms of both matricies results in:

$$\cos\theta_m = \cos\theta_x + X_A Y_x \sin\theta_x \quad (3)$$

$$Z_m \sin\theta_m = -2X_A \cos\theta_x + \sin\theta_x (Z_x - X_A^2 Y_x) \quad (4)$$

The prior two equations provide the information necessary to solve for the two unknowns, Z_x and θ_x. To obtain design equations, let:

$$Z_m = Z_o \quad (5)$$

and

$$\theta_m = 90° \quad (6)$$

which is what the ideal line should be in the two branch-line couplers. Substituting Eqs. 5 and 6 into Eqs. 3 and 4, and performing algebraic manipulation yields:

$$Z_x = \sqrt{Z_o^2 - X_A^2} \quad (7)$$

and

$$\theta_x = \pi - \tan^{-1} \sqrt{\left(\frac{Z_o}{X_A}\right)^2 - 1} \quad (8)$$

Using the same procedure to solve Eq. 3b produces:

$$Z_y = \eta^2 \sqrt{\frac{Z_o^2}{2} - X_B^2} \quad (9)$$

$$\theta_y = \tan^{-1} \sqrt{\frac{Z_o - \sqrt{2}\,X_B}{Z_o + \sqrt{2}\,X_B}} \quad (10)$$

To analyze the circuit in Fig. 3c a somewhat different approach is followed, that is values of Z_Z and θ_Z are sought that will minimize the mismatch. To determine these unknowns, the input impedance of the circuit is derived and appropriate conditions imposed:

$$\text{Im} \left| Z_{in} \right| = 0 \quad (11)$$

$$\text{Re} \left| Z_{in} \right| = \rho_m Z_o \quad (12)$$

(continued on p. 186)



Satellite and RF Telemetry Receivers

Microdyne's 1100-AR and 1100-LS receivers are world standards for versatile and reliable Meteorological Satellite Earth Terminals and RF Telemetry applications. By simply selecting the appropriate plug-in modules, one basic 1100-AR receiver will process and provide antenna tracking information for all of the following Meteorological and RF Telemetry data link formats: Landsat USB, Seasat, VHRR, AVHRR, Stretched VISSR, DMSP and WEFAX/APT, plus all IRIG RF telemetry data.

Where extra wideband requirements such as Landsat (MSS/RBV) are involved, Microdyne's 1100-LS will handle data rates up to 15 megabits NRZ and IF bandwidths up to 40 MHz with a demodulated video output of 10 MHz.

For complete details, or before any make or buy decision, do yourself an important favor and send for our new 24 page General Equipment and Applications Catalog describing our receivers, ancillary equipment and latest design innovations. Copies are also available in French and German.

Visit our display at the Paris Air Show, U.S. Pavillion, State of Maryland Booth E-10 June 2 thru 12, 1977

MICRODYNE CORPORATION

P. O. Box 1527 – 627 Lofstrand Lane
Rockville, Maryland 20850
Telephone (301) 762-8500 TWX 710-828-0477
Cable MICRODYNE Rockville, Maryland USA

READER SERVICE NUMBER 57

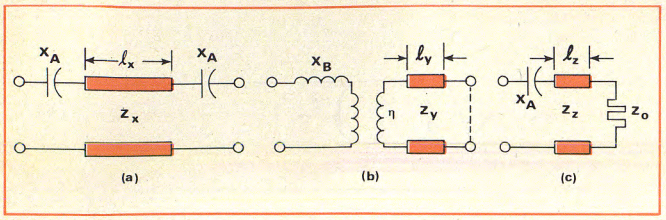

3. Further dividing the coupler into three sections *(a, b and c), the complex analysis becomes easier to undertake.*

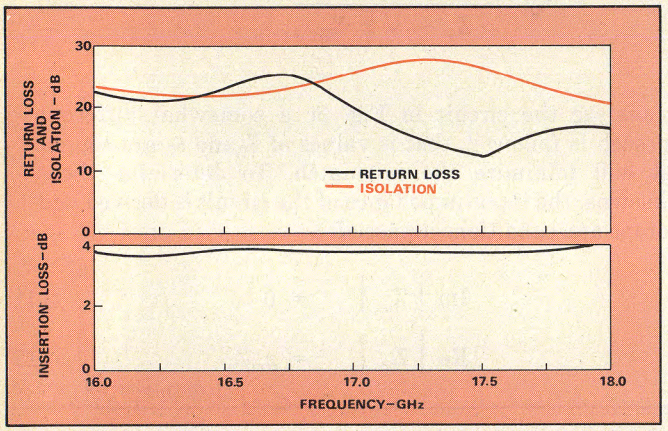

4. Excellent coupler performance *proves the practicality of the design approach.*

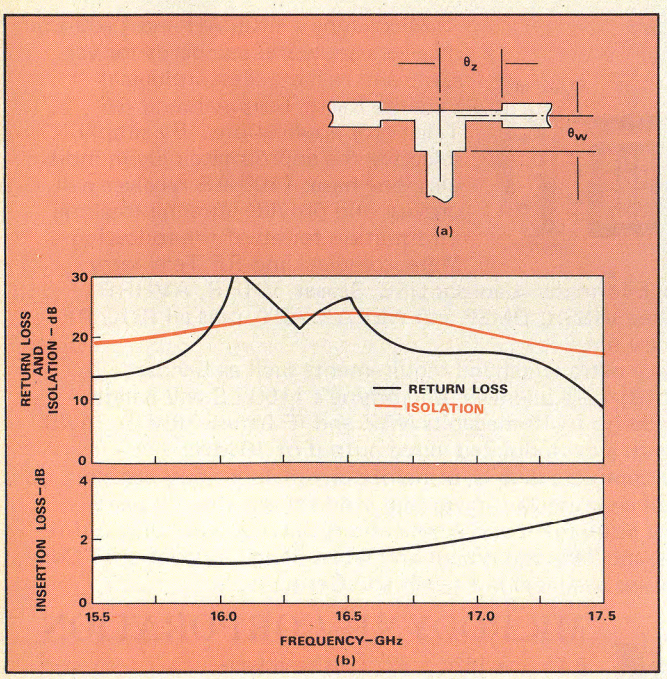

5. An SPDT switch, designed taking full account of T-junction discontinuities *(a), provides 10 dB minimum return loss (b).*

where ρ_m is the minimum VSWR desired which has to be greater than unity.
Following the previously outlined approach:

$$Z_z = \sqrt{\frac{\rho_m Z_o^2 + X_A^2}{\rho_m - 1}} \quad (13)$$

and

$$\theta_z = \tan^{-1} \sqrt{(\rho_m - 1)\left[1 + \rho_m (\rho_m - 1)\left(\frac{Z_o}{X_A}\right)^2\right]} \quad (14)$$

Like the final section of the line coupler, the design of a SPDT switch also relies on a minimum mismatch solution. Taking the T-junction discontinuities into account, the values of Z_Z and θ_Z (Eqs. 13 and 14) can be used to find the unknowns for the branch containing the transformer. Completing the calulations yields two new unknowns:

$$Z_w = \eta \sqrt{\frac{\eta^2 X_B^2}{\eta^2 - 1} + Z_o^2} \quad (15)$$

$$\theta_w = \tan^{-1} \left\{ (\eta^2 - 1) \left[1 + (\eta^2 - 1)\left(\frac{Z_o}{\eta X_B}\right)^2\right]^{1/2} \right\} \quad (16)$$

where Z_w and θ_w represent the characteristic parameters of a length of line that will match the branch with the transformer.

Using the two sets of design equations, a branch-line coupler and SPDT switch were fabricated and evaluated to test the validity of the approach. Both the coupler and the switch were designed for Ku-band operation with results closely tracking predictions. The coupler's performance, fully detailed in Fig. 4, showed a maximum 4-dB insertion loss at 18 GHz with 20-dB minimum isolation across a 16 to 18 GHz band. The SPDT switch, designed for a 15.5 to 17.5 GHz band, exhibited less than 3-dB loss across the entire frequency range (Fig. 5). ••

References

1 W. H. Leighton, Jr., and A. G. Milnes, "Junction Reactance and Dimensional Tolerance Effects on X-band 3-dB Directional Couplers, *"IEEE Trans. Microwave Theory Tech.*, Vol. MTT-19, pp. 818-824, (October, 1971).
2 H. M. Altschuler and A. A. Oliner, "Discontinuities in the Center Conductor of Symmetric Strip Transmission Line," *IRE Trans. Microwave Theory Tech.*, Vol. MTT-8, pp. 328-339, (May, 1960).
3 Lewin, L., "Radiation from Discontinuities in Stripline," *Proc. IEEE (London)*, Vol. 107, Pt. C, pp. 163-1, (February, 1960).
4 J. Reed and G. J. Wheeler, "A Method of Analysis of Symmetrical Four-Port Networks," *IRE Trans. Microwave Theory Tech.* (Special Assy: Symp. Microwave Techniques), Vol. MTT-4, pp. 246-252. (Oct., 1, 1965).
5 J. L. Altman, *Microwave Circuits*, New York, D. Van Nostrand Company, Inc., (1964), pp. 72-133.
6 R. V. Garver, "Theory of TEM Diode Switching," *IRE Trans. Microwave Theory Tech.*, vol. MTT-9, pp. 224-238, (May, 1961).

Careful MIC Design Prevents Waveguide Modes

Channels protect and isolate suspended substrate transmission lines, but also propagate unwanted waveguide modes. This calculator program provides cutoff frequency based on dimensions and substrate material.

RECENT years have seen the advent of the "supercomponent" approach to circuit design—large-scale integration of microwave devices on a single printed-circuit substrate. The development of complex assemblies within a single package has led to significant improvements in performance as well as important size reductions.[1] Precautions must be taken, however, to avoid unwanted coupling between adjacent transmission lines and components. This design aspect becomes particularly important in X and Ku bands.

Suspended substrate transmission lines are isolated by placing them within a channel milled in a metal block (Fig. 1). Selection of both depth and width of the channel is important. Dimensions must be sufficiently small to avoid propagation of waveguide modes within the channel: these modes would actually produce the unwanted coupling one is trying to prevent. On the other hand, if the channel dimensions are too small, the propagation characteristics of the transmission line itself would be significantly modified. Remember that these lines are often designed and measured in the absence of packaging.

Little information is available concerning the selection of the channel dimensions needed to avoid moding. For instance, one "rule of thumb" method utilizes increments of the experimentally determined magic number of 3 mm.[1] While a complete study of the suspended-substrate structure shown in Fig. 1 would be rather involved, considerable information can be gathered by considering the simplified geometry of Fig. 2. The cutoff frequencies of the waveguide modes in this structure can be calculated exactly,[2] and provide an approximation for the channel modes in suspended substrate line.

Theoretical studies[2] have considered the case of an H-plane slab of dielectric, centrally located within the waveguide. The dominant waveguide mode can be either the first longitudinal-section magnetic (LSM_{11} or quasi-TE_{10} mode), or the distorted TE_{01} mode, depending on the dielectric permittivity and guide dimensions. The cutoff frequencies of these two modes are obtained from transcendental equations for the LSM_{11} mode,

$$\epsilon_r p_a \tanh (p_a d) - p_d \tan (p_d t/2) = 0 \qquad (1)$$

where:

$$p_a = \sqrt{(\pi/a)^2 - (\omega/c)^2}$$

$$p_d = \sqrt{\epsilon_r (\omega/c)^2 - (\pi/a)^2}$$

$$d = (b - t)/2$$

Fred E. Gardiol, Professor, Ecole Polytechnique Fédérale, Chemin de Bellerive 16, CH-1007 Lausanne, Switzerland.

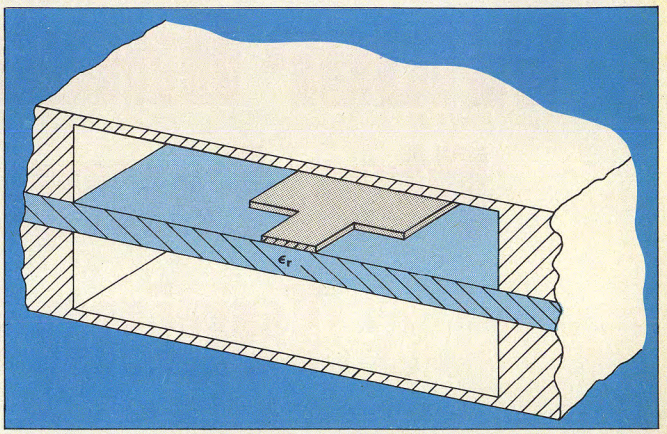

1. Metal channels *support and isolate suspended substrate transmission line.*

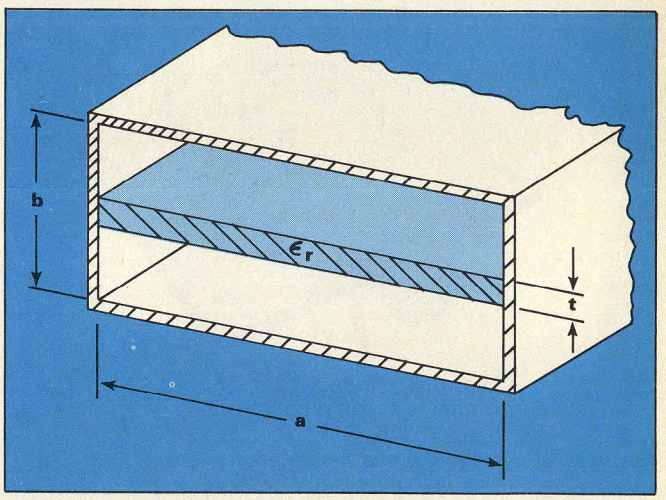

2. A slab-loaded waveguide *is a good approximation of an MIC package.*

The cutoff frequency for the LSM_{11} is obtained by an iterative process using the relation,

$$f_{n+1} = \frac{1}{5}\left[4f_n + \sqrt{f_d^2 + \frac{1}{\beta^2}\left\{\tan^{-1}\left(\frac{\epsilon_r p_a}{p_d}\tanh p_a d\right)\right\}^2}\right] \qquad (2)$$

For the TE_{01} mode,

$$\sqrt{\epsilon_r} \tan (p_d t/2) \tan (p_a d) - 1 = 0$$

where:

$$p_d = (\omega/c)\sqrt{\epsilon_r}$$

$$p_a = \omega/c$$

(continued on p. 190)

CUTOFF: A calculator program for MIC design

```
001   *LBL A
      RAD
      √X
      STO I        √εr in I
      R ↓
      STO 3        t in 3
      R ↓
      STO 2        b in 2
      R ↓
010   STO 1        a in 1
      RCL I
      X²
      1/X
      1
      —
      CHS
      STO 6
      RCL 3
      RCL 2
020   :
      STO x 6
      RCL 6
      1
      —
      CHS
      √X
      STO 6        √(1-(t/b)(1-1/εr)) in 6
      π
      3
030   0
      0
      :
      STO x 3
      STO x 2
      RCL 3
      STO - 2      α in 2
      RCL I
      STO x 3      β in 3
      1
040   5
      0
      ENTER ↑
      RCL 1
      :
      STO 4        fa in 4
      STO 9
      ENTER ↑
      RCL I
      :
050   STO 5        fd in 5
      1
      .
      0
      5
      x
      STO C        1.05 fd in C
      0
      .
      9
060   5
      STO x 9      0.95 fa in 9
      RCL 4
      RCL 6
      x            approximate f0
      ENTER ↑
      ENTER ↑
      RTN
      R/S
      *LBL C
070   R ↓
      R ↓
      STO A        fn in A
      RCL 2
      x
      TAN
      RCL I
      x            SEARCH LOOP
      1/X          FOR TE01
      TAN⁻¹        CUTOFF
080   RCL 3
      :
      RCL A
      +
      2
      :
      PSE          1 second pause
      ENTER↑
      ENTER ↑
      RCL A
090   % CH
      ABS
      0            test on
      .            frequency
      0            change
      1            change
      X≤Y ?
      GTO C        end of search loop
      R ↓
      R ↓
100   ENTER ↑
      ENTER ↑
      RTN
      R/S
      *LBL B
      R ↓
      R ↓
      RCL 4        TESTS TO AVOID
      X⇄Y          ERRORS IN
      X>Y ?        SQUARE ROOTS
110   RCL 9
      RCL 5
      X⇄Y
      X≤Y ?
      RCL C
      STO A        fn in A
      X²
      CHS
      RCL 4
      X²
120   +
      √X
      RCL 2
      x
      STO 6
      RCL A
      X²
      RCL 5
      X²
      —
130   √X
      RCL 3        SEARCH
      x
      STO 7        LOOP
      RCL 2
      x            FOR
      RCL 6
      :            LSM11
      RCL 3
      :            CUTOFF
140   RCL I
      :
      STO 8
      RCL 6
      2
      x
      CHS
      eˣ
      1
      —
150   ENTER ↑
      ENTER ↑
      2
      +
      :
      CHS
      RCL 8
      :
      TAN⁻¹
      RCL 3
160   :
      X²
      RCL 5
      X²
      +
      √X
      RCL A
      4
      x
      +
170   5
      :
      PSE          1 second pause
      ENTER ↑
      ENTER ↑
      RCL A
      % CH
      ABS
      0
      .
180   0            test on
      1            frequency
      X≤Y ?        change
      GTO B        end of search loop
      R ↓
      R ↓
      ENTER↑
      ENTER ↑
      RTN
      R/S
```

The iterative relation used to determine the cutoff frequency for the TE_{01} mode then is:

$$f_{n+1} = \frac{1}{2}\left[f_n + \frac{1}{\beta}\tan^{-1}\{1/(\sqrt{\epsilon_r}\ \tan\ \alpha f_n)\} \right]$$

Where, for Eqs. 2 and 4:

$$\alpha = \pi\ (b - t)/300 \qquad \beta = \pi\sqrt{\epsilon_r}\ \ t/300$$
$$f_a = 150/a \qquad f_d = 150/(\sqrt{\epsilon_r}\ a)$$
$$p_a\ (b\text{-}t)/2 = \alpha\sqrt{f^2_a - f^2_n} \qquad p_d t/2 = \beta\sqrt{f^2_n - f^2_d}$$

The cutoff frequencies for various situations are shown in Fig. 3 as a function of substrate permittivity. The effect of the filling ratio (t/b) for a fixed height-to-width ratio (b/a) is shown in Fig. 3(a); in Fig. 3(b), the b/a ratio varies and the t/b ratio is kept constant. The cutoff frequency, in both instances, is normalized with respect to the TE_{10} mode cutoff frequency ($f_{de} = c/2a$) in an empty rectangular waveguide of width a. The dotted lines refer to the approximate relation for waveguide cutoff ventured by Schneider:[3]

$$f_0 = \frac{c}{2_a}\sqrt{1 - \frac{t}{b}\left[\frac{\epsilon_r - 1}{\epsilon_r}\right]}$$

where c is the velocity of light and ϵ_r the relative permittivity of the dielectric board. The dimensions a, b and t are defined in Fig. 2.

Figure 3 illustrates that, for low values of substrate permittivity, the lowest waveguide mode cutoff is that of the LSM_{11}. In this case, the curves follow closely the approximate value of Schneider and, in fact, remain fairly close to the empty waveguide cutoff value. For heavier loading, however, the TE_{01} mode becomes dominant and significantly lower cutoff frequencies are observed. The crossover point between the two modes depends upon the geometry.

The strategy to apply in order to avoid channel waveguide modes depends strongly on which mode is dominant. The cutoff of the LSM_{11} mode is increased by reducing the width of the waveguide, but is less affected by a reduction in height. On the other hand, a reduction in height raises the TE_{01} cutoff frequency.

A computer program was prepared for the iterative resolution of these equations on an HP 67 or HP 97 calculator. The program allows the cutoff frequencies of the two modes to be rapidly determined for any combination of dimensions and dielectric. Armed with this information, one can determine the dimensions of the transmission-line channel in such a way that moding phenomena do not appear.

The complete program is listed as "CUTOFF: A calculator

program for MIC design". Input data are introduced as follows:

- value of a in mm: ENTER ↑
- value of b in mm: ENTER ↑
- value of t in mm: ENTER ↑
- value of ϵ_r

Pressing A then yields the approximate cutoff frequency (in GHz) given by Eq. (15) which is used as the starting point for the iterative search of the exact solution. *This is a necessary step.* If a better approximation is available, it can be introduced at this point, and followed by pressing the ENTER button twice.

Pressing B yields (after some calculation time) the cutoff frequency in GHz of the LSM_{11} mode (Eq. 2). The pauses, approximately one second long, permit the calculator to examine the intermediate values in the calculation and determine if the iteration is converging correctly.

Pressing C yields, in a similar fashion, the cutoff frequency in GHz for the TE_{01} mode (Eq. 4).••

References

1. S. V. Bearse, "Supercomponents Come Of Age," *MicroWaves*, Vol. 15, No. 2, pp. 36-43, (December, 1976).
2. F. E. Gardiol, A. S. Vander Vorst, "Wave Propagation In A Rectangular Waveguide Loaded With An H-Plane Dielectric Slab," *IEEE Transactions Microwave Theory Techniques*, Vol MTT-17, No. 1, pp. 56-57, (January, 1969).
3. M. V. Schneider, "Millimeter-Wave Integrated Circuits," *Proceedings Of the 1973 IEEE G-MTT International* Microwave Symposium, Boulder, CO, pp. 16-18, (June, 1973).

3. Cutoff frequency of the dominant mode, *(LSM_{11} or TE_{01}) varies with substrate dielectric permittivity. By holding waveguide dimensions in a constant ratio (b/a = 0.5), one can see the influence of substrate thickness (a). Likewise, if the waveguide height to substrate thickness ratio is constant (t/b = 0.2), the behavior of waveguide ratios other than 2:1 is seen.*

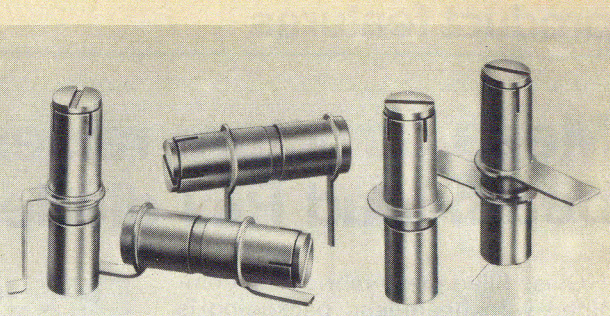

GIGA-TRIM CAPACITORS FOR MICROWAVE DESIGNERS

GIGA-TRIM (gigahertz-trimmers) are tiny variable capacitors which provide a beautifully straightforward technique to fine tune RF hybrid circuits and MIC's into proper behavior.

APPLICATIONS

- Impedance matching of GHz transistor circuits
- Series or shunt "gap trimming" of microstrips
- External tweaking of cavities

Available in 5 sizes and 5 mounting styles with capacitance ranges from .3 - 1.2 pf to 7 - 30 pf.

Johanson®

MANUFACTURING CORPORATION
Rockaway Valley Road
Boonton, N.J. 07005
(201) 334-2676 TWX 710-987-8367

READER SERVICE NUMBER 60

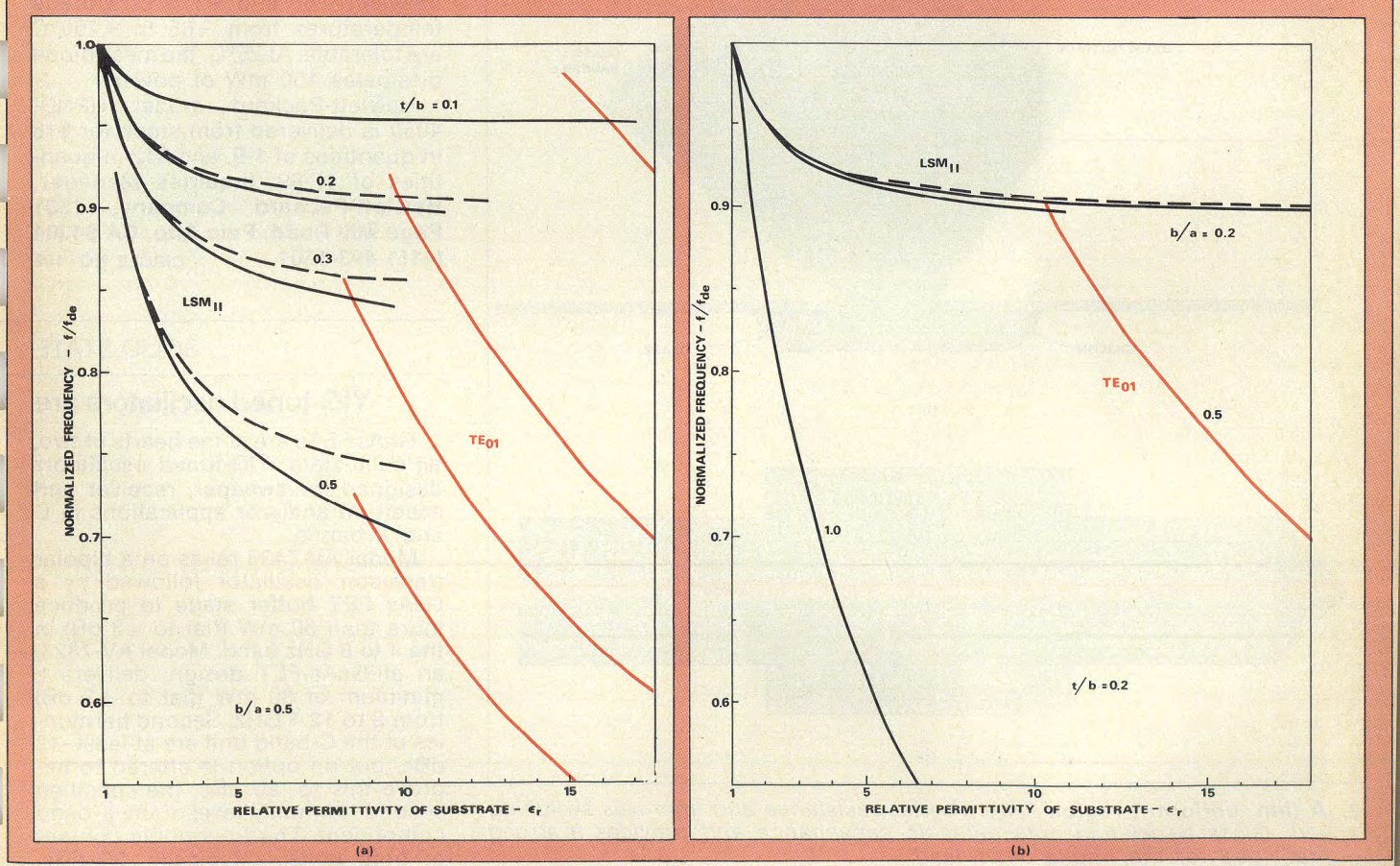

Mesa structure raises beam-lead PIN diode performance

Glass-filled mesa fabrication combined with beam-lead packaging is the secret behind the low series resistance and fast recovery time specifications of a new generation of PIN diodes from Hewlett-Packard. Typical series resistance of 1.3 ohms, a recovery time in the order of 2 ns and an RC product of 0.16 ps make the device an ideal shunt switching element in microstrip and stripline circuits.

Conventional planar PIN diodes are characterized by relatively long minority carrier lifetimes and reverse recovery times due to unequal carrier path lengths in the I region. In HP's new fabrication technology, a mesa structure provides a uniformly thin I region, resulting in minority carrier lifetime of 15 ns and reverse recovery time of 2 ns. This improvement in recovery time meets requirements for most fast-acting switches, modulators and attenuators. At low current, the beam-lead PIN diode exhibits lower series resistance (1.3 ohms @ 10 mA) making it ideal for applications using the diode in shunt configurations.

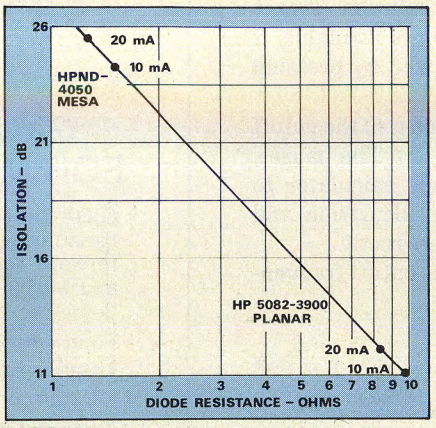

***1. Lower series resistance** gives the mesa device an edge in isolation over typical planar diodes.*

As a series switch, the mesa beam-lead PIN diode with lower R_S, offers lower insertion loss than planar types. Lower I^2R losses in the diode allows greater power handling, but C_T causes lower isolation. Used as a shunt switch, the mesa beam-lead PIN diode improves isolation due to lower R_S at a given bias current. The diode is limited at higher frequencies because the higher C_T causes greater insertion loss (0.55 dB @ 18 GHz).

Immunity from contaminants is provided by a nitride passivation layer. During handling and assembly, protection from scratches is afforded by a deposited glass layer. Glass backfilling reduces parasitic capacitance and provides an exceptionally high lead pull strength of 4 grams. The mesa beam-lead PIN diode operates through a range of temperatures between −65 and +175°C. Storage temperatures from −65 to +200°C are tolerable. At 25°C, the mesa diode dissipates 150 mW of power.

Hewlett-Packard model HPND-4050 is delivered from stock for $16 in quantities of 1-9, and $12 in quantities of 10-99. **Inquiries Manager, Hewlett-Packard Company, 1501 Page Mill Road, Palo Alto, CA 94304 (415) 493-1501.** CIRCLE NO. 109

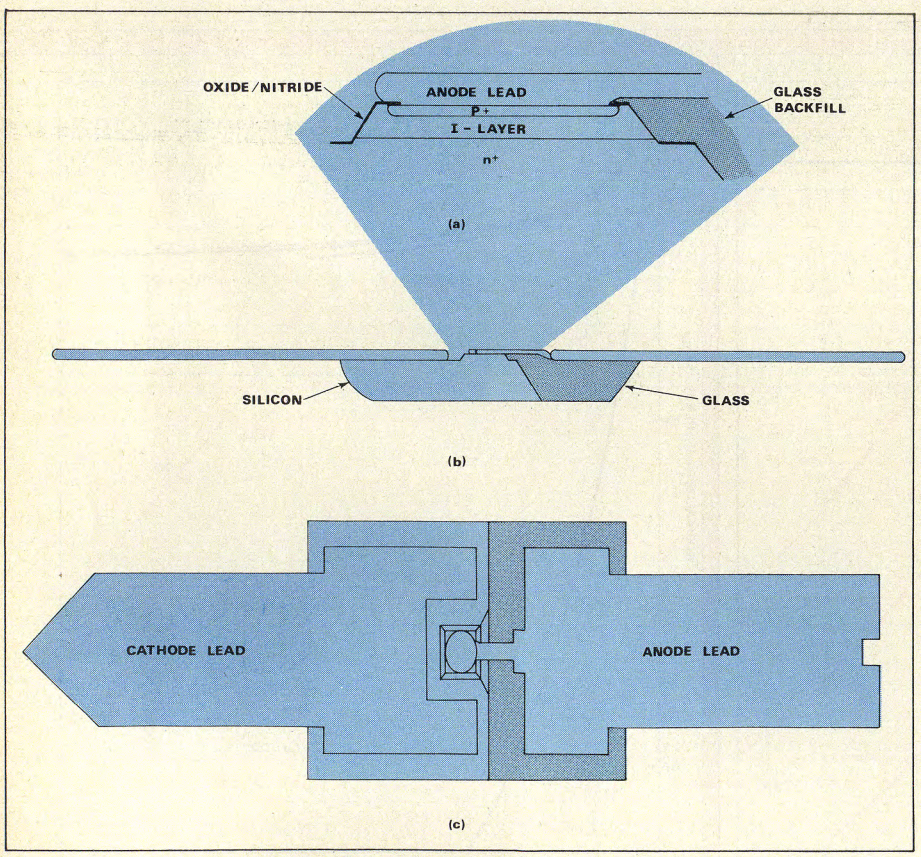

***2. A thin, uniform I region** lowers series resistance and improves switching speed. Glass backfilling cuts parasitic capacitance and provides a strong contact pad for the fragile beam lead.*

SOLID-STATE

YIG-tuned oscillators are

GaAs FETs are at the hearts of two, all solid-state, YIG-tuned oscillators designed for sweeper, receiver and spectrum analyzer applications in C and X bands.

Model AV-7433 relies on a bipolar transistor oscillator followed by a GaAs FET buffer stage to produce more than 50 mW (flat to ±3 dB) in the 4 to 8 GHz band. Model AV-7823, an all-GaAs-FET design, delivers a minimum of 30 mW (flat to ±2 dB) from 8 to 12.4 GHz. Second harmonics of the C-band unit are at least -12 dBc, but an option is offered to improve this to -20 dBc, the specified second-harmonic level of the X-band component. Third-harmonic content of both units is typically -30 dBc,

JUNE
1977

MICROWAVES

laser technology

BALANCED TRANSISTORS

A New Horizon For Amplifier Design

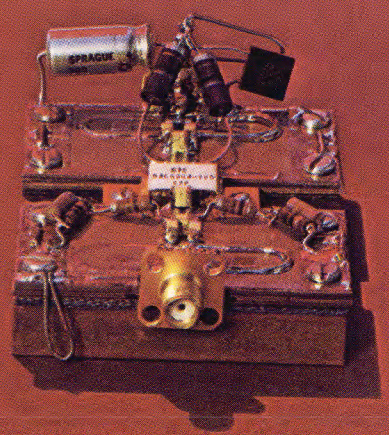

COMPUTER-AIDED DESIGN

CAD: Maturity Brings Flexibility

Computer Modeling Speeds Circulator Design

Also: Modified backfire cuts cross-polarization ■ GaAs FETs gain ground in oscillators, mixers and limiters

MICROWAVES

June 1977
Vol. 16, No. 6

news

9 GaAs FETs gain ground in oscillators, mixers and limiters
12 Superconductor may be the new RF attenuation standard
14 Ku-band front-ends shrink to meet big demands
17 British hope to be first with commercial fiber optics
Power transistor elevates emitters
18 Industry
21 Washington
26 International
28 Meetings
36 R & D
38 For Your Personal Interest. . .

editorial

40 Indecision could sink a global MLS standard

technical

42 **Balanced Transistors: A New Option For RF Design.** Lee B. Max of Communications Transistor Corp., introduces a new type of transistor that bonds chips in series for higher power over broader bandwidths.

49 **CAD: Programs grow in flexibility as designers learn about optimization.** A survey of computer-aided circuit design in the microwave industry reveals a renaissance in sophistication, flexibility and acceptance. Designers are regaining confidence in optimization by investing more time in basic analysis.

54 **Speed Circulator Design With Computer Modeling.** G.W. Renken of Honeywell Corp., derives a mathematical model for circulator design, and applies it to the problem of realizing MICs on ferrite substrates.

70 **Modified Backfire Lowers Cross-Polarization Levels.** Dr. A. Kumar of Queen Mary College, and Dr. Ing. H. D. Hristov of the Bulgarian Higher Institute of Mechanical and Electrical Engineering, modify a long backfire antenna with a small strip reflector to permit operation in two discrete frequency bands with low cross-polarization.

departments

74 Application Notes
75 New Products
82 Feedback
83 New Literature
84 Catalog Update
87 Advertisers' Index
88 Product Index

About the cover: The sun rises on a new concept in RF transistor design: The balanced bipolar. The new devices have two inputs and two outputs, and demand a new approach to circuit design. See page 42 for details. Cover design and photography by Art Director Robert Meehan; devices courtesy of Communications Transistor Corp.

coming next month: Sources

GaAs FET oscillators: A look at their design and application. GaAs FET sources are attractive alternatives to TEOs at frequencies to Ku-band. High efficiency, low voltage requirements and simple heat sinking are just a few advantages. Here's how to select a device, design a circuit and specify a source for system applications.

Design waveguide cavity oscillator with computer analysis. A unified approach to oscillator design using computer analysis allows the designer to juggle 23 critical parameters to arrive at a near optimum circuit. The method is applicable to waveguide circuits from L through Q bands with any type of two-terminal negative resistance device.

VCO subsystems: What to test, how to test it (Part II). This concluding installment addresses the difficult problem of making transient measurements.

Publisher
Howard Bierman

Editor
Stacy V. Bearse

Washington Editor
Paul Harris
Snyder Associates
1050 Potomac St. NW
Washington, DC 20007
(202) 965-3700

Editorial Assistant
Gail Murphy

Production Editor
Sherry Lynne Karpen

Art Director
Robert Meehan

Art Illustrator
Janice Tapp

Production
Dollie S. Viebig, Mgr.
Anne Molfetas

Circulation
Barbara Freundlich, Dir.
Sherry Karpen,
Reader Service

Directory Coordinator
Janice Tapp

Editorial Office
50 Essex St.,
Rochelle Park, NJ 07662
Phone (201) 843-0550
TWX 710-990-5071

A Hayden Publication
James S. Mulholland, Jr.,
President

MICROWAVES is sent free to individuals actively engaged in microwave work. Prices for non-qualified subscribers:

	1 Yr.	2 Yr.	3 Yr.	Single Copy
U.S.	$25	$40	$ 60	$3.00
Foreign	$40	$70	$100	$4.00

Additional Product Data Directory reference issue, $15.00 each (U.S), $27.00, (Foreign). POSTMASTER, please send Form 3579 to Fulfillment Manager, MicroWaves, P.O. Box 13801, Philadelphia, PA. 19101.

Back Issues of MicroWaves are available on microfilm, microfiche, 16mm or 35mm roll film. They can be ordered from Xerox University Microfilms, 300 North Zeeb Road, Ann Arbor, MI 48106. For immediate information, call (313) 761-4700.

Hayden Publishing Co., Inc., James S. Mulholland, President, printed at Brown Printing Co., Inc., Waseca, MN. Copyright © 1977 Hayden Publishing Co., Inc., all rights reserved.

Balanced Transistors: A New Option For RF Design

Yes, the RF transistors on this month's cover have two inputs and two outputs! Their balanced design places two chips in a series circuit to boost input and output impedances by a factor of four.

DEVICE designers have traditionally relied on refinements in semiconductor technology to nudge the microwave bipolar transistor to higher and higher power levels. Today, however, it is no longer semiconductor technology that limits RF transistor power levels available for many applications. In most cases, the transistor vendor can still place even larger silicon chips in a given package. By doing so, however, he produces a device with extremely low input and output impedance levels, limiting high-power performance to relatively narrow bandwidths.

A new concept in microwave transistor design, called the *balanced transistor*, overcomes this handicap by increasing input and output impedances by a factor of four compared with conventional bipolars using the same size transistor chip. The balanced device is easier to assemble, has fewer internal parts and offers better efficiency than conventional devices. Most impressive of all is that the balanced transistor for the first time allows octave and multioctave bandwidths with 100 watts of continuous power output. Experimental devices now under evaluation include:

- 125 watts, CW, over 225 to 400 MHz
- 100 watts, CW, from 750 to 1000
- MHz
- 80 watts, CW, from 500 to 1000
- MHz

Two other devices are currently finding applications in the field. (circle reader service no. 153 for more information):

- 100 watts, CW, from 30 to 400 MHz
- 100 watts, CW, from 90 to 500 MHz

The conventional approach to designing a higher power transistor is essentially to combine more transistor cells in parallel within a package (Fig. 1(a)). This leads directly to ever lower input and output impedances. One alternative to combining in parallel is to combine in series (See Fig.1(b)). This approach has many advantages. For the same power delivered and the same resistor value R, the resultant impedance level achieved by combining in series (Z_s) is four times the impedance available from combining in parallel (Z_p), or $Z_s = 4\ Z_p$.

Lee B. Max, Director, Military and SSB Products, Communications Transistor Corporation, 301 Industrial Way, San Carlos, CA 94070.

To relate this to the design of higher power microwave transistors, consider the RF chip as being split into two equal halves. With the conventional approach, these halves would be combined in parallel. Using the balanced transistor concept, these halves would be combined in series to present four times the impedance available from the conventional approach. Combining the chips in series, however, requires that the two transistor halves be operated 180 degrees out of phase (see Fig. 2). External networks on the input and output of the device drive the two chips in a balanced (push-pull) mode of operation.

In-package RF ground opens new doors

In addition to the increased impedance levels, an RF ground is created inside the package (see Fig. 2). This is forced automatically by the external balanced circuitry. The result is that the common lead from the package is only a DC connection and thus, a non-critical external circuit connection. The critical low-impedance RF ground is totally self-contained within the transistor package.

A packaged device would then have two input leads and two output leads as opposed to the conventional device which

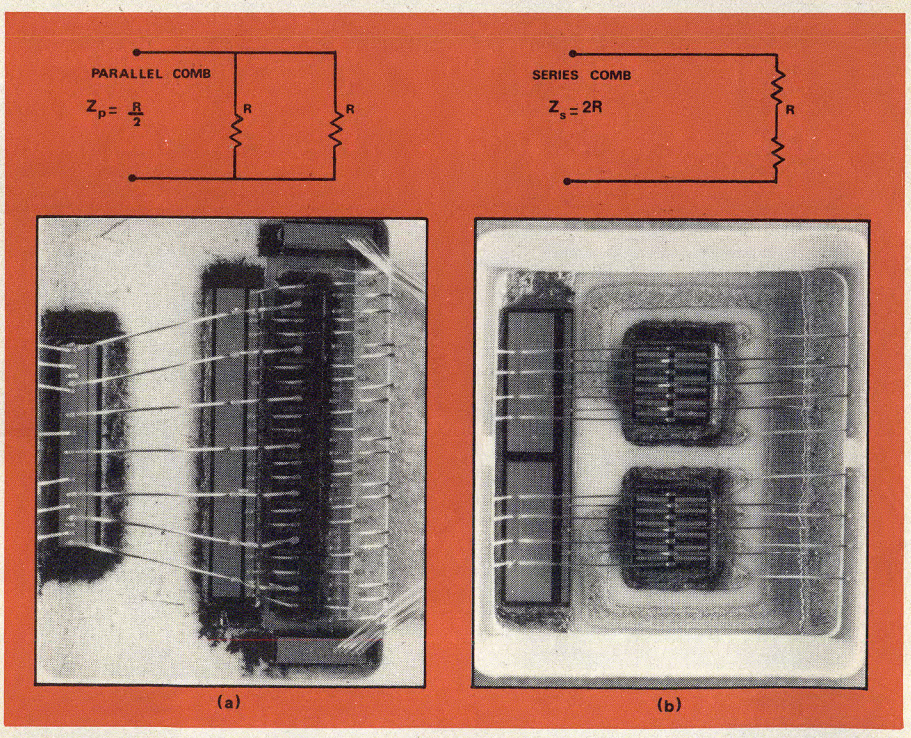

***1. The traditional approach** to designing higher-power transistors is to bond a greater number of cells in parallel (a). By arranging two chips in series, however, input impedance is increased by a factor of four (b).*

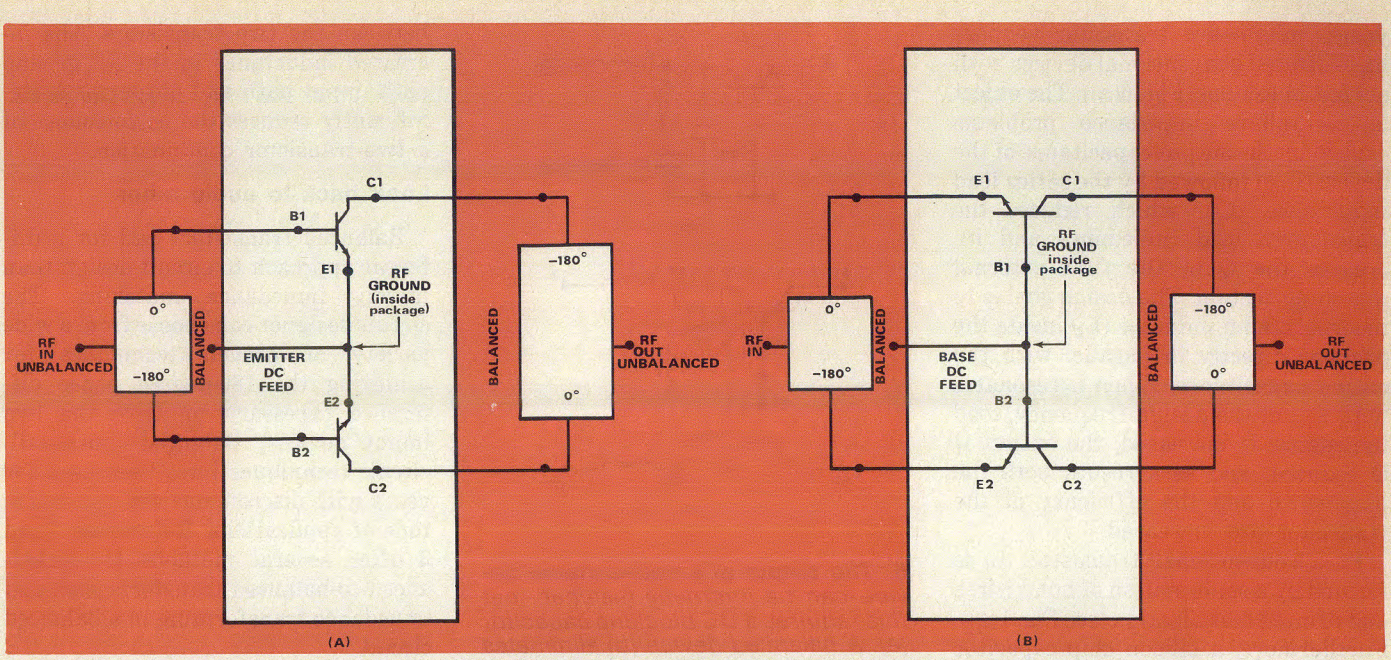

2. Common-emitter (a) and common-base (b) *balanced transistors have two inputs and two outputs. External circuitry must drive the inputs and combine the outputs 180 degrees out of phase.*

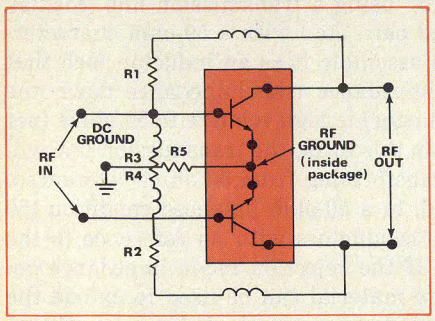

3. Since RF ground is established within the package, *the emitter ballast resistor (R5) of this class-A circuit need not have an RF bypass.*

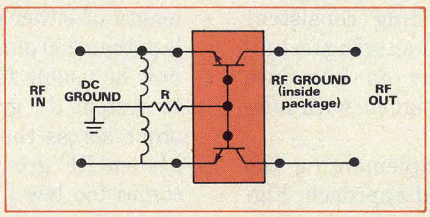

4. High-power common-base circuits may be reverse-biased *by inserting resistance between base leads and DC ground.*

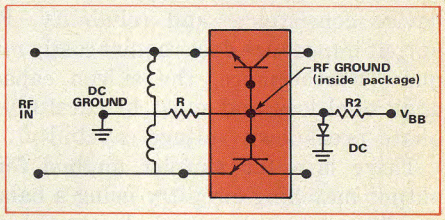

5. High-power, common-base circuits may be forward-biased *with circuitry commonly used with common-emitter designs.*

has one of each. All leads on the new package are electrically isolated from the flange. The electrical connections are all made on the top side of the circuit board. Since there is no low-impedance RF ground path through the flange, the mounting of the transistor package and the circuit board are less critical.

The unique RF ground aspect of the balanced transistor offers several bias options for using RF power transistors that were not previously available. For example, external emitter ballast can be used to operate high power, common emitter devices in class-A operation (Fig.3). Since RF ground is already established inside the package, the emitter ballast resistor (R5) need not be RF bypassed. With this extra (DC only) emitter resistance, it is now possible to use the simple resistive networks that have, in the past, provided excellent thermal stability for high-power, class-A audio transistors. There is no need for fancy constant current circuitry or active device bias schemes.

Another new option created by the balanced device is the ability to reverse-bias high-power, common-base circuits (Fig. 4). The designer must simply put a resistor between the base leads and DC ground (RF ground is established within the package)! This is a far easier option than the conventional method of adding DC resistance in the emitter path. For example, a 0.1-ohm, 2.5-watt resistor would be necessary to provide 0.5-volt reverse bias on a device running with a collector current of 5-amperes. The same bias point on a balanced device could be achieved by placing a 5-ohm, 0.05-watt resistor between the base and DC ground (DC β is assumed to be 50). The larger resistor between emmitter and base would improve low-frequency stability.

A third important advantage of in-package grounding is brought out by the circuit in Fig. 5. Note that it is possible to easily forward bias high-power, common-base devices with the same simple DC circuitry that has been used with high-power, common-emitter devices for years. This is possible with a balanced transistor since all DC connections for the emitter, base and collector can be made at points of RF ground.

Easier internal output matching

Still another simplification offered by the balanced approach to transistor design is the implementation of output matching within the device's package. For the past several

(continued on p. 44)

years, microwave transistor vendors have offered conventional devices with output matching (Fig. 6(a)). The object is to relieve impedance problems caused by the output capacitance of the device (C_{oB}) followed by the series lead inductance (L_c), which reduces the transistor's load impedance and increases the Q of the first external matching section. The design goal is to incorporate an inductor (L_l) inside the package directly in parallel with the output capacitance. When L_l resonates with C_{oB} at the design frequency, load impedance is increased, the output Q is reduced, and as a result, both the bandwidth and the efficiency of the transistor are increased.

In a conventional transistor, L_l is formed by a combination of bond wires and printed metalization (see Fig. 1(a)). Furthermore, a silicon chip capacitor group (C_l) must be introduced to DC block the collector from ground. This assembly structure for output matching functions admirably and is used by all microwave transistor vendors, but it does have its drawbacks. Due to the extra components and the increase in complexity of assembly, there are added concerns about device consistency and reliability. Providing consistent output impedance does require costly manufacturing techniques. Furthermore, the silicon capacitors do introduce additional loss and must be carefully designed with adequate breakdown voltage capability.

There is a far simpler method for implementing the output matching circuitry using a balanced approach. Figure 6(b) shows that an inductor (L) can be introduced in parallel with the total device output capacitance by connecting the collector of one side of the device (C_1) to the collector of the other side (C_2). Since both collectors are at the same DC level, no capacitor is required for blocking. Figure 1(b) shows that the entire output matching circuitry (L) can be a printed line on the ceramic substrate connecting one collector pad to the other. With the entire inductor metalized on the ceramic, it is well heat sunk and free of thermal problems. Obviously, there are no additional bond wires or capacitors and no added assembly steps.

The advantages available by using the balanced transistor concept may initially seem achievable by using two discretely packaged transistors. This, however, is not realizable due to the added inductance resulting from the physical distance between the two transistors. The increased inductance in the RF ground path, input path and output path significantly reduces the performance of a two-transistor combination.

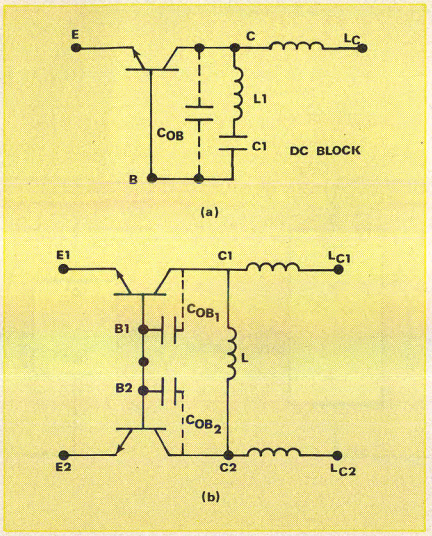

***6. The output of a conventional device** can be internally matched, but this requires a DC blocking capacitor (a). A balanced device (b) eliminates this requirement since both collectors are at the same DC level.*

Look back to audio amps

Balanced transistors call for a different approach to circuit design than merely impedance matching. The circuit designer can choose from a wide variety of proven techniques for achieving the 180-degree phase difference necessary to drive the two imput devices. Balanced (push-pull) circuit techniques have been used for years with discrete devices in a multitude of applications. References 1 and 2 offer several methods for unbalanced-to-balanced transformation and impedance transforming in a balanced circuit.

One very basic approach to creating a balanced condition starting in a 50-ohm system can be seen in Fig. 7. Start by using a transmission line (coaxial, parallel strip, twisted pair, etc.) with a 50-ohm characteristic impedance, and assemble it as an inductor such that the rejection-mode impedance (the impedance down the length of either conductor) is high relative to 50 ohms (not less than 250 ohms). In this form, the transmission line will now be usable for transforming from 50 ohms referenced, to system RF ground, to a 50-ohm balanced condition (50 ohms across the two conductors with no reference to the system RF ground). If the rejection mode impedance becomes too low (ferrite material can be used to extend the usable frequency range downward), the balanced condition will not be maintained and the circuit performance will be degraded.

The circuit shown in Fig. 8 employs a modified version of this coax transformer technique.[3] Fifty-ohm, semi-rigid coax is used, but it is intentionally made short resulting in a low rejection-mode impedance, which will appear as a shunt inductance to ground on one half of the balanced side of the transformer. However, the symmetry or balance can be regained if an equal inductance is placed from the other half to ground. This can be achieved by printing two identical shorted-stub transmission lines, as the schematic in Fig. 8 shows. Then, continuously solder the semi-rigid coax down to one stub and connect the center conductor

(continued on p. 46)

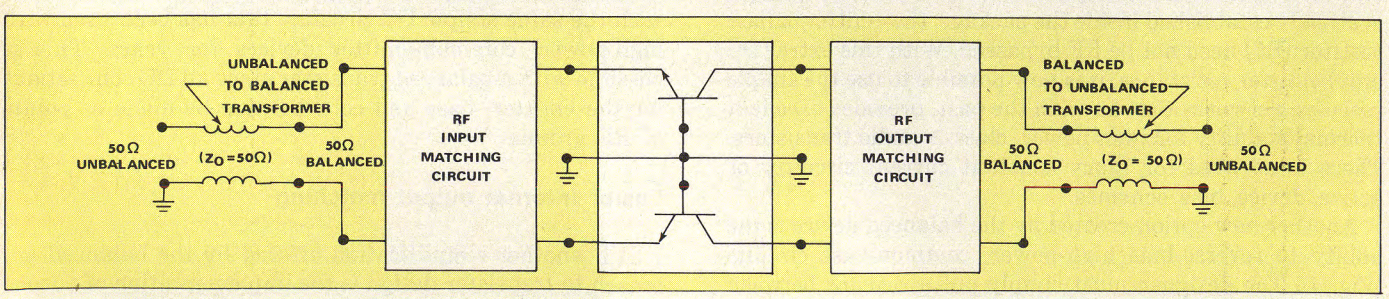

***7. A transmission line,** such as a coax cable, parallel strip or twisted pair, can be used to create balanced input and output circuitry.*

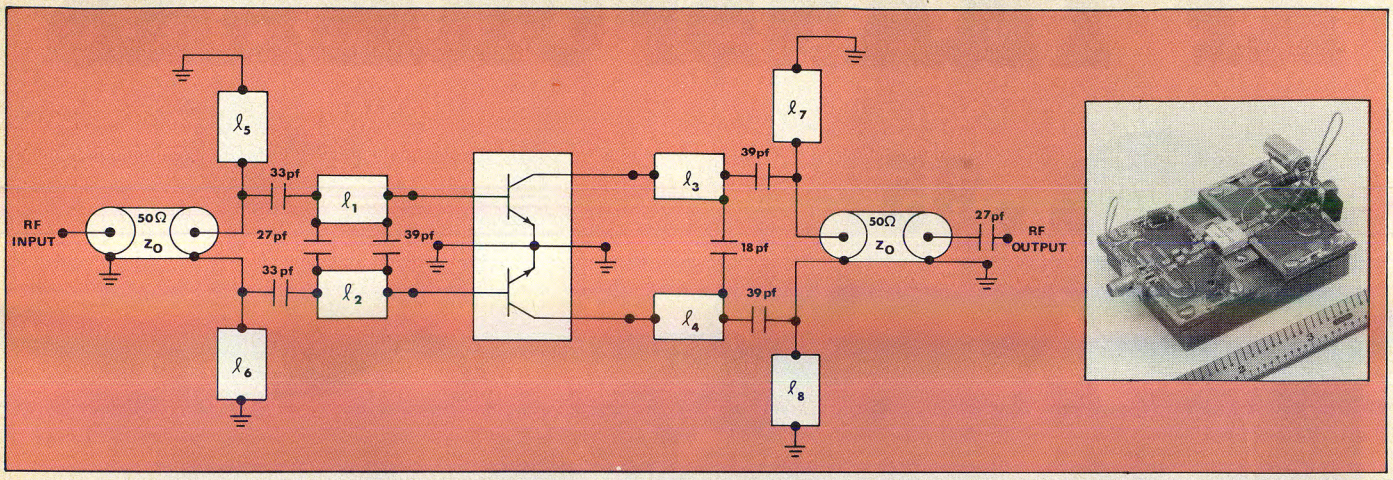

***8. Semi-rigid coax** is used as the transformer in this 125-watt, 225 to 400 MHz balanced circuit. The high-pass impedance transformer created by a combination of chip capacitors and strip inductors reduces the size of the coax transformers.*

of the coax across to the other stub. In effect, the printed stub controls the shunt inductance and, thus, makes it possible to have the same amount of shunt inductance on each half of the circuit. Instead of each half of the circuit providing 25 ohms purely real, each half presents 25 ohms real in parallel with an inductor.

By following the shunt inductance with a series capacitor on each half, a high-pass impedance transforming section is now created. Using this technique, the circuit can be designed to use ultra-short unbalanced to balanced transformers. The first impedance matching section and DC blocking are achieved in combination with the short transformers while maintaining the balanced state.

Once a balanced condition is achieved, impedance matching techniques are the same as with conventional transistors except that parallel matching components may be connected directly across the circuit.

To achieve maximum performance from a conventional transistor, zero-degree phase splitting and recombining occur inside the package. This is affected by factors inside the package that only the semiconductor vendor can control, such as the consistency of the die, resistive balancing, inductive balancing and symmetry of assembly. Maximum performance from a balanced transistor relates to a 180-degree phase split and recombination that occurs in the external circuit. The same factors that control the relative phasing inside the package of a conventional device, control relative phasing inside the package of the balanced device, but in addition, the circuit designer has control of the external combining circuitry.

Comparisons with the conventional

Comparisons between the performance of a balanced transistor that will soon be marketed and the closest conventional device may be appropriate. For over a year, a 100-watt CW, 225 to 400 MHz transistor (the CTC C2M100 -28A) has been available. The minimum collector efficiency wideband is 50 per cent at a 100-watt output; the device load impedance is approximately 2.5 ohms. The new 125-watt, balanced, output matched, UHF device has a load impedance of approximately 10 ohms and can operate with a minimum collector efficiency of 60 per cent. That means that the new balanced device will be dissipating less power while delivering 125 watts than the conventional device was dissipating while delivering 100 watts. Furthermore, the 10-ohm load impedance makes the impedance matching circuitry far simpler.

Since balanced (push-pull) circuit techniques are used with balanced transistors, harmonic distortion is less than with conventional devices. The even harmonic levels specifically are reduced. When covering an octave in bandwidth, the balanced device will offer approximately 20 dB lower second harmonic content than a conventional transistor.••

References

1. Octavius Pitzalis, T.P. Course, "Broadband Transformer Design For RF Transistor Power Amplifiers," *1968 Electronic Components Conference* Proceedings, (May, 1968).
2. C. L. Ruthroff, "Some Broadband Transformers," *Proc. IEEE*, Vol. 47, pp. 1337-1342, (August, 1959).
3. Lee B. Max, Communications Transistor Corporation's Application Note 2.2.8.8E, (September, 1974).

Redirect Your Career

Looking for a new way to apply your engineering skills? Invest ten seconds in this simple test:

YES	NO	
☐	☐	**I thrive on intellectual stimulation.**
☐	☐	**Travel turns me on.**
☐	☐	**I have a voice for self-expression.**
☐	☐	**The pen is mightier than the soldering gun.**
☐	☐	**My boss should send me to more tech conferences.**
☐	☐	**Broad horizons beat narrow knowledge.**
☐	☐	**State-of-the-art is where it's at.**

If you've checked YES for all statements, you might be the person we want to add to the staff of MicroWaves. We're looking for a graduate EE with basic writing skills, who is flexible enough to deal with all aspects of microwave technology. As an editor, you'll visit leading firms and labs, talk to the top people in the industry, and write stories aimed at the RF design engineer. If you're the person we're looking for, rush your resume to:

Stacy V. Bearse, Editor
MicroWaves
50 Essex Street
Rochelle Park, NJ 07662

transistors is compiled to form a data base, which may be addressed by satellite terminals distributed throughout the laboratory. Final tweaking is minimized since any circuit is designed around the measured performance of the actual device that will be soldered or bonded in place.

But the RCA data base is just a forerunner of what might come. RCA's Barry Perlman suggests that a tolerance analysis might be incorporated into the system that indicates how circuit characteristics are affected by variations in s-parameters. Alternately, the designer could specify a fixed circuit, and instruct the computer to search through the data base and select the best devices in inventory to provide performance within specified limits.

COMPACT recently incorporated a comprehensive transistor data bank, listing the design parameters of more than 120 devices from 13 manufacturers. Although this file is updated regularly, many designers polled by *MicroWaves* are somewhat skeptical about basing a final design on even the most current "data sheet" values. Even the COMPACT user's manual includes the statement, "Important: The databank contains representative data of "typical" devices and should not be interupted for specifications." It must be mentioned that Besser has approached transistor manufacturers with the idea of using data windows, but the firms were reluctant to provide such specifications.

Acceptance is still a problem

The CAD authorities polled by *MicroWaves* have differing views on optimization, measurement and in-house versus time-shared programming, but they at least seem to agree on the largest problem facing the growth of CAD today. And they identify this obstacle as you, the design engineer.

"Many engineers are convinced they need the tools which computer-aided design and analysis provides," comments Sergio Bernstein, "yet they do not know how, or cannot convince their management to "juggle" the accounting in some way and perform the greatest alchemist feat: That of transforming wasted internal dollars into a useful and productive development of CAD programs."

This problem of convincing management to invest in something as costly as computers and talented programmers, or as intangible as time-shared computer time has many perspectives, but they all seem traceable to (1) a misunderstanding of how the mechanics of computer-aided analysis, synthesis and optimization actually work, and (2) how these mechanics must economically combine with good engineering judgement in the RF design process.

COMPACT's Les Besser relates the not untypical tale of one circuit engineer who spent hundreds of dollars optimizing a relatively simple filter design. Naturally, the fellow's management was a bit upset over the matter, so the engineer turned back to Besser in an effort to keep CAD alive in that particular shop. Besser studied the problem for a few minutes, then demonstrated that the same optimized result could be reached with about $35 of computer time. The moral: The more you know about the programs you run, the more shortcuts you will find to analyzing complex problems. And it is these shortcuts, combined with sound design judgement, that will lower your computer costs.

"And so," summarizes Bernstein, "the current challenge for researchers and developers is maxi-computations with mini-computers and micro-budgets."••

Millimeter Sources from TRG

12.4 to 300 GHz

- fundamental oscillators to 65 GHz
- high power sources up to ½ watt
- varactor tuned GUNN oscillators
- high efficiency multipliers to 300 GHz

Need flatness? TRG GUNN oscillators are varactor tuned and offer ±0.25 dB (max power variation over ±100 MHz). For more bandwidth our ±200 MHz unit has a flatness level of ±0.4 dB.

Want high power? Our high power oscillators can deliver up to ½ watt over ±100 MHz mechanical tuning range with ±0.25 dB flatness.

Up there in frequency and bandwidth? The TRG series 9400 55 GHz GUNN oscillator has 4 GHz mechanical tuning with 50 mW power output and ±2dB flatness. For operating above 65 GHz, the TRG series 936 doublers and triplers develop 35% efficiency at up to 300 GHz. Call or write the Millimeter Team at TRG for more information.

TRG DIVISION Alpha **Our limits are your imagination.**

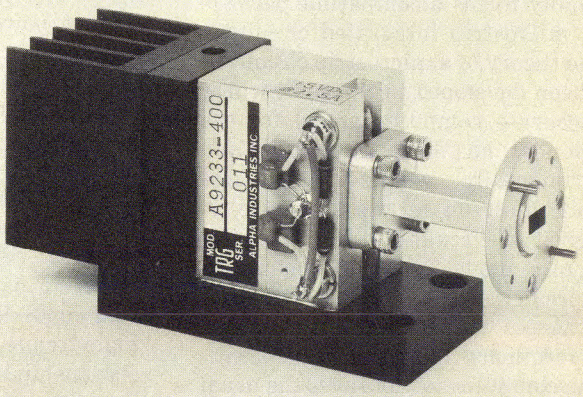

35 GHz, 400 mW GUNN Oscillator

ALPHA INDUSTRIES, INC. • 20 Sylvan Road, Woburn, Massachusetts 01801 • (617) 935-5150 • TWX: 710-393-1236 • TELEX 949436

READER SERVICE NUMBER 44

Speed Circulator Design With Computer Modeling

A comprehensive computer model provides a fast, cost-effective way to design microstrip junction circulators. But before the model is applied, be sure to have a grasp of the fundamentals.

MICROSTRIP junction circulators have found use recently within microwave integrated circuits. Circulators have been used in waveguide and stripline systems for much longer than in microstrip. These two package arrangements of the junction circulator, however, have been incompatible with that of the MIC. In the past, the circuit designer had to transition from microstrip to a waveguide or stripline packaged circulator then back to the microstrip substrate to use a circulator in an integrated circuit. Microstrip circulators eliminate such transition problems; they are easily made as part of the microstrip substrate layout.

There has also been work on the use of ferrites as the dielectric substrate in a microstrip system. Since circulators use ferrite in their operation, microstrip junction circulators built on a ferrite substrate are a natural combination of the microstrip substrate and the ferrite (see "Ferrite: An intriguing substrate for MICs"). Such an assembly forms a compatible package with microstrip integrated circuits.

The theory of a microstrip circulator has been developed to the point where an accurate computer model for the component has been developed, and experimentally verified. The test circuit, built on ferrite substrate, is designed to circulate at 5.0 GHz. The computer model provided dimensions and predicted performance; measured data agrees with the predicted circulation frequency to within 2 per cent.

The computer model saves the usual design iterations normally associated with a "cut-and-try" approach to circulator development. Aside from adjusting the magnetic bias on the circuit, no "tweaking" was necessary to achieve the close parity with theory.

G. W. Renken, P.E., Honeywell Corporation, Systems and Research Center, Millimeter-wave Group, 2600 Ridgway Parkway, Minneapolis, MN 55413.

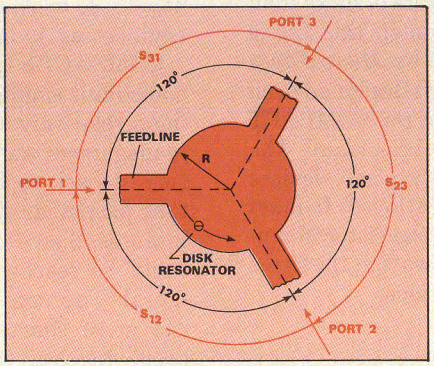

1. The familiar shape of a circulator is formed by three equally spaced radial lines eminating from a disk resonator.

The junction circulator is a non-reciprocal, three-port device used to control the flow of microwave power within a system. As shown in Fig. 1, any power incident at port 1 is transferred in its entirety to port 3 (S_{31} = 1). No power is delivered to port 2, (S_{21} = 0). When port 2 is made the incident power port, then all of the input power is delivered to port 1 (S_{12} = 1) and no power is delivered to port 3 (S_{13} = 0). The same non-reciprocal relationships between the scattering parameters hold between ports 1, 2 and 3, when port 3 is the input port.

For proper circulation, the relationships between the component's scattering parameters as given above must hold. In the ideal case, at the single frequency of circulation, f_c, this relationship holds exactly. As frequency moves away from f_c, the desired scattering matrix relationship will remain approximately as given above.

The acceptable bandwidth over which the scattering matrix departs from the ideal case, but for which the circulator works in the desired manner, is the isolation bandwidth. A good figure of merit is 20 dB or more of isolation over the isolation bandwidth.

This condition imposed on the circulator scattering parameters is aptly termed the circulation condition. In the circulator analysis that follows, this condition is used to derive the theoretical expressions for the circulator. The computer model of the microstrip junction circulator follows from these expressions. For proper operation, the junction circulator must simultaneously satisfy three conditions:

- The disk resonator of the circulator must resonate at the circulation frequency, f_c.
- The standing wave pattern within the disk resonator must be rotated sufficiently within the plane of the disk to satisfy the circulation condition.
- Feedlines to the disk resonator must match the resonator impedance to 50-ohm lines over the circulator's isolation bandwidth, and at f_c.

Load the disk properly

When any one of the three feedlines is used as input to the resonator, the disk will resonate at a frequency, f_c, largely determined by R, the radius of the resonator. If there is no load on the resonator, then R determines the resonant frequency of the disk. When the other two feedlines load the disk, the resonant frequency changes slightly due to feedline loading.

The disk resonates because the input power to it splits: Some of the power propagates clockwise rotating fields, while the remaining power propagates counter-clockwise rotating fields within the disk resonator. The sum of these two oppositely rotating fields produces a standing wave distribution in the θ direction within the plane of the disk, as shown in Fig. 2(a).

If the feedlines are not too wide, the resonator is lightly loaded and the standing wave pattern is easily maintained. There is equal power flow to

Ferrite: An intriguing substrate for MICs

The earlier microstrip junction circulators were designed using a ferrite puck placed under the disk resonator. A hole of the same diameter as the puck was machined into the substrate at the location of the circulator junction. The puck was fitted tightly into the hole. The substrate was then metallized, and the microstrip circulator pattern was etched into the metallized substrate. After etching, the circulator's disk resonator with the three radial feedlines coming into it remained on the substrate. The disk resonator was centered over the enclosed ferrite puck.

This approach to microstrip circulator design works well when the microstrip substrate is easily machined, and the ferrite puck can be made to fit tightly into the substrate hole. If a substrate such as quartz is used, the designer is faced with boring a hole into a brittle and fragile dielectric. Even if the quartz substrate is not broken when the hole is bored, there could likely be problems with the hole itself. In addition, the surface of the substrate around the circumference of the hole is likely to chip in places, leaving an erose ring around the ferrite puck. This roughness will have adverse effects on the circulation symmetry, line losses, and the circulator resonator input impedance.

While the more brittle substrates are ruled out for use in ferrite puck type microstrip circulators, one may still design such microstrip circulators using more workable substrates such as Rexolite or Duroid. When these machineable substrates are used, however, there still remains the problem of holding the puck in the hold under the disk resonator.

The ferrite puck itself is brittle and fragile. Since the ferrite puck is the same thickness as the substrate (typically 0.050 to 0.010 inch), great care must be taken not to damage the puck as it is placed into the substrate hole. A tight fit to the hole risks breaking the ferrite puck. If a looser fit is desired to reduce any possible puck damage, then the puck must be glued into the hole. The designer is then faced with making certain that the glue used fills all the void between the rim of the puck and the substrate hole to provide a continuum of dielectric. In addition, the glue used must have the same dielectric constant and loss tangent as the substrate to prevent reflections of the input microwave power from dissimilar dielectric interfaces at the substrate hole. By contrast, if one uses ferrite for the substrate itself, there is no need for any tedious and precise boring or cutting. If the DC magnetic field, H_{DC}, is confined to the disk resonator; proper circulation will result. Since the ferrite substrate is thin, magnetic fringing fields in the radial direction pose no serious problem. Over the remaining, non-magnetized area of the ferrite, the substrate will behave in the same manner as any other dielectric substrate, given these two considerations:

- The relative dielectric constant, ϵ_f, of most ferrites is fairly large—in the order of 10.0 to 15.0. This large a value of dielectric constant will shrink the size of the microstrip layout by a factor of $1/\epsilon_f$ in the worse case, an important consideration for overall component size at millimeter-wave frequencies. For a given and small enough R, the specified feedline width to the circulator can be made to yield an acceptable range of quarter-wave transformer impedances that match the disk to the 50-ohm feedlines over the desired isolation bandwidth.
- The ferromagnetic resonant radian frequency, ω_m, must not be approached by ω, the microwave radian frequency. The normal dielectric loss of the ferrite increases sharply at frequencies near ω_m.

Pucel and Masse[4] have rigorously studied the subject of microstrip on a ferrite substrate with a theoretical analysis confirmed very closely by experimental data for several different ferrite substrates. They have derived expressions for the characteristic impedance of a microstrip line on the ferrite substrate, the microstrip guide wavelength, λ_g, and the substrate dielectric loss per guide wavelength, $\alpha\lambda_g$. The behavior of the ferrite substrate itself may be accurately computed using their formulation. For finer expressions of total circulator insertion losses, these ferrite substrate losses may be subtracted from the total measured circulator insertion losses.••

either feedline, although the power delivered to each is considerably less than one half the input power. As the feedlines are made wider, each line receives more power until the resonator's Q is lowered to the point where resonance is impossible.

As explained later, the designer must choose a feedline width somewhere between these two extremes. The lines must be wide enough to couple power into and out of the disk resonator efficiently; but they cannot be made too wide or the disk will not resonate.

Add magnetic bias

Once the disk resonates at the circulation frequency, the second condition involves rotating the standing wave pattern in the θ direction. The standing wave pattern must be rotated to obtain the preferential flow of power described earlier in the description of the ideal circulator.

Magnetized ferrite material, placed directly underneath the disk resonator, accomplishes this rotation. When an axial DC magnetic field, H_{DC}, is applied perpendicularly to the plane of the ferrite-resonator combination, the unperturbed standing wave pattern in the circulator rotates. In the ideal case, the rotation in the θ direction is such that one feedline receives all the input power, and the other line receives zero power.

This rotation occurs because the axially magnetized ferrite has a different permeability for the clockwise rotational magnetic fields than it does for the counter-clockwise rotating magnetic fields. Since the permeabilities are different, the two rotational fields are affected differently. The net result is for the one field to be advanced in the plus θ direction, while the oppositely rotating magnetic field is retarded in the minus θ direction. The change in standing wave pattern as H_{DC} is applied is shown in Fig. 2(b).

In the figure, the necessity for 120-degree feedline symmetry is evident, if one would have the circulator operate as a three-terminal device. Each rotational magnetic field is moved in the

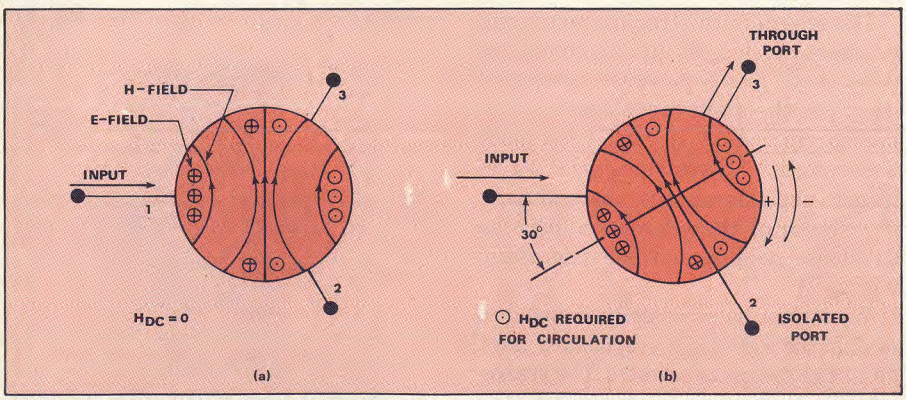

2. The application of a DC magnetic field shifts the standing wave pattern in the resonator by 30 degrees to meet the circulation condition.

(continued on p. 56)

θ direction just far enough so that the resulting standing wave pattern isolates one feedline and delivers all the input power to the other feedline. From Fig. 2(b), the necessary standing wave pattern rotation required for the circulation condition is 30 degrees.

When the circulation condition is imposed upon the junction scattering matrix, the relationship between these first two conditions of disk resonance and standing wave rotation are easily studied and examined using a computer model.

As mentioned previously, the resonator radius, R, determines the resonant frequency of the disk. The ferrite, also of radius R, placed underneath the disk and magnetized by H_{DC}, determines the isolation bandwidth through its saturation magnetization, $4\pi M_s$. The greater the value of the ferrite's $4\pi M_s$, the wider the frequency range over which the standing wave pattern in the disk can be maintained at the 30 degrees of rotation, satisfying the circulation condition.

Don't put off impedance matching!

Matching the impedance of the disk resonator and feedlines is an important design task. If the circulation condition is satisfied but the resonator is not matched to its feedlines, the circulator will work poorly or not at all. With a mismatch between the resonator and the feedlines, some of the output power sent from the resonator to the unmatched output feedline will be reflected back into the disk resonator. This reflected output power will then be considered as input power from the through-port. It will propagate around the disk resonator and be delivered as output to the supposedly isolated port.

Poor impedance matching limits the actual maximum isolation achieved with a circulator due to the type of internally reflected power described above. The impedance matching network used must have an impedance matching bandwidth greater than the expected isolation bandwidth from the circulator disk resonator.

The circulator test fixture design also deserves some comment. If one uses waveguide to microstrip or coaxial to microstrip transition, the mismatch from the transitions must also be considered when designing a circulator for a specified isolation bandwidth. Likewise, if a given circulator design does not provide the expected magnitude or bandwidth of isolation, transitions should be examined.

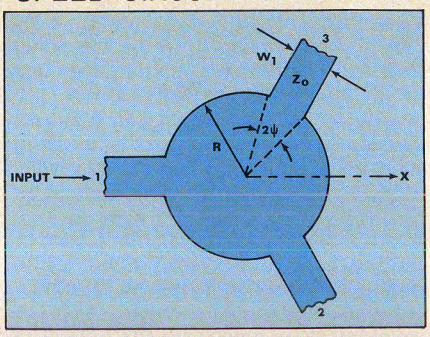

3. The angle subtended by each radial line, ψ, is an important design parameter. Note how it is related geometrically to the disk radius, R, and the line width, W_1.

There is usually only one type of impedance matching network used to match the disk resonator to its feedlines, the quarter-wave transformer. More involved and complex networks can be used, but microstrip line losses become prohibitive when these networks are used, especially at higher frequencies.

Generally, a quarter-wave transmission line section is used for the impedance transformer. If more bandwidth is required, a two-section transformer can be used, and so on. The more sections used, however, the greater the line losses become. Since the model computes the microstrip line width, W_1, at the rim of the disk resonator, the characteristic impedance, Z_1, for that line is determined. The quarter-wave transmission line transformer design is simple. The single-stage transformer characteristic impedance, Z_T, is given by:

$$Z_T = \sqrt{Z_1 \, Z_o} \qquad (1)$$

where Z_o is the characteristic impedance of the system where the circulator is to be used (Z_o = 50 ohms in most cases).

The length of the transformer is one quarter-wavelength at the circulation frequency. Note, however, that this length is the guide wavelength in the microstrip and is not freespace wavelength. Microstrip guide wavelength depends on the characteristic impedance of the microstrip line, the substrate height, and the microstrip width, W.

W_1 cannot be arbitrarily changed to match the resonator impedance later on in the design procedure. The reason for this restriction is given later. The designer is free, however, to choose the substrate thickness and dielectric constant, in order to simplify impedance matching problems. If the substrate's dielectric constant and thickness can be successfully juggled to make $Z_1 = Z_o$, no transformer is required at all. When such is the case and $Z_1 = Z_o$, the circulator is said to be directly coupled.

Thus, the designer should carefully consider impedance matching when planning a microstrip circulator. This is one area that must be addressed at the outset, and not as the last step in the circulator design.

Analysis leads to a model

Bosma[1], Fay and Comstock[2] have written excellent papers describing the operation of stripline junction circulators. Bosma uses a Green's function to solve for the field distribution within the circulator's disk resonator. From the Green's function development and the conditions imposed to the circulator disk resonator scattering matrix to satisfy the circulation condition, Bosma derives theoretical expressions for the disk resonator input wave impedance, Z_{IN}, through-port and isolated-port insertion losses.

In their paper on continuous tracking, wideband microstrip circulators, Wu and Rosenbaum[3] develop these expressions into complex infinite series expansions suitable for computer study and modeling techniques. While their analysis focuses on octave bandwidth circulation as a function of feedline width to the disk resonator, their work is applicable to any microstrip junction circulator, or arbitrary isolation bandwidth.

From the Green's function formulation, Wu and Rosenbaum derive expressions for the E_z and H_θ field components within the disk resonator. By defining the input wave impedance of the disk resonator, Z_{IN}, as the ratio of E_z/H_θ, they derive the corresponding scattering matrix for the circulator's disk resonator (see Fig. 3):

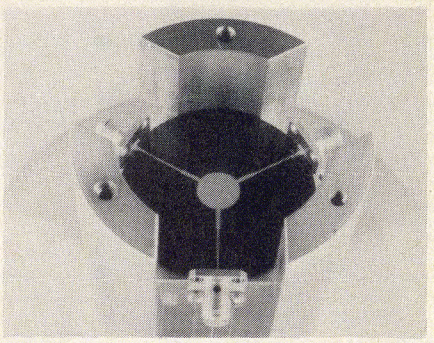

4. This 5.0 GHz microstrip junction circulator is built on a ferrite substrate.

$$[S] = \begin{bmatrix} \alpha & \gamma & \beta \\ \beta & \alpha & \gamma \\ \gamma & \beta & \alpha \end{bmatrix} \quad (2)$$

where

$$\alpha = 1 + \frac{\pi Z_d (C_1^2 - C_2 C_3)}{D} = S_{11} = S_{22} = S_{33} \quad (3)$$

$$\beta = \frac{\pi Z_d (C_2^2 - C_1 C_3)}{D} = S_{12} = S_{23} = S_{31} \quad (4)$$

$$\gamma = \frac{\pi Z_d (C_3^2 - C_1 C_2)}{D} = S_{21} = S_{32} = S_{13} \quad (5)$$

where

$$D = j Z_{eff} (C_1^3 + C_2^3 + C_3^3 - 3C_1C_2C_3) \quad (6)$$

$$C_1 = \frac{\Psi J_o(SR)}{2 J_o^1(SR)} + \sum_{n=1}^{\infty} \left(\frac{\sin^2 n\Psi}{n^2\Psi} \right) \cdot \left(\frac{J_n^1(SR) J_n(SR)}{D_n} \right) - \frac{\pi Z_d}{j 2 Z_{eff}} \quad (7)$$

$$C_2 = \frac{\Psi J_o(SR)}{2 J_o^1(SR)} + \sum_{n=1}^{\infty} \left(\frac{\sin^2 n\Psi}{n^2\Psi} \right) \cdot \left(\frac{P_n - j Q_n}{D_n} \right) \quad (8)$$

$$C_3 = \frac{\Psi J_o(SR)}{2 J_o^1(SR)} + \sum_{n=1}^{\infty} \left(\frac{\sin^2 n\Psi}{n^2\Psi} \right) \cdot \left(\frac{P_n + j Q_n}{D_n} \right) \quad (9)$$

or $C_3 = C_2^*$.

where

$$D_n = \left(J_n^1(SR)\right)^2 - \left((1/SR) \left(\frac{\kappa}{\mu} \right) (n) \right)^2 \left(J_n(SR) \right)^2 \quad (10)$$

$$P_n = \left(J_n^1(SR) \right) \left(J_n(SR) \right) \cos(2n\pi/3) \quad (11)$$

$$Q_n = \left((1/SR) \left(\frac{\kappa}{\mu} \right) (n) \right) \left(J_n(SR) \right)^2 \sin(2n\pi/3) \quad (12)$$

$J_n(SR)$ is the Bessel function of the first kind, order n.

$J_n^1(SR)$ is the first derivative with respect to its argument, SR, of the Bessel function of the first kind, n.

S = the radial wave propagation constant of the magnetized ferrite under the disk resonator ($S = (\omega/c)(\mu_{eff}\epsilon_f)^{1/2}$)

μ_{eff} = $(\mu^2 - \kappa^2)/\mu$ = effective permeability of the magnetized ferrite.

ω = microwave radian frequency ($2\pi f$).

c = velocity of light in free space.

$Z_d = \frac{120\pi}{\sqrt{\epsilon_d}}$ = the intrinsic wave impedance within the microstrip dielectric substrate.

$Z_{eff} = 120\pi \sqrt{\frac{\mu_{eff}}{\epsilon_f}}$ = the intrinsic wave impedance within the magnetized ferrite beneath the junction disk resonator.

R = disk resonator radius.

Ψ = the half-angle subtended by the feedlines where they meet the edge of the disk resonator.

W_1 = microstrip feedline width.

Z_1 = microstrip characteristic impedance corresponding to W_1.

Z_0 = desired microstrip feedline system impedance, usually 50 ohms.

ϵ_f = relative dielectric constant of the ferrite.

ϵ_d = relative dielectric constant of the microstrip substrate.

In the ideal case of perfect circulation, with all ports perfectly matched, one output port is perfectly isolated and from the scattering matrix, $\beta = 0$. The other output port will have perfect transmission under these conditions, and $\gamma = 1$. The input reflection coefficient at the port of incidence, α, is zero when the intrinsic wave impedance, Z_{eff}, for the disk resonator is matched to the intrinsic wave impedance of the microstrip substrate, Z_d.

When there is some impedance mismatch between the disk resonator and the feedlines, $Z_{eff} = Z_d$ and the following expressions hold:

Return loss = $20 \log_{10} | \alpha |$ dB (13)

Isolated port insertion loss or circulator's isolation = $20 \log_{10} | \beta |$ dB (14)

Through-port insertion loss = $20 \log_{10} | \gamma |$ dB (15)

The circulator resonator input impedance, Z_{IN}, is related to the complex reflection coefficient at the input port, α, by:

$$Z_{IN} = - \frac{(\alpha + 1)}{(\alpha - 1)} Z_d \quad (16)$$

In Eq. 16, note that at circulation frequency, f_c, $\alpha = 0$ in the ideal case and the intrinsic input wave impedance, $Z_{IN} = Z_d$, the circulator's resonator is impedance matched to the dielectric substrate at f_c (i.e., $Z_{IN} = Z_d = Z_{eff}$). Substitution of Eq. (3) for α gives:

$$Z_{IN} = - \left(Z_d + \frac{j2D}{\pi(C_1^2 - C_2C_3)} \right) \quad (17)$$

(continued on p. 58)

dubbeldee
type IIa
diamond
heat sinks

for:
• impatt, trapatt and gunn diodes
• semiconductor lasers
• high power transistors
• semiconductor switching devices etc.

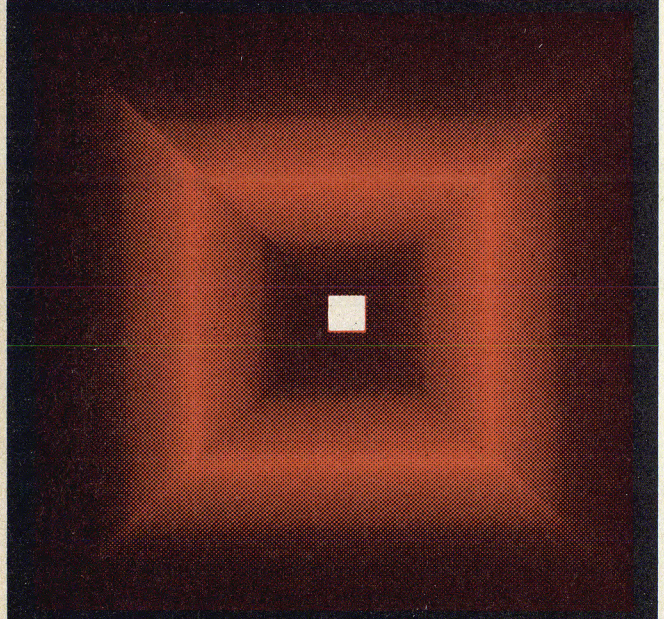

DIAMONDS

D. DRUKKER & ZN N.V.

12 SARPHATIKADE, AMSTERDAM-HOLLAND,
TELEPHONE: 26 73 21, TELEX: 14143 D DAM-NL.

REPRESENTED IN USA:
DUBBELDEE DIAMOND CORPORATION,
2 WEST 46 TH STREET SUITE 1604, NEW YORK N.Y. 10036,
TELEPHONE 582-89 76, TELEX 236064, CABLE: DUBBELDEE

READER SERVICE NUMBER 45

Where D has already been expressed in Eq. (6). More explicitly,

$$Z_{IN} = -\left(Z_d + j\left(\frac{2Z_{eff}}{\pi}\right)\left(\frac{C_1^3 + C_2^3 + C_3^3 - 3C_1 C_2 C_3}{C_1^2 - C_2 C_3}\right)\right) \quad (18)$$

The disk resonator input impedance is referenced to Z_d, the intrinsic wave impedance of the dielectric substrate surrounding the ferrite under the disk resonator, since that substrate is the dielectric media up to the magnetized ferrite located under the junction resonator. If a ferrite were used for the entire substrate, then Z_d would be the intrinsic wave impedance of the unmagnetized ferrite.

As for the ferrite itself, the Polder tensor, μ, relates the applied magnetic field, H_{DC}, to the magnetic field within the ferrite:

$$\bar{\bar{\mu}} = \begin{vmatrix} \mu & -j\kappa & o \\ j\kappa & \mu & o \\ o & o & \mu \end{vmatrix} \quad (19)$$

The magnetic properties of the ferrite are characterized by its saturation magnetization, $4\pi M_s$. In a circulator, the ferrite may be magnetized to a value less than or equal to its saturation $4\pi M_s$. For minimum dielectric losses within the ferrite and for widest isolation bandwidth, the ferrite should be saturated with $H_{DC} = 4\pi M_s$. H_{DC} is usually supplied with small permanent magnets.

When the ferrite is saturated, the elements of the Polder tensor simplify to:

$$\mu = 1$$
$$\kappa = -\omega_m/\omega$$
and
$$\mu_{eff} = 1 - (\omega_m/\omega)^2$$

where:

$$\omega_m = 2\pi\gamma(4\pi M_s)$$
$$\gamma = 2.8 \text{ MHz/Oe}$$

With the ferrite analysis given above, this information can then be entered into Eqs. 7, 8, 9, 10, 11 and 12 to form a computer model for circulator design.

Shaping the equations

The circulator junction analysis outlined above is in terms of ψ, the half angle subtended by the junction feedlines where they meet the edge of the disk resonator. This angle relates the feedline width, W_1 to the disk radius, R, by:

$$W_1 = 2R \sin(\Psi) \quad (20)$$

or

$$\Psi = \sin^{-1}(W_1/2R) \quad (21)$$

Earlier, it was mentioned that the circuit designer is often not free to change W in an effort to match impedances. It can be seen that this comes from the fact that ψ is not arbitrary; Wu and Rosenbaum use ψ as the design parameter relating together the substrate dielectric, the ferrite and the isolation bandwidth.

Since the predicted isolation bandwidth is derived from the sums of complex infinite series for C_1, C_2 and C_3, the actual explicit effect of ψ on the circulator design comes out from some implicit relationships in the expressions for C_1, C_2 and C_3. The relationship of ψ to the overall operation of the circulator will be made evident as the circulation condition is imposed on the scattering matrix.

(continued on p. 60)

Imposing the circulation condition upon the scattering matrix specifies the implicit relationships between ψ, $4\pi M_s$, ϵ_f, ϵ_d and R necessary for the circulator to work as designed. For perfect circulation, one of the three ports must be completely isolated. This condition may be stated mathematically by setting in the scattering matrix equal to zero. For $\beta = 0$, Eq. 4 becomes:

$$C_2^2 = C_1 C_3 \qquad (22)$$

In the rigorous case of imposing the circulation condition, the roots to Eq. 22 must be derived given the fact that C_1, C_2 and C_3 are themselves complex numbers and that each of them is the sum of an infinite series expansion of complex terms. Equation 22 may be decomposed into the following two conditional equations:

$$P = \frac{M(M^2 - 3N^2)}{(M^2 + N^2)} \qquad (23)$$

$$Q = \frac{N(3M^2 - N^2)}{(M^2 + N^2)} \qquad (24)$$

where:

$$P = \mathrm{Re}(C_1) = \frac{\Psi J_o(SR)}{2J_o^1(SR)} + \sum_{n=1}^{\infty} \left(\frac{\sin^2 n\Psi}{n^2\Psi}\right)\left(\frac{J_n(SR)J_n^1(SR)}{D_n}\right)$$

$$Q = \mathrm{Im}(C_1) = \frac{\pi Z_d}{2Z_{eff}}$$

$$M = \mathrm{Re}(C_2) = \frac{\Psi J_o(SR)}{2J_o^1(SR)} + \sum_{n=1}^{\infty} \left(\frac{\sin^2 n\Psi}{n^2\Psi}\right)\left(\frac{J_n(SR)J_n^1(SR)\cos(2n\pi/3)}{D_n}\right)$$

$$N = \mathrm{Im}(C_2) = \sum_{n=1}^{\infty} \left(\frac{\sin^2 n\Psi}{n^2\Psi}\right) \cdot \left(\frac{(n)(1/SR)(\kappa/\mu)(J_n(SR))^2 \sin(2n\pi/3)}{D_n}\right)$$

where D_n was given earlier in Eq. 10; Eqs. 23 and 24 give the two conditions to be satisfied for perfect circulation. The quantities P, M and N are infinite series with each term corresponding to one particular resonator mode. If the circulator disk resonator is to satisfy all the particular boundary conditions, then it is necessary to keep an infinite number of terms for P, M and N.

For practical applications, not all terms are important. Most circulators operate close to the n = 1 resonance, so most designers consider only the n = 1 term. With this simplification, the solutions to Eq. 23 and 24 reduce to the following relationships:

$$SR = 1.84 \qquad (25)$$

$$\psi = \psi_c = \frac{\pi}{\sqrt{3}\,(1.84)} \frac{Z_d}{Z_{eff}} \left|\frac{\kappa}{\mu}\right| \qquad (26)$$

For a magnetized ferrite ($H_{DC} = 4\pi M_s$) operated at frequencies over which $\omega < \omega_m$, the ratio of Z_{eff} to Z_d becomes:

$$\frac{Z_{eff}}{Z_d} = \left(\frac{\epsilon_d}{\epsilon_f}\right)^{1/2} \left(1 - \left(\frac{\kappa}{\mu}\right)^2\right)^{1/2} \qquad (27)$$

These approximate solutions for the circulation condition can be the basis of a computer model for circulator design. A more detailed description of the computer design algorithm is given a bit later. Expressing the equations of R and ψ in those terms more closely descriptive of the ferrite and microstrip substrate, we have:

$$R = \frac{1.84}{S} = \frac{1.84}{\sqrt{(\omega/c)(\mu_{eff}\epsilon_f)}} = \frac{1.84}{\sqrt{(\omega/c)(\epsilon_f)(1 - (\frac{\kappa}{\mu})^2)}} \qquad (28)$$

$$\psi_c = \frac{\pi}{1.84\sqrt{3}} \times \frac{\kappa}{\mu} \times \sqrt{\frac{\epsilon_f}{\epsilon_d}} \times \frac{1}{\sqrt{1 - (\frac{\kappa}{\mu})^2}} \qquad (29)$$

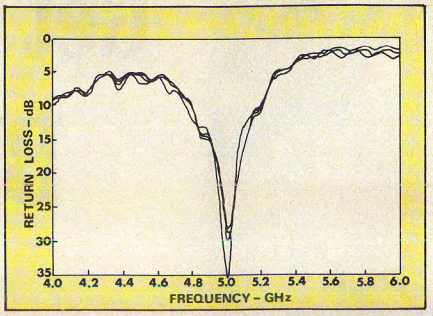

5. The measured return loss (20 log$_{10}$ (ρ)) plot reveals a 20-dB isolation bandwidth of about 3 per cent.

where

$$\frac{\kappa}{\mu} = -\frac{\omega_m}{\omega} = \frac{-(2\pi)(\gamma)(4\pi M_s)}{2\pi f} \qquad (30)$$

Molding the model

The actual computer modeling procedure is an iterative process. (It is assumed at this stage of the design that the ferrite and dielectric substrate material have already been chosen). By specifying the circulation center frequency, f_c, the corresponding microwave circulation radian frequency, ω_c, is substituted for ω in Eq. 28, and the disk radius, R, for the unloaded resonator with no feedlines is computed.

The solution of Eq. 28 is used only as a starting value for R in the computer model, since this equation was derived for the unloaded resonator. When the feedlines are added to the resonator, the value of R must decrease in order for the loaded resonator to resonate at the circulation frequency. The computer model iterates on R until the loaded disk resonator with its feedlines attached resonates at f_c.

Before the final value of R can be determined from iteration, the value of $\psi = \psi_c$ satisfying the circulation condition must be determined; ψ_c is computed from Eq. 29. With this value of ψ_c determined, the rest of the microstrip circulator design follows. Once ψ_c is computed, however, the remainder of the circulator design and analysis will be based on this value of $\psi = \psi_c$.

To match the microstrip feedline impedance, Z_1, at the edge of the disk resonator to 50-ohm lines requires proper selection of substrate thickness to make $Z_1 = Z_0$. Quarter-wave transformer matching as described previously may also be used if the designer

(continued on p. 62)

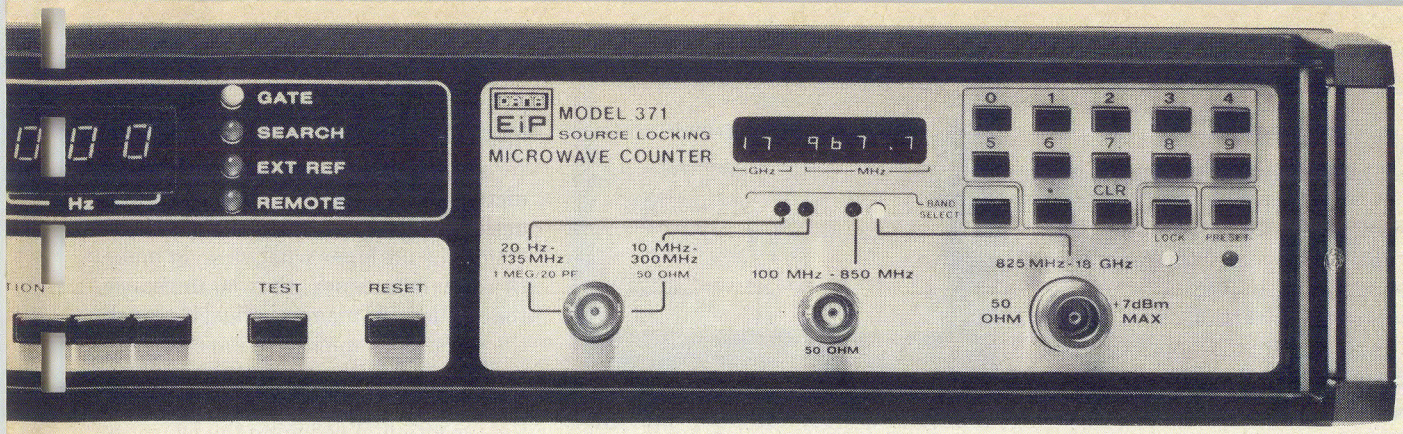

source to the same long term accuracy and stability as the counter's timebase, and does so over the broad frequency range from 10 MHz to 18 GHz in 100 KHz increments.

Simple to operate.

A microprocessor-based keyboard input and automatic bandwidth and polarity control make source locking easy. The 371 requires only 2 interconnections; a sample of the output from the source, and an FM input to the source. To lock a signal, simply tune the source to within 20 MHz of the desired frequency, enter that frequency on the front panel keyboard, and press the LOCK button.

In its role as a premium automatic frequency counter, the 371 offers frequency coverage from 20 Hz to 18 GHz, −30 dBm sensitivity, greater than 40 MHz FM tolerance, 2 watt burnout protection, and multiple signal discrimination.

Economical, too.

The price—$6,800, only slightly more than a dedicated microwave counter alone. And far less than a counter and separate lockbox.

We've got counters for every application; low cost, pulsed RF, general purpose, and ruggedized environmental.

For more details or a demonstration, phone or write EIP.



EIP, Inc.
3230 Scott Boulevard, Santa Clara, CA 95051
Phone 408/244-7975. TWX: 910 338 0155.

In Europe:
EIP International, Brussels, Belgium
Phone 2/660 48 70. TELEX 846-23662.

READER SERVICE NUMBER 48

Table 1: Description of experimental circulator

Microstrip dielectric constant (ϵ_d) = 14.3
Ferrite dielectric constant (ϵ_f) = 14.3
Circulation frequency (f_c) = 5.0 GHz
Disk resonator radius (R) = 0.192 in.
Substrate thickness (H_s) = 0.025 in.
λ/4 transformer impedance (Z_T) = 32.2 ohms
λ/4 transformer line width (W_1) = 0.038 inches
λ/4 transformer length (l_T) = 0.194 in.
Resonator half-angle (ψ) = 0.100 radian
Saturation magnetization ($4\pi M_s$) = 550 Gauss
Initial DC magnetic bias (H_{DC}) = 550 Gauss
Final DC magnetic bias (H_{DC}) = 185 Gauss

When tested in the lab, this circulator did not circulate. The initial design of the component was based upon another circulator analysis paper and did not work due to severe impedance mismatch from the resonator to the feedline transformers. For the DC magnetic field strength of 550 Gauss applied to the ferrite, the resulting impedance mismatch between Z_d and Z_{eff} could not be matched out. All of the input to the resonator was internally reflected and sent to the supposedly isolated port.

The model finds the fault

Wu and Rosenbaum's paper, and the computer model based on that paper, confirmed this impedance mismatch as the problem. The model also predicted that if the field strength H_{DC} was reduced from 550 Gauss to 185 Gauss, the disk-resonator impedance would be the proper value to be matched to the 50-ohm feedlines by 32.3-ohm quarter-wave transformers. The field strength was reduced from 550 Gauss until circulation was observed on the network analyzer; the field strength was then measured at 180 Gauss.

The circulator was built using metalization on the ferrite substrate. Connector tabs were tapered to improve their impedance match. Silver epoxy under the transitions provided good connection from the tapered tabs to the 50-ohm input feedlines. The 50-ohm feedlines connect to the 32.2 ohm quarter-wave transformers, which in turn, connect to the disk resonator.

All data for this circulator was taken with a network analyzer on a swept frequency basis from 4 to 6 GHz. The degree of match between the 50-ohm feedlines and disk resonator was measured in terms of the input impedance looking into the circulator from the microstrip launchers. The input impedance data was recorded on an X-Y plotter from the network analyzer in rectangular and polar forms (Figs. 5 and 6). Figure 5 is a composite plot of the return loss looking into the three circulator ports taken one at a time. Note that the plots are nearly coincident, indicating a very good degree of symmetry within the circulator. The

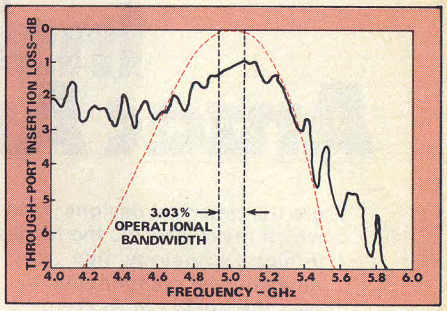

***7. Measured through-port insertion loss** is corrected for return loss and ferrite dielectric loss.*

(continued on p. 64)

return loss varies from −27 to −30 dB, and all of the return loss curves fall very close to 5.0 GHz.

The Smith chart impedance plots shown in Fig. 6 are for port 2 as the input port. The other two ports gave similar loci by virtue of the circulator symmetry shown in Fig. 5.

Through-port insertion loss, shown in Fig. 7, ideally should approach zero at f_c. The measured through-port insertion loss does not fall below 1.0 dB for two reasons:

- Losses in the coaxial to microstrip transitions in the test fixture.
- Additional ferrite losses in the partially magnetized ferrite under the disk resonator.

The through-port insertion loss generally should not be this large. Note that the 50-ohm feedlines are longer than necessary (Fig. 4) contributing more line loss.

Insertion loss for the isolated and through-ports was also measured on a swept frequency basis from 4 to 6 GHz. Figure 8 shows a composite isolation plot for all three ports being the isolated port, taken one at a time. Again, the isolation curves are coincident, displaying good circulator symmetry. Impedance matching Z_{IN} from the ferrite to the magnetized ferrite under the resonator, combined with the value of $\psi_c = 0.100$ radian, results in a very narrow 3.03 per cent isolation bandwidth of 20 dB or more of isolation. Maximum measured isolation is greater than 35 dB. Wider isolation bandwidth could have been obtained by saturating the ferrite to its full $4\pi M_s = 550$ Gauss instead of only 185 Gauss. The value for ψ_c would be larger and the larger ψ_c would give a wider isolation bandwidth since the resonator would be more heavily loaded.

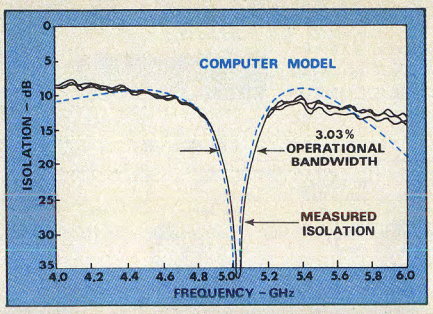

***8. This composite, overly plot** of the circulator's isolated-port insertion loss considers all three ports.*

It is important to remember that if the computer model had been working at the time that this circulator was originally designed, the fault in this design would have been seen. As it turned out, the computer model predicted after the fact that the original design would not work. The model also "told" the designer what to do to make the circulator work; that is, to reduce the applied DC magnetic field to match the resonator input wave impedance to the intrinsic wave impedance of the unmagnetized ferrite substrate. With the exception of reducing the DC magnetic field from 550 Gauss to 180 Gauss, there was no "tweaking" done to the circulator itself to make it work. In essence, the designer adjusted the circulator according to the model rather than fudging a non-functional circulator to make it work in terms of its surrounding microwave connections.••

References

1. H. Bosma, "On Stripline Y-Circulation AT UHF," *IEEE Transactions On MTT* (1963 Symposium Issue), Vol. MTT-12, pp. 61-72, (January, 1964).
2. C.E. Fay and R.L. Comstock, "Operation of the Ferrite Junction Circulator," *IEEE Transactions On MTT* (1964 Symposium Issue), Vol. MTT-13, pp. 15-27, (January, 1965).
3. Y.S. Wu and F.J. Rosenbaum, "Wideband Operation of Microstrip Circulators," *IEEE Transactions On MTT*, Vol. MTT-22, pp. 849-856, (October, 1974).
4. R.A. Pucel and D.J. Masse, "Microstrip Propagation On Magnetic Substrates, Part I: Design Theory, Part II: Experimental," *IEEE Transactions On MTT*, Vol. MTT-20, pp. 304-313, (May, 1972).

Inside Anzac Amplifiers

are the patented designs which make ANZAC the leader in high technology/high reliability RF components... plus the quality of workmanship you can expect from our MIL-Q-9858A approved facility.

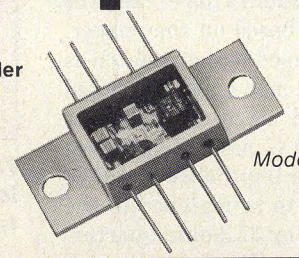

Model AM-123

10 dB Gain, Wide Dynamic Range
5 - 500 MHz

Noise Figure	4 dB typical
Power Output	+22 dBm (1 dB compression)
3rd Order Intercept	+40 dBm
Bias Power	1 watt typical

Call or write for the latest ANZAC Full Line Catalog.

All Amplifiers Available from Stock

anzac ELECTRONICS
Division of Adams-Russell

39 Green Street • Waltham, MA 02154 • Tel. (617) 899-1900 • TWX 710 324-6484

READER SERVICE NUMBER 49

If the Microminiature Connector insert is missing, circle number 179 for your personal catalog. For a complete description of this catalog see our ad in the Catalog Update section, page 84.



International Telephone and Telegraph Corporation

World Headquarters
666 East Dyer Road
P.O. Box 929
Santa Ana, California 92702
(714) 557-4700

Cannon Electric Division

WHAT'S BETTER THAN SPEED READING?

SPEED LEARNING

(SPEED PLUS COMPREHENSION)

Speed Learning is replacing speed reading because it's easy to learn . . . lasts a lifetime . . . applies to everything you read . . . and is the only fully accredited course with the option of 3 college credits.

Do you have too much to read and too little time to read it? Do you mentally pronounce each word as you read? Do you frequently have to go back and re-read words or whole paragraphs you just finished reading? Do you have trouble concentrating? Do you quickly forget most of what you read?

If you answer "yes" to any of these questions — then here at last is the practical help you've been waiting for. Whether you read for business or pleasure, school or college, you will build exceptional skills from this major breakthrough in effective reading, created by Dr. Russell Stauffer at the University of Delaware.

Not just "speed reading" — but speed reading-thinking-understanding-remembering-and-learning

The new *Speed Learning Program* shows you step-by-proven-step how to increase your reading skill and speed, so you understand more, remember more and use more of everything you read. The typical remark made by the 75,000 slow readers who completed the *Speed Learning Program* was: "Why didn't someone teach me this a long time ago?" They were no longer held back by the lack of skills and poor reading habits. They could read almost as fast as they could think.

What makes Speed Learning so successful?

The new *Speed Learning Program* does not offer you a rehash of the usual eye-exercises, timing devices, costly gadgets you've probably heard about in connection with speed reading courses or even tried and found ineffective.

In just a few spare minutes a day of easy reading and exciting listening, you discover an entirely new way to read and think — a radical departure from anything you have ever seen or heard about. Research shows that reading is 95% *thinking* and only 5% eye movement. Yet most of today's speed reading programs spend their time teaching you rapid eye movement (5% of the problem) and ignore the most important part (95%) *thinking*. In brief, *Speed Learning* gives you what speed reading *can't*.

Imagine the new freedom you'll have when you learn how to dash through all types of reading material *at least* twice as fast as you do now, and with greater comprehension. Think of being able to get on top of the avalanche of newspapers, magazines and correspondence you have to read . . . finishing a stimulating book and retaining facts and details more clearly and with greater accuracy than ever before.

Listen-and-learn at your own pace

This is a practical, easy-to-learn program that will work for you — no matter how slow a reader you think you are now. The *Speed Learning Program* is scientifically planned to get you started quickly . . . to help you in spare minutes a day. It brings you a "teacher-on-cassettes" who guides you, instructs, encourages you, explaining material as you read. Interesting items taken from *Time* Magazine, *Business Week*, *Wall Street Journal*, *Family Circle*, *N.Y. Times* and many others, make the program stimulating, easy and fun . . . and so much more effective.

Executives, students, professional people, men and women in all walks of life from 15 to 70 have benefited from this program. Speed Learning is a fully accredited course . . . costing only 1/5 the price of less effective speed reading classroom courses. Now you can examine the same, easy, practical and proven methods at home . . . in spare time . . . without risking a penny.

Examine Speed Learning FREE for 10 days

You will be thrilled at how quickly this program will begin to develop new thinking and reading skills. After listening to just one cassette and reading the preface you will quickly see how you can achieve increases in both the speed at which you read and in the amount you understand and remember.

You must be delighted with what you see or you pay nothing. Examine this remarkable program for 10 days. If, at the end of that time you are not convinced that you would like to master Speed Learning, simply return the program and owe nothing. See the coupon for low price and convenient credit terms.

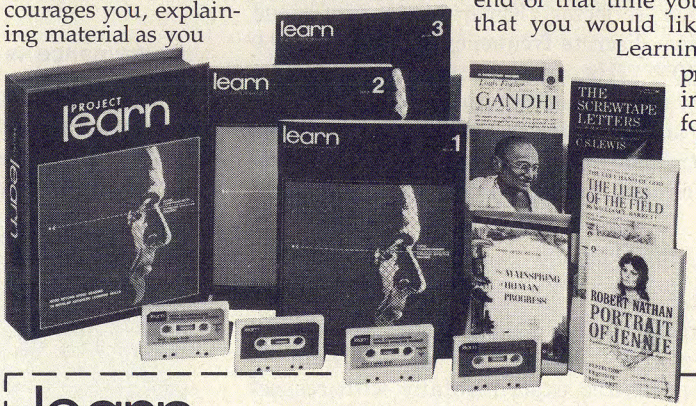

In most cases, the entire cost of your Speed Learning Program is Tax Deductible.

EARN 3 COLLEGE CREDITS

The program may be taken as a 3 credit university-level course. Complete details and enrollment application are included with each program. With this option, SPEED-LEARNING becomes eligible for coverage under most corporate tuition-assistance plans.



Dr. Russell G. Stauffer, originator and research director of this program, has been Editor of the International Reading Association Journal, Professor of Education, University of Delaware.

learn INCORPORATED
113 Gaither Drive, Mount Laurel, N.J. 08054
MicroWaves, 50 Essex Street, Rochelle Park, N.J. 07662, Dept. CMM

Please send me the Speed Learning Program at $79.95 plus $3.00 for handling and insured delivery.

Please check the method of payment below:

☐ Check or money order enclosed for items ordered.

☐ Please charge my credit card under their regular payment terms: ☐ Bank Americard ☐ Master Charge Interbank No. _____ ☐ American Express ☐ Diners Club

Card No. _____ Exp. Date _____

I understand that if after 10 days I am not delighted in every way, I may return the materials and obtain a full refund with no questions asked.

Name _____

Address _____

City _____ State _____ Zip _____

x Signature _____

New Jersey Residents add 5% sales tax

If you don't already own a cassette player, you may order this Deluxe Cassette Recorder for only $49.95. (Includes handling and delivery.)

Check here to order ☐



Modified Backfire Lowers Cross-Polarization Levels

A long backfire antenna can be modified with a small strip reflector to operate in two discrete frequency ranges with symmetrical radiation patterns and low cross-polarization levels.

SUITABLY modified with a small strip reflector, the long backfire antenna is an attractive component for frequency-reuse applications where a low level of cross-polarization is required between signals transmitted in the E and H planes. The antenna may be useful in satellites, ships, aircraft and space vehicles because of its structural simplicity, light weight, small size, low cross-polarization and directive, symmetrical radiation pattern.

To review, the backfire antenna is essentially a leaky cavity antenna with electromagnetic characteristics which are, in a certain sense, comparable to those of a laser cavity. The smaller reflector is the RF analogy of the partially transparent optical end mirror in a laser. Transparency of both types of reflectors is comparable.

Since 1959, when Ehrenspeck claimed patent protection for the "backfire principle"[1, 2], there has been extensive experimental and theoretical work in many countries on several backfire antenna modifications.[3–8] Our investigations have centered on a long backfire structure, with a small, strip reflector located four wavelengths from the surface of the main reflector. Experiments performed simultaneously at two discrete frequency bands, 8.6 to 9.0 GHz and 9.9 to 10.4 GHz, illustrate that peak cross-polarization levels of this type of antenna are less than −27 dB, making it very attractive for frequency-reuse systems where signals are transmitted and received on orthogonal linear or opposite circular polarizations.

Phase velocity is modified

The backfire antenna under consideration consists of a linearly corrected reflector R_m, dielectric structure D, and a small strip-reflector R_s (Fig. 1). The size of the strip reflector has been optimized experimentally with respect to the pattern quality and input matching. Plexiglass ($\epsilon_r = 2.6$) is used for the dielectric structure. To obtain a larger effective aperture for the backfire antenna, the surface wave velocity, V_s, was chosen according to the approximate design method proposed by Zucker[10]; however, a more accurate expression for the optimum velocity is:[7]

$$V_s = \frac{c}{1 + 0.234\,\frac{\lambda}{\ell} + 0.021\left[\frac{\lambda}{\ell}\right]^2} \qquad (1)$$

where c = velocity of light,
ℓ = length of the backfire antenna and
λ = wavelength.

Because the length of the long backfire antenna for optimum performance has to be an integral multiple (n) of half wavelengths, the phase velocity of an optimized backfire is

$$V_s = \frac{c}{1 + \frac{0.234}{n} + \frac{0.021}{n^2}} \qquad (2)$$

or approximately

$$V_s \approx \frac{c}{1 + \frac{0.234}{n}} \qquad (3)$$

Performance is encouraging

The experimental antenna operates as a backfire component from 9.9 to 10.4 GHz and as an endfire antenna from 8.6 to 9 GHz when strips of the small reflector are parallel to E-vector (Fig. 2(a)). The radiation patterns for these cases,

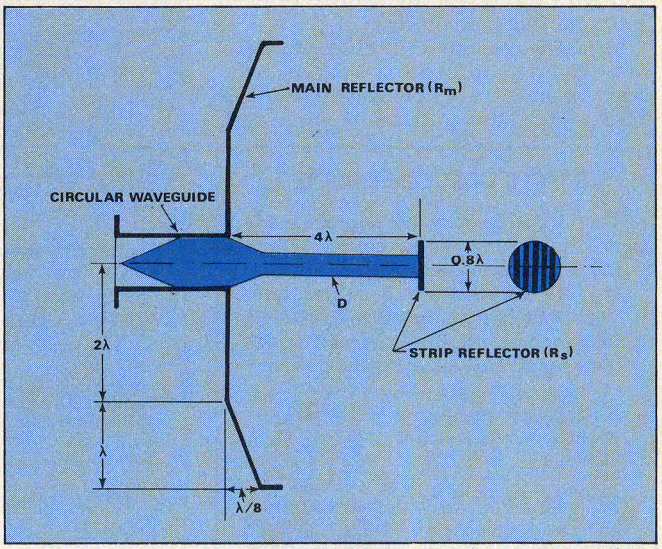

*1. **Metal strips** mounted on a plexiglass dielectric structure act as a partially transparent reflector.*

Dr. Akhileshwar Kumar, Department of Electrical & Electronic Engineering, Queen Mary College, University of London, Mile End Road, London E1 4 NS, England, and **Dr. Ing. H. D. Hristov**, Head, Department of Radiotechnics, Higher Institute of Mechanical and Electrical Engineering, (VMEI) Varna, Bulgaria.

in both E-plane and H-plane at 8.8 and 10.2 GHz, are shown in Fig. 3. If the small strip reflector is rotated by 90 degrees (strips are now perpendicular to E-vector, Fig. 2(b)), the backfire antenna works as an endfire antenna; radiation patterns are illustrated in Fig. 3 by dotted lines. Experiments confirm that the E and H-plane radiation patterns are symmetrical with the earlier case when the strip reflector is removed (Fig. 2(c)).

For two positions of the small strip reflector, the radiation patterns are quite different in beamwidth and sidelobes, but each pattern is axially symmetrical. Radiation patterns for case A (Fig. 2(a)) at 8.8 GHz, case B (Fig. 2(b)) at 10.2 GHz and case C (Fig. 2(c)) are approximately the same; the small reflector for case B is electromagnetically invisible at 10.2 GHz. The 3-dB beamwidth for the backfire case, tuned for 10.2 GHz, is 11 degrees in both E and H planes, and the sidelobes in the E and H planes are less than −20 dB and −23 dB, respectively. The 3-dB beamwidth for the endfire case for same frequency is 28 degrees in both planes, and the sidelobes in the E and H planes are less than −12 dB and −13 dB, respectively. Similar patterns for the latter case have been obtained at another frequency range (8.6

(continued on p. 73)

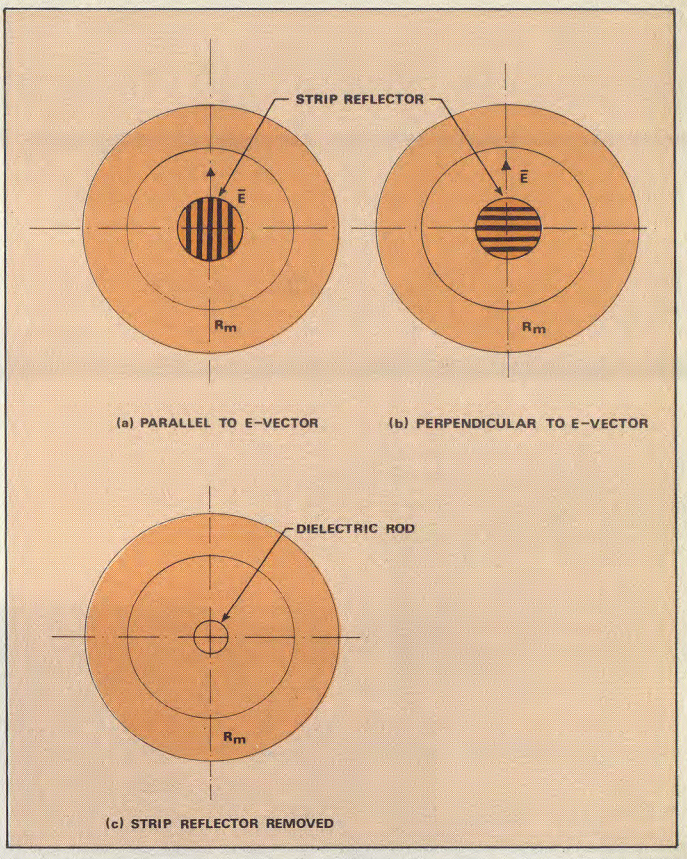

***2. Orientation of the strips** with respect to the E-plane gives backfire (a) or endfire (b) performance. Radiation pattern generated with reflector removed (c) is identical to the endfire case.*

ENGELMANN MAKES IT!

the microcube™ oscillators

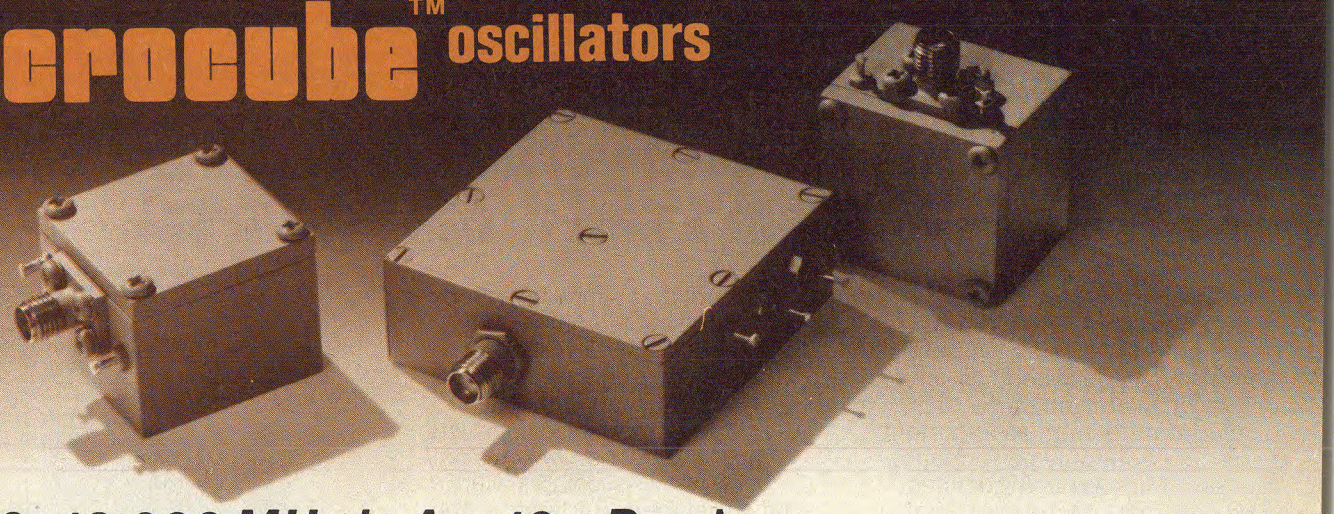

750-18,000 MHz in Any 10% Band

- Precise Resolution . . . Mechanical Tuning
- 12 VDC Operation
- High Efficiency
- Fundamental Transistor Up To 7 GHz
- Temperature Stability to ± .05%
- AFC Provision . . . plus many other options

READER SERVICE NUMBER 67

Setting New Standards in Reliabili

ENGELMANN

Engelmann Microwave Co.— Subsidiary of Pyrofilm Corpora

Skyline Drive, Montville, New Jersey 07045 • (201) 334-5

to 9 GHz), which is out of the frequency range for the long backfire case.

Measured VSWR is less than 1.8 in both discrete frequency ranges, and less than 1.08 and 1.04 at 8.8 and 10.2 GHz, respectively.

The directivity of the backfire antenna has been calculated by the pattern integration method.[11] The calculated value of directivity is 24.8 dB at 10.2 GHz for the backfire case. The loss in the radiated power due to poor matching and loss in dielectric structure is approximately 0.3 dB. The gain of the antenna is approximated by subtracting the loss in the radiated power. The final gain of the long backfire antenna is 24.5 dB, referred to an isotropic source. In the case of endfire operation, the average gain is 14 dB from 8.6 to 9 GHz.

The cross-polarization performance of the antenna for both frequency ranges is summarized in Table 1. Note that the peak cross-polarization levels are less than −27 dB and −30 dB over the two discrete frequency ranges.••

Table 1:

Cross-polarization in two bands

Frequency, GHz	Peak cross-polarization level, dB
8.6	−27.0
8.7	−28.0
8.8	−28.0
8.9	−27.5
9.0	−27.0
9.9	−30.5
10.0	−31.0
10.1	−31.5
10.2	−31.0
10.3	−30.5
10.4	−30.0

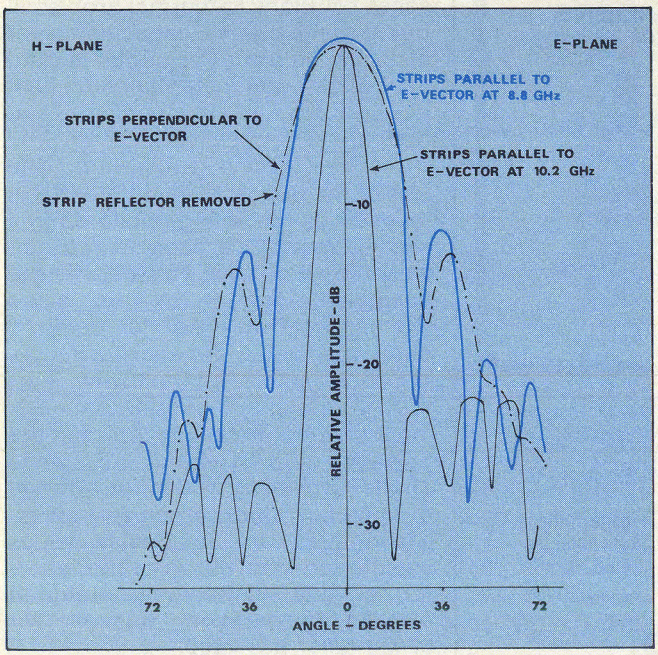

***3. E and H-plane patterns** show a high degree of symmetry for all cases.*

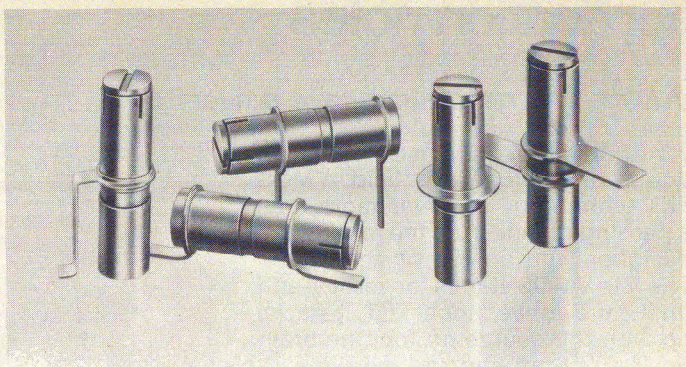

GIGA-TRIM CAPACITORS FOR MICROWAVE DESIGNERS

GIGA-TRIM (gigahertz-trimmers) are tiny variable capacitors which provide a beautifully straightforward technique to fine tune RF hybrid circuits and MIC's into proper behavior.

APPLICATIONS

- Impedance matching of GHz transistor circuits
- Series or shunt "gap trimming" of microstrips
- External tweaking of cavities

Available in 5 sizes and 5 mounting styles with capacitance ranges from .3 - 1.2 pf to 7 - 30 pf.

Johanson®

MANUFACTURING CORPORATION
Rockaway Valley Road
Boonton, N.J. 07005
(201) 334-2676 TWX 710-987-8367

READER SERVICE NUMBER 53

References

1. H. W. Ehrenspeck, "The Backfire Antenna, A New Type Of Directional Line Source," *Proc. IRE*, 48, pg. 109, (1960).
2. H. W. Ehrenspeck, "Reflection Antenna Employing Multiple Director Elements and Multiple Reflection Of Energy To Effect Increased Gain," US Patent 3 122 745, (February, 1964).
3. H. W. Ehrenspeck, "The Backfire Antenna: New Results," *Proc. IEEE*, 53, pg. 639, (1965).
4. H. W. Ehrenspeck, "Backfire Antenna," *NTZ*, 22, 5, pg. 286, (1969).
5. H. D. Hristov, "Some Experiences With Backfire Antennas, Discussion Meeting On Novel Types Of Aerials," *IEE*, London, (January, 1972).
6. H. D. Hristov, "X-Band Rectangular Backfire Antenna," Bulgarian Patent 18149, (July, 1972).
7. H. D. Hristov, "Backfire Antennas With Surface-Wave Structure," Ph.D. Thesis, The Higher Inst. of Mech. and Elect. Engr., Varna, Bulgaria, (1973), (In Bulgarian).
8. J. A. Strom, "A Dielectric Rod Backfire Antenna," AFCRL Report 69-0347, (August, 1969).
9. H. D. Hristov and A. Kumar, "X-Band Long Backfire Antenna With Surface Wave Structure," Research report - Queen Mary College, (1976).
10. F. J. Zucker, "The Backfire Antenna: Qualitative Approach To Its Design," *Proc. IEEE*, 53, pg. 746, (1965).
11. S. Silver, *Microwave Antenna Theory and Design*, Dover Publication, NY, (1965).

VMOS: The next microwave power FET?

Although not quite ready to revolutionize the microwave field, VMOS FET technology deserves more than a passing glance from the microwave designer with an eye on the future. The V in VMOS stands for vertical and unlike the conventional FET, it stacks up with the source on top, the drain on the bottom and the gate in a V-groove antisotropically etched into the substrate.

Siliconix, Inc., has put together a number of notes on this exciting new technology, but the one most interesting to the microwave designer is AN76-3: "VMOS—A Breakthrough In Power MOSFET Technology." The 11-page note reviews the VMOS structure and expands the subject to include applications ranging from general switching networks to a VHF linear amplifier circuit.

Using the VMP 1, a number of switching networks are developed. Teamed with a CMOS driving gate, the FET is capable of about 25 nsec switching time, and by increasing the drive current a 10 nsec switch is possible. The VMP 1 also interfaces nicely with TTL and if more current is needed to pull the output up higher, open collector TTL can be used with a 10 or 15 volt supply. In all, about 15 applications are discussed for a switching VMOS FET. Space is also devoted to temperature considerations.

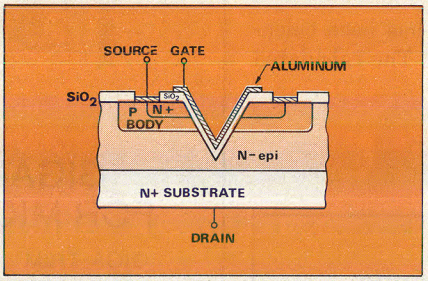

***Gate metalization** is deposited on the surface of a V-shaped groove.*

The final circuit is a 144-146 MHz linear amplifier with a 5-watt peak output power when used as a transmitter. As a preamp, a 2.4-dB noise figure and an 11-dB gain make it ideal for receiver applications. **Siliconix, Inc., 2201 Laurelwood Road, Santa Clara, CA 95054 (408) 246-8000.**

CIRCLE NO. 109

Designing with beryllia

Beryllia has a long and successful history for microwave designers because of its high thermal conductivity, good insulating properties, strong makeup and transparency to microwave radiation. But how much do you *really* know about this work-horse material?

"Designing With Beryllia" from National Beryllia Corporation will answer most of your questions and probably some you didn't even have. The note, which actually made its debut as a seminar handbook a few months ago, describes beryllia design from three viewpoints: material properties, manufacture and component design.

Beginning with the second law of thermodynamics (heat flows from a higher to a lower temperature body), important thermal relationships are developed. If the study of thermodynamics leaves you cold, remember all thermal properties have analogous electrical terms.

With that in mind, Ohm's law becomes Fourier's law, $P\theta = \Delta T$. The temperature difference, ΔT, is analogous to voltage. So the thermal resistance, θ, times the heat flow, P, is proportional to ΔT. This expression points out what's thermally happening within a component and clears the path to more complex expressions. Actual solved problems are the vehicle that describe each individual parameter and their series/parallel conditions.

There are no tricks, just common sense solutions to thermal problems. Dealing with thermal capacitance, for instance, an electrical circuit is used to explain non-instantaneous heat rise. As heat is first applied, temperature difference will increase until it reaches thermal equilibrium. The rate of the temperature differential is identical to the voltage build-up in a similiar resistance capacitance network. Current flow, voltage and capacitance interact in the same manner as heat flow, temperature differential and thermal capacitance.

Shock, stress, conductivity, thermal spreading and intermittent heating are other interesting topics in the 38-page note. Thermal resistance charts, providing values for a range of materials, thicknesses and cross-section areas are included as well as some interesting views of the future for beryllia technology. **National Beryllia Corporation, Haskell, NJ 07420 (201) 839-1600.**

CIRCLE NO. 110

Miniature Stripline Components

0.2 to 18 GHz

HYBRIDS 90°/180°

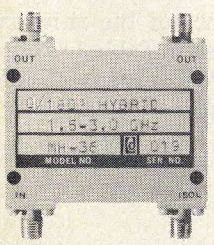

DIRECTIONAL COUPLERS

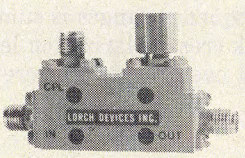

POWER DIVIDERS
In-Phase, 2-4-n Way

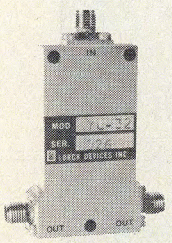

Complete in-plant design, manufacture and environmental testing of quality-assured miniature stripline components covering the 0.2 GHz—18 GHz band in octave and multi-octave ranges is one of our specialties. The units shown above are produced with peak power handling capacity to 25 KW.

Lorch Devices' complete line of stripline components includes mixers, switches, limiters, attenuators, detectors and custom integrated assemblies. All operate over the temperature range from −55° to +125°C, and can be readily adapted for Hi-Rel applications.

Send for a copy of our 64 page Catalog 749 and consult with our application engineering department about your specific requirements.

LORCH DEVICES INC.
105 CEDAR LANE, ENGLEWOOD, N.J. 07631
201-569-8282 • TWX: 710-991-9718

READER SERVICE NUMBER 54